

UNCLASSIFIED

AD NUMBER
AD921093
NEW LIMITATION CHANGE
TO Approved for public release, distribution unlimited
FROM Distribution authorized to U.S. Gov't. agencies only; Test and Evaluation; 30 Apr 1974. Other requests shall be referred to Air Force Avionics Lab., Wright-Patterson AFB, OH 45433.
AUTHORITY
AFAL ltr, 21 Sep 1978

THIS PAGE IS UNCLASSIFIED

THIS REPORT HAS BEEN DELIMITED  
AND CLEARED FOR PUBLIC RELEASE  
UNDER DOD DIRECTIVE 5200.20 AND  
NO RESTRICTIONS ARE IMPOSED UPON  
ITS USE AND DISCLOSURE.

DISTRIBUTION STATEMENT A

APPROVED FOR PUBLIC RELEASE;  
DISTRIBUTION UNLIMITED.

L

AFAL-TR-74-104

PERFORMANCE SYNTHESIS OF  
ELECTRO-OPTICAL SENSORS

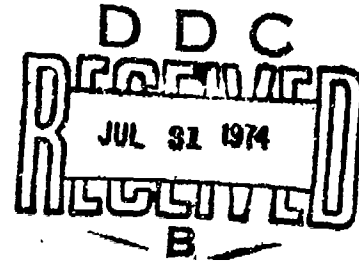
Frederick A. Rosell  
Robert H. Willson

Westinghouse Defense and Electronic Systems  
Systems Development Division  
Baltimore, Maryland

TECHNICAL REPORT AFAL-TR-74-104

April 1974

AD921093



Distribution limited to United States government agencies only; test and evaluation: 30 April 1974. Other requests for this document must be referred to Air Force Avionics Laboratory (NVA-698DF), Wright-Patterson Air Force Base, Ohio 45433

Air Force Avionics Laboratory  
Air Force Systems Command  
Wright Patterson Air Force Base, Ohio

## NOTICE

When Government drawings, specifications, or other data are used for any purpose other than in connection with a definitely related Government procurement operation, the United States Government thereby incurs no responsibility nor any obligation whatsoever; and the fact that the Government may have formulated, furnished, or in any way supplied the said drawings, specifications, or other data, is not to be regarded by implication or otherwise as in any manner licensing the holder or any other person or corporation, or conveying any rights or permission to manufacture, use, or sell any patented invention that may in any way be related thereto.

Copies of this report should not be returned unless return is required by security considerations, contractual obligations, or notice on a specific document.



PERFORMANCE SYNTHESIS OF  
ELECTRO-OPTICAL SENSORS

Frederick A. Rosell  
Robert H. Willson

Distribution limited to United States Government agencies only:  
test and evaluation; 30 April 1974. Other requests for this  
document must be referred to Air Force Avionics Laboratory  
(NVA-698DF), Wright Patterson Air Force Base, Ohio 45433

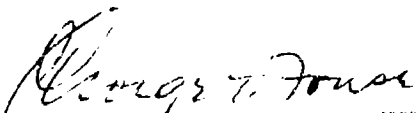
## FORWORD

This program involved the refinement of mathematical models and performance of psychophysical experiments as part of the continuation effort of the 698DF development project for a high-resolution low-light-level television system for tactical airborne application. These studies have led to a better understanding of system tradeoffs, dynamic range, image motion and range analysis of electro-optical sensors and the use of the results has lead to a realistic system specification and can lead to a reduced need for costly laboratory and flight testing of systems.

The Air Force Project Director on this program was Frank A. McCann, AFAL/NVA(698DF). The Westinghouse effort was conducted principally by Frederick A. Rosell and Robert H. Willson. The program was performed by the Westinghouse Systems Development Division, Baltimore, Maryland, under Air Force Contract F33615-73-C-4132.

This report was submitted by Frederick A. Rosell and Robert H. Willson.

This technical report has been reviewed and is approved for publication.

  
GEORGE T. FOUSE  
Acting Deputy Director  
Navigation & Weapon Delivery Division

## ABSTRACT

This effort is a continuation of the Performance Synthesis Study (Electro-Optical Sensors) reported in Technical Report AFAL-TR-73-260, dated August 1973 analytical sensor models are updated and refined. Procedures for performing systems trade-off analysis are discussed, general requirements and specifications for typical electro-optical imaging sensors are derived and reported. Psychophysical testing was performed in order to determine grey scale detection and other dynamic range requirements and to further improve the understanding of image motion effects. Finally computer programs for system resolution prediction are developed.

## TABLE OF CONTENTS

<u>Section</u>	<u>Page</u>
I INTRODUCTION AND SUMMARY . . . . .	1
II MODEL UPDATE . . . . .	9
2.1 The Elementary Model . . . . .	9
2.2 The Effect of Finite Apertures . . . . .	21
2.3 Observer thresholds . . . . .	36
2.4 Observer Requirements - Periodic Bar Patterns . . . . .	46
2.5 Higher Discrimination Levels . . . . .	49
III SYSTEM TRADEOFF ANALYSIS . . . . .	57
3.1 Scene Characteristics . . . . .	59
3.1.1 Scene Characteristics (Passive) . . . . .	60
3.1.2 Scene Characteristics (Active) . . . . .	69
3.2 Objective Lens, Sightline Instability and Photosurface Parameters . . . . .	82
3.2.1 Objective Lens Parameters (Passive) . . . . .	91
3.2.2 Objective Lens Parameters (Active) . . . . .	93
3.3 Image Tube Parameters, Image Motion Effects . . . . .	94
3.3.1 Threshold Resolution of the TV Camera . . . . .	103
3.3.2 Effective Magnification of an Electro-Optical Sensor . . . . .	104
3.4 Range Analysis. . . . .	115
3.4.1 Range Analysis (Active) . . . . .	116
3.4.2 Range Analysis- (Passive Case) . . . . .	121

TABLE OF CONTENTS  
(continued)

<u>Section</u>	<u>Page</u>
IV ELECTRO-OPTICAL SYSTEM REQUIREMENTS AND SPECIFICATIONS . . .	127
4.1 Component Specifications . . . . .	129
4.1.1 System Component Blocks (Passive). . . . .	129
4.1.2 System Component Blocks (Active) . . . . .	129
4.1.3 System Source (Active) . . . . .	129
4.1.4 Window Assembly . . . . .	130
4.1.5 Stabilization and LOS Sterring Mechanisms . . . . .	130
4.1.6 Objective Lens Assembly . . . . .	131
4.1.7 Television Camera Assembly . . . . .	132
4.1.8 Television Camera Assembly (Active) . . . . .	133
4.1.9 Signal Processor. . . . .	133
4.1.10 Display . . . . .	134
4.2 Predicted Laboratory Performance . . . . .	134
4.2.1 Standardized Laboratory Test Patterns . . . . .	135
4.2.2 The Idealized Scene . . . . .	136
4.2.3 Overall System MTF's . . . . .	137
4.2.4 Signal-to-Noise Ratio . . . . .	139
4.2.5 Display Signal-to-Noise Ratio Required . . . . .	141
4.3 Predicted Field Performance . . . . .	141
4.3.1 Effect of Sightline Vibration on Motion . . . . .	142
4.3.2 Effect of Atmosphere (Passive) . . . . .	143
4.3.3 Effect of Atmosphere (Active) . . . . .	143
4.3.4 Scene Irradiator - Sensor Gating Characteristics . . . . . (Active)	144

TABLE OF CONTENTS  
(continued)

<u>Section</u>	<u>Page</u>
4.3.5	Miscellaneous Environmental Considerations . . . . . 144
4.3.6	System Resolution (Passive). . . . . 145
4.3.7	System Resolution (Active) . . . . . 145
4.4	Mission Requirements . . . . . 146
4.4.1	Expectation of Meeting Mission Requirements. . . . . 147
4.4.2	Levels of Discrimination . . . . . 148
4.4.3	Targets and Range Prediction . . . . . 148
4.4.4	Mission Profile Recommendations. . . . . 148
4.5	Nomenclature, Symbols and Units . . . . . 148
V	DYNAMIC RANGE . . . . . 151
5.1	Signal Transfer Characteristics and Video. . . . . 154 Signal-to-Noise Ratio
5.2	Shades of Grey . . . . . 164
5.3	Psychophysical Experiments - Shades of Gray . . . . . 165
VI	EFFECTS OF IMAGE MOTION . . . . . 177
6.1	Psychophysical Experiments Involving Image Motion. . . 178
VII	COMPUTER PROGRAMS FOR SYSTEM RESOLUTION PREDICTION. . . . . 193
7.1	Calculation of $N_e$ . . . . . 194
7.2	Calculation of $\xi$ and $\Gamma$ . . . . . 196
7.3	Calculation of $R_{SF}(N)$ . . . . . 197
7.4	Calculation of $\beta(N)$ . . . . . 199
7.5	Calculation of $R_{om}(N)$ . . . . . 200
7.6	Calculation for Passive Day Operation. . . . . 202

TABLE OF CONTENTS  
(continued)

<u>Section</u>	<u>Page</u>
7.7 Calculation for Passive Night . . . . .	210
7.8 Calculation for Active System . . . . .	216
REFERENCES . . . . .	221

LIST OF ILLUSTRATIONS

<u>Figure</u>	<u>Page</u>
1 Perceived Signal-to-Noise Ratio for a Square Image as a Function of the Image's Linear Size for Various Input Photocurrents. Also shown are the Threshold SNR for $C_M = 1.0$ and Apparent Thresholds for $C_M = 0.3$ and $0.1$ . . . . .	.14
2 Minimum Detectable Photocurrent for Square Images of Linear Dimension Z as Limited by Photoelectron Noise at Three Values of Input Image Contrast. . . . .	.16
3 Probability of Detection for Rectangular Images as a Function of the Image Signal-to-Noise Ratio . . . . .	.17
4 Perceived Signal-to-Noise Ratio for a Bar Pattern Image as a Function of Spatial Frequency for Various Input Photocurrents. Also shown are the Threshold SNR for $C_M = 1.0$ and the Apparent Thresholds for $C_M = 0.3$ and $0.1$ . . . . .	.19
5 Threshold Resolution vs Average Input Photocurrent for a Bar Pattern Image as Limited by Photoelectron Noise at 3 Values of Input Image Contrast . . . . .	.20
6 Figure for Deriving the Square Wave Flux Amplitude $A_I$ for a Sensor with MTF, $R_O(N)$ . Figure is Drawn for the First Harmonic ( $k = 1$ ). . . . .	.31
7 Actual Image Amplitude, $A_I$ , and Waveshape (————) Compared to Equivalent Square Wave Flux Amplitude, $A_T$ , and Waveshape (- - -) . . . . .	.32
8 $SNR_D$ vs Spatial Frequency for the 25/25/20 I-EBSICON for Three Values of Input Photocurrent ( . . . ) $3.16 \times 10^{-14}$ A, (————) $3.16 \times 10^{-13}$ A and ( - - - ) $1 \times 10^{-10}$ A. If $N_1$ is the Threshold Frequency, $N_2$ is the New Threshold Frequency when $SNR_D$ at $N_1$ is Doubled. . . . .	.35
9 Relative Increase in Threshold Resolution $N_2/N_1$ as the $SNR_D$ at $N_1$ is Increased by a Factor of 2 Above the Threshold Value at $N_1$ . . . . .	.35



LIST OF ILLUSTRATIONS  
(continued)

<u>Figure</u>		<u>Page</u>
10	Corrected Probability of Detection vs $SNR_D$ required for Rectangular Images of Size $\bigcirc 4 \times 4$ , $\square 4 \times 64$ , $\triangle 4 \times 128$ , and $\diamond 4 \times 180$ Scan Lines. Televised Images at 30 frames per second and 525 Scan Lines. $D_V/D_H = 3.5$ . . . . .	37
11	Corrected Probability of Detection vs $SNR_D$ required for Square Images of Size $\square 8 \times 8$ , $\bigcirc 16 \times 16$ , $\triangle 32 \times 32$ and $\times 64 \times 64$ Scan Lines. Televised Images at 30 frames per second and 525 Scan Lines. $D_V/D_H = 3.5$ . . . . .	38
12	Threshold $SNR_D$ required to detect Square Images of Various Size and Angular Extent. Televised Images at 30 frames/second, 525 Scan Line Raster. $D_V/D_H = 3.5$ . . . . .	39
13	Threshold $SNR_D$ vs Size of Squares in Scan Line Width Dimensions for Simple Detection (—) and for Liminal Perception of the Square Edges (- - -). . . . .	41
14	Geometric Shapes Used for Edge Discrimination. Photographs show (left to right, up to down) Decreasing $SNR_D$ Values. Attenuation of Signal in db is- upper left 23db, upper Right 25db lower left 27db lower right 29db. . . . .	43
15	Geometric Shapes Used for Edge Discrimination. Photographs Show (left to right, up to down) Decreasing $SNR_D$ Values. Upper left 15 db, upper right 17 db, lower left 19db, lower right 21 db attenuation of Signal . . . . .	44
16	Threshold $SNR_D$ vs Bar Pattern Spatial Frequency for Display-to-Observer Viewing Distances of $\bigcirc 14"$ , $\square 28"$ and $\bullet 56"$ . . . . .	48
17	Threshold Display Signal-to-Noise Ratio vs. Bar Pattern Spatial Frequency for $\square$ Optimum Viewing Distance and $\bigcirc 28"$ Viewing Distance for One Observer. . . . .	48
18	Threshold Display Signal-to-Noise Ratio required to recognize the Presence of, $\bigcirc$ Horizontally Oriented and, $\bullet$ Vertically Oriented Bar Patterns vs. Bar Pattern Spatial Frequency Televised Images at 25 Frames/Sec., 875 Scan Lines, $D_V/D_H = 3.5$ Bar Height-to-Width Ratio was 5 . . . . .	49
19	Levels of Object Discrimination. Object Area to be Used in the $SNR_D$ Calculation is $\Delta y$ by $L$ . . . . .	53

LIST OF ILLUSTRATIONS  
(continued)

<u>Figure</u>	(continued)	<u>Page</u>
20	Probability of Recognition vs SNR <sub>D</sub> for a $\circ$ Tank, $\diamond$ Radar Half Track, $\square$ Van Truck and $\bullet$ Derrick Bulldozer. Uniform Background, Televised Imagery at 875 Lines, 25 frames/sec $D_V/D_H = 3.5$ . . . . .	53
21	Equivalent Bar Pattern Criterion for Object Identification. . . . .	55
22	Illuminance Levels on the Surface of the Earth due to the Sun, the Moon, and the Light of the Night Sky . . . . .	63
23	Approximate ratio of the Atmospheric Extinction Coefficient, $\alpha_h$ at altitude h to its value $\alpha_0$ at Sea Level for slant and Horizontal Paths neglecting Water Vapor and Carbon Dioxide Absorption . . . . .	66
24	Ratio of Apparent to Inherent Contrast vs Range for Various Values of Sky-to-Ground Ratio for a Meteorological Visibility of 10 Nautical Miles . . . . .	68
25	Geometry for Backscatter Calculation - Sensor Not Range Gated. . . . .	76
26	Geometry for Backscatter Calculation - Range Gated Sensor . . . . .	77
27	Ratio of Apparent-to-Inherent Contrast for (—) Range Gated Active and (- - -) Passive Sensors for Background Reflectivity of 20% and 10 Nautical Mile Visibility . . . . .	79
28	Ratio of Apparent to Inherent Object Contrast vs Range for a Near Point Range Gate Fixed at $R_{Ln}$ for Objects in the Range Interval $R_{Ln}$ to $R_{Ln}+1$ . Visibility at 0.86 micrometers is 10 n.m. with Average Scene Reflectance = 0.2. $T=2 \mu s$ . . . . .	81
29	Ratio of Apparent to Inherent Contrast vs Range for Objects in the Middle of the Range Gate Limits. Visibility at 0.86 micrometers is 10 n.m. with Average Scene Reflectance = 0.2. $T = 2 \mu s$ . . . . .	82
30	Relationship Between Focal Length and Image Size . . . . .	86
31	Modulation Transfer Function for a Typical Image Intensifier . . . . .	96
32	Modulation Transfer Function for a Typical Image Intensifier with (—) 40, (—) 25 and (- - -) 16 $\mu m$ Phosphor Diameter . . . . .	97

LIST OF ILLUSTRATIONS  
(continued)

<u>Figure</u>		<u>Page</u>
33	Schematic of an Intensified-EBSICON Camera Tube . . . . .	98
34	Typical MTF's for EBSICON Camera Tubes with Targets of Diameter (————) 25 mm, (———) 20 mm and (——.——) 10 mm. Targets are of the Deep Etch Variety . . . . .	99
35	SNR <sub>D</sub> vs Spatial Frequency for the 25/20 mm EBSICON at Various Average Input Photocurrents. Lens MTF Assumed to be Unity. Horizontal Lines Represent Observer Thresholds for Various Image Modulation Contrasts. . . . .	106
36	Threshold Resolution vs Input Photocurrent for the EBSICON Camera Tub for Various Input Image Contrasts. . . . .	107
37	Threshold Resolution vs Input Photocurrent for the D <sub>pc</sub> /25/20 I-EBSICON. The Above Result is Independent of <sup>pc</sup> the Input Photosurface Diameter, D <sub>pc</sub> , to a Good Approximation. . . . .	108
38	MTF of Typical Lenses with Various Fields-of-View (in the Vertical) . . . . .	112
39	MTF Due to Random Image Motion Expressed in Lines/Picture Height for Various Fields-of-View. . . . .	112
40	SNR <sub>D</sub> vs Spatial Frequency for the Assumed Camera with 4 Different Fields-of-View. Sightline Instability is 30 Microradians rms (random). . . . .	113
41	Input Photocurrent vs Range for Various Sea Level Visibilities. System Source Power is 40 watts, Lens T Stop is 4, Average Scene Reflectivity is 0.2. Field-of-View is 1.5 x 2 and Photoresponse is 15 mA/W. . . . .	117
42	SNR <sub>D</sub> vs Spatial Frequency as a Function of Range for the Assumed Active System . . . . .	119
43	Threshold Resolution vs Range for the Assumed Active System with Various Input Image Contrasts . . . . .	120
44	Threshold Angular Resolution vs Range for the Assumed Active System with Various Input Image Contrasts . . . . .	121
45	Threshold Resolution vs Range for the Assumed Active System with Various Input Image Contrasts . . . . .	121

LIST OF ILLUSTRATIONS  
(continued)

<u>Figure</u>		<u>Page</u>
46	Ratio of the Sum of Photoelectron and Preamp Noise to the Photoelectron Noise . . . . .	123
47	Display Signal-To-Noise Ratio vs Range for the Assumed Passive System. SNR <sub>d</sub> Thresholds are for a 10 n.m. Visibility of 10 n.mi. and a Sky to Ground Ratio of 4. Inherent Image Contrast is 100% . . . . .	124
48	Threshold Angular Resolution vs Range for the Assumed Passive System for Two Values of AVERAGE Input Photocurrent . . . . .	125
49	Typical Output Signal Current vs Input Photocurrent for the Intensified-EBSICON Camera . . . . .	155
50	Typical Broad Area Video Signal-to-Noise Ratio vs Input Photocurrent for the Intensified-EBSICON Camera . . . . .	161
51	Video Waveform for a Typical Linear Grey Scale . . . . .	166
52	Video Waveform Used for the Double Rectangle Experiments. . . . .	168
53	The Display Signal-to-Noise Ratio Experiment. . . . .	169
54	Video Signal-to-Noise Ratio for Electronically Generated Shades of Grey as a Function of the Number of Scan Lines in a Bar Width . . . . .	169
55	Test Pattern Showing Grey Scale Pattern . . . . .	172
56	Video Signal-to-Noise Ratio for EIA Grey Scale as a Function of Number of Shades of Grey . . . . .	173
57	Threshold SNR <sub>v</sub> as a Function of # of Shades of Grey in EIA Grey Scale $\odot$ 10 FL in Step #2, $\square$ 10 FL in Step #10. . . . .	175
58	Experimental Set-up for the Television Camera Generated Imagery . . . . .	178
59	Experimental Set Up for Motion Experiments. . . . .	179
60	Photographs of Models Used for Recognition Experiments - Upper Left, Tank; Upper Right, Van Truck; Lower Left, Half Track with Antenna; and Lower Right, Derrick Half Track . . . . .	180
61	Static Tank-Detection Experiment. . . . .	184
62	Tank in Motion-5 Sec/P.W. Detection Experiment. . . . .	184

LIST OF ILLUSTRATIONS  
(continued)

<u>Figure</u>		<u>Page</u>
63	Static Tank - A Trace Waveform . . . . .	185
64	Tank Moving 5 sec/P.W. - A Trace Waveform. . . . .	185
65	The Display Signal-to-Noise Ratio Experiment . . . . .	186
66	Threshold $SNR_D$ vs Number of Raster Lines in Square for $\bigcirc$ Stationary Patterns $\square$ 20 Seconds/Picture Width Motion and $\blacksquare$ 5 Seconds/Picture Width Motion . . . . .	187
67	Bar Patterns of Variable Aspect, Isolated Bars and Isolated Circles Used for Experiments . . . . .	188
68	Threshold $SNR_D$ vs Spatial Frequency for Pattern Speeds of $\bigcirc$ 10 Sec/P.W. and $\bigcirc$ 5 Sec/P.W. . . . .	190
69	Dynamic Square Wave Response - Theory $\bigcirc$ Measured - $\bigcirc$ for 10 Sec/ P.W Linear Pattern Speed. . . . .	191
70	Dynamic Square Wave Response - Theory $\bigcirc$ Measured - $\bigcirc$ for 5 Sec/P.W. Linear Pattern Speed . . . . .	191
71	Threshold $SNR_D$ vs Line Number for Aperiodic Bars Moving at a Speed of $\bigcirc$ 10 Seconds per Picture Width. . . . .	192
72	$SNR_D$ vs $\Delta\theta$ for 6, 12, 18, 24 and 30 K ft . . . . .	209
73	Required vs Available Resolution, $\Delta\theta$ vs Slant Range . . . . .	210

LIST OF TABLES

<u>Table</u>	<u>Page</u>
1 SNR <sub>D</sub> Required to Detect and to Shape Detect Various Geometric Shapes. . . . .	42
2 Table Constructed to Test the Hypothesis that the Ability of an Observer to Discern Regular Geometric Shapes is Proportional to the Square Root of Side Length. . . . .	45
3 Levels of Object Discrimination. . . . .	52
4 Johnson's Criteria for the Resolution Required per Minimum Object Dimension vs Discrimination Level. . . . .	52
5 Atmospheric Extinction Coefficient as a Function of Meteorological and Subjective Visibility. . . . .	66
6 Typical Values of the Sky to Ground Ratio in the Visible Spectrum .	68
7 Values of Attenuation Coefficient/km as a Function of Altitude for Laser Wavelength of .488 um (k = molecular absorption, $\sigma_m$ = molecular scattering, $k_a$ = aerosol <sup>m</sup> absorption, $\sigma_a$ = aerosol <sup>m</sup> scattering) . . . . .	70
8 Values of the Extinction Coefficient at 0.86 Micrometers vs Meteorological Visibility . . . . .	73
9 Values of Attenuation Coefficient/km as a Function of Altitude for Laser Wavelength = .86 um (k = molecular absorption, $\sigma_m$ = molecular scattering, $k_a$ = aerosol <sup>m</sup> absorption, $\sigma_a$ = aerosol <sup>m</sup> scattering) . . . . .	83
10 Amplitude and Flux Responses and Noise Filtering Factor vs Spatial Frequency for the 25/20 EBSICON. . . . .	105
11 MTF and MTF Related Quantities for the 25/25/20 Intensified EBSICON . . . . .	108
12 Effect of Field of View Decrease and Sightline Motion on Effective Magnification . . . . .	114
13 International Systems (SI) for Fundamental Photometric and Radiometric Units . . . . .	149

LIST OF TABLES  
(continued)

<u>Table</u>		<u>Page</u>
14	Values Used for Tactical Image Detection Calculations . . . . .	182
15	Program For Calculation of $N_e$ . . . . .	195
16	Program For Calculation of $X_1$ and Gamma . . . . .	196
17	$X_1$ and Gamma Calculated With Program . . . . .	197
18	Program For Calculation of Flux Factor . . . . .	198
19	Flux Factor as Calculated with Program . . . . .	198
20	Program For Calculation of Beta Factor. . . . .	199
21	Beta Factor as Calculated with Program . . . . .	200
22	Program For Calculating $R_0$ due to Random Motion . . . . .	201
23	$R_0$ as Calculated with Program . . . . .	201
24	Program For Passive Day. . . . .	204
25	Continuation of Passive Day Program . . . . .	205
26	Correspondence Between Symbols. . . . .	206
27	Passive Day Calculations . . . . .	207
28	More Passive Day Calculations. . . . .	208
29	Program for Passive Night. . . . .	211
30	Continuation of Program For Passive Night. . . . .	212
31	Calculations For Passive Night . . . . .	213
32	More Calculations For Passive Night. . . . .	214
33	More Passive Night Calculations. . . . .	215
34	Yet More Passive Night Calculations. . . . .	216
35	Program For Active System. . . . .	217
36	Rest of Program For Active System. . . . .	218
37	Calculations For Active Calculation. . . . .	219

## 1.0 Introduction and Summary

The objectives of the Performance Synthesis of Electro-Optical Sensors study performed under Air Force Contract No. F33615-70-C-1461 are to determine the fundamental limitations of long range air-to-ground detection, recognition and identification of tactical military targets, to determine methods of realizing maximum range performance through optimum spatial, temporal and electrical filtering of the received image signals and to devise methods of predicting maximum range performance taking into account the parameters of real targets, backgrounds, illumination sources, atmospherics and sensory systems. The results are to be applicable to all imaging sensors whether passive or active and are to include low light level television, forward-looking infrared scanners and direct view light amplifiers.

The current effort is a continuation of the programs previously reported in Ref. 1 (Technical Report AFAL-TR-71-137), Ref. 2 (Technical Report AFAL-TR-72-229) and Ref. 3 (Technical Report AFAL-TR-73-260). As before, the approach taken is to devise analytical models to describe sensory system performance including the observer as an integral part of the system. Psychophysical experiments are performed to obtain the necessary constants of the observers to quantitatively evaluate the analytical models. Through these efforts, it is hoped to promote a better understanding of the operation of electro-optical sensors, guide the further development of systems components, improve methods of sensory system



performance and reduce the necessity of costly laboratory and flight evaluation of prototype systems.

In the previous efforts reported, the early emphasis in analysis and experimentation was on images of simple or regular geometry such as rectangles and bar patterns. Real images of tactical objects were also considered with a concerted effort to correlate the discernibility of bar patterns with various levels of real object discrimination -- particularly real object recognition and identification. Some success with the equivalent bar pattern approach was realized as noted in Ref. 2. However, further efforts were, and still are, required.

The discernibility of an image projected onto the photosurface of an electro-optical sensor and ultimately displayed to an observer is limited by the sensor's sensitivity to the received radiation and by noises generated either in the primary photoconversion process or in subsequent signal processing. Also, the image's discernibility is limited by finite sensor apertures that decrease the image modulation. Preliminary efforts to account for the effects of these apertures were reported in Ref. 1. The theory, then presented, though leading to reasonable system predictions was intuitively unsatisfying. An advanced theory was presented in Ref. 2 that was more satisfying but still had deficiencies -- particularly in the treatment of aperiodic (rectangular) images.

Concurrent with the effort reported in Ref. 2, a separate effort was undertaken under Air Force Contract No. F33615-70-C-1461 by Sendall and Rosell to analyze FLIR and TV on a common basis. In this program, the aperiodic image treatment was considerably improved due in large part to Sendall. These advances in the modeling were reported in Ref. 3 in

some detail. While much of the ground work for the present models must be attributed to Otto Schade, Sr., the translation of the theory to practice did not prove to be trivial. In any event, a mathematically rigorous and consistent theory of apertures was devised and put to experimental test. The experimentation involves psychophysical effects which are subject to statistical variation. Also, to test the theory, the test objects must be small -- close to the limit of sensor resolution. Near these limits, accurate sensor parameter measurements become difficult to make. However, to within the accuracy of the measurements, the theory was shown to hold. However, more work remains to be done in this area.

In each of the continuation efforts, we have attempted to concentrate on the most critical problems involved in the image discrimination field. In the current effort we have concentrated on image motion effects, shades of grey specification, dynamic range, system tradeoff analysis, the specification of systems and on the development of computer programs for range analysis.

Section 2 of this report, entitled model update, reviews the analytical model previously reported partly to serve as a reference for Section 4, system specifications. In the development, we discuss for the first time the interaction of signal to noise ratio and threshold resolution. In an ideal system, a doubling of the display signal to noise ratio or  $SNR_D$  at a given threshold line number results in a doubling of the threshold resolution. In a real system this effect will be observed at very low spatial frequencies. However, at high line numbers, a doubling of  $SNR_D$  may result in almost no resolution increase. This is due to the

sensor MTF. It becomes apparent that an increase in  $SNR_D$  at low spatial frequencies is more effective than a comparable increase at high line numbers. This  $SNR_D$ -resolution product may be likened to the gain bandwidth theory of information theory. We feel that this concept is worthy of further study.

Also, in Section 2, we explore a new shape discrimination concept. Using rather large images (unlimited by sensor MTF), we desired to determine the increase in  $SNR_D$  required before an object, just barely detected as a blob, could be recognized as a definite shape. The increase in  $SNR_D$  required averaged about 2.2 for 5 geometric figures. However, a more detailed analysis showed that the increase in  $SNR_D$  needed was proportional to the square root of the side length (the geometric shapes were regular). Further efforts in this area could lead to some alternate, and possibly, more fruitful criteria for object recognition.

In Section 3, we discuss system trade-off analyses. Part of this work is a review of previous efforts for the dual purpose of introducing the trade-off analysis and for use in the system specifications of Section 4. Section 3 begins with a discussion of the passive and active scene characteristics. Next, we consider the sensor's objective lens and sightline stability requirements and the trade-offs between objective lens and photosurface parameters. We follow with sensor parameters and their interaction with image motion. In the discussion, we devise an effective magnification concept which serves as a reference with which to compare the performance of an unaided observer under daylight conditions to that of an observer augmented by an electro-optical sensor.

This concept is used in range analysis to show the atmospheric and sightline stability limitations to magnification increase.

Section 4 represents an attempt to write a general specification for television systems. The approach is to first require that sensor component requirements be fully detailed. Next, it is asked that a potential contractor predict or document the system performance to be expected in the laboratory where image vibration and atmospheric effects are not expected to be a factor. Finally, the potential contractor is asked to document the performance he expects to realize in a field environment including the best estimates of the degradation to be expected due to image motion and atmospherics. The emphasis in this section is on system parameters bearing on the capability of the imaging system to convey information to the user as opposed to physical details such as finish of parts, etc.

Section 5 is devoted to a topic which is loosely designated as dynamic range. This subject has, so far, defied both description and definition. Usable data has not existed. It is thus unreasonable to expect that this long standing problem should be solved in the small effort allotted to this portion of the program. While a precise definition was not expected to, nor did it, result from our program, considerable understanding of the nature of the problem was generated. In essence, a specification of dynamic range must include the limitations of the observer's eye. The darker shades of grey are obscured by fluctuations in the observer's primary photoprocess. In the course of our investigations it became abundantly clear that the number of observable shades of grey that can be seen depends upon the background luminance

of the grey scale and unless precisely defined, a grey scale will be an unreliable dynamic range indicator.

In section 6, motion experiments were discussed to test the validity of certain of the image motion concepts and to gain further insight into the image motion problem. Specifically, psychophysical experiments were performed using moving bar patterns moving isolated bars and moving complex images (vehicles). The vidicon camera was used to generate the imagery. In these experiments, the light level was high enough so that sensor time constants are usually negligible and the primary effect of motion is due to exposure time.

For bar patterns, the current motion MTF model was used (motion effects only -- not lag), and it appears to be adequate for the particular cases considered. For the vehicular imagery, an aperiodic model was applied with apparent success but the results must be considered tentative.

It is quite common to judge electro-optical system performance in terms of the overall systems ability, including the observer, to resolve simple geometric patterns which are easy to make and to quantitatively describe. The most common test pattern used, by far, is the square wave bar pattern consisting of alternating black and white stripes. A number of patterns are employed, each of a different spatial frequency. The higher the spatial frequency that can be resolved, the better the system is presumed to be. Bar patterns are used both in the laboratory and in the field. In the 698DF Performance Synthesis Program (Ref.'s 1 - 3) efforts have been made to correlate the ability to resolve bar patterns with the ability to detect, recognize and identify real scene objects. It would be presumptuous to claim that a one-to-one correlation was

observed but a degree of correlation does definitely exist.

In any event, real imagery is almost impossible to describe quantitatively and is generally unsuitable for use in an analytical model and thus the bar pattern has been adopted by most workers as the standard of performance. In general, the ability of an electro-optical sensor augmented observer to resolve a bar pattern on the sensor's display can be analytically predicted, knowing the sensor's parameters. The prediction is ordinarily quite precise, subject mainly to the statistical variation from observe-to-observer.

In section 7, we provide computer programs for the purpose of predicting a system's ability to resolve bar patterns. In general, the procedure is to calculate the bar pattern signal-to-noise ratio as it appears on the display and then compare that to the signal-to-noise ratio required by the observer. While we have suggested methods of correlating the discernability of bar patterns with real images, these methods must be considered preliminary and subject to further improvement and revision in the future. Thus, while the prediction of bar pattern resolution should be quite accurate, the estimation of the range at which real objects are recognized must be considered to be an approximation.

The various computer programs developed in section 7 are suitable for both component tradeoff and overall system analysis. Before discussing the main programs, smaller speciality programs are discussed which generate the system functions and constants needed as inputs to the main programs.

## 2.0 Model Update

Basic models have been derived for the probability of detecting rectangular and periodic test patterns in Ref. 3. These models will be briefly reviewed herein and extended to include the latest results obtained in the analysis and psychophysical experimentation.

Throughout the work in this program the procedure has been to associate a signal-to-noise ratio with an image produced by a sensor and then determine the signal-to-noise ratio required by an observer to discern the image at a given level of discrimination. By matching the image signal-to-noise ratio obtainable from the sensor to that required by the observer, measures of the overall sensory system performance, including the observer as an integral part of the system, can be estimated. This same procedure is continued in the current effort.

### 2.1 The Elementary Model

A slightly different approach to the elementary model is adopted here than was used in Ref. 3 in order to give further insight into the image detection process.

Suppose the image projected on the photosurface of a sensor is rectangular of dimensions  $x_0 \cdot y_0$  and of absolute irradiance level  $E_0$  Watts/m<sup>2</sup>. The absolute irradiance level of the background is taken to be  $E_B$ . The photosurface converts the image and background irradiances to densities of magnitude  $\dot{n}_0$  and  $\dot{n}_b$  photoelectrons respectively. The photoelectron images are greatly amplified in a signal processor. Eventually, the amplified

electron image is reconverted to a visible light image by a phosphor (the display). The displayed image is made bright enough and big enough so that the observer's eye is not limited by the image's size or luminance.

The observer's eye-brain combination has the ability to integrate the image in space and time. Thus, the signal we associate with the displayed image is

$$s_p = G\Delta n t \iint_{-\infty}^{\infty} f(x,y) dx dy \quad , \quad (1)$$

where  $G$  is the image amplification,  $\Delta n = n_s - n_b$ ,  $t$  is the integration time of the observer's eye and  $f(x,y)$  is the image's spatial waveform over which the eye integrates. For the special case of a rectangular image of uniform amplitude,

$$s_p = G\Delta n t x_o y_o \quad . \quad (2)$$

Thus, the perceived signal is proportional to the image area. It is important to note that the image area is referenced to the sensor's photosurface and not to the display. The signal is a count of the number of photoelectron events generated within the area  $x_o y_o$  during time,  $t$ , by the primary photoprocess.

The photon to electron conversion process is noisy. The mean square noise density is given by

$$\hat{n}_p^2 = G^2 \sigma^2 t [a(x,y)]^2 \Delta B_N \quad , \quad (3)$$



where  $\sigma^2$  is the mean square noise density (equal to  $(\dot{n}_o + \dot{n}_b)/2$ ),  $t$  is the eye integration time,  $a(x,y)$  is the area over which the noise is integrated and  $\Delta B_N$  is the noise bandwidth as limited by the eye. The area function  $a(x,y)$  is simply equal to  $x_o \cdot y_o$  for the elementary case. The noise bandwidth  $\Delta B_N$  is given by the function

$$\Delta B_N = \iint_{-\infty}^{\infty} F^2(N_x, N_y) dN_x dN_y, \quad (4)$$

where  $F(N_x, N_y)$  is the Fourier transform of  $f(x,y)$  and  $F(o)$  is the value of  $F(N_x, N_y)$  at zero frequency.  $N_x$  and  $N_y$  are spatial frequencies expressed in lines or half cycles per picture height. For the rectangular image cases,

$$\begin{aligned} \Delta B_N &= \frac{(x_o y_o)^2}{(x_o y_o)^2} \iint_{-\infty}^{\infty} \left[ \frac{(\sin \pi N_x x_o / 2)(\sin \pi N_y y_o / 2)}{(\pi N_x x_o / 2)(\pi N_y y_o / 2)} \right]^2 dN_x dN_y \\ &= \frac{1}{x_o y_o}, \end{aligned} \quad (5)$$

and thus the perceived noise is

$$\begin{aligned} n_p &= G \left[ \frac{(\dot{n}_o + \dot{n}_b)t}{2} \right]^{\frac{1}{2}} \frac{x_o y_o}{(x_o y_o)^{\frac{1}{2}}} \\ &= G \left[ \frac{(\dot{n}_o + \dot{n}_b)}{2} x_o y_o t \right]^{\frac{1}{2}} \text{ photoelectrons.} \end{aligned} \quad (6)$$

It is seen that the perceived rms noise is proportional to the square root of the image area.

The perceived signal-to-noise ratio is found by dividing Eq. (2) by Eq. (6) to obtain

$$\text{SNR}_p = \frac{\Delta \dot{n}(x_o y_o t)^{\frac{1}{2}}}{[(\dot{n}_o + \dot{n}_p)/2]^{\frac{1}{2}}} \quad (7)$$

The perceived  $\text{SNR}_p$  is thus proportional to the square root of image area. The above formula is identical to that developed as the elementary model in Ref.'s 2 and 3.

It is a convenience to express the photoelectron rates  $\dot{n}$  in terms of a photocurrent  $i$ ,

$$\dot{n} = i/eA \quad , \quad (8)$$

where  $e$  is the charge of an electron and  $A$  is the effective area of the photosurface. Then, Eq. (7) reads

$$\text{SNR}_p = \left[ \frac{a}{tA} \right]^{\frac{1}{2}} \frac{Ai}{(ei_{AV})^{\frac{1}{2}}} \quad , \quad (9)$$

where  $a$  is the image area ( $x_o \cdot y_o$  for a rectangular image) and  $i_{AV} = (i_o + i_p)/2$ . It is also handy to express the dimensions of a rectangular image in dimensionless form, i.e.,

$$\frac{x_o y_o}{A} = \frac{\epsilon x_o^2}{\alpha Y^2} = \frac{\epsilon}{\alpha} z^2 \quad , \quad (10)$$

where  $\epsilon$  is the length to width ratio of the rectangle,  $\alpha$  is the width to length or aspect ratio of the photosurface (assumed rectangular),  $Y$  is the "picture height" or height of the photosurface and  $z = x_o/Y$ . The dimension of  $z$  is in picture heights. Using Eq. (10), Eq. (9) becomes

$$\text{SNR}_p = \left[ \frac{te}{\alpha} \right]^{\frac{1}{2}} z \frac{2C_M i_{av}^{\frac{1}{2}}}{e^{\frac{1}{2}}} \quad (11)$$

In the above, we have made use of the image modulation contrast definition

$$\begin{aligned} C_M &= (i_o - i_b)/(i_o + i_b) \\ &= \Delta i / 2i_{av} \quad (12) \end{aligned}$$

As discussed in Ref. 3, the perceived signal-to-noise ratio required by an observer to detect a rectangular image is approximately a constant so long as the image is bright enough (i.e., sufficiently amplified by the sensor) and not too large or too small. For rectangles, this constant has been found to be 2.8 for a 50% probability of detecting the rectangle. Thus, if the image SNR provided by the sensor and calculated using Eq. (11) exceeds 2.8, the observer has a 50% or better probability of detecting the image.

The Eq. (11) is plotted in Fig. 1 for a square image ( $\epsilon = 1$ ), an observer time constant equal to 0.1 seconds, a picture aspect ratio of  $\alpha = 4/3$ , a modulation contrast of 1.0 and various values of  $i_{av}$ . The threshold signal-to-noise ratio  $\text{SNR}_{pT}$  required by the observer of 2.8 is also plotted. As can be observed from Eq. (11), the image SNR produced by the sensor decreases as  $C_M$  decreases. However, in order to minimize the number of curves to be plotted, we elect to assume that the SNR required by the observer increases instead using the formula

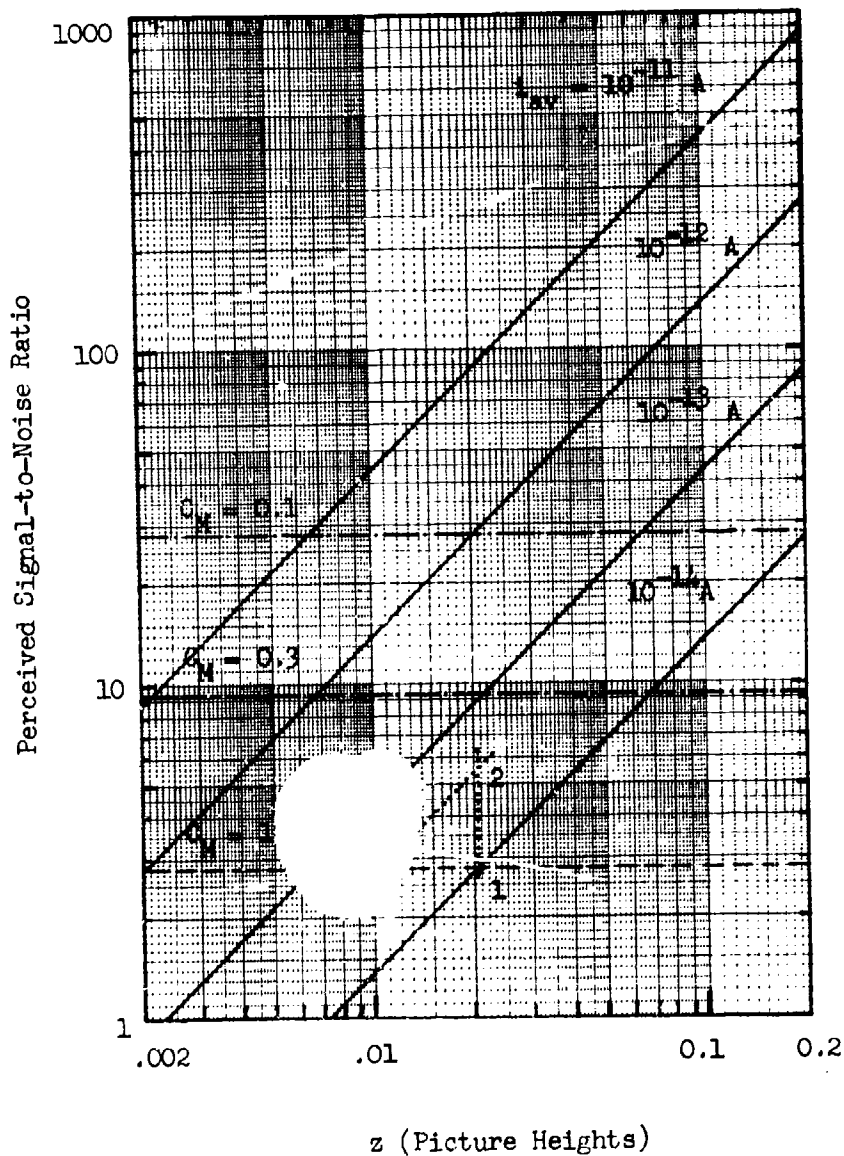


Fig. 1. Perceived Signal-to-Noise Ratio for a Square Image as a Function of the Image's Linear Size for Various Input Photocurrents. Also Shown are the Threshold SNR for  $C_M = 1.0$  and Apparent Thresholds for  $C_M = 0.3$  and  $0.1$ .

$$\text{SNR}_{pT}(C_M) = \frac{\text{SNR}_{pT}(C_M = 1)}{C_M} . \quad (13)$$

It is important to note that this is an analytical and graphical convenience only. When the observer is limited by the SNR developed by the sensor, rather than the properties of his own eye, the observer's threshold SNR is independent of the input image contrast. Observe that the displayed image contrast is adjustable by means of a contrast (video gain) control in TV and need not be the same as the input image contrast.

Using the concept leading to Eq. (13), we plot the  $\text{SNR}_{pT}$  for  $C_M = 0.3$  and  $C_M = 0.1$  on Fig. 1 (in addition to the  $\text{SNR}_{pT}$  for  $C_M = 1.0$  already plotted). The intersection of the  $\text{SNR}_p$  obtainable curves with the  $\text{SNR}_{pT}$  required-by-the-observer curves gives the minimum size of the square which can be detected or alternatively, we can determine the minimum photocurrent required as a function of the square size as shown in Fig. 2. Note on Fig. 1, that as we increase the image SNR developed by the sensor from point 1 to point 2 (a factor of 2 increase in  $\text{SNR}_p$ ), the minimum detectable square size is halved. The area of the minimum detectable square is decreased by  $\frac{1}{4}$ . The effect of increasing the SNR of the large square is to increase the probability of detecting it. As we discussed in Ref. 1, the probability of detection is given by

$$P_d(-\infty < \zeta < \zeta_2) = \frac{1}{\sqrt{2\pi}} \int_{-\infty}^{\infty} \exp(-\zeta^2/2) d\zeta , \quad (14)$$

which is the integral of the normal probability curve. The value of  $\zeta$  is given by

$$\zeta = \text{SNR}_p - \text{SNR}_{pT} . \quad (15)$$

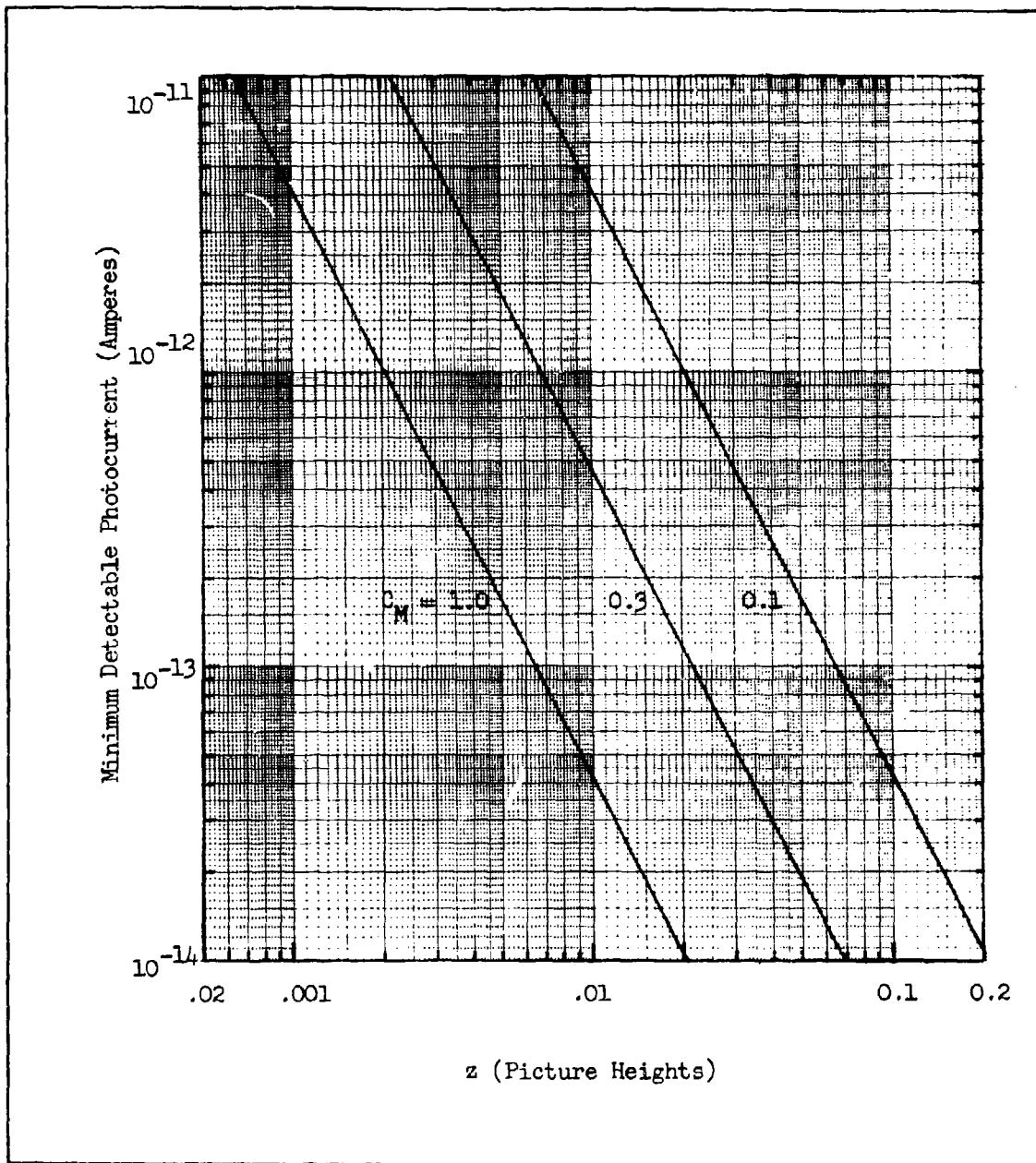


Fig. 2. Minimum Detectable Photocurrent for Square Images of Linear Dimension  $z$  as Limited by Photoelectron Noise at Three Values of Input Image Contrast.

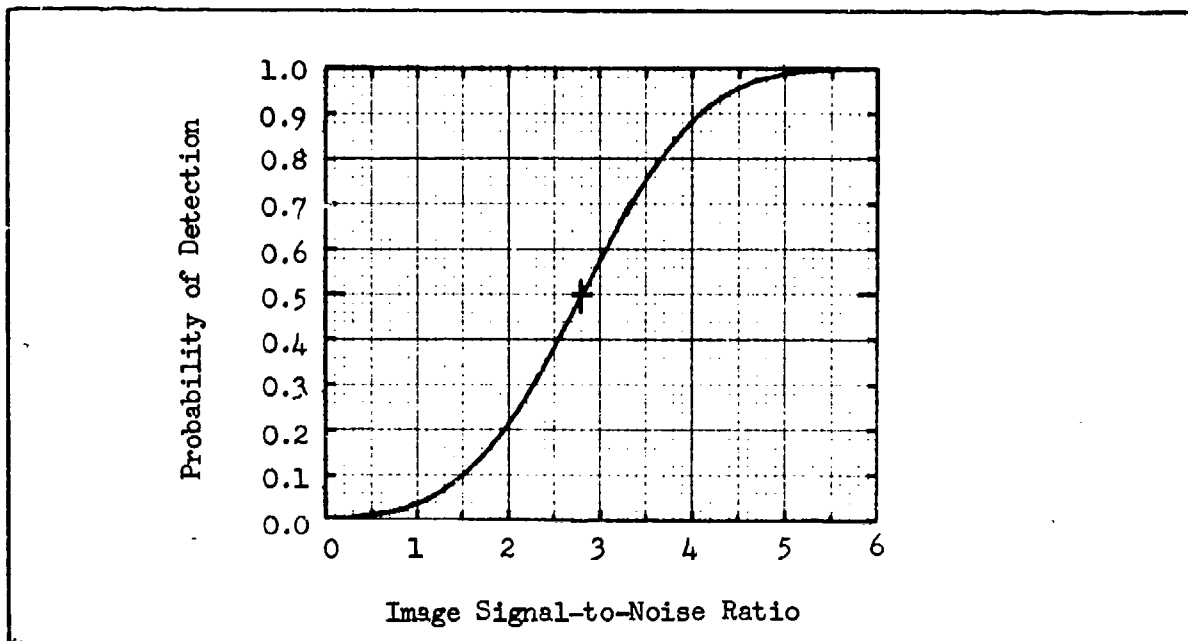


Fig. 3. Probability of Detection for Rectangular Images as a Function of the Image Signal-to-Noise Ratio.

Using this relation, we plot  $\text{SNR}_{pT}$  vs  $\text{SNR}_p$  on Fig. 3 using Eq. (15).

As can be seen doubling  $\text{SNR}_p$  from 2.8 to 5.6 increases the probability of detection to essentially 100%.

In Ref. 2, we hypothesized that to detect the presence of a bar pattern, an observer must discern a single bar in the pattern. Thus the Eq. (11) applies to the detection of a bar pattern as well. For later convenience, we will express the width of the bar in terms of the reciprocal dimensions

$$N = \frac{1}{z} \quad , \quad (16)$$

with the units of  $N$  being lines/picture height. Then Eq. (11) reads

$$\text{SNR}_p = \left( \frac{et}{\alpha} \right)^{\frac{1}{2}} \frac{1}{N} \frac{2C M_{av}^{\frac{1}{2}}}{e^{\frac{1}{2}}} \quad (17)$$

Using this equation, we plot the  $SNR_D$  for the bar pattern in Fig. 4. For simplicity in the present discussion, we assume that the threshold is 2.8 (for  $C_M = 1.0$ ) as for the rectangular image. Observe once again that as the  $SNR_D$  obtainable from the sensor is doubled from point 1 to point 2 on Fig. 4, that the threshold resolution is doubled from 105 TVl/pict. ht. at point 1 to 210 TVl/pict. ht. at point 3. The limiting resolution vs input photocurrent characteristic is plotted in Fig. 5 for 3 values of input contrast.

In the above analysis, it was assumed that the only noise affecting image perception is that generated in the primary photoprocess. In a typical TV camera tube of high sensitivity, the photoelectron signals and noises are first amplified and read out by a scanning electron beam. The read-out signal is then passed to a preamplifier which is generally noisy. If the preamplifier noise is white and of mean square density,  $I_p^2/2\Delta f_V$ , then Eq. (17) takes the form

$$SNR_p = \left(\frac{et}{\alpha}\right)^{\frac{1}{2}} \frac{1}{N} \frac{2C_M G i_{av}}{\left[eG^2 i_{av} + I_p^2/2\Delta f_V\right]^{\frac{1}{2}}} \quad (18)$$

Note that if the gain,  $G$ , prior to the preamplifier is large, the preamplifier noise may be neglected.

Up to this point, we have implied that Eq. (18) applies to both bar patterns and rectangles. However, it is common experience that bar patterns are much more difficult to discern on the output of a sensor's display than is an isolated bar of dimensions equal to a single bar in the bar pattern. This is due more to the way a bar pattern is processed in the electro-optical sensor than any difference in the visual detection process although differences in the visual process may also have to be considered.



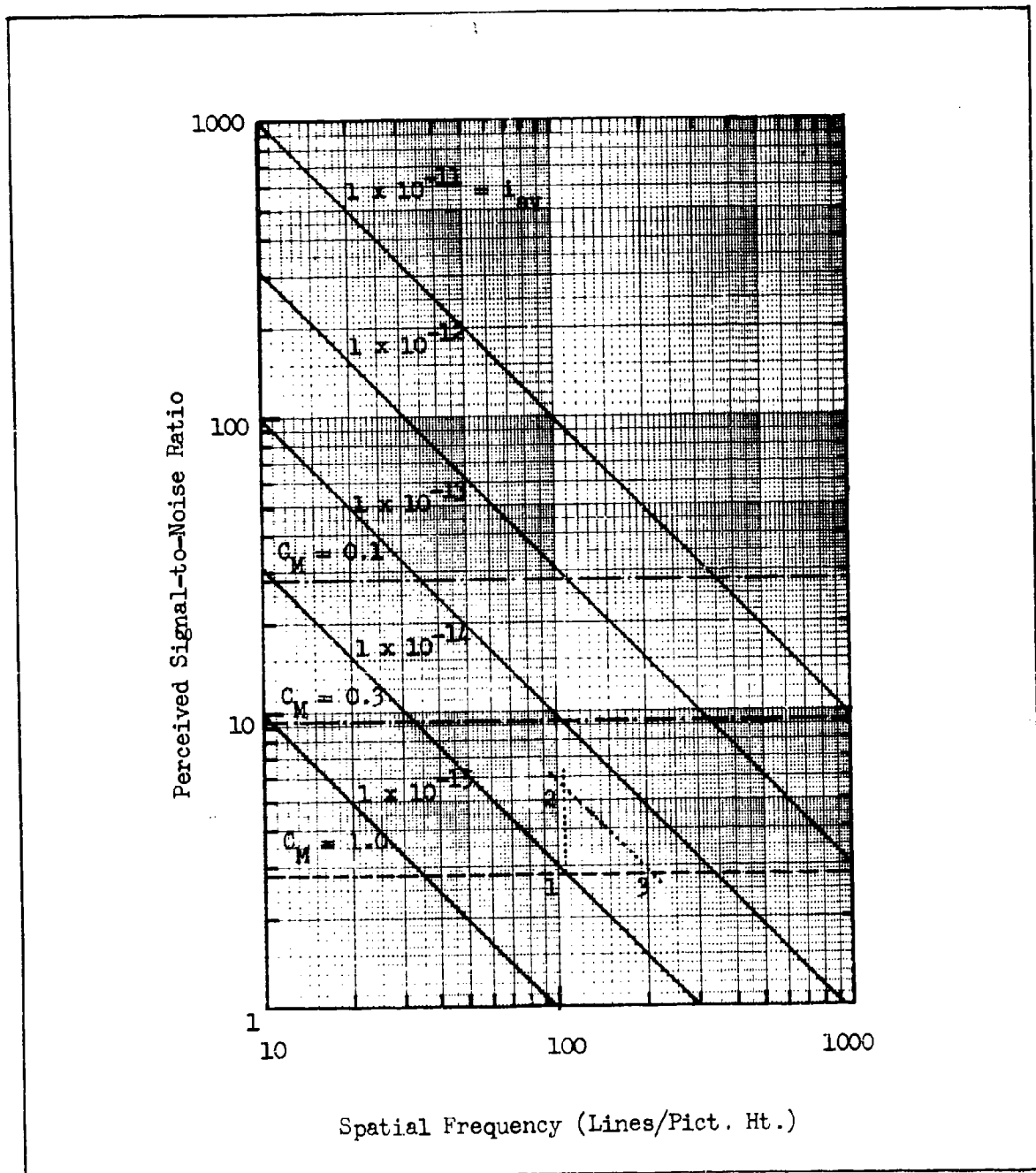


Fig. 4. Perceived Signal-to-Noise Ratio for a Bar Pattern Image as a Function of Spatial Frequency for Various Input Photocurrents. Also Shown are the Threshold SNR for  $C_M = 1.0$  and the Apparent Thresholds for  $C_M = 0.3$  and  $0.1$ .

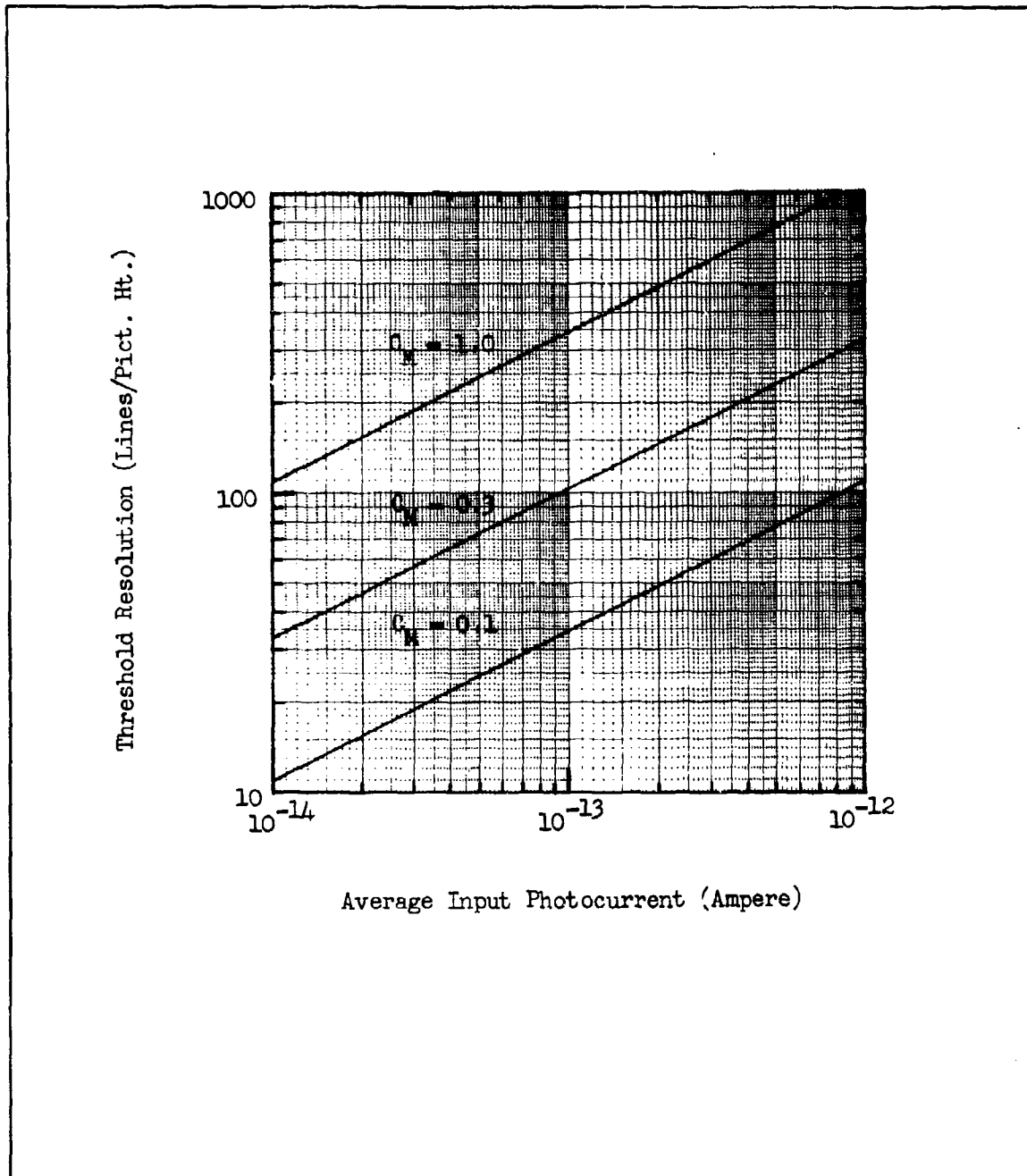


Fig. 5. Threshold Resolution vs Average Input Photocurrent for a Bar Pattern Image as Limited by Photoelectron Noise at 3 Values of Input Image Contrast.

## 2.2 The Effect of Finite Apertures

As is well known, point images in object space end up as blurs on an electro-optical sensor's display. The blurred images may differ from the actual scene object in amplitude, shape and/or phase (position). These image changes are due to finite imaging apertures such as those associated with a lens, a fiber optic, an electron scanning beam, a phosphor particle, etc. These effects have been treated in great detail in Ref. 3 and the results are summarized here.

Suppose first that the image is a rectangle of dimensions  $l/N$  and  $e/N$  in the horizontal and vertical respectively. If  $e$  is large, the bar is long with respect to its width and aperture effects along the length can be neglected. Let the aperture response of the system be designated  $r_o(x)$  and let the input signal waveform be  $k_1 f(x)$ . The output signal is equal to  $k_1 g(x)$  where  $g(x)$  is the convolution of  $r_o(x)$  and  $f(x)$ , i.e.,

$$g(x) = r_o(x) * f(x) \quad . \quad (19)$$

Similarly in the spatial frequency domain,

$$G(N) = R_o(N) \cdot F(N) \quad , \quad (20)$$

where  $G(N)$ ,  $R_o(N)$  and  $F(N)$  are the Fourier transforms of  $g(x)$ ,  $r_o(x)$  and  $f(x)$ , respectively.

In the elementary theory of imaging, it is assumed that the eye, within certain bounds, can expand its limits of integration as necessary to match the dimensions of the displayed image and that the perceived signal,  $s_p$ , will be proportional to the area of the displayed image. Specifically,

$$s_p = k_1 t \int_{-\infty}^{\infty} g(x) dx , \quad (21)$$

where  $k_1$  is the incremental amplitude of the displayed pulse and  $t$  is the integration time of the observer's eye. Observe that by definition of the Fourier transform

$$G(N) = \int_{-\infty}^{\infty} g(x) \exp(-2j\pi Nx) dx , \quad (22)$$

and that

$$G(0) = \int_{-\infty}^{\infty} g(x) dx . \quad (23)$$

That is, the integral over the output image area is equal to the Fourier transform of the output image at zero frequency. Also, since  $G(N) = R_o(N) \cdot F(N)$ ,

$$G(0) = R_o(0) \cdot F(0) , \quad (24)$$

and since  $R_o(0)$  is unity by definition of the aperture response (or optical transfer function)

$$\begin{aligned} s_p &= k_1 t G(0) = k_1 t F(0) \\ &= k_1 t \int_{-\infty}^{\infty} f(x) dx . \end{aligned} \quad (25)$$

That is, the area under the output pulse is identical to the area under the input pulse. Thus, the aperture has no effect on the perceived signal.

While the aperture does not affect the perceived signal, it can affect the perception of noise added either prior to or subsequent to an aperture. To begin, assume that noise is added after the image has passed through

the aperture. In general, the signal must be perceived in the presence of noise. The eye integrates noise in a manner similar to signal as we previously noted. If the image had not been smeared out, the eye would then integrate the noise only over the input image boundaries. However, with the pulse smeared out, the eye would then integrate the noise over some larger distance. Thus, while an aperture does not add noise nor decrease signal in the isolated image case, it can increase perceived noise generated elsewhere in the imaging process. We note, for future reference, that the effects of noise added before an aperture is less serious than a noise added after an aperture for in the former case, the aperture also has a filtering effect on the noise.

The fundamental noise expression of Eq. (3) applies here as well. The principal changes required to account for the effects of the aperture are to redefine the area function  $a(x,y)$  and the bandwidth  $\Delta B_N$ . The area function (in one dimension) will be designated the duration variable  $\delta_u$  and is equal to the integral of the output image divided by the output pulse amplitude, i.e.,

$$\delta_u = \frac{k_2 \int_{-\infty}^{\infty} g(x) dx}{k_2 g(o)} = \frac{\int_{-\infty}^{\infty} g(x) dx}{g(o)} = \frac{F(o)}{g(o)} \quad (26)$$

The output pulse amplitude is shown in Ref. 3, page 99. Next, the noise equivalent bandwidth  $\Delta B_N$  is given by

$$\Delta B_N = \frac{\int_0^{\infty} |F(N)R_o(N)|^2 dN}{F(o)^2} \quad (27)$$

which is the integral of the noise power density spectrum normalized to its value at zero frequency. Now, the Eq. (3) can be written as

$$n_p^2 = G^2 \sigma^2 t \frac{F(o)^2}{g(o)^2} \frac{\int_0^\infty |F(N)R_o(N)|^2 dN}{F(o)^2}, \quad (28)$$

which can be simplified to

$$n_p^2 = G^2 \sigma^2 t \frac{\int_0^\infty |F(N)R_o(N)|^2 dN}{g(o)^2}. \quad (29)$$

In Ref. 3, we show that when the input image is large with respect to the aperture line spread function  $r_o(x)$ , then

$$n_p^2 = G^2 \sigma^2 t x_o, \quad (30)$$

where  $x_o$  is the width of the assumed rectangular input image. When the noise equivalent line spread function width is large with respect to the input image width

$$n_p^2 = G^2 \sigma^2 t \delta_e, \quad (31)$$

where the noise equivalent line spread function is given by

$$\delta_e = \frac{1}{N_e} = \frac{1}{\int_0^\infty |R_o(N)|^2 dN}. \quad (32)$$

For the more general case where  $x_o$  and  $\delta_e$  are both significant, the following approximations can be made without undue error,

$$\delta_u^2 = \delta_e^2 + x_o^2, \quad (33)$$

or

$$\frac{1}{N_u^2} = \frac{1}{N_e^2} + \frac{1}{N^2}, \quad (34)$$

when  $\delta_e$  and  $x_o$  ( $= \frac{1}{N}$ ) are given in units of picture heights. With this form,

$$n_p^2 = G^2 \sigma^2 \left[ t(\delta_e^2 + x_o^2)^{\frac{1}{2}} \right] \quad (35)$$

For analytical purposes, we define a noise increase factor  $\xi$  as

$$\xi = \frac{\delta_u}{x_o} = \left[ 1 + \left( \frac{\delta_e}{x_o} \right)^2 \right]^{\frac{1}{2}} \quad (36)$$

or alternatively,

$$\xi = \left[ 1 + \left( \frac{N}{N_e} \right)^2 \right]^{\frac{1}{2}} \quad (37)$$

with this factor, Eq. (35) may be written as

$$n_p^2 = G^2 \sigma^2 (t \xi x_o) \quad (38)$$

The above equation applies when the aperture precedes the point of noise insertion. When the aperture follows a point of noise insertion, the aperture has two effects; it increases the noise integration distance but it also filters the noise. Again, as shown in Ref. 3 the noise expression now becomes

$$n_p^2 = (G\sigma)^2 t \delta_u^2 \Gamma \Delta B_{NW} \quad (39)$$

where  $\Gamma$  is the noise filtering factor for a finite noise spectrum and  $\Delta B_{NW}$  is the noise bandwidth as previously computed for a white noise spectrum. The filter factor  $\Gamma$  is the actual bandwidth divided by the white noise bandwidth and is given by

$$\Gamma = \frac{\Delta B_{NF}}{\Delta B_{NW}} \quad (40)$$

$\Delta B_{NF}$  is the actual noise bandwidth given by

$$\Delta B_{NF} = \int_0^{\infty} \left| \frac{G(N)}{F(O)} \right|^2 dN = \int_0^{\infty} \left| \frac{F(N)R_o(N)}{F(O)} \right|^2 dN, \quad (41)$$

which in approximate form becomes

$$\Delta B_{NF} \approx \frac{1}{[x_o^2 + 2\delta_e^2]^{\frac{1}{2}}}, \quad (42)$$

so that

$$\Gamma = \frac{[x_o^2 + \delta_e^2]^{\frac{1}{2}}}{[x_o^2 + 2\delta_e^2]^{\frac{1}{2}}}. \quad (43)$$

It is clear that  $\Gamma$  is a number less than one. The noise increase factor  $\xi$  is a number greater than one. The product of  $\xi$  and  $\Gamma$  is larger than one which implies that the effect of an aperture following a point of noise insertion is to increase the noise perceived by the observer but by an amount less than it would be if the aperture precedes the point of noise insertion.

Suppose there are two apertures; one preceding a point of noise insertion with noise equivalent aperture  $\delta_{eL}$  and one following it with noise equivalent aperture  $\delta_{eT}$ . Both apertures increase the noise by a factor

$$\xi_{xLT} = \left[ 1 + \frac{\delta_{eL}^2}{x_o^2} + \frac{\delta_{eT}^2}{x_o^2} \right]^{\frac{1}{2}}, \quad (44)$$

but the second aperture  $\delta_{eT}$  filters the noises. The noise filtering function is

$$\Gamma_{xLT} = \frac{\xi_{xLT}}{\left[ 1 + \frac{\delta_L^2}{x_o^2} + 2\frac{\delta_T^2}{x_o^2} \right]^{\frac{1}{2}}}, \quad (45)$$



and the noise becomes

$$n_p^2 = G^2 \sigma^2 T_{xLT}^2 x_o \quad (46)$$

For photoelectron noise generated in the primary photoprocess, the noise density  $\sigma^2$  is equal to  $e i_{av}$  where  $e$  is the charge of an electron and  $i_{av}$  is the average photocurrent in the vicinity of the image of interest.

For a typical EBSICON camera system as described in Ref.'s 2 and 3, the principal MTF's are those due to the lens and the camera tubes gain-storage target. In operation, a lens focuses the image of a scene onto the photocathode. This image can be considered to be essentially noise-free. Noise is generated by the photosurface as the scene photons are converted to photoelectrons. The MTF of the lens,  $R_{OL}(N)$  therefore precedes the point of photoelectron noise insertion. The photoelectron image is then accelerated to the target which both amplifies and stores the image for subsequent readout by the scanning electron beam. The MTF of the combined target structure and scanning electron beam,  $R_{OT}(N)$  follows the point of photoelectron noise generation. The signal stored on the target is sequentially read off by the beam and preamplified. Noise is generated by the preamplifier. Both the lens and target MTF's precede the point of preamplifier noise insertion. The video bandwidth, which is an MTF, has a major effect on preamp noise but not on the image signal nor the signal related noises. The display also has an MTF which follows all of the noises generated but ordinarily the display MTF can be either com-

compensated or ignored because it is sufficiently better than that of the camera tube except when the display is of very small size.

Assuming the display to be essentially perfect, the display signal-to-noise ratio for an isolated rectangular object may be written as

$$\text{SNR}_D = \left[ \frac{te}{\alpha} \right]^{\frac{1}{2}} \frac{1}{(\xi_{xLT} \cdot \xi_{yLT})^{\frac{1}{2}} N} \frac{2C_M G_T i_{av}}{\left[ G_T^2 e \Gamma_{xT} \Gamma_{yT} i_{av} + \frac{I_p^2}{2\Delta f_V} \right]^{\frac{1}{2}}}, \quad (47)$$

where

- $t$  = the integration time of the eye (sec)
- $\epsilon$  = the rectangular images length-to-width ratio
- $\alpha$  = the image plane width-to-height ratio
- $\xi_{xLT} \cdot \xi_{yLT}$  = the noise increase factors in the x and y directions respectively due to the lens and target
- $N$  = the reciprocal width of the rectangular object in picture heights<sup>-1</sup>
- $C_M$  = the input image modulation contrast
- $G_T$  = the gain of the gain storage target
- $i_{av}$  = the average input photocurrent in the vicinity of the test object (Ampere)
- $\Gamma_{xT} \cdot \Gamma_{yT}$  = the noise filtering factor in the x and y directions respectively due to the target
- $e$  = the charge of an electron (coulomb)
- $I_p^2$  = the mean square preamp noise (Amp<sup>2</sup>)
- $\Delta f_V$  = the video bandwidth (Hz) .

In the above, it is assumed that the aperture effects are independent and separable in the x and y directions and that the preamp noise is random white noise. The target gain term  $G_T$  includes the scan efficiency of the electron beam in reading out the target, i.e., if the true target gain is  $G_T'$ , the effective target gain is

$$G_T = G_T' / e_v e_h, \quad (48)$$

where  $e_v e_h$  are the vertical and horizontal scan efficiencies respectively. The scan efficiency term results in an increase in the signal current because the same amount of charge is read out in less time with a low scan efficiency than with a scan efficiency of unity. The penalty is an increase in the video bandwidth required to transmit the image.

We noted previously that the elementary model of section 2.1 and specifically Eq. (18) applies to both bar patterns and rectangles. However, the effect of the system apertures on the two types of images will be far different. In the case of the isolated rectangular image, the apertures were found to have no effect on the signal. This is not the case for a train of square waves, i.e., a bar pattern.

A vertically oriented bar pattern is aperiodic in the y direction along the length of the bars and periodic in the x direction across the width of the bars. The effect of a sensory system aperture along the length of the bars is to elongate the bars in the y direction and to decrease the modulation of the image in the x direction. If the bar lengths are long relative to their width, the aperture effects along the length can be neglected with respect to their effect on the displayed image signal-to-

noise ratio.

A bar pattern input image can be quantitatively described by a square wave function in the x direction. Written in terms of a Fourier transform, the square wave function is

$$S_q(x) = \frac{Am}{2} + \frac{2Am}{\pi} \sum_k \frac{1}{k} \cos(\pi N k x) \quad (49)$$

$k = 1, 3, 5, \dots$

Suppose that the overall MTF of the sensor is  $R_o(N)$ . Then the overall response of the sensor to a unit amplitude square wave may be written as

$$g(x) = \frac{1}{2} + \frac{2}{\pi} \sum_k \frac{R_o(kN)}{k} \cos(\pi N k x) \quad (50)$$

where  $g(x)$  is normalized to unit amplitude at  $N = 0$ . It is postulated that the observer, in detecting the presence of a bar pattern, must make his decision on the basis of detecting a single bar and that the signal associated with the bars in the x direction is proportional to the mean signal amplitude which will be designated the square wave flux response  $R_{SF}(N)$ . Ignoring the d-c term, the mean value of  $g(x)$  is derived as follows using Fig. 6\*

$$\begin{aligned} R_{SF}(N) &= \frac{4N}{\pi} \sum_k \frac{R_o(kN)}{k} \int_{-\frac{1}{2}N}^{\frac{1}{2}N} \cos(\pi N k x) dx \\ &= \frac{8}{\pi^2} \sum_k \frac{R_o(kN)}{k^2} \quad (51) \end{aligned}$$

$k = 1, 3, 5, 7, \dots$

In effect,  $R_{SF}(N)$  represents the amplitude of an equivalent square wave

\* Drawn for the first harmonic  $k = 1$ .

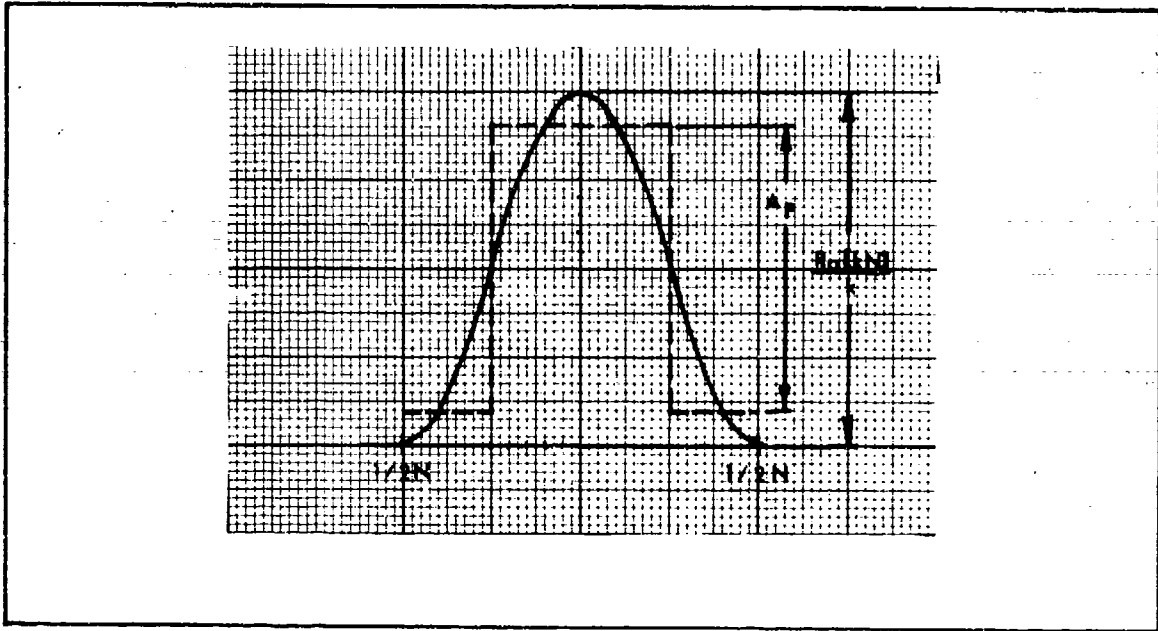


Fig. 6. Figure for Deriving the Square Wave Flux Amplitude  $A_1$  for a Sensor with MTF,  $R_0(N)$ . Figure is Drawn for the First Harmonic ( $k = 1$ ).

having the same mean signal as the actual function  $g(x)$  as shown in Fig. 7. This new measure is made necessary, according to Schade, because the square wave amplitude response bears no fixed relationship to the average value of flux as in the case of sine waves but instead, depends upon the harmonic components of the waveform.

The above derivation implies that the number of bars in the bar patterns are sufficient so that the pattern's Fourier spectrum approaches a line and that any end effect transients are damped out. In practice, the number of bars in the pattern may be as few as 3 or 4 which makes difficult a precise estimate of the signal level.

If an imaging system is linear, the response (displayed image) to a periodic test pattern will also be periodic with the same spatial

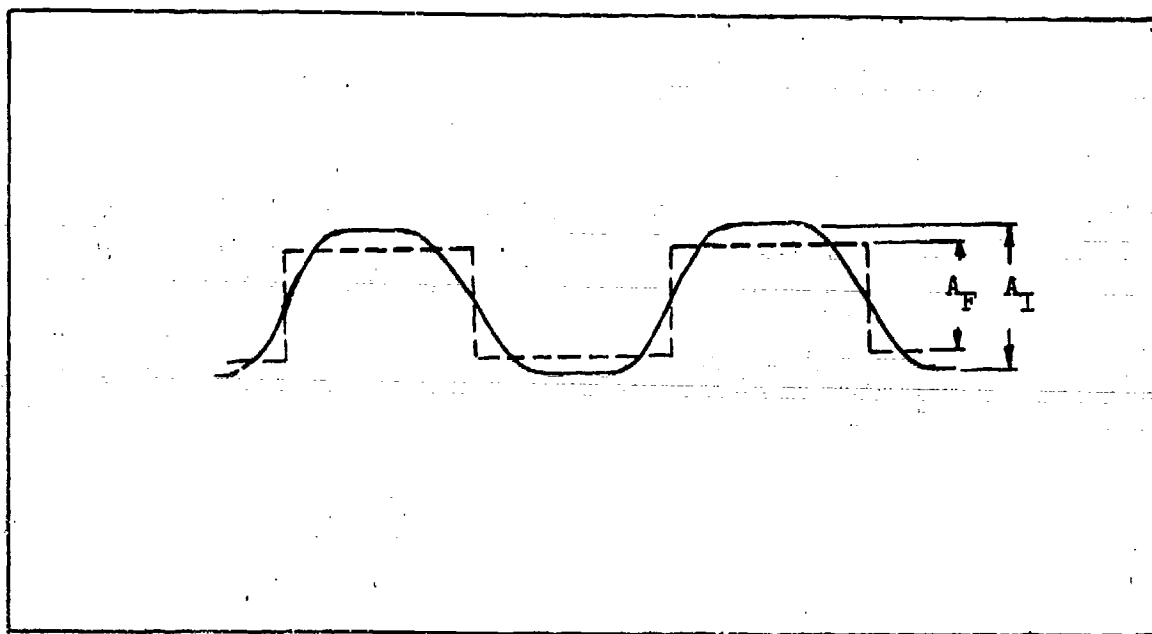


Fig. 7. Actual Image Amplitude,  $A_I$ , and Waveshape (—) Compared to Equivalent Square Wave Flux Amplitude,  $A_F$ , and Waveshape (- - -).

frequency as the test pattern. The effect of the sensor's apertures is to decrease the signal amplitude but the noise integration distance is unchanged being from trough-to-trough in the displayed image of a bar in the pattern. In short, the primary effect of an aperture on a periodic pattern in the direction across the bars is to reduce signal leaving noise unchanged. However, in direct analogy to the aperiodic case, the noise will be filtered by the aperture if it follows the point of noise insertion. The noise filtering factor  $\beta$  is given by

$$\beta(N) = \frac{1}{N} \int_0^N R_o^2(N) dN, \quad (52)$$

where  $R_o(N)$  represents the product of all of the MTF's which follow the point of noise insertion.

Before progressing, it is desired to note that most manufacturers

of TV camera tubes do not supply the MTF of their tubes but rather, provide the square wave amplitude response which is also known as the contrast transfer function or CTF. If the camera tube is linear, the MTF can be found knowing the square wave amplitude response  $R_{SQ}(N)$  from the formula

$$R_o(N) = \frac{\pi}{4} \left[ R_{SQ}(N) + \frac{R_{SQ}(3N)}{3} - \frac{R_{SQ}(5N)}{5} + \frac{R_{SQ}(7N)}{7} + 0 + \frac{R_{SQ}(11N)}{11} - \frac{R_{SQ}(13N)}{13} - \frac{R_{SQ}(15N)}{15} - \frac{R_{SQ}(17N)}{17} + \frac{R_{SQ}(19N)}{19N} + \frac{B_K(kN)}{k} + \dots \right], \quad (53)$$

where

$$B_K = \begin{cases} (-1)^m (-1)^{\frac{k-1}{2}} & \text{if } n = m \\ 0 & \text{if } n < m \end{cases}, \quad (54)$$

and

$m$  is the total number of primes into which  $k$  can be factored and  $n$  is the number of different prime factors in  $k$ .

Returning to the consideration of the periodic bar pattern, we will again consider the case of the EBSICON camera system as used in the example for the aperiodic case. The bar pattern is considered to be aperiodic in the  $y$  direction and periodic in the  $x$  direction. Again, we assume that there are two principal apertures, that of the lens and that of the gain storage target. For this case, the  $SNR_D$  equation becomes

$$SNR_D = \left[ \frac{t_e}{\alpha} \right]^{\frac{1}{2}} \frac{1}{t_{yLT}^{\frac{1}{2}}} \frac{R_{SF}(N)}{N} \frac{2C_{MT} i_{av}}{\left[ G_T^2 e \Gamma_{yLT}^2 x T_{av}^2 + I_p^2 / \Delta f_V \right]^{\frac{1}{2}}}, \quad (55)$$

where the terms are the same as described in connection with Eq. (47)

except for the following .

$\xi_{yLT}$  = the noise increase factor along the length of the bars in the y direction due to the lens and gain-storage target

$R_{SF}(N)$  = the square wave flux response due to both lens and gain-storage target

$\Gamma_{yLT}$  = the noise filtering factor in the y direction due to the gain-storage target

$\beta_{xT}$  = the noise filtering factor in the x direction due to the gain-storage target.

In the earlier analysis, we showed that with an ideal sensor (unity MTF), a doubling of the  $SNR_D$  at a given line number at threshold, results in a new threshold line number which is twice as large as the original line number. This is not true for sensors with finite apertures. To illustrate, we consider the  $SNR_D$  obtainable from an Intensified-EBSICON using the parameters discussed in section 3 and plotted in the region  $SNR_D = 1$  to 10 in Fig. 8. Suppose that the spatial frequency  $N_1$  represents the threshold resolution. If we then increase the  $SNR_D$  by a factor of 2 (by increasing input image photocurrent), we would expect the threshold resolution to increase to a value  $N_2 = 2N_1$ . However, due to the sensor's finite apertures,  $N_2$  increases by a smaller amount. For the case at the lowest photocurrent,  $N_2 = 1.75N_1$  at the middle value of photocurrent  $N_2 = 1.54N_1$  and at the highest,  $N_2 = 1.15N_1$ . In other words, when finite sensor apertures are involved, a substantial increase in  $SNR_D$  may result in only slight further increase in threshold resolution. To show the result graphically, we plot the ratio  $N_2/N_1$  vs  $N_1$  in Fig. 9



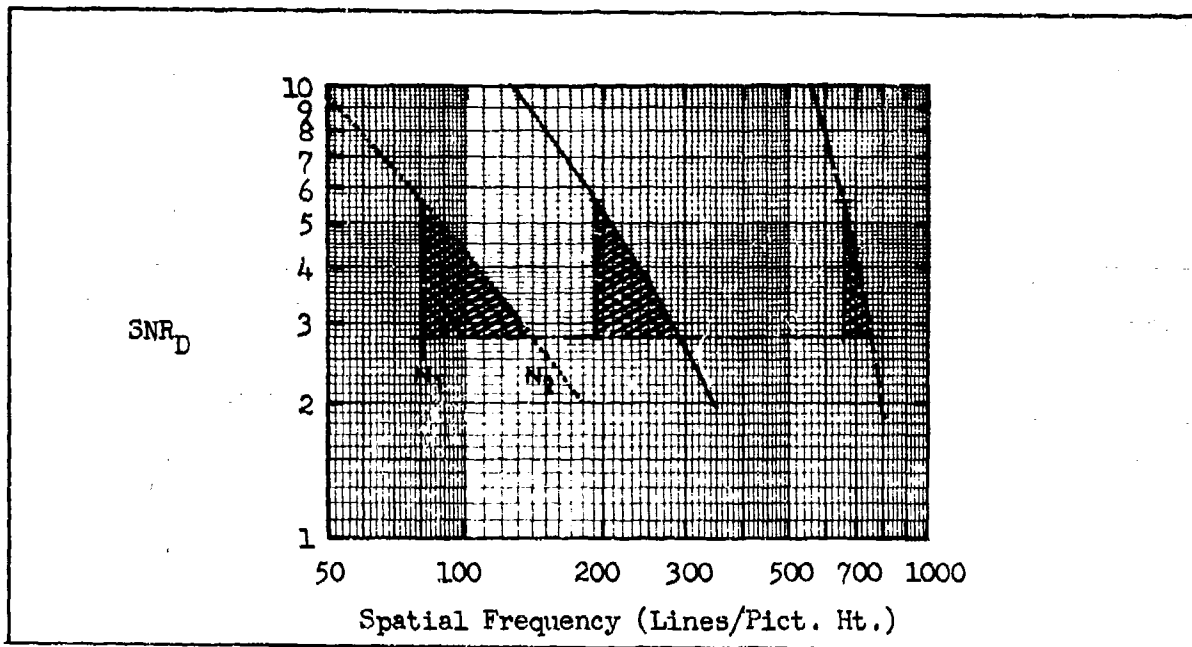


Fig. 8.  $SNR_D$  vs Spatial Frequency for the 25/25/20 I-EBSICON for Three Values of Input Photocurrent ( $\cdots$ )  $3.16 \times 10^{-14}$  A, ( $\text{---}$ )  $3.16 \times 10^{-13}$  A and ( $\text{- - -}$ )  $1 \times 10^{-10}$  A. If  $N_1$  is the Threshold Frequency,  $N_2$  is the New Threshold Frequency when  $SNR_D$  at  $N_1$  is Doubled.

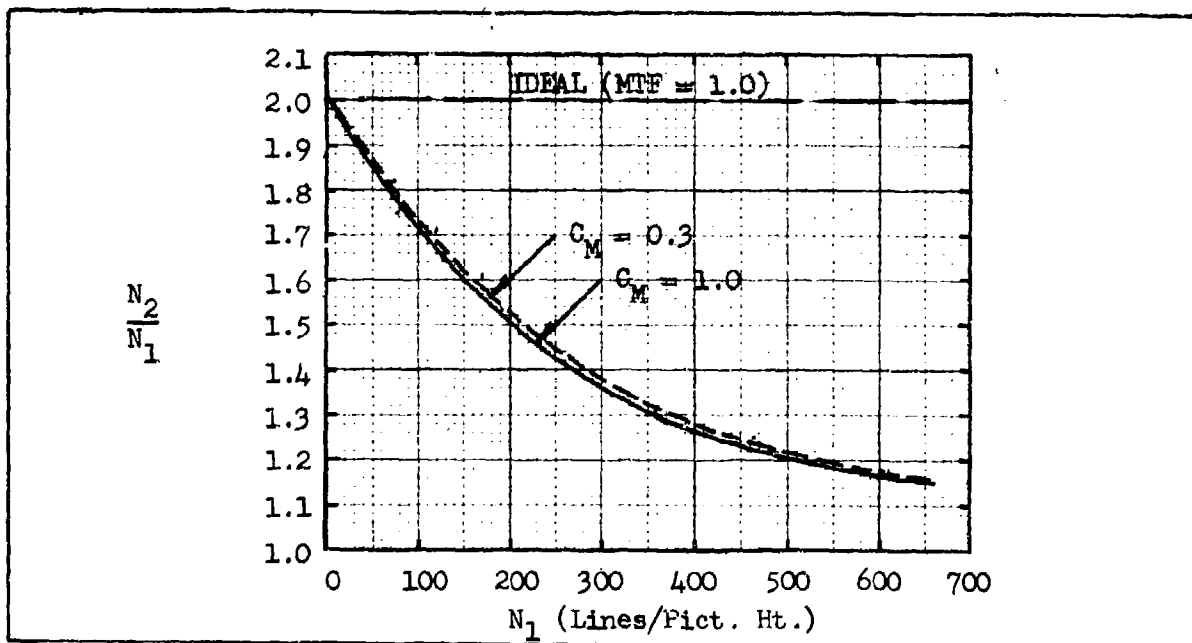


Fig. 9. Relative Increase in Threshold Resolution  $N_2/N_1$  as the  $SNR_D$  at  $N_1$  is Increased by a Factor of 2 Above the Threshold Value at  $N_1$ .

for the assumed camera tube. Also shown is the result when the input image modulation contrast is 0.3 instead of 1.0.

It has been hypothesized that the increase in performance of a sensor, as  $SNR_D$  is increased might be related to the integral of  $SNR_D$  between the limits  $N_1$  and  $N_2$ . These areas are shown as shaded in Fig. 8. At low input photocurrents (low light levels), the area is large indicating that a small amount of additional light gives a large improvement in image quality while at the higher input photocurrents, the area is small indicating that a large amount of additional light gives only a small increase in image quality (assuming that image quality is a product of resolution and signal-to-noise).

This concept, though it is an integral of excess signal under an MTF curve above a threshold, is not the same as Snyder's MTF concept reported in Ref. 4, because Snyder integrates from a fixed low spatial frequency to the intersection of  $SNR_D$  with  $SNR_{DT}$ . This gives no weight to the effect of increasing  $SNR_D$  at any specific frequency. We believe the above concept merits further study and experimentation because it may bear strongly on the subject of image quality, whose quantitative measure has proved so elusive over the years.

### 2.3 Observer Thresholds

The previous sections were primarily devoted to the subject of image signal-to-noise ratios obtainable from a sensor. If the observer's image signal-to-noise ratio requirements are known for the images displayed by the sensor, then measures of overall sensory system performance can be devised by matching that obtainable to that required. In Ref.'s 2 and 3, the results of a large number of psychophysical experiments performed

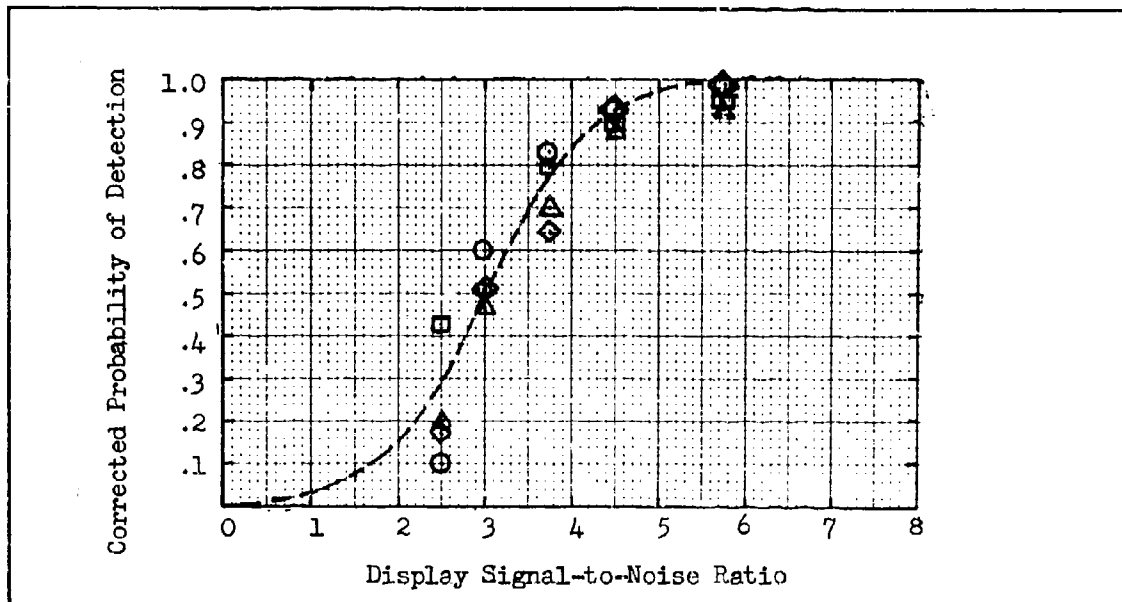


Fig. 10 Corrected Probability of Detection vs  $SNR_D$  required for Rectangular Images of Size  $\circ$  4 x 4,  $\square$  4 x 64,  $\Delta$  4 x 128, and  $\diamond$  4 x 180 Scan Lines. Televised Images at 30 frames per second and 525 Scan Lines.  $D_v/D_H = 3.5$ .

to obtain observer requirements were reported. These results will be briefly reviewed here.

The first images used in the experimentation were squares and rectangles. In the elementary model, it is assumed that the eye will integrate the image signal over the entire image area. The results of an initial experiment to determine both the observer requirements and the limits of his ability to integrate in space are shown in Fig. 10 as the probability of detection vs  $SNR_D$ . In this experiment, the image width was held constant (equal to 4 scan lines or 4/490 of the picture height) and the height was varied from 4 to 180 lines. The  $SNR_D$  required for 50% detection was approximately 2.8 in all cases. The angular extent of the displayed images were  $0.13^\circ$  in width and from  $0.13^\circ$  to  $6.02^\circ$  in height. The ability of the eye to integrate over a  $6^\circ$  angle without loss was larger than was previously

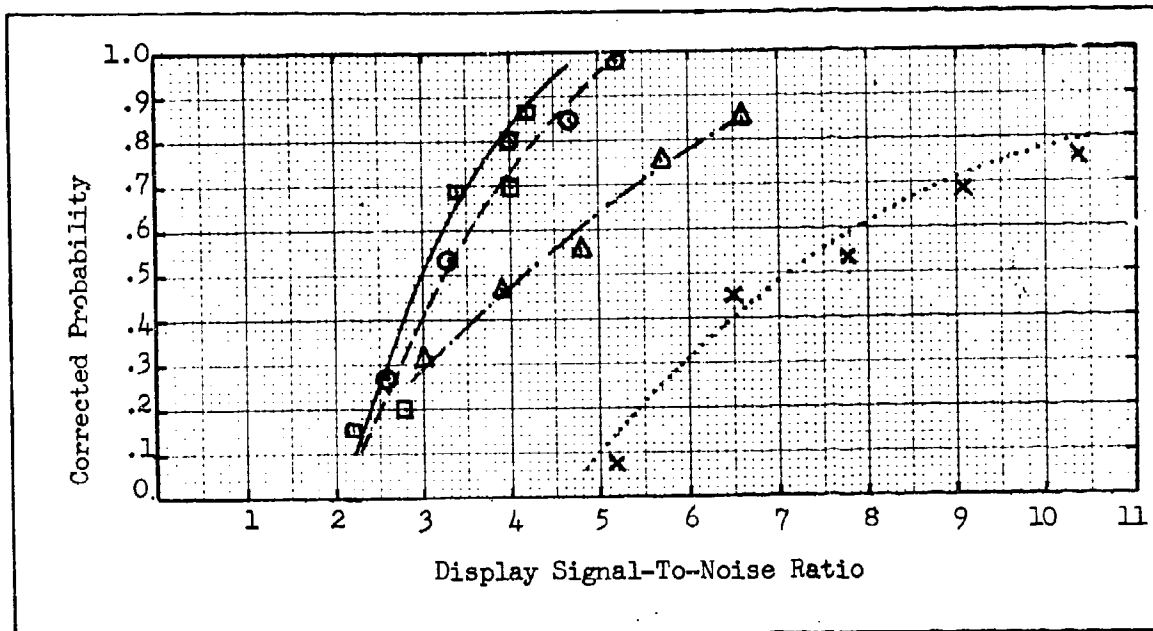


Fig. 11 Corrected Probability of Detection vs  $SNR_D$  required for Square Images of Size  $\square$  8 x 8,  $\circ$  16 x 16,  $\triangle$  32 x 32 and  $\times$  64 x 64 Scan Lines. Televised Images at 30 frames per second and 525 Scan Lines.  $D_V/D_H = 3.5$ .

thought possible.

Seeking further verification, squares were next used with the result shown in Fig. 11. As can be seen, the  $SNR_D$ , computed on the basis that the eye integrates over the entire image, increases as the square size increases. These results, together with others are summarized in Fig. 12, where we plot the threshold SNR or  $SNR_{DT}$  as a function of square size and the angular extent of the squares relative to the observer's eye. The larger  $SNR_{DT}$  required for the smallest square is tentatively attributed to eye MTF effects. However, the increase in thresholds noted for the large squares is interpreted as being due to incomplete spatial integration over the entire image area within the observer's eye. To explain these effects, it is hypothesized that the eye actually integrates signal from an area around the perimeter of the image area rather than the total area. From our

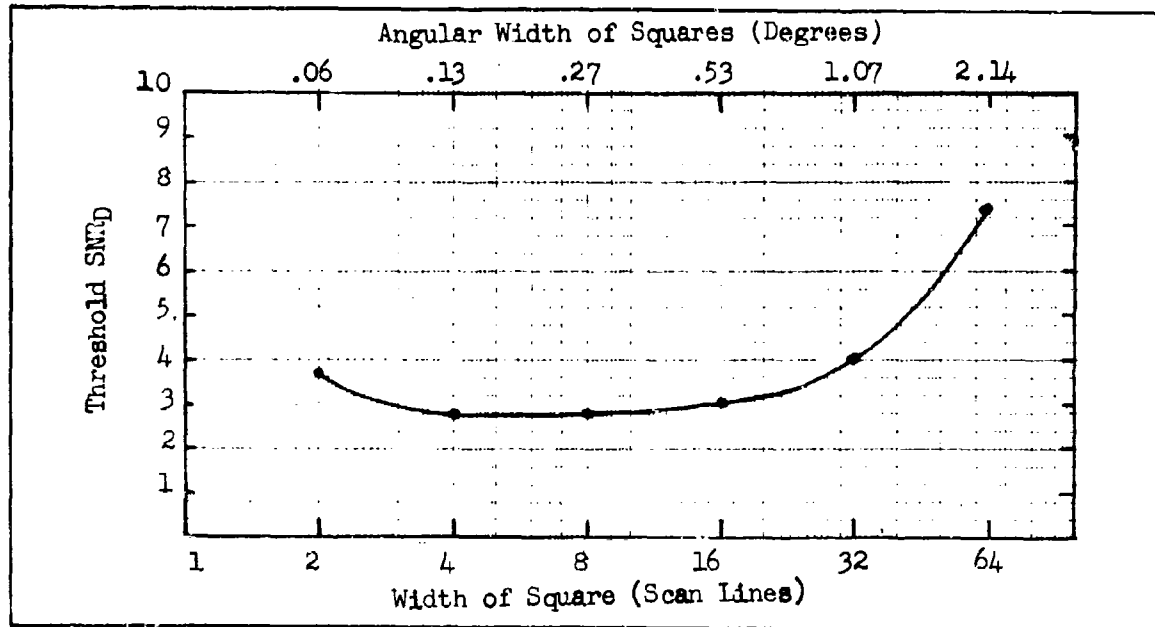


Fig. 12 Threshold SNR<sub>D</sub> required to detect Square Images of Various Size and Angular Extent. Televised Images at 30 frames/second, 525 Scan Line Raster.  $D_V/D_H = 3.5$ .

measurements, the increase in the threshold noted for the large squares is interpreted as being due to incomplete integration over the total area of image. It has been hypothesized that the eye integrates signal from an area around the perimeter of the area rather than the total area. From our measurements, the integration distance appears to be about 10 minutes of arc. The result obtained for the long thin rectangles is explained on the basis that these images are nearly all edge (perimeter).

The result obtained for the large squares, while interesting, are not particularly important to the sensory system performance prediction problem which is almost always concerned with the detection of rather small images. Thus, the area model, previously postulated is considered appropriate for most of the tasks which will be of interest. Note that when we speak of images of large angular extent we refer to the angular

extent of the image on the display relative to the observer's eye. When the angular extent is greater than about  $0.4^\circ$ , the eye ceases to integrate all of the image signal and the threshold  $SNR_{DT}$  appears to increase. By simply increasing the distance from the observer, to the display, the objects angular subtense will decrease. The eye will now be able to integrate over the entire area and the threshold  $SNR_D$ , as calculated from the measurements, will decrease.

The result obtained from the large squares, although interesting, are not particularly important to the sensory system performance prediction problem which is almost always concerned with the detection of small images. Thus, the area model, previously postulated is considered appropriate for most of the tasks which will be of interest. The area model holds for images whose angular extent is less than about  $0.5^\circ$  (actually the error is small even for images of  $1^\circ$  angular extent). Note that an image of large angular extent can be made of smaller angular extent by simply moving back away from the display. If this is done, the  $SNR_{DT}$  will decrease as we have shown experimentally. Note that by increasing the signal-to-noise ratio by a factor of about 2 over its value at threshold, the probability of detection increases to near 100%.

At the  $SNR_D = 2.8$  level, a rectangular image appears as a blob with no discernable shape. It was desired to determine how much the  $SNR_D$  had to be increased before the shape became apparent. In the first experiment, electronically-generated squares were employed. The square sizes were  $2 \times 2$ ,  $4 \times 4$ ,  $8 \times 8$ ,  $16 \times 16$ , and  $32 \times 32$  scan lines (a scan line width is  $1/490$ th of the picture height). The  $SNR_{DT}$  were determined for threshold detection of the square and for liminal perception of the edges of the square and are

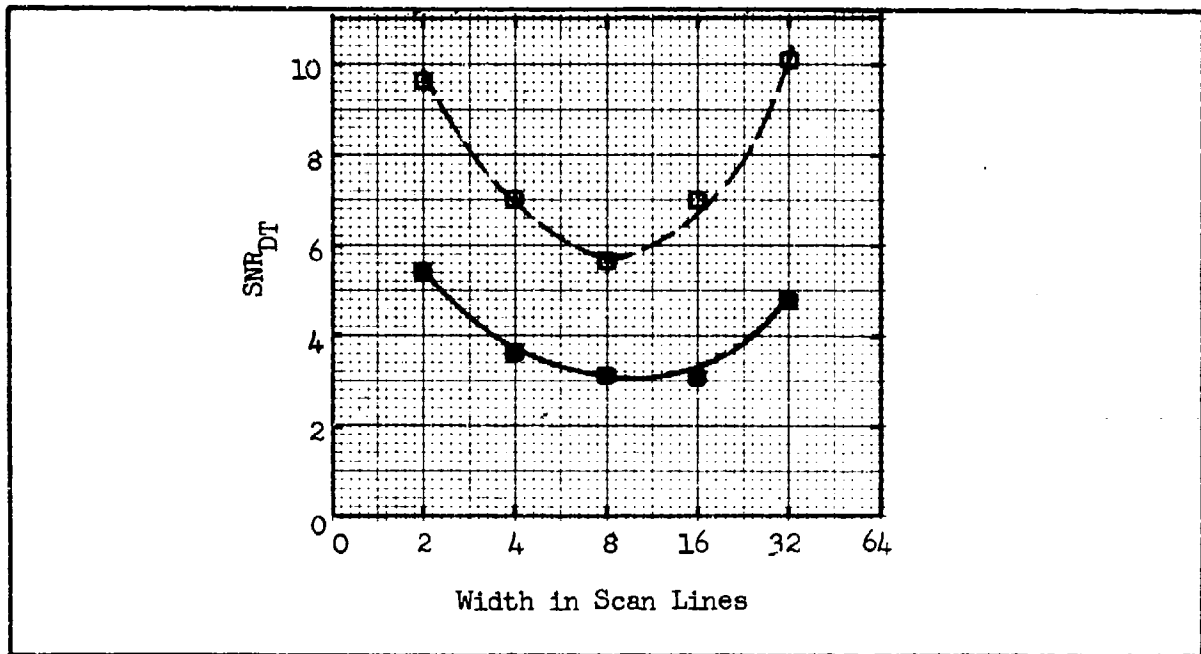


Fig. 13 Threshold  $SNR_{DT}$  vs Size of Squares in Scan Line Width Dimensions for Simple Detection (—) and for Liminal Perception of the Square Edges (- - -).

plotted in Fig. 13. As can be seen, approximately 2 times more  $SNR_{DT}$  is required for edge detection than for simple detection of the square. In this experiment a total of 790 data points were taken using a single observer. The TV display was operated with 490 active scan lines per picture height at 30 frames/sec. The observer-to-display distance was 28" from a display of 8" height and 1 ft-Lambert luminance. The ambient lighting about the display was also 1 ft-Lambert.

In the second set of experiments, the test patterns were geometric shapes including a triangle, a square, a pentagon, a six-pointed star and a circle. These shapes were simultaneously televised by a vidicon camera operated at 25 frames/sec and 875 scan lines/picture height. Again, the display was 8" high and viewed by an observer at 28" from the display. The display and its surround was 1 ft-Lambert. Using a single

<u>Target</u>	<u>Shape Discrimination</u>	<u>Detection</u>	<u>Ratio</u>
Star	18.7	5.79	3.23
Pentagon	14.4	5.40	2.67
Square	11.6	6.53	1.78
Triangle	10.8	6.44	1.68
Circle	<u>10.3</u>	<u>5.73</u>	<u>1.80</u>
	Av. 13.16	Av. 5.98	Av. 2.20

Table 1.  $SNR_D$  Required to Detect and to Shape Discriminate Various Geometric Shapes.

observer, 950 data points were taken. The results are shown in Table 1. Each of the geometric shapes were of approximately the same area and the  $SNR_D$  calculation was based on the total area within the shape.

For detection, the values of threshold  $SNR_D$  for each shape are nearly the same and the average  $SNR_{DT}$  is about 20% higher than for the more ideal electronically generated squares. The  $SNR_D$  required to discern the shape varies more than the  $SNR_D$  to simply detect as would be expected. In order of easiest to hardest to discern are the circle, triangle, square, pentagon and the star. Photographs of the geometric shapes at various  $SNR_D$  levels are shown in Figs. 14 and 15. In the photographs, the star appears to be more discernable than the pentagon but the reverse was true in the experimentation.

In reviewing the results of the above experiment it was observed that





Fig. 14 Geometric Shapes Used for Edge Discrimination. Photographs Show (left to right, up to down) Decreasing SNR Values. Attenuation of Signal is Lower Right 21 db, Lower Left 19 db, Upper Right 17 db, Upper Left 15 db.

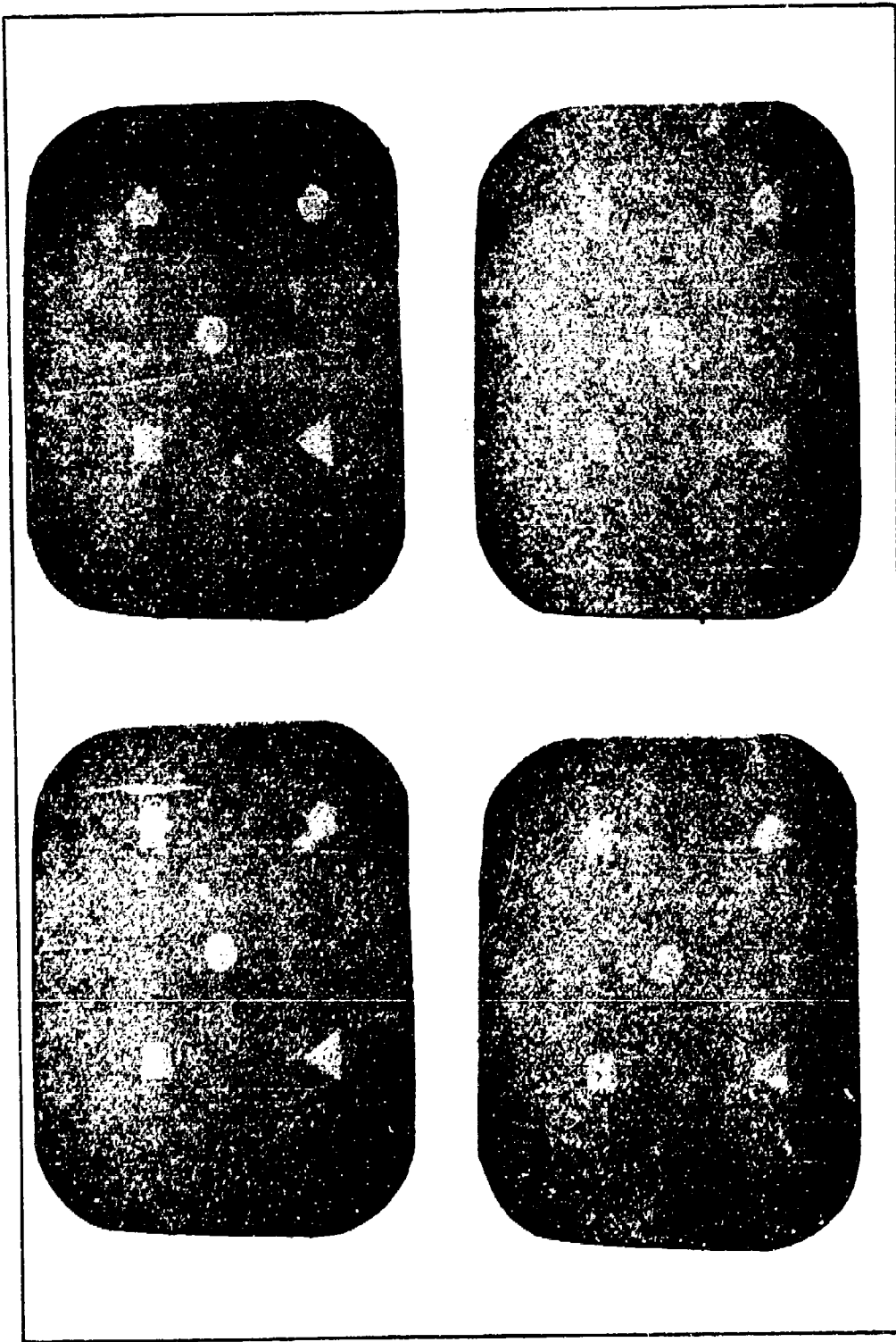


Fig. 15 Geometric Shapes Used for Edge Discrimination. Photographs Show (left to right, up to down) Decreasing  $SNR_D$  Values. Attenuation of Signal is Lower Right 29 dB, Lower Left 27 dB, Upper Right 25 dB, Upper Left 23 dB.

1	2	3	4	5	6
Object	Ratio of Triangle Side Length to Object Side Length ( $x_o$ )	$x_o^{\frac{1}{2}}$	$10.8 x_o^{\frac{1}{2}} = y_o$	Measured $SNR_{DT} = y_m$	$\frac{100(y_o - y_m)}{y_o}$
Triangle	1.00	1.00	10.8	10.8	0
Square	1.43	1.12	12.1	11.6	4.1
Pentagon	2.12	1.46	15.7	14.4	8.3
Star	3.24	1.80	19.5	18.7	4.1
					Av. = 4.13

Table 2. Table Constructed to Test the Hypothesis that the Ability of an Observer to Discern Regular Geometric Shapes is Proportional to the Square Root of Side Length.

of the objects with straight lines, the object with the longest straight line (the triangle) was the one that required the least  $SNR_{DT}$  while the objects with the shortest straight line (the star) required the most. It was then hypothesized that the discernability is proportional to the length of the straight line in the shapes. To test this notion we constructed the Table 2. In column 2, we form the ratio of the length of the straight line in the triangle to that of any other shapes. In column 3, we take the square root of the line length and multiply the result by 10.8\* in column 4 which is the  $SNR_{DT}$  required to recognize the triangle.

\* Because all of the shapes were of approximately equal area, the  $SNR_{DT}$ 's can all be interpreted as  $SNR_V$ , the video signal-to-noise ratios if note is made of the proportionality constant between  $SNR_{DT}$  and  $SNR_V$  (which is the same for all the shapes).

Column 4 is then compared to the measured value of  $SNR_D$  in column 5 with the percentage of error being shown in column 6.

While not conclusive, it appears that the discernability of regular geometric shapes with equal sides is proportional to the square root of the side length. It would be of interest to continue this investigation using both regular and irregular shapes since shape recognition is of considerable interest in the art of making range predictions.

#### 2.4 Observer Requirements - Periodic Bar Patterns

The most important test image in current use for system evaluation is the periodic bar pattern. As previously noted, it is assumed that the eye, in detecting the presence of a bar pattern, must discern a single bar in the pattern. In the elementary model, the area over which the eye integrates is the total area of one bar. One question which arose early in the investigation concerned the eye's ability to integrate over the entire bar length. This was found to be the case when the bar did not exceed about  $0.5^\circ$  in the vertical relative to the observer's eye (compared to an ability to integrate over an angle of at least  $6^\circ$  for an isolated bar). However, even when the bar length exceeds  $0.5^\circ$ , an increase in bar length increases its discernability. The increase, for angular subtenses larger than  $0.5^\circ$  was, however, only at the  $\frac{1}{4}$ th power of the length rather than the  $\frac{1}{2}$  power as is the case for bars of less than  $0.5^\circ$  subtense.

In Fig. 16, we show the threshold  $SNR_D$  for bar patterns with the observer at 14", 28" and 56" from a display of 8" picture height. The  $SNR_{DT}$  required at  $N = 100$  lines is seen to decrease with an increase in

viewing distance. At higher line numbers (above  $N = 200$ ),  $SNR_{DT}$  decreases with a decrease in viewing distance. The  $SNR_{DT}$  for bar patterns, at an optimum viewing distance is shown in Fig. 17. Previously we found that the  $SNR_{DT}$  for isolated bars was 2.8. At an optimum viewing distance, the  $SNR_{DT}$  for a bar pattern is about 2.7 at 100 lines and decreases with increase in spatial frequency to a value of about 1.4 at 630 lines. Note in this connection that the bar pattern images were generated by a vidicon camera and that the bars displayed were square waves at low line numbers and more nearly sine waves at high line numbers due to the camera's MTF. The  $SNR_{DT}$ 's plotted are corrected for square wave flux factor, i.e., the signal is the mean flux in the displayed pattern above background. The fall in  $SNR_{DT}$  at the high line numbers is however unexpected and as yet, unexplained.

When horizontally oriented bar patterns are used, the television raster structure may interfere with the bar patterns discernability. The result of an experiment using horizontal bars is shown in Fig. 18. For our particular camera, the  $SNR_{DT}$  required was essentially independent of the bar patterns orientation, whether vertical or horizontal for spatial frequencies of 400 lines and below. At 485 lines the  $SNR_{DT}$  required increases noticeably for horizontal bars while the 635 lines pattern could only be seen with no noise added to the signal. Note, however, that the results are specific for the camera used. In principle, a pattern of spatial frequency 875 lines per picture height could be resolved if the shape of the scanning beam were such that its Fourier transform is an ideal low pass filter. The shape of the beam, in the vertical, across-scan direction, would be an ideal low pass filter if

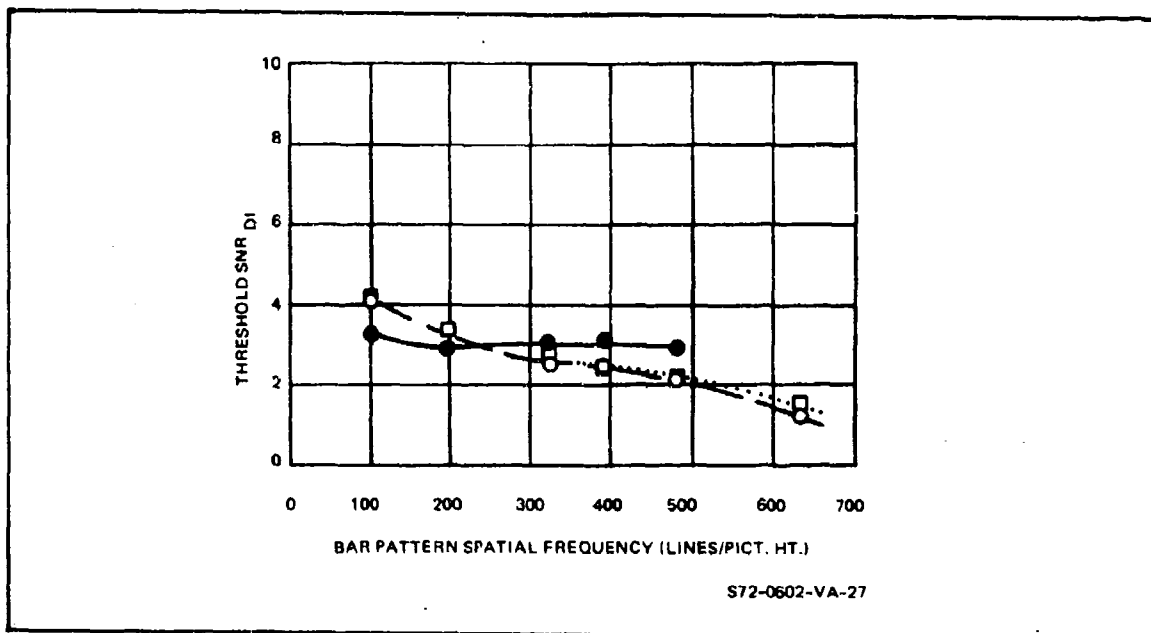


Fig. 16 Threshold SNR<sub>D-I</sub> vs Bar Pattern Spatial Frequency for Display-to-Observer Viewing Distances of  $\circ$  14",  $\square$  28" and  $\bullet$  56".

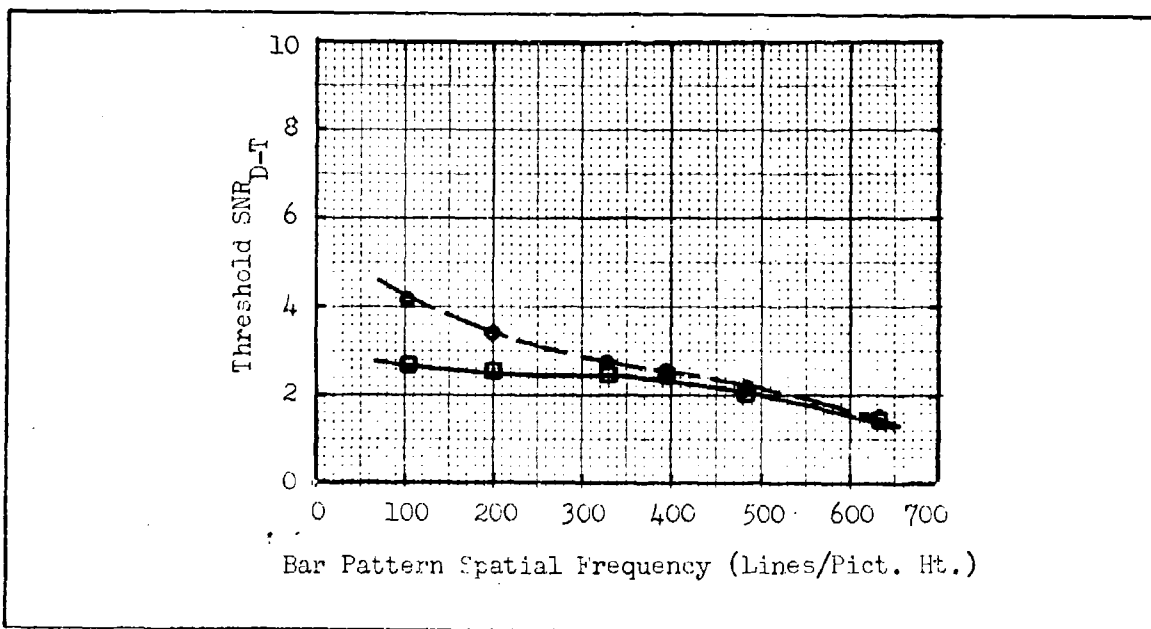


Fig. 17 Threshold Display Signal-to-Noise Ratio vs. Bar Pattern Spatial Frequency for  $\square$  Optimum Viewing Distance and  $\circ$  28" Viewing Distance for One Observer.

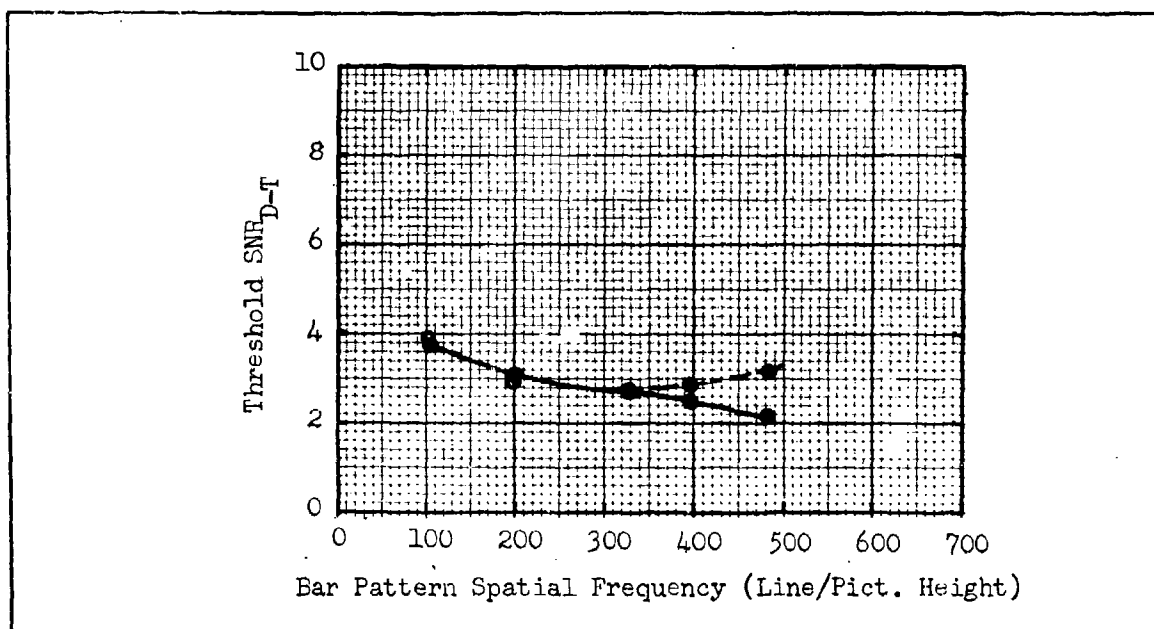


Fig. 18 Threshold Display Signal-to-Noise Ratio required to recognize the Presence of, ○ Horizontally Oriented and, ● Vertically Oriented Bar Patterns vs. Bar Pattern Spatial Frequency. Televised Images at 25 Frames/Sec., 875 Scan Lines,  $D_V/D_H = 3.5$ . Bar Height-to-Width Ratio was 5.

its shape were  $\sin x/x$ . However, such a shape is physically unrealizable. In any event, the Nyquist limit of resolution, of 1 cycle per two scan lines may be approached either more or less closely in cameras other than in the one we used.

#### 2.5 Higher Discrimination Levels

In the shape recognition task using the simple geometric shapes of Section 2.3, it was seen that a larger  $SNR_D$  was needed to discern the shape than to merely detect it. The geometric shapes televised were large enough that the sensor MTF's could be ignored. The only limit on the shape recognition was the signal or noise level. The more complex images such as the star required a higher  $SNR_D$  to recognize than the simpler, such as the triangle. In general, it would be desirable if  $SNR_{DT}$  were a constant for all images if it were possible. One approach toward this goal might

be to select a subarea on the more complex images. For example, a single point (actually a triangle) might be used on the star. However, while the area of the point of a star might be a logical selection for the subarea of a star, the choice of a subarea on a pentagon is more difficult. To define a subarea in general, would be a formidable problem.

As we have observed in the previous analysis, the ability to resolve scene detail can be limited by noise alone. On the other hand, a noise-free picture can be resolution limited. Consider trying to discern the star as such, when the stars subtense is but one scan line wide on a television monitor. The star may be readily detected but may be completely unrecognizable. For specific simple objects, such as a rectangle or a bar pattern, we can write a signal-to-noise expression including resolution as a parameter. It is unlikely that one could be constructed for randomly oriented stars with undeterminate numbers of points.

For the above reasons, and because of the similarity of radio communications with optical image communication, optical system parameters are discussed in terms of spatial frequency response. In audio systems, the goal, when reproducing music is to maintain a flat frequency response to beyond the limit of the ear's response. However, when reproducing speech, a lesser response may be tolerated to conserve telephone line bandwidth provided that the bandwidth is sufficient to maintain the speaker's intelligibility. In imagery, the same principles apply.

As we observed above, the ability to resolve scene detail can be limited by sensor apertures or by noise or by both. Analytically we have models for the rectangles and bar patterns which include both noise and resolution and for this reason, it would be highly desirable to



find a correlation between the objects we can analyze and real scene objects even if the correlation is not perfect. This desire led to the equivalent bar pattern approach discussed in Ref. 2. Basically the idea is to perform recognition experiments with a real object and then replace the real object with an equivalent bar pattern. In the initial attempt reported in Ref. 2, we adopted Johnson's criteria for detection, recognition and identification as given in Table 3. According to Johnson's experiments, the resolution required to perform the various levels of discrimination are as shown in Table 4. In creating an equivalent bar pattern we made the pattern bars as long as the object is long and of width equal to the object's width divided by the number of resolution lines required for the level of discrimination wanted as illustrated in Fig. 19.

In performing the "real" object recognition experiment, we calculated the  $SNR_D$  for the real image on the basis of peak to peak signal excursion in the video and an area equal to the minimum dimension divided by 8. The results for 4 types of vehicles against a uniform background are shown in Fig. 20. The  $SNR_{DT}$  for 50% recognition probability average 3.3, being a bit larger for the radar half track than the derrick bulldozer. The value needed for an equivalent bar pattern was 2.9 which is only 14% different from 3.3. The results of the experiment are not however clear cut since a number of interpretations are possible. The first difficulty is in the method of defining the signal as peak to peak signal current excursion for the real object rather than some mean value or some average excursion about the mean. Had some smaller value of signal excursion been used in the calculation, then the

<u>Classification of Discrimination Level</u>	<u>Meaning</u>
Detection	An object is present.
Orientation	The object is approximately symmetrical or unsymmetrical and its orientation may be discerned.
Recognition	The class to which the object belongs may be discerned (e.g., house, truck, man, etc.).
Identification	The target can be described to the limit of the observer's knowledge (e.g., motel, pick-up truck, policeman, etc.).

Table 3. Levels of Object Discrimination.

<u>Discrimination Level</u>	<u>Discrimination Factor, <math>k_d</math>, in terms of the Number of Resolution Lines Required per Minimum Object Dimension (TV Lines)</u>
Detection	2.0 + 1.0 - 0.5
Orientation	2.8 + 0.8 - 0.4
Recognition	8.0 + 1.6 - 0.4
Identification	12.8 + 3.2 - 2.8

Table 4. Johnson's Criteria for the Resolution Required per Minimum Object Dimension vs Discrimination Level.

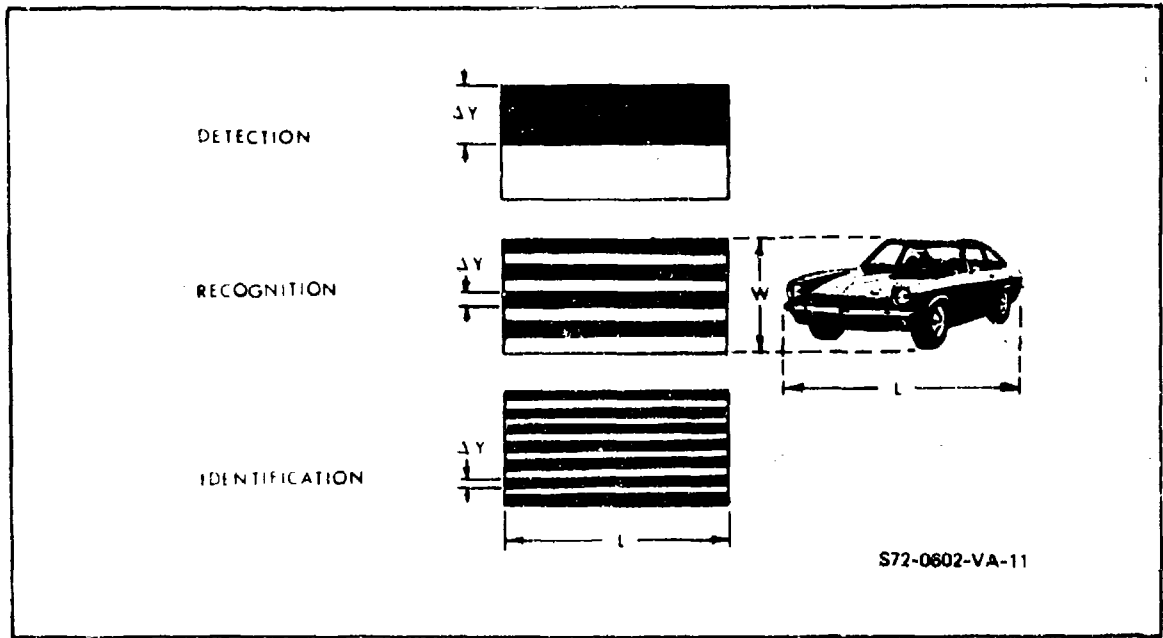


Fig. 19 Levels of Object Discrimination. Object Area to be Used in the  $SNR_D$  Calculation is  $\Delta Y$  by  $L$ .

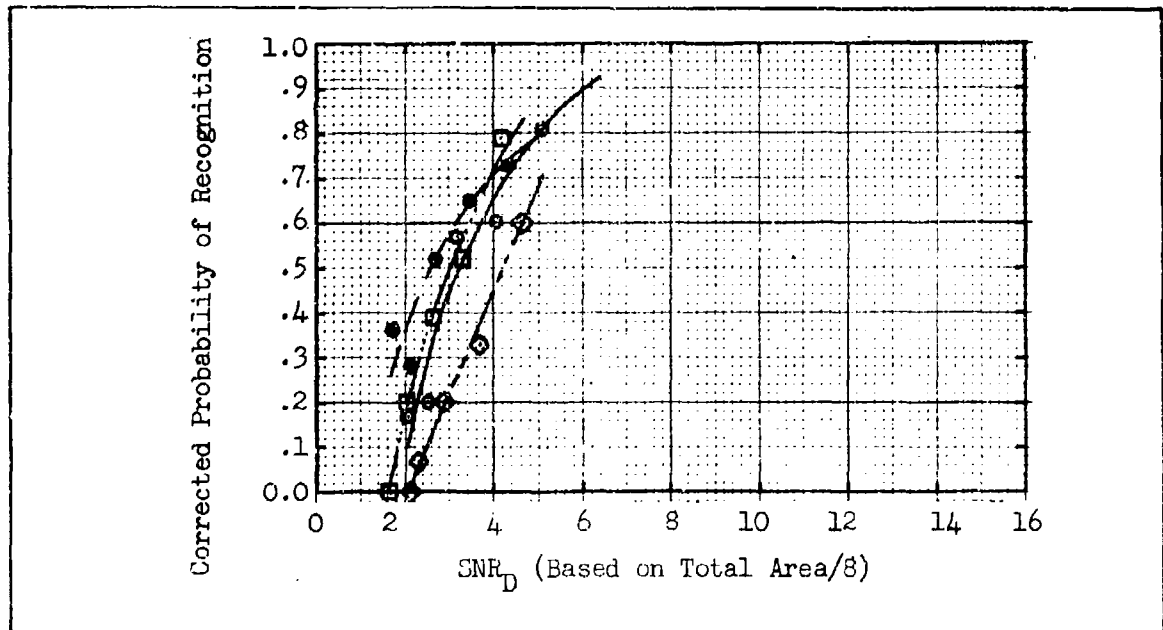


Fig. 20 Probability of Recognition vs  $SNR_D$  for a ● Tank, ◇ Radar Half Track, □ Van Truck and ● Derrick Bulldozer. Uniform Background, Televised Imagery at 875 Lines, 25 frames/sec  $D_V/D_H = 3.5$ .

$SNR_{DT}$  would have been smaller and the complication might be that the vehicles could be recognized with lower resolution. In subsequent experiments using more complex backgrounds, the radar half track tended to remain more difficult to recognize than the derrick bulldozer and it is easy to believe that more resolution is needed to recognize the half track than the bulldozer. However, it is not possible to conclude that 8 lines of resolution across a minimum dimension will be sufficient or even in excess of that needed to recognize an object.

As the background complexity increases the  $SNR_{DT}$  also increases indicating a need for more resolution. If the amount of resolution needed with a uniform background were known then the further amount needed with more complex backgrounds could be estimated but this is not the case. Observe further, that in a real camera, increases in  $SNR_D$  are accompanied by increases in resolution as was discussed in connection with Fig. 8. Thus, resolution and noise effects are difficult to separate.

In future recognition and identification experiments, it is suggested that an attempt be made to obtain as nearly a noise-free picture as possible and then imposing resolution limits by suitable optical and electrical filtering. In the past some efforts were made to do this by strip mapping photographs, i.e., raster limiting the picture but the results are not directly useable in the analytical models. In any such process care must be taken to avoid aliasing effects and to equalize resolution in two directions. Having established an aperture limited picture, it would then be desirable to add noise.

Until further progress is made, it is felt that the equivalent bar pattern approach as proposed in Ref. 2 and reviewed here is a viable

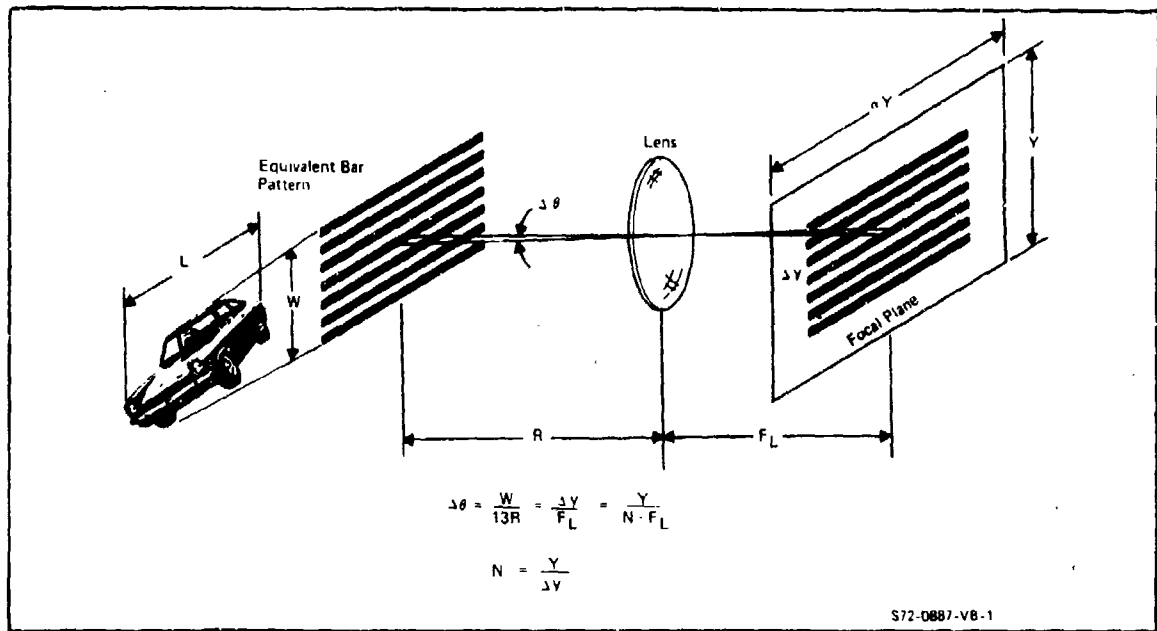


Fig. 21 Equivalent Bar Pattern Criterion for Object Identification.

and useful means of estimating performance. In practical use, such as identifying the automobile shown in Fig. 21 the equivalent bar pattern is of length  $L$  and of bar spacing  $W/13$ . At range  $R$ , the angular subtense  $\Delta\theta = W/13R$ . On the image plane of the sensor the bar spacing  $\Delta y = F_L \Delta\theta$  where  $F_L$  is the lens focal length. The spatial frequency  $N$  which must be resolved by the sensor is then  $Y/\Delta y$  lines/picture height where  $Y$  is the picture height. The sensory system must then be analyzed to determine whether or not  $N$  lines can be resolved.

### 3.0 System Tradeoff Analysis

The primary function of an imaging system as used in industrial security, law enforcement or military applications is to enable an observer to resolve scene details with sufficient clarity to perform some desired function. This desired function must be performed over an acceptably large fraction of the time that the equipment should have applicability. The fraction of the time when the equipment will not perform the desired function should mainly depend upon factors beyond the designer's control such as scene contrasts or atmospheric visibilities which are well below the expected average. The maximum level of scene resolution depends upon the designed-in system parameters and must perforce reflect a compromise between the user's desires and needs, the levels of performance physically realizable and the very real constraints of system size, weight, power and cost.

A system requirement usually stems from a real need to perform a given task. Sometimes, however, the requirement calls for performance beyond that needed to perform the task and the excess capability should fall in the class of a "desirement". While excess capability can often be provided, the excess capability will entail a penalty in either the equipment itself such as its size or cost or in some other area such as aerodynamic drag.

In a typical aerial bombing problem, the range at which an object must be detected must include time to search for and acquire the object,

to make the necessary computations with regard to the bomb release and yet leave time enough for the bomb to fall without overshooting the object's location. While this would seem to be a straightforward problem, the range required is not necessarily a fixed number. A pilot will probably wish to fly as fast as possible over the target area to maximize survivability. However, the extra range needed to permit fast fly-over may be acquired only at considerable expense in aerodynamic drag. The increased drag could in turn substantially decrease aircraft speed, increase fuel requirements or decrease aircraft range. Similarly, the time to acquire can be a large variable. Much longer ranges will be required with pessimistic view of acquisition time. On the other hand, a too optimistic view would result in a high proportion of missed targets which would be equally undesirable.

A complete tradeoff analysis must include the effect of a change in any sensor parameter on all of the other parameters involved in meeting the total mission requirement. In a usual systems synthesis, a first cut baseline system is devised which appears to meet the mission requirements. A fairly detailed configuration is devised and judged in terms of its suitability for the intended use. In successive iterations, the overall design is optimized. It should be clear from the above discussion that the optimum system is not necessarily one that provides maximum object detection range but rather, one that has a high probability of meeting the mission requirements without other undesirable side effects such as excessive size, weight, cost, complexity or drag. The decision that an optimum has been reached is not clear cut but requires judgment on the part of the designer.

A treatment of a complete and general systems tradeoff procedure is obviously beyond the scope of this effort. However, we will discuss sensory system parameter tradeoffs in some detail but with minimum regard for the effects of the tradeoffs on the system's mechanical configuration. For example, we will discuss the effect of increasing optical aperture on range, but we will not dwell on the effect of increased aperture on overall system weight, on window area or on aerodynamic drag.

### 3.1 Scene Characteristics

In the discussion below, we will consider both active and passive electro-optical systems. An active system is one which employs an auxiliary scene irradiator while a passive system relies entirely on light from natural scene sources such as the sun or moon. The scene to be viewed consists of the source of scene irradiance, the atmosphere intervening between the source and an object in the scene, the object itself and the atmosphere intervening between the object and the sensor.

For either active or passive sensors, the scene is characterized by spatial distributions of spectral irradiance  $E(\lambda)$  and spectral reflectivity  $\rho(\lambda)$ . If the scene is diffusely reflecting, as we assume here, the scene spectral radiance  $L(\lambda)$  will be

$$L(\lambda) = \frac{\rho(\lambda)E(\lambda)}{\pi} \frac{\text{Watts}}{\text{m}^2 - \text{ster}} \quad (56)$$

It is usual in first order analysis to assume that the reflectivity of the scene object and its background are independent of wavelength, i.e.,



the average differential object-to-background reflectivity is specified. In this case, we define the inherent object-to-background contrast for diffuse scenes as

$$\begin{aligned} C_{M_o} &= (\rho_o - \rho_b) / (\rho_o + \rho_b) \\ &= (\rho_o - \rho_b) / 2\rho_{av} \quad , \end{aligned} \quad (57)$$

where  $\rho_{av} = (\rho_o + \rho_b) / 2$  and  $\rho_o$  and  $\rho_b$  are the object and background reflectivities respectively. If this is the case, we can write the incremental scene irradiance  $\Delta L(\lambda)$  as

$$\Delta L(\lambda) = 2\rho_{av} C_{M_o} E_s(\lambda) / \pi \quad . \quad (58)$$

### 3.1.1 Scene Characteristics (Passive)

A wide variety of "natural" sources can exist, including the sun, the stars, the moon and the skyglow. "Unnatural" sources such as city lights reflected off low clouds and even scene floodlighting when the floodlights are not at or near the sensor's location will nevertheless be considered as natural sources on the basis that the scene radiance passes only once through the atmosphere from the object to the sensor rather than twice as is the case for the auxiliary source. The two primary classes of natural sources are those which provide mainly diffuse scene irradiance and those which provide predominantly directional scene radiance. Clear night starlight and heavy overcast sunlight or moonlight represent diffuse sources while clear day sunlight and clear night moonlight would be examples of directional sources.

There are obviously cases where both classes of source exist together and are of near equal importance such as in light overcast sun or moonlight or when the moon is new, or when either the sun or moon are low on the horizon sky.

In diffuse light, the detectability of objects would be expected to be relatively independent of viewing angle since the lighting is nearly uniform in all directions, and the objects are shadowless or nearly so. The average scene contrasts also would be expected to be lower than in the case where lighting is directional. With the directional lighting, one expects sharp contrasty shadows but object features may become unrecognizable except at certain viewing and source angles. For example, a black and white bar pattern on a panel may be clearly discerned when the moon is behind the observer, but with the moon behind the panel, the panel appears black.

Naturally irradiated scenes can assume an infinite variety depending on the relative aspect angles between the scene object, observer and the source, or type of source and it becomes most difficult to divide the number of objects into a reasonable number of cases for analytical purposes. Hence, it is usual to assume that the source is primarily directional or primarily diffuse. If directional, it is assumed that an equivalent diffuse source can be defined.

The irradiance levels we expect to find, whether day or night, are ordinarily tabulated for typical scenes. Usually, the irradiance levels are measured with photometers which are compensated to have a spectral response similar to that of the unaided human eye. The resulting curves

such as that shown in Fig. 22 may or may not be relevant to electro-optical sensors which can have an entirely different spectral bandpass. This subject is discussed in some detail in Ref. (1) and (2).

In the daytime, light levels are generally sufficient so that camera tubes can be operated at near maximum performance levels. In this case, light level is of little concern. However, it is always of interest to know what the minimum light level can be and yet obtain an acceptable image. The natural levels of scene illumination and irradiance are discussed and tabulated in some detail in Ref. (5) for daylight and the nocturnal hours. It is rather difficult to characterize twilight which is a period of time during which the light level is falling very rapidly. In the visible, the light level may drop 8 orders of magnitude in a short space of time as indicated in Fig. 22.

The sensitivities of many photocathodes are measured using a 2854° K tungsten source. The sensitivity itself is given in terms of micro-ampere per lumen. Although this sensitivity term only applies when the test source is a tungsten lamp, it is often used to predict performance for a naturally lighted scene. As discussed in Ref. (1) and (2) this may not be a bad approximation in all cases. For example, in Ref. (2), Figs. 24 - 27 show that with an S-25 photosurface using the luminance sensitivity rather than the radiometric sensitivity results in an error of only 25 - 30% in estimating camera tube signal current (for a grey scene object, i.e., one whose reflectivity is uniform with respect to wavelength). But note that this applies only when the S-25 photocathode is not spectrally filtered. However, spectral filtering is quite often used.

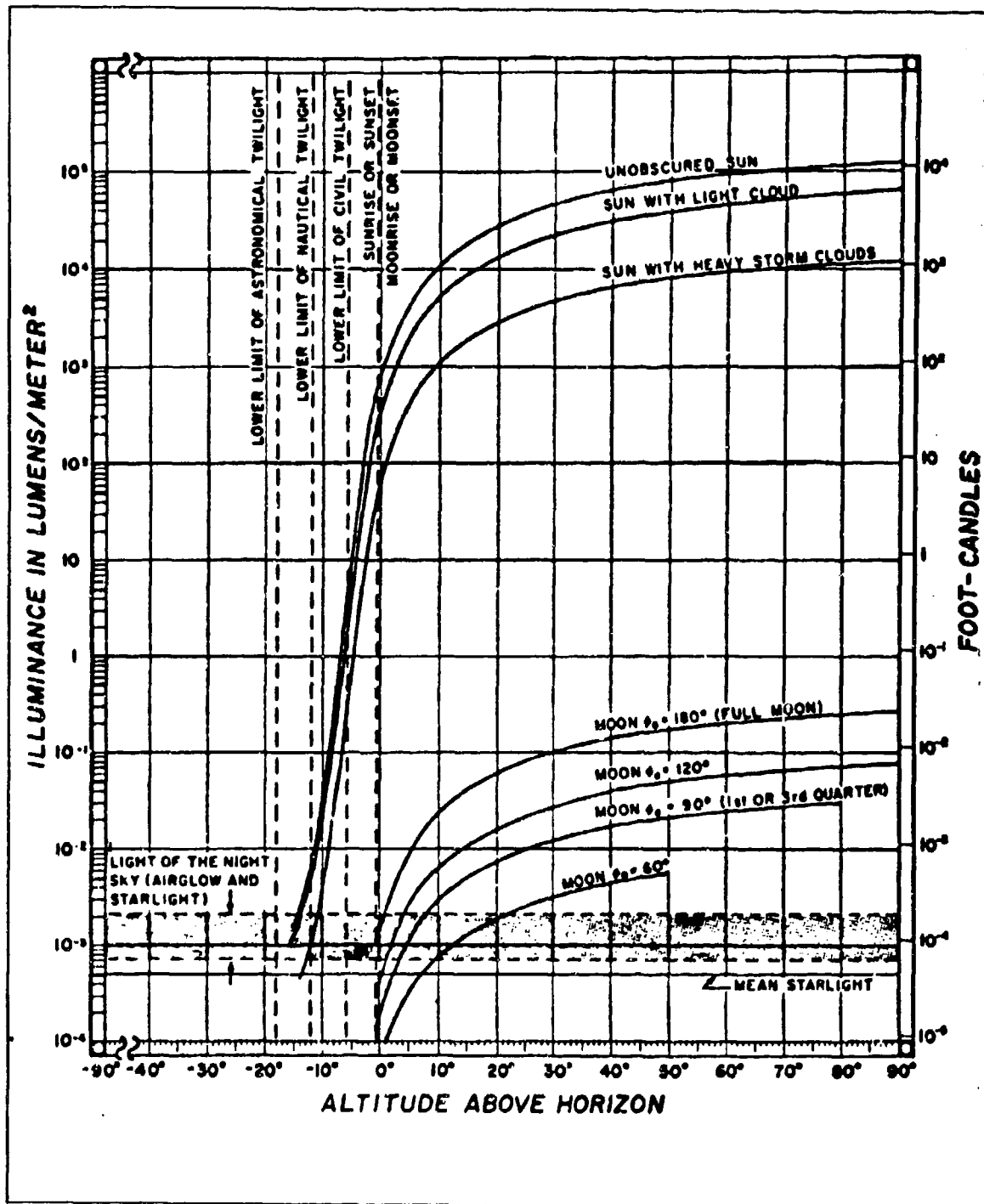


Fig. 22 Illuminance Levels on the Surface of the Earth due to the Sun, the Moon, and the Light of the Night Sky.

The typical illuminance levels of the earth under many conditions are well known and are common knowledge. For this reason, it is sometimes useful to relate the sensor's sensitivity to the illuminance level as was done in the case of the S-25 photocathode using the procedures of Ref. (1).

The atmosphere between the source and object, or surrounding the object has three principal effects on passive imaging sensors. First, the atmosphere may be, in effect, the natural source as is the case of the sun just below the horizon. In this case, the light scattered by the atmosphere is the principal source. Secondly, the scene irradiance is diminished due to absorption and to scattering of the natural source radiation out of the path between the source and object and finally, a portion of the sources radiant energy may be scattered into the sensors line-of-sight. The levels of natural scene irradiance are not ordinarily calculated except in special instances but rather, are taken from tables and curves as we noted above.

The main effect of atmosphere scattering of radiation into the line of sight is to decrease image contrast. The inherent image contrast  $C_0^*$  is the contrast at zero range. At range R, the apparent contrast is generally smaller. It is designated  $C_R$ . The general law of contrast reduction is given by Middleton (Ref. 6) as

$$C_R = C_0 \left( \frac{N_{o0} - N_{b0}}{N_{oR} - N_{bR}} \right) e^{-\alpha \bar{R}}, \quad (59)$$

where  $N_{o0}$  and  $N_{b0}$  are the object and background radiance at zero range respectively and  $N_{oR}$  and  $N_{bR}$  are the corresponding quantities at range, R.

---

\* Contrast as defined by Middleton is  $\Delta L/L$  background.

Also,  $\alpha_0$  is the value of the atmospheric attenuation, or extinction, coefficient at zero range and  $\bar{R}$  is the "optical slant range" and represents the equivalent distance in a homogeneous atmosphere for which the attenuation is the same as that actually encountered along the true path of length  $R$ .

The optical slant range is obtained from an equation of the form

$$\bar{R} = \int f(r) dr . \quad (60)$$

For an optical standard atmosphere, Middleton (after Duntley) gives

$$\bar{R} = \int_{R_1}^{R_2} e^{-r \sin\theta/30,000} dr , \quad (61)$$

where  $r \sin\theta$  is the altitude of either object or observer above sea level and  $\theta$  is the angle between the observer and the horizontal. For the above formulation, a single vertical structure is assumed for the atmosphere which is usually not the case. An alternative approach is to use the actual slant path and correct the sea level extinction coefficient,  $\alpha_a$  of Table 5 by means of the curves of Fig. 23 (Ref. 7).

The general law of contrast reduction has been specialized for three cases by Middleton as follows.

1. Horizontal Vision - When the observer is looking at an object imaged against a horizon sky background, the general case simplifies to

$$C_R = C_0 e^{-\alpha_0 R} , \quad (62)$$

Visibility n. miles	Extinction Coefficient			Subjective Visibility
	n. miles <sup>-1</sup>	ft <sup>-1</sup>		
- 100	- 0.039	- 6.52 x 10 <sup>-6</sup>		Exceptionally Clear
- 38	- 0.012	- 1.58 x 10 <sup>-5</sup>		Very Clear
- 10	- 0.39	- 6.52 x 10 <sup>-5</sup>		Clear
- 5	- 0.78	- 1.30 x 10 <sup>-4</sup>		Light Haze
- 2	- 1.95	- 3.26 x 10 <sup>-4</sup>		Haze
- 1	- 3.9	- 6.52 x 10 <sup>-4</sup>		

Table 5. Atmospheric Extinction Coefficient as a Function of Meteorological and Subjective Visibility.

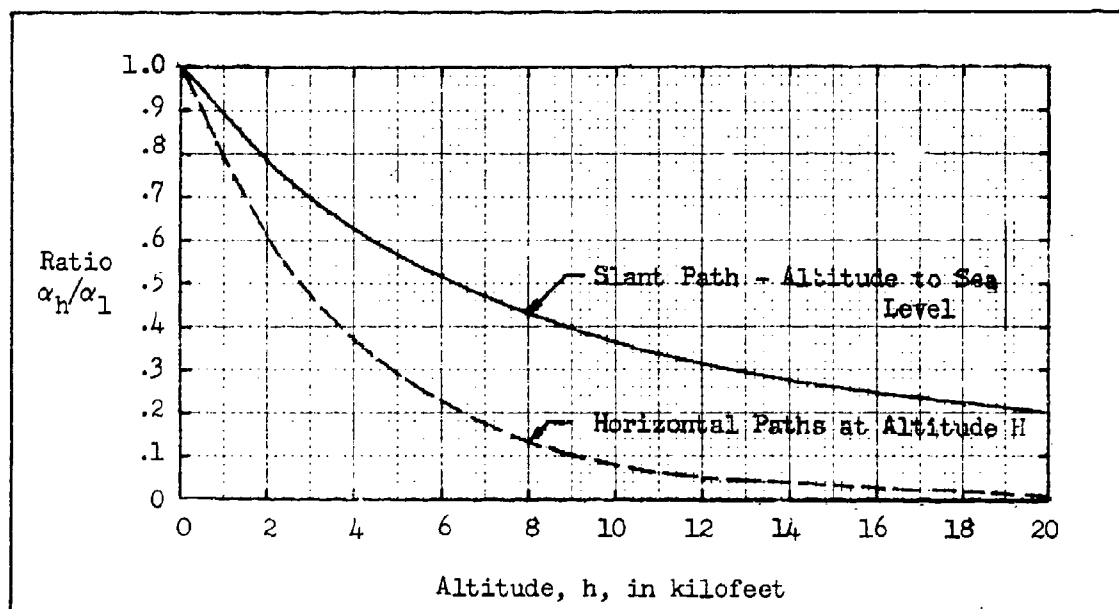


Fig. 23 Approximate ratio of the Atmospheric Extinction Coefficient,  $\alpha_h$ , at Altitude h to its value,  $\alpha_1$ , at Sea Level for Slant and Horizontal Paths neglecting Water Vapor and Carbon Dioxide Absorption.

which holds for objects of both positive and negative contrast. This equation is often erroneously used even when the object is not imaged against the horizon sky.

2. The Observer Looking Upward - For this case, Middleton gives

$$C_R = C_0 e^{-\alpha_0 \bar{R}} \left[ \frac{1 - \exp(-\alpha_0 \bar{R}_{R \rightarrow \infty})}{1 - \exp(-\alpha_0 \bar{R}_{O \rightarrow \infty})} \right], \quad (63)$$

where

$$\bar{R}_{R \rightarrow \infty} = \int_R^{\infty} f(r) dr \text{ and, } \bar{R}_{O \rightarrow \infty} = \int_0^{\infty} f(r) dr. \quad (64)$$

3. Vision Downward - This is the most important case in aerial surveillance. For this case,

$$C_R = C_0 \left[ 1 - \frac{S_k}{G_d} (1 - e^{-\alpha_0 \bar{R}}) \right]^{-1}, \quad (65)$$

where  $S_k/G_d$  is a quantity dubbed the "sky-to-ground ratio" and represents the sky-to-ground brightness ratio. Its value is estimated to be inversely proportional to the background reflectivity,  $\rho$ , i.e.,

$$\begin{aligned} \frac{S_k}{G_d} &= \frac{1}{\rho} \quad (\text{overcast sky}) \quad , \\ &= \frac{0.2}{\rho} \quad (\text{clear sky}) \quad . \end{aligned} \quad (66)$$

Typical values of  $S_k/G_d$  are given in Table 6 for the visible spectrum. The Eq. (65) is plotted in Fig. 24 for a meteorological visibility of



<u>Sky Condition</u>	<u>Ground Condition</u>	$\frac{S_k}{G_d}$
Clear	Fresh Snow	0.2
Clear	Desert	1.4
Clear	Forest	5.0
Overcast	Fresh Snow	1.0
Overcast	Desert	7.0
Overcast	Forest	25.0

Table 5. Typical Values of the Sky to Ground Ratio in the Visible Spectrum.

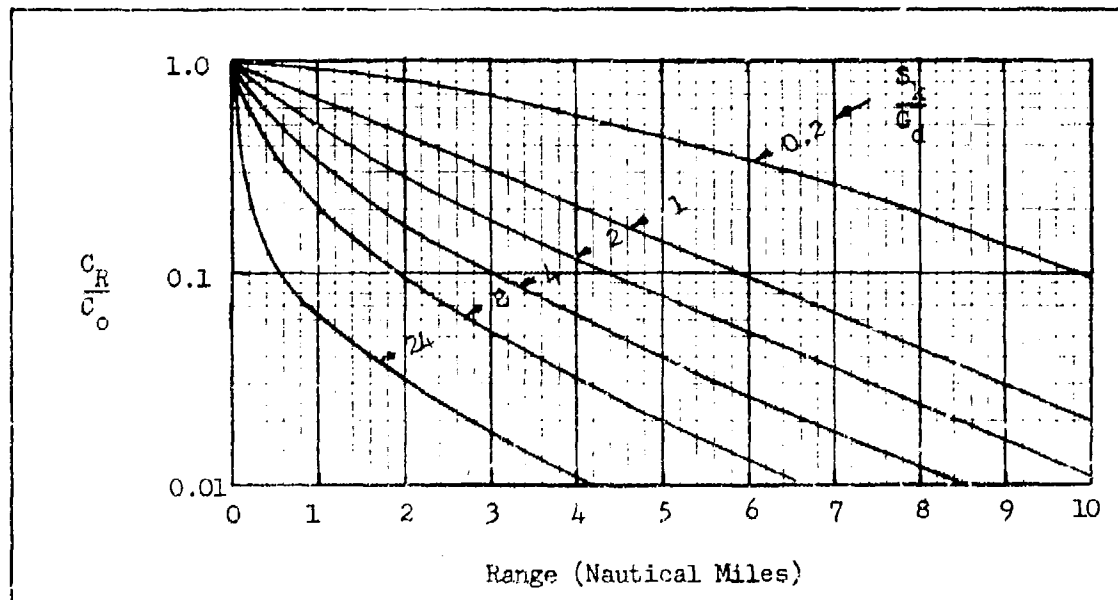


Fig. 24 Ratio of Apparent to Inherent Contrast vs Range for Various Values of Sky-to-Ground Ratio for a Meteorological Visibility of 10 Nautical Miles.

10 n. miles. Note that these curves apply to the visible spectrum. In the near infrared, the reflectivity of forests is much higher than in the visible and, hence, the sky-to-ground ratio is correspondingly lower.

The main point of the above discussion is to note that the reduction in contrast due to atmosphere is not always a simple exponential as is commonly taken to be the case but instead varies with the sky condition, the background and the viewing direction. The reader is urged to read Middleton (Ref. 6) for a more detailed treatment of the atmospheric visibility problem.

In the above discussion, we have used the standard or generally accepted values of extinction coefficients in the visible spectrum. In Ref. (8), data is given for the scattering and absorption coefficients for a number of wavelengths from the visible to the infrared. Five geographic zones are assumed ranging from the arctic to the tropical. For each zone, two aerosol models (clear and hazy), are considered. A typical table from Ref. (8) for  $\lambda = 0.488$  micrometers is reproduced in Table 7.

As an example of the use of the table, consider a clear day at sea level and a midlatitude summer. For this case,  $\sigma_m = 1.88 \times 10^{-2} \text{ k}_m^{-1}$  and  $\sigma_a = 1.76 \times 10^{-1}$  and  $k_a$  is negligible. The total extinction coefficient is then the sum of  $\sigma_m$  and  $\sigma_a$  or  $.195 \text{ k}_m^{-1}$ .

### 3.1.2 Scene Characteristics (Active)

The scene object and its background is presumably the same for an active system as it is for a passive system and is characterized by the same parameters, i.e., spectral reflectivity  $\rho(\lambda)$  and an inherent contrast  $C_{MO}$ . The contrast may, of course, be different in value from that of a

		$\lambda = 0.488 \mu\text{m}$												
H (ft/m)	TROPICAL		MIDLATITUDE SUMMER		MIDLATITUDE WINTER		SUBARCTIC SUMMER		SUBARCTIC WINTER		CLEAR		HAZY	
	$k_m$ ( $\text{km}^{-1}$ )	$\sigma_m$ ( $\text{km}^{-1}$ )	$k_m$ ( $\text{km}^{-1}$ )	$\sigma_m$ ( $\text{km}^{-1}$ )	$k_m$ ( $\text{km}^{-1}$ )	$\sigma_m$ ( $\text{km}^{-1}$ )	$k_m$ ( $\text{km}^{-1}$ )	$\sigma_m$ ( $\text{km}^{-1}$ )	$k_m$ ( $\text{km}^{-1}$ )	$\sigma_m$ ( $\text{km}^{-1}$ )	$k_m$ ( $\text{km}^{-1}$ )	$\sigma_m$ ( $\text{km}^{-1}$ )	$k_a$ ( $\text{km}^{-1}$ )	$\sigma_a$ ( $\text{km}^{-1}$ )
0	<E-06	1.21E-02	<E-06	2.03E-02	<E-0	2.03E-02	<E-06	1.80E-02	<E-06	1.80E-02	<E-06	1.70E-01	<E-06	8.38E-01
0-1		1.74E-02	1.77E-03	1.93E-02	1.86E-03	1.93E-02	1.80E-02	1.80E-02	1.80E-02	1.80E-02	1.80E-02	1.17E-01	1.17E-01	4.18E-01
1-2		1.58E-02	1.65E-02	1.70E-02	1.65E-02	1.70E-02	1.65E-02	1.65E-02	1.65E-02	1.65E-02	1.65E-02	9.09E-02	9.09E-02	1.90E-01
2-3		1.43E-02	1.45E-02	1.32E-02	1.42E-02	1.32E-02	1.42E-02	1.42E-02	1.42E-02	1.42E-02	1.42E-02	2.17E-02	2.17E-02	5.94E-02
3-4		1.30E-02	1.31E-02	1.36E-02	1.36E-02	1.36E-02	1.36E-02	1.36E-02	1.36E-02	1.36E-02	1.36E-02	1.02E-02	1.02E-02	2.53E-02
4-5		1.18E-02	1.18E-02	1.22E-02	1.22E-02	1.22E-02	1.22E-02	1.22E-02	1.22E-02	1.22E-02	1.22E-02	6.45E-03	6.45E-03	8.25E-03
5-6		1.06E-02	1.06E-02	1.05E-02	1.05E-02	1.05E-02	1.05E-02	1.05E-02	1.05E-02	1.05E-02	1.05E-02	4.70E-03	4.70E-03	4.70E-03
6-7		9.56E-03	9.54E-03	9.68E-03	9.68E-03	9.68E-03	9.68E-03	9.68E-03	9.68E-03	9.68E-03	9.68E-03	3.80E-03	3.80E-03	3.80E-03
7-8		8.41E-03	8.55E-03	8.40E-03	8.40E-03	8.40E-03	8.40E-03	8.40E-03	8.40E-03	8.40E-03	8.40E-03	3.72E-03	3.72E-03	3.72E-03
8-9		7.72E-03	7.63E-03	7.82E-03	7.82E-03	7.82E-03	7.82E-03	7.82E-03	7.82E-03	7.82E-03	7.82E-03	3.70E-03	3.70E-03	3.70E-03
9-10		6.99E-03	6.89E-03	6.83E-03	6.83E-03	6.83E-03	6.83E-03	6.83E-03	6.83E-03	6.83E-03	6.83E-03	3.42E-03	3.42E-03	3.42E-03
10-11		6.10E-03	6.05E-03	5.88E-03	5.88E-03	5.88E-03	5.88E-03	5.88E-03	5.88E-03	5.88E-03	5.88E-03	3.32E-03	3.32E-03	3.32E-03
11-12		5.48E-03	5.40E-03	5.03E-03	5.03E-03	5.03E-03	5.03E-03	5.03E-03	5.03E-03	5.03E-03	5.03E-03	3.34E-03	3.34E-03	3.34E-03
12-13		4.83E-03	4.77E-03	4.31E-03	4.31E-03	4.31E-03	4.31E-03	4.31E-03	4.31E-03	4.31E-03	4.31E-03	3.16E-03	3.16E-03	3.16E-03
13-14		4.27E-03	4.15E-03	3.78E-03	3.78E-03	3.78E-03	3.78E-03	3.78E-03	3.78E-03	3.78E-03	3.78E-03	3.05E-03	3.05E-03	3.05E-03
14-15		3.75E-03	3.53E-03	3.17E-03	3.17E-03	3.17E-03	3.17E-03	3.17E-03	3.17E-03	3.17E-03	3.17E-03	2.88E-03	2.88E-03	2.88E-03
15-16		3.27E-03	3.01E-03	2.72E-03	2.72E-03	2.72E-03	2.72E-03	2.72E-03	2.72E-03	2.72E-03	2.72E-03	2.76E-03	2.76E-03	2.76E-03
16-17		2.82E-03	2.57E-03	2.33E-03	2.33E-03	2.33E-03	2.33E-03	2.33E-03	2.33E-03	2.33E-03	2.33E-03	2.73E-03	2.73E-03	2.73E-03
17-18		2.41E-03	2.16E-03	1.99E-03	1.99E-03	1.99E-03	1.99E-03	1.99E-03	1.99E-03	1.99E-03	1.99E-03	2.47E-03	2.47E-03	2.47E-03
18-19		1.93E-03	1.88E-03	1.71E-03	1.71E-03	1.71E-03	1.71E-03	1.71E-03	1.71E-03	1.71E-03	1.71E-03	1.84E-03	1.84E-03	1.84E-03
19-20		1.62E-03	1.60E-03	1.46E-03	1.46E-03	1.46E-03	1.46E-03	1.46E-03	1.46E-03	1.46E-03	1.46E-03	1.41E-03	1.41E-03	1.41E-03
20-21		1.35E-03	1.35E-03	1.25E-03	1.25E-03	1.25E-03	1.25E-03	1.25E-03	1.25E-03	1.25E-03	1.25E-03	1.04E-03	1.04E-03	1.04E-03
21-22		1.13E-03	1.13E-03	1.08E-03	1.08E-03	1.08E-03	1.08E-03	1.08E-03	1.08E-03	1.08E-03	1.08E-03	8.37E-04	8.37E-04	8.37E-04
22-23		9.48E-04	9.48E-04	8.89E-04	8.89E-04	8.89E-04	8.89E-04	8.89E-04	8.89E-04	8.89E-04	8.89E-04	6.17E-04	6.17E-04	6.17E-04
23-24		8.04E-04	8.04E-04	8.45E-04	8.45E-04	8.45E-04	8.45E-04	8.45E-04	8.45E-04	8.45E-04	8.45E-04	5.04E-04	5.04E-04	5.04E-04
24-25		6.83E-04	7.23E-04	6.83E-04	6.83E-04	6.83E-04	6.83E-04	6.83E-04	6.83E-04	6.83E-04	6.83E-04	2.54E-04	2.54E-04	2.54E-04
25-30		4.58E-04	4.85E-04	4.42E-04	4.42E-04	4.42E-04	4.42E-04	4.42E-04	4.42E-04	4.42E-04	4.42E-04	7.15E-05	7.15E-05	7.15E-05
30-35		2.08E-04	2.24E-04	1.99E-04	1.99E-04	1.99E-04	1.99E-04	1.99E-04	1.99E-04	1.99E-04	1.99E-04	1.88E-05	1.88E-05	1.88E-05
35-40		9.80E-05	1.07E-04	8.84E-05	8.84E-05	8.84E-05	8.84E-05	8.84E-05	8.84E-05	8.84E-05	8.84E-05	4.93E-06	4.93E-06	4.93E-06
40-45		4.86E-05	5.24E-05	4.13E-05	4.13E-05	4.13E-05	4.13E-05	4.13E-05	4.13E-05	4.13E-05	4.13E-05	1.81E-06	1.81E-06	1.81E-06
45-50		2.47E-05	2.69E-05	2.04E-05	2.04E-05	2.04E-05	2.04E-05	2.04E-05	2.04E-05	2.04E-05	2.04E-05	1.31E-06	1.31E-06	1.31E-06
50-70		9.24E-06	1.01E-05	7.47E-06	7.47E-06	7.47E-06	7.47E-06	7.47E-06	7.47E-06	7.47E-06	7.47E-06	<E-06	<E-06	<E-06
70-100		<E-06	<E-06	<E-06	<E-06	<E-06	<E-06	<E-06	<E-06	<E-06	<E-06	<E-06	<E-06	<E-06

Table 7. Values of Attenuation Coefficient/km as a Function of Altitude for Laser Wavelength of .488  $\mu\text{m}$  ( $k_m$  = molecular absorption,  $\sigma_m$  = molecular scattering,  $k_a$  = aerosol absorption,  $\sigma_a$  = aerosol scattering).

naturally lighted scene due to the spectral characteristics of the scene irradiator.

The auxiliary, or system, source may be a simple searchlight, or a complex light-emitting diode array or laser. These sources may be used in conjunction with a simple passive sensor or with a range gated sensor. In either case, the system is considered to be an "active" system if an auxiliary source of scene irradiance is used and if the system source is near the observer.

The primary system source parameters are the average transmitted source power,  $\phi_s$ , and the solid angle  $\Omega_s$  into which it radiates. Thus, the average source radiant intensity,  $I_s$ , is

$$I_s = \frac{\phi_s}{\Omega_s} . \quad (67)$$

The system source may be continuous wave, CW, as in the case of an ordinary searchlight, or a pulsed wave, PW, as in the case of a pulsed laser. If pulsed, the pulse duration, T, will be a primary source parameter. Also, the pulsed source is often monochromatic.

In the absence of atmosphere, the scene radiance normal to the line-of-sight is given for a diffuse reflector by

$$L_s = \frac{\rho_{av} \phi_s}{\pi \Omega R^2} , \quad (68)$$

where  $\rho_{av}$  is the average scene reflectance,  $\phi_s$  is the source radiant power in  $\text{Wav}^{-2}$ , and  $\Omega$  is the solid angle into which the source radiates

in steradians. In normalized form, this equation becomes

$$\frac{L_s}{\rho_{av} \Phi_s} = \frac{1}{\pi R^2} \frac{\text{Watts/m}^2 - \text{sr}}{\text{Watt}} \quad (69)$$

The atmosphere intervening between the source and object has two principal effects on active imaging systems. First, the scene radiance is diminished due to scattering of source radiation out of the line-of-sight and secondly, a portion of the source radiation may be back-scattered into the sensor's line-of-sight. The reduction of source radiant intensity by the atmosphere at range,  $R$ , compared to that in a vacuum is given by

$$\frac{I_s}{I_{sv}} = e^{-\alpha_o \bar{R}}, \quad (70)$$

where  $I_{sv}$  is the radiant intensity under vacuum condition. Then, the actual scene radiance becomes

$$L_s = \frac{\rho_{av} \Phi_s \exp(-\alpha_o \bar{R})}{\pi R^2} \quad (71)$$

However, the reflected scene radiance must travel through the atmosphere once more on its trip to the observer and thus, the apparent scene radiance becomes

$$L_{sa} = \frac{\rho_{av} \Phi_s \exp(-2\alpha_o \bar{R})}{\pi R^2}, \quad (72)$$

The value of  $\alpha_o$  may be obtained from the relation given by Steingold and Strauch (Ref. 9) as

Visibility <u>n. miles</u>	Extinction Coefficient		
	$\alpha$ (ft) <sup>-1</sup>	$\alpha$ (n. miles) <sup>-1</sup>	$\alpha$ (meters) <sup>-1</sup>
1	4.72 x 10 <sup>-4</sup>	2.27	9.15 x 10 <sup>-4</sup>
2	2.18	1.33	6.65
3	1.37	0.832	4.18
4	9.82 x 10 <sup>-5</sup>	0.597	2.99
5	7.58	0.461	2.31
6	6.1	0.371	1.86
7	5.1	0.310	1.55
8	4.32	0.263	1.32
9	3.8	0.231	1.16
10	3.3	0.201	1.0
15	1.99	0.12	6.08 x 10 <sup>-5</sup>
20	1.39	0.0845	4.24

Table 8. Values of the Extinction Coefficient at 0.86 Micrometers vs Meteorological Visibility.

$$\alpha_0(\lambda) = \frac{3.91 \cdot 10^{-3}}{V} \left[ \frac{0.55}{\lambda} \right] 0.585V^{\frac{1}{3}}, \quad (73)$$

where  $\alpha_0(\lambda)$  is the attenuation per meter when  $V$  is the meteorological visibility in kilometers and  $\lambda$  is in micrometers. The Eq. (73) is tabulated in Table (8) for  $\lambda = 0.86$  micrometers. As can be seen from Eq. (72), the atmosphere strongly influences the apparent scene radiance.

Before proceeding, it is desired to note the tradeoff relations between the apparent scene irradiance and the irradiator parameters. At any given range, it is apparent by observation of Eq. (72) that the apparent scene irradiance is doubled if the irradiator power is doubled. However, suppose it is desired to determine the amount that system

source power must be increased in order to obtain the same scene irradiance at some longer range  $R_2$  as was obtained at a shorter range  $R_1$ . Then, by solving Eq. (72) for  $\phi_s$  and taking the ratio, we obtain

$$\begin{aligned} \frac{\phi_{s2}}{\phi_{s1}} &= \left(\frac{R_2}{R_1}\right)^2 \exp[+ 2\alpha_o(R_2 - R_1)] \\ &= k^2 \exp[2\alpha_o R_1(k - 1)] \end{aligned} \quad (74)$$

where  $k = R_2/R_1$ . It is seen that under vacuum conditions ( $\alpha_o = 0$ ), the system source power must be quadrupled in order to obtain the same scene irradiance at twice the range. With a visibility of 10 n.mi. and an initial range ( $R_1$ ) of 5 n.mi., the source power must be increased 30 fold to obtain the same irradiance at double the range.

It is important to note that detection or recognition range is not doubled just because the apparent scene irradiance is increased to the same value at double the range. With the field of view held constant, detection and recognition range will depend on the overall system resolution.

An alternative method of increasing the apparent scene irradiance is to decrease the field of view. The change in field of view required to obtain the same level of apparent scene irradiance at range  $R_2$  as at some shorter range  $R_1$  is

$$\frac{\Omega_1}{\Omega_2} = k^2 \exp[2\alpha_o R_1(k - 1)] \quad (75)$$

by similarity to Eq. (74). If the sensor field of view is reduced in direct proportion, then detection range will also increase but not necessarily at the same rate as the decrease the linear field of view ( $\Omega^{\frac{1}{2}}$ ) due to atmospheric and perhaps other system defects such as sightline instability. The field of view tradeoffs will be further discussed below.

The second major effect of atmosphere on an active system is to decrease image contrast as is discussed in some detail by Rampolla in Ref. (5). The contrast reduction in general terms is given by

$$\frac{C_R}{C_0} = \left[1 + \frac{F_b}{F_s}\right]^{-1}, \quad (76)$$

where  $F_b$  is the total flux returned to the sensor by backscattering and  $F_s$  is the total signal flux.

For continuous wave, or CW, systems, the ratio  $F_b/F_s$  is given by \*

$$\frac{F_b}{F_s} = \frac{\alpha_a R_s^2 (\exp 2\alpha_a R)}{8\rho} \int_{R_0}^{R_s} \frac{\exp(-2\alpha_a R) dR}{R^2}, \quad (77)$$

where the distance limits,  $R_0$  and  $R_s$ , are obtained from the geometry of Fig. 25.

For the range gated active system, the contrast reduction by the atmosphere can be expected to be smaller, but the contrast reduction

---

\* In this formulation, we use the extinction coefficient,  $\alpha_a$ , which is corrected for slant path.



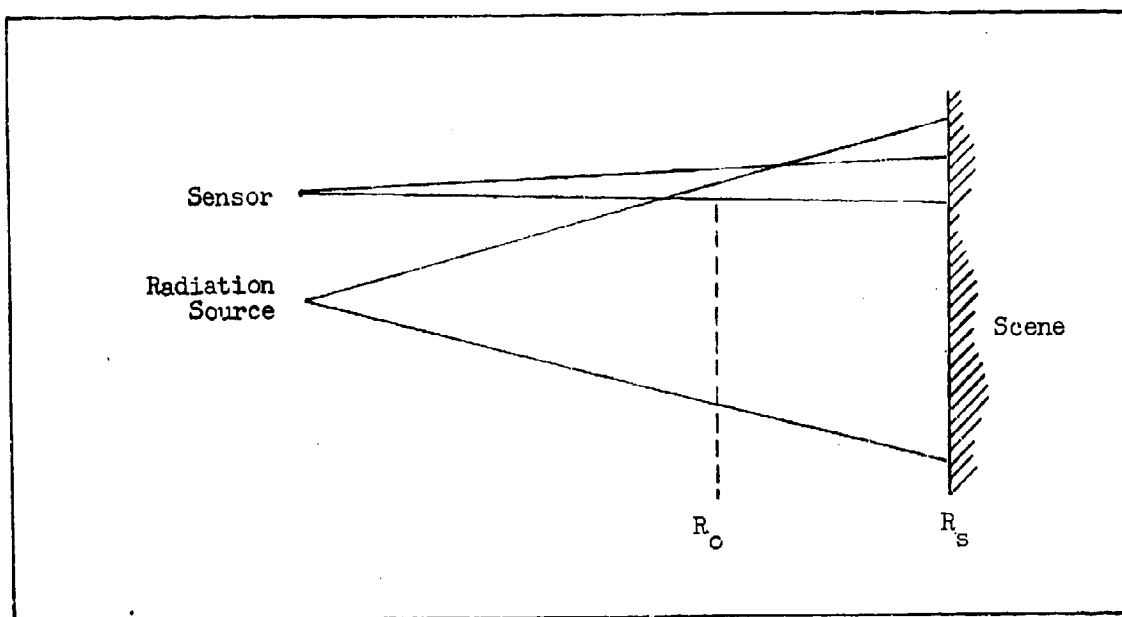


Fig. 25 Geometry for Backscatter Calculation - Sensor Not Range Gated.

calculations will be found to be much more complex. Hence, a number of simplifications are in order. The simplified geometry to be used is shown in Fig. 26. The duration of the radiation pulse is taken to be  $T$  seconds, and, the range increment corresponding to the pulse packet is  $cT/2$  where  $c$  is the velocity of light ( $9.835 \times 10^8$  ft/sec). If the radiation pulse is initiated at time zero, and if the sensor is gated on at time  $t_1$ , then we can locate the ranges from which echoes are received. The leading edge of the pulse can be located at range  $R_L$  and the trailing edge at range  $R_T$ . These ranges are

$$R_L = ct_1/2 \quad (78)$$

$$R_T = c(t_1 - T)/2 \quad (79)$$

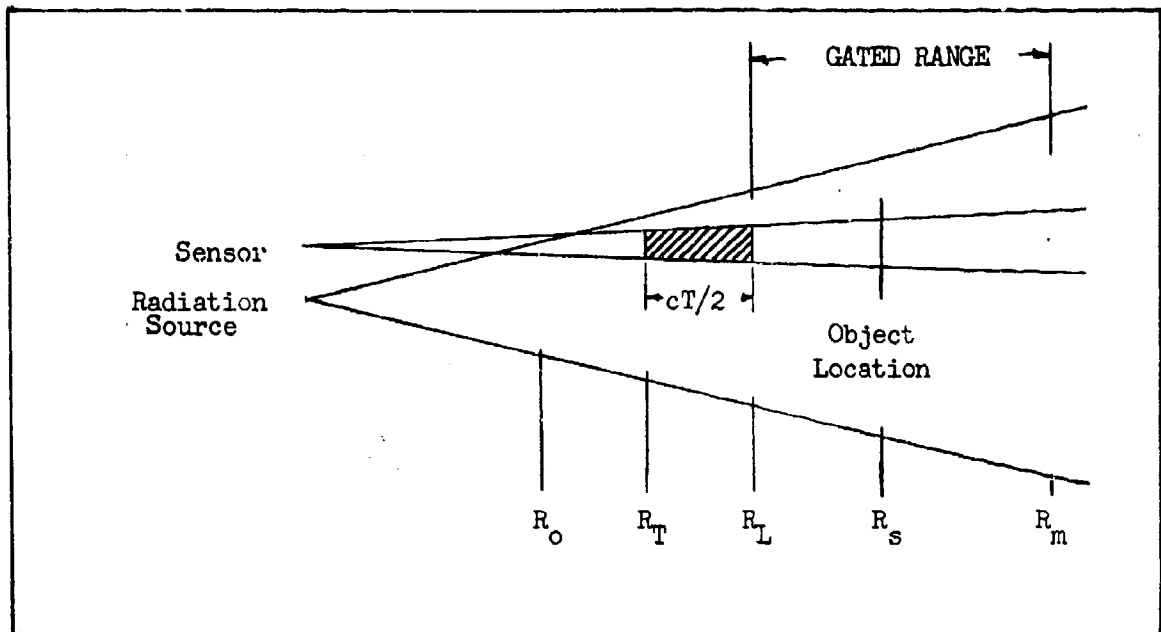


Fig. 26 Geometry for Backscatter Calculation - Range Gated Sensor.

The sensor is gated off at some time  $t_2$  and there will be a range  $R_m$  corresponding to this time. A scene object to be detected must be located approximately between the range limits  $R_L$  and  $R_m$ . (At slightly longer or shorter ranges, the object may be detected because of the radiator's finite pulse duration but the effective object radiance is reduced because only a part of the returned pulse is sensed.)

The ratio of  $F_b/F_s$  is determined from the relation

$$\frac{F_b}{F_s} = \frac{\alpha_a \left[ \int_{R_L}^{R_2} \frac{\exp(-2\alpha_a R)}{R^2} \left( \frac{R - R_T}{cT/2} \right) dR + \int_{R_2}^{R_s} \frac{\exp(-2\alpha_a R)}{R^2} dR \right]}{8\rho \exp(-2\alpha_a R_s) / R_s^2} \quad (80)$$

where limits are

$$\begin{aligned}
R_1 &= R_o \text{ if } R_o \geq R_T @ t_1 , \\
R_1 &= R_T \text{ if } R_o < R_T @ t_1 , \\
R_2 &= R_L \text{ if } R_s > R_L @ t_1 , \\
R_2 &= R_s \text{ if } R_s \leq R_L @ t_1 .
\end{aligned}
\tag{81}$$

The first term in Eq. (80) which is designated  $(F_b/F_s)_1$ , is repeated below as

$$\left[ \frac{F_b}{F_s} \right]_1 = \frac{\alpha_a \left[ \int_{R_1}^{R_2} \frac{\exp(-2\alpha_a R)}{R^2} \left( \frac{R - R_T}{cT/2} \right) dR \right]}{8\rho \exp(-2\alpha_a R_s)/R_s^2} ,
\tag{82}$$

is the component of backscatter due to the range interval from  $R_T$  to  $R_L$  in Fig. 26. Suppose that the object is at distance  $R_L$ . Then, the second term in Eq. (80) is zero and only Eq. (82) applies. A typical result for this special case is calculated using Eq.'s (76 and 82) and is plotted in Fig. 27. For this calculation, the radiation wavelength was taken to be 0.86 microns and a visibility of 10 n. miles was assumed for the purpose of obtaining the atmospheric extinction coefficient. The scene reflectivity used was 0.2.

For comparison purposes, the contrast degradation due to atmosphere is shown for a passive system on the same figure. Observe that at short ranges, that the active system is inferior to the passive system while the converse is true at long range. The inferior result at short range is due to the fact that very little of the atmosphere is range gated for close

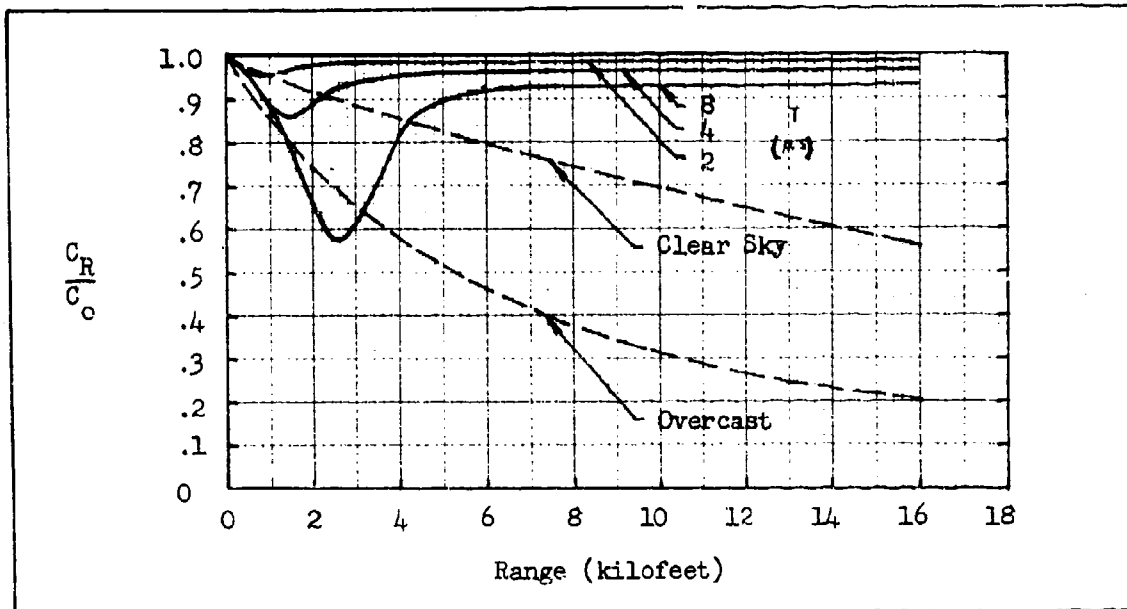


Fig. 27 Ratio of Apparent-to-Inherent Contrast for (—) Range Gated Active and (---) Passive Sensors for Background Reflectivity of 20% and 10 Nautical Mile Visibility.

in targets and the backscatter from the radiation source is larger than from an atmosphere irradiated by a natural source such as the moon.

In the general case, the object will be at some range  $R_s$  greater than  $R_L$ . In this case, we will prefer to determine the ratio  $F_b/F_s$  in the form

$$\frac{F_b}{F_s} = \frac{K}{\rho} \left[ [F_b'(T, R_L)]_1 + [F_b'(R_s)]_2 - [F_b'(R_L)]_2 \right], \quad (83)$$

where

$$K = \frac{R_s^2}{8 \exp(-2\alpha_a R_s)}, \quad (84)$$

and

$$[F_b'(T, R_L)]_1 = \alpha_a \int_{R_L - cT/2}^{R_L} \frac{\exp(-2\alpha_a R) [R - (R_L - cT/2)] dR}{R^2}, \quad (85)$$

and

$$[F_b'(R_s)]_2 = \alpha_a \int_{R_k}^{R_s} \frac{\exp(-2\alpha_a R) dR}{R^2}, \quad (86)$$

and

$$[F_b'(R_L)]_2 = \alpha_a \int_{R_k}^{R_L} \frac{\exp(-2\alpha_a R) dR}{R^2}. \quad (87)$$

The function  $[F_b'(T, R_L)]_2$  cannot be solved in closed form and is best computer calculated. This function has been calculated and tabulated in Ref. 2 for two pulse durations and various visibilities. To give insight to the operation of an active sensor two cases are considered. In the first case, the leading edge, or the near point range gate, of the pulse is fixed at a range  $R_{L1}$  and the ratio of apparent-to-inherent contrast is calculated as the object is moved from range  $R_{L1}$  to  $R_{L2}$ . Then, the leading edge is moved to  $R_{L2}$  and the object is moved from  $R_{L2}$  to  $R_{L3}$ , etc., as shown in Fig. 28. In this figure, and the next, the radiation wavelength was 0.86 micrometers, the scene reflectivity was 0.2, the pulse duration was 2  $\mu$ s, and the meteorological visibility was 10 n. m. With the visibility of 10 n. m., and radiation pulse duration of 2  $\mu$ s, the contrast degradation due to the finite pulse duration [the first term in Eq. (83)] can be neglected. Note in the Fig. 28, that the observer can increase the apparent contrast of the object to nearly

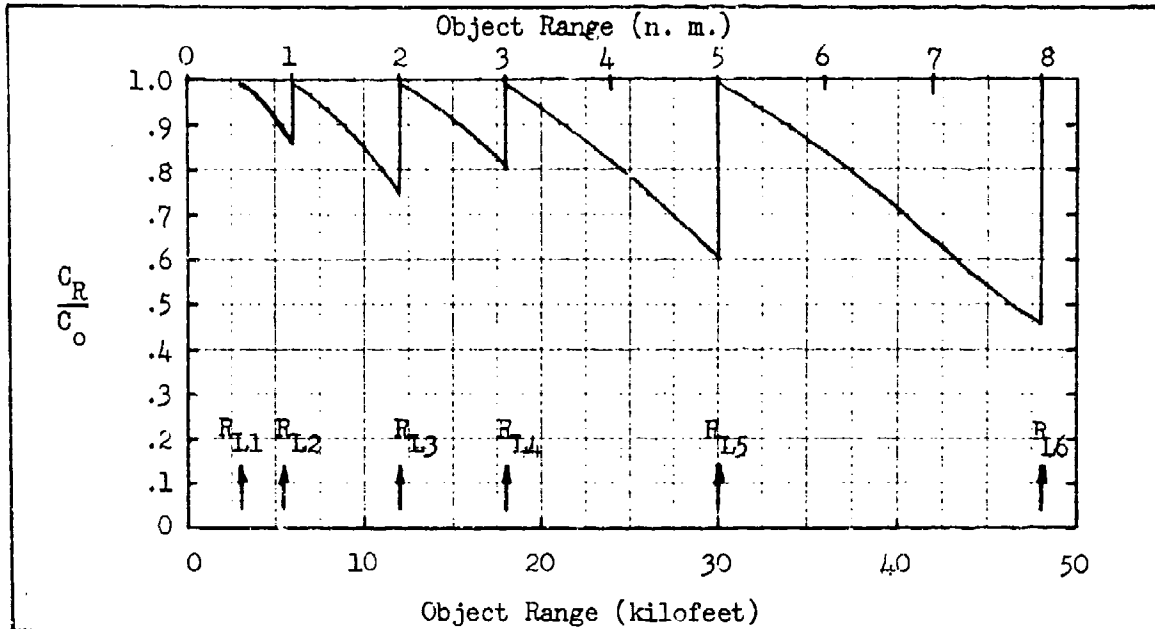


Fig. 28 Ratio of Apparent to Inherent Object Contrast vs Range for a Near Point Gate Fixed at  $R_{L0}$  for Objects in the Range Interval  $R_{Ln}$  to  $R_{Ln+1}$ . 10 n. mi. Visibility at 0.86 micrometers with Scene Reflectance = 0.2 and  $T = 2 \mu s$ .

its inherent value at anytime by adjusting the near point range gate so that it falls just in front of the object being viewed.

In a more practical situation, we assumed that the range gate was movable and that the object was located in the center of the range gate, i.e., midway between the near point as set by sensor turn on time,  $t_1$ , and the far point as set by the sensor turn off time,  $t_2$ . The results are shown in Fig. 29. In this calculation, the range gate was made progressively larger as distance was increased to illustrate the effect of various range gate widths. This figure is probably representative of the typical search condition. Once an object has been detected, the observer will probably adjust the range gate near point to increase the object contrast.

Instead of the Steingold and Strauch relation of Eq. (73), the

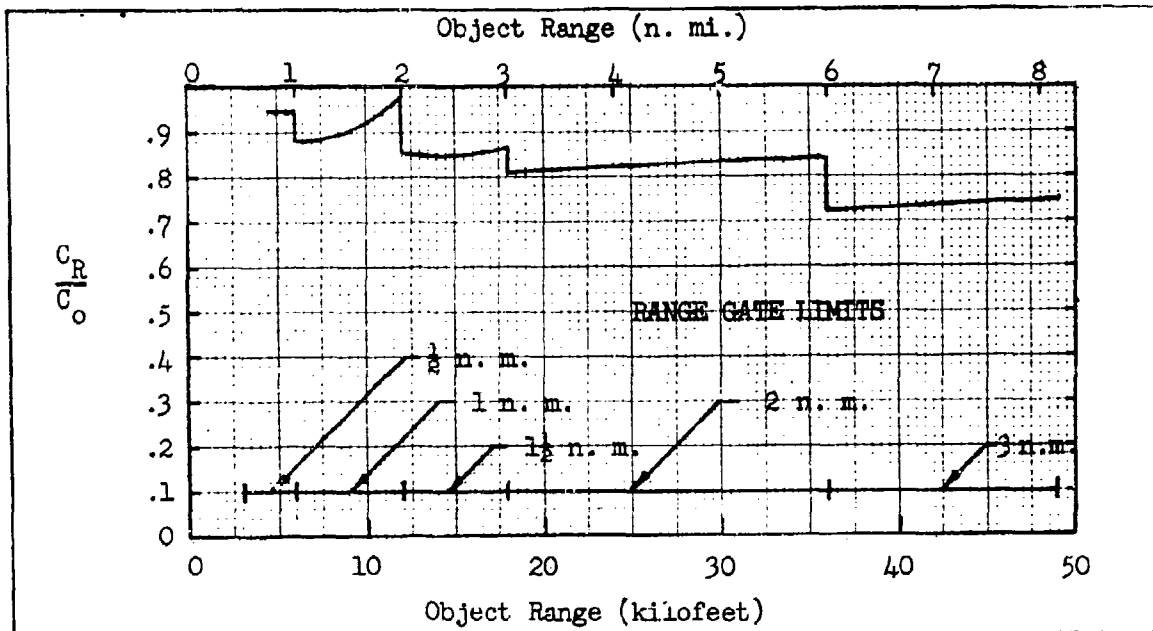


Fig. 29 Ratio of Apparent to Inherent Contrast vs Range for Objects in the Middle of the Range Gate Limits. Visibility at 0.86 micrometers is 10 n. m. with Average Scene Reflectance = 0.2.  $T = 2 \mu s$ .

table of Ref. (8) may be used. The table for  $\lambda = 0.86$  micrometer is reproduced here on Table 9. For an altitude of 2 - 3 km and a clear midlatitude winter,  $\sigma \approx 0.0127 \text{ km}^{-1}$ .

### 3.2 Objective Lens, Sightline Instability and Photosurface Parameters

In many, but not all cases, it is possible to resolve scene detail at longer range by increasing the lens focal length. However, the increase in range may be smaller than first thought due to inadequate sensitivity or to sightline instability. For example, when the focal length of the lens is increased, the lens f-number decreases (assuming constant aperture) and the light level on the photosurface decreases. Then, the signal-to-noise ratio obtainable from the sensor may decrease, reducing the overall sensory system resolution.

$\lambda = 0.86 \mu\text{m}$

Altitude (km)	TROPICAL		MIDLATITUDE SUMMER		MIDLATITUDE WINTER		SUBARCTIC SUMMER		SUBARCTIC WINTER		CLEAR AEROSOL		HAZY AEROSOL	
	$k_m$ ( $\text{km}^{-1}$ )	$\sigma_m$ ( $\text{km}^{-1}$ )	$k_m$ ( $\text{km}^{-1}$ )	$\sigma_m$ ( $\text{km}^{-1}$ )	$k_m$ ( $\text{km}^{-1}$ )	$\sigma_m$ ( $\text{km}^{-1}$ )	$k_m$ ( $\text{km}^{-1}$ )	$\sigma_m$ ( $\text{km}^{-1}$ )	$k_m$ ( $\text{km}^{-1}$ )	$\sigma_m$ ( $\text{km}^{-1}$ )	$k_m$ ( $\text{km}^{-1}$ )	$\sigma_m$ ( $\text{km}^{-1}$ )	$k_m$ ( $\text{km}^{-1}$ )	$\sigma_m$ ( $\text{km}^{-1}$ )
0	<E-06	1.89E-03	<E-06	1.93E-03	<E-06	2.09E-03	<E-06	1.97E-03	2.27E-03	<E-06	1.52E-02	9.03E-02	7.43E-02	4.40E-01
0-1		1.91E-03		1.84E-03		1.98E-03		1.87E-03	2.06E-03		1.01E-02	5.99E-02	4.49E-02	2.66E-01
1-2		1.64E-03		1.66E-03		1.77E-03		1.69E-03	1.81E-04		4.41E-03	2.61E-02	1.64E-02	8.72E-02
2-3		1.49E-03		1.50E-03		1.58E-03		1.53E-03	1.60E-04		1.89E-03	1.11E-02	6.00E-03	2.56E-02
3-4		1.34E-03		1.36E-03		1.41E-03		1.37E-03	1.42E-04		8.04E-04	5.24E-03	2.18E-03	1.30E-02
4-5		1.22E-03		1.22E-03		1.26E-03		1.23E-03	1.27E-04		5.58E-04	3.30E-03	8.00E-04	4.71E-03
5-6		1.10E-03		1.10E-03		1.13E-03		1.11E-03	1.13E-04		4.07E-04	2.41E-03	4.07E-04	2.41E-03
6-7		9.92E-04		9.90E-04		1.00E-03		9.93E-04	1.01E-04		3.29E-04	1.94E-03	3.29E-04	1.94E-03
7-8		8.94E-04		8.97E-04		8.92E-04		8.90E-04	8.94E-04		3.22E-04	1.91E-03	3.22E-04	1.91E-03
8-9		8.00E-04		7.95E-04		7.90E-04		7.95E-04	7.84E-04		3.20E-04	1.90E-03	3.20E-04	1.90E-03
9-10		7.15E-04		7.11E-04		6.98E-04		7.08E-04	6.78E-04		3.10E-04	1.83E-03	3.10E-04	1.83E-03
10-11		6.38E-04		6.32E-04		6.08E-04		6.19E-04	5.78E-04		2.96E-04	1.75E-03	2.96E-04	1.75E-03
11-12		5.67E-04		5.60E-04		5.22E-04		5.32E-04	4.94E-04		2.94E-04	1.74E-03	2.94E-04	1.74E-03
12-13		5.01E-04		4.95E-04		4.47E-04		4.57E-04	4.22E-04		2.89E-04	1.71E-03	2.89E-04	1.71E-03
13-14		4.43E-04		4.30E-04		3.84E-04		3.93E-04	3.61E-04		2.75E-04	1.63E-03	2.75E-04	1.63E-03
14-15		3.93E-04		3.67E-04		3.29E-04		3.37E-04	3.08E-04		2.64E-04	1.56E-03	2.64E-04	1.56E-03
15-16		3.39E-04		3.12E-04		2.82E-04		2.90E-04	2.64E-04		2.49E-04	1.48E-03	2.49E-04	1.48E-03
16-17		2.92E-04		2.67E-04		2.42E-04		2.50E-04	2.26E-04		2.42E-04	1.43E-03	2.42E-04	1.43E-03
17-18		2.45E-04		2.28E-04		2.07E-04		2.15E-04	1.94E-04		2.36E-04	1.40E-03	2.36E-04	1.40E-03
18-19		2.03E-04		1.88E-04		1.77E-04		1.85E-04	1.66E-04		2.13E-04	1.26E-03	2.13E-04	1.26E-03
19-20		1.68E-04		1.66E-04		1.52E-04		1.59E-04	1.42E-04		1.68E-04	1.68E-04	1.68E-04	9.94E-04
20-21		1.40E-04		1.42E-04		1.29E-04		1.36E-04	1.22E-04		1.22E-04	7.25E-04	1.22E-04	7.25E-04
21-22		1.17E-04		1.21E-04		1.10E-04		1.17E-04	1.04E-04		9.04E-05	5.36E-04	9.04E-05	5.36E-04
22-23		9.84E-05		1.03E-04		9.43E-05		1.01E-04	8.89E-05		6.96E-05	4.06E-04	6.96E-05	4.06E-04
23-24		8.35E-05		7.50E-05		6.88E-05		7.41E-05	7.60E-05		5.34E-05	3.16E-04	5.34E-05	3.16E-04
24-25		7.09E-05		6.48E-05		5.98E-05		6.41E-05	6.49E-05		4.36E-05	2.59E-04	4.36E-05	2.59E-04
25-30		4.73E-05		5.64E-05		4.59E-05		5.01E-05	4.31E-05		2.20E-05	1.30E-04	2.20E-05	1.30E-04
30-35		2.16E-05		2.32E-05		2.07E-05		2.35E-05	1.91E-05		6.19E-06	3.67E-05	6.19E-06	3.67E-05
35-40		1.03E-05		1.11E-05		9.27E-06		1.11E-05	8.60E-06		1.63E-06	8.63E-06	1.63E-06	8.63E-06
40-45		5.04E-06		5.44E-06		4.71E-06		5.48E-06	3.94E-06		<E-06	<E-06	<E-06	<E-06
45-50		2.56E-06		2.79E-06		2.31E-06		2.85E-06	1.88E-06		<E-06	<E-06	<E-06	<E-06
50-70		<E-06		1.05E-06		<E-06		1.05E-06	1.05E-06		<E-06	<E-06	<E-06	<E-06
70-100				<E-06		<E-06		<E-06	<E-06		<E-06	<E-06	<E-06	<E-06

Table 9. Values of Attenuation Coefficient/km as a Function of Altitude for Laser Wavelength = .86  $\mu\text{m}$  ( $k_m$  = molecular absorption,  $\sigma_m$  = molecular scattering,  $k_a$  = aerosol absorption,  $\sigma_a$  = aerosol scattering).



In object space, the most meaningful measure of resolution from an imaging system point of view is an object's angular subtense. Specifically, let  $\Delta\theta$  be the angular subtense of an object of size  $y_o$ , at range  $R$ .

For small angles

$$\Delta\theta = y_o/R \quad (88)$$

In the image space of an infinity focused object,

$$\Delta\theta = \Delta y/F_L \quad (89)$$

Alternatively, resolution is often expressed in terms of an angular frequency  $k_\theta$  where

$$k_\theta = \frac{1}{2\Delta\theta} \frac{\text{cycles}}{\text{radian}} \quad (90)$$

The primary objective lens parameters are its light transmission,  $\tau_o$ , diameter,  $D_o$ , focal length,  $F_L$ , and modulation transfer function,  $R_o(k_\theta)$ . For a simple, infinity focused objective lens, the focal plane irradiance  $E$ , is related to the scene radiance,  $L$ , by the approximate relation

$$E \approx \frac{\pi\tau_o L}{4f^2} \quad (91)$$

where  $f$ , the focal ratio or "f-number" is equal to  $F_L/D_o$ .

A circular, diffraction-limited lens has an MTF (for monochromatic light) equal to

$$R_o(k) = \frac{2}{\pi} (\varphi - \cos\varphi \sin\varphi)(\cos\varphi)^\gamma \quad (92)$$

where  $\theta$  is the half field angle,  $\gamma = 1$  for radial lines and 3 for tangential

lines and

$$\varphi = \cos^{-1}\left(\frac{\lambda k}{f}\right), \quad (93)$$

$k$  is a spatial frequency in cycles/millimeter, and  $\lambda$  is the light's wavelength. When resolution is given, in terms of  $k_{\theta}$  cycles/radian,

$$\Phi = \cos^{-1} \lambda k_{\theta} D_o, \quad (94)$$

which shows that the angular resolution of a diffraction limited lens is a function of the lens diameter only. The spatial frequency goes to zero when  $\varphi = 0$ . This spatial frequency is

$$k_c = \frac{1}{\lambda f} \frac{\text{cycles}}{\text{mm}}, \quad (95)$$

and

$$k_{\theta c} = \frac{D_o}{\lambda} \frac{\text{cycles}}{\text{radian}}. \quad (96)$$

It should be apparent that with a diffraction limited lens image plane resolution cannot be increased by simply increasing lens focal length. Increases in image plane resolution are obtained only by an increase in lens diameter. However, as will be seen overall system resolution can be improved by increasing the lens focal length when the sensor parameters are considered.

A point is imaged by a lens as a blur. The effective blur width, defined by a rectangle of amplitude equal to the actual blur amplitude and of area equal to the actual blur area is approximately equal to  $2\lambda/D$  radians. An insight to the above discussion can be gained by reference to Fig. 30. The diffraction limited optical blur  $\Delta\theta$  is independent of focal length for

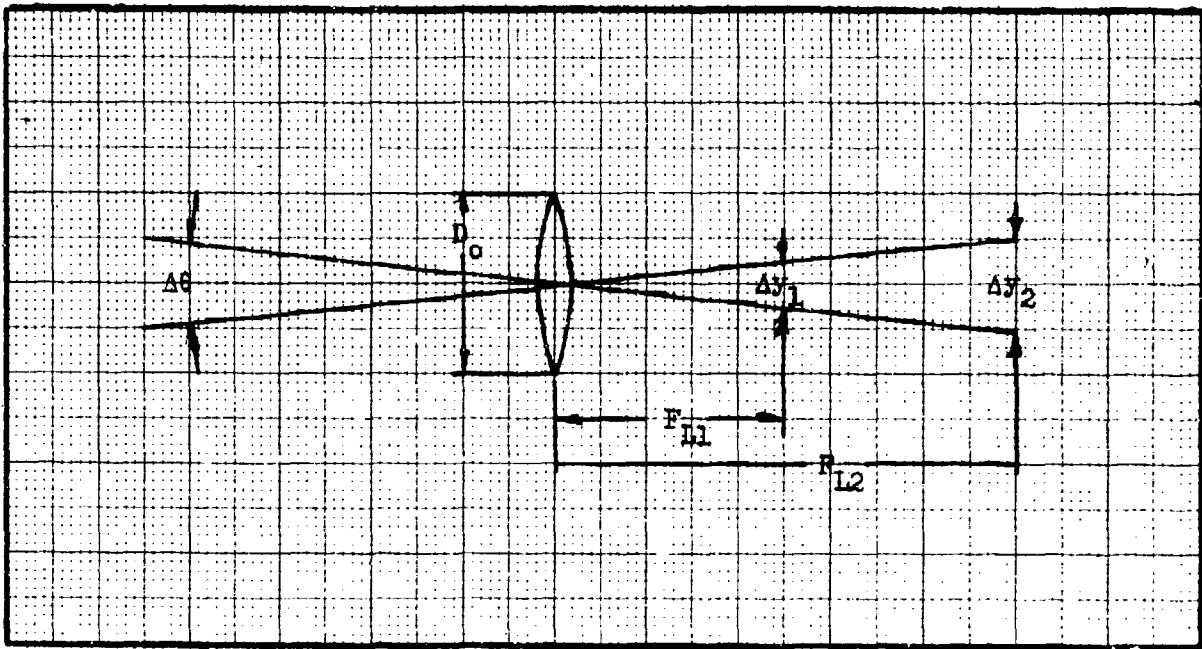


Fig. 30 Relationship Between Focal Length and Image Size

a lens of fixed diameter. Thus, it will be of size  $\Delta y_1$  with focal length  $F_{L1}$  and of larger size  $\Delta y_2$  at longer focal length  $F_{L2}$ . The longer focal length represents a longer lens and a larger effective focal plane area for a given field of view but may be an advantage from two other points of view. First, the f-number is larger for the lens of longer focal length and a lens with a high f-number is generally cheaper and easier to manufacture. In addition, the lens elements of a lens with a higher f-number will have less curvature and higher transmittance. The smaller curvature of the lens elements usually results in smaller aberrations and thus a higher MTF for lenses which are not diffraction limited.

The focal plane irradiance is smaller for a lens of longer focal length. For equal fields of view, however, the photosurface area will be

larger for the longer focal length. Thus, the product of irradiance ( $\text{Watts/m}^2$ ) and total areas ( $\text{m}^2$ ) is the same for both the long and short focal length configurations, i.e., the same total amount of light falls on both focal planes. In television practice, the sensitivity of the total system (remembering the assumed constraints of equal optic diameter and field of view) is independent of lens focal length. In photographic practice, this is also generally true but what the photographer has in mind when he goes to larger film formats, is to obtain increased scene resolution by virtue of the superior MTF of the larger film. More light is required to achieve this goal. In TV, the resolution is more often limited by scan line number and bandwidth constraints and a larger photosurface/longer focal length combination results in no sensitivity and little or no resolution change when lens diameter is fixed.

A larger photosurface is sometimes necessary. As we will see, the overall sensitivity of a photoelectron noise limited system is directly proportional to the lens diameter. As a practical rule, lens f-numbers cannot be much less than one. Hence, the diameter of a 3" focal length lens cannot be much larger than about 3". If more lens diameter is needed, it is necessary to increase lens focal length and photosurface area in turn (to obtain the same field of view).

The photosurface current for a linear photoemitter is given by

$$i_s = \int_0^\infty S(\lambda)AE(\lambda)d\lambda \quad , \quad (97)$$

where  $S(\lambda)$  is the spectral responsivity,  $A$  is the effective area and  $E(\lambda)$  is the spectral irradiance of the photosurface. For a specific

test source  $E_T$ , a specific responsivity  $S_T$  may be defined. In this case, the simpler relation

$$i_T = S_T E_T \quad , \quad (98)$$

may be written.

A specific responsivity to tungsten light at a color temperature of  $2854^\circ$  K is commonly used in commercial broadcast practice. Since broadcast cameras are often spectrally filtered to have a response similar to the eye and because of the availability of photometers, it is common to give specific response in Amperes/lumen. Quantitatively,

$$S_T = \frac{\int_0^\infty S(\lambda)M(\lambda)d\lambda}{\int_0^\infty 680 \bar{y}(\lambda)M(\lambda)d\lambda} \quad \frac{\text{Ampere}}{\text{lumen}} \quad , \quad (99)$$

where  $M(\lambda)$  is the radiant exitance of the tungsten lamp and  $\bar{y}(\lambda)$  is the relative response of the human eye. The specific response of the S-20 photosurface, when unfiltered, is typically 150 micro-Amperes/Watt.

A noise is generated in the photoconversion process. The elementary imaging model gives the signal to noise ratio for an elementary image area,  $a$ , as

$$\text{SNR}_{PC} = \left[ t \left( \frac{a}{A} \right) \right]^{\frac{1}{2}} \frac{\Delta i_T}{[e i_{TAV}]^{\frac{1}{2}}} \quad , \quad (100)$$

where  $t$  is the integration time of the photoelectron signal,  $a/A$  is the relative image area,  $\Delta i_T$  is the incremental image signal,  $i_{TAV}$  is the

average photocurrent and  $e$  is the charge of an electron. Actually, the integration time may be near zero at the point of photoemission, i.e., the photoemission is near instantaneous. The actual signal and noise integration takes place later in the signal processor or in the observer's eye. Aside from temporal integration, the signal-to-noise ratio in the system is nowhere higher than it is at the output of the photosurface.

Observe that  $SNR_{PC}$  may be written in terms of the scene and lens parameters using Eq. 91 as

$$\begin{aligned}
 SNR_{PC} &= \left[ t \left( \frac{a}{A} \right) \right]^{\frac{1}{2}} \frac{S_T A \pi \tau_o \Delta L_T / 4f^2}{[S_T A \pi \tau_o e A L_{Tav} / 4f^2]^{\frac{1}{2}}} \\
 &= \left[ \frac{t a S_T \pi \tau_o}{e} \right]^{\frac{1}{2}} \frac{D_o}{2F_L} \frac{\Delta L_T}{(L_{Tav})^{\frac{1}{2}}}, \quad (101)
 \end{aligned}$$

which shows that for a photoelectron noise limited system, the SNR is directly proportional to the lens diameter. If the photoelectron noise is negligible compared to the system noise then the SNR (at some later point in the system) takes the form

$$SNR_S = \left[ \frac{t a S_T \pi \tau_o}{e} \right]^{\frac{1}{2}} \frac{D_o^2}{4F_L^2} \frac{\Delta L_T}{(L_N/A^{\frac{1}{2}})}, \quad (102)$$

where it is seen that the SNR is proportional to the lens diameter squared.

The photosurface MTF is usually, but not always, quite high so that it can be neglected.

Suppose next that the optical line of sight is in motion. Assume that the photocathode is a photoemitter and that the photoemission process is nearly instantaneous. Then the photoelectron image formed will be in apparent motion. By apparent motion we mean that the intensity distribution of an image will move in accord with the movement of the line of sight. The photoelectron image is next accelerated to either a phosphor or to a gain storage target in the case of a camera tube. A phosphor usually has a significant time constant and a camera tube usually has both an integration period and a time constant. In either case, a moving point image is smeared out and the amount of smearing can be quantitatively described in terms of an optical transfer function. The photoelectron image however moves in direct correspondence with the image of the scene and therefore no motion MTF exists at the point of photoconversion. We will discuss the motion MTF in connection with the camera tube gain-storage target.

We observed that the lens has an optical transfer function. The effect of the lens OTF, as we noted in section 2, on periodic bar patterns is to reduce signal in the periodic direction and increase perceived noise in the aperiodic direction. Using the periodic form of the SNR equation, we find that the  $SNR_P$ , including the lens, becomes

$$SNR_{PC} = \left[ \frac{t_f \epsilon}{\alpha} \right]^{\frac{1}{2}} \frac{R_{SF}(N)}{\xi^{\frac{1}{2}} \cdot N} \frac{2C M_{av} i}{[e i_{av}]^{\frac{1}{2}}}, \quad (103)$$

where  $R_{SF}(N)$  is the square wave flux factor for the lens and  $\xi$  is the lens' noise increase factor as defined in section 2 [see Eqs. (37) and (51)], and  $t_f$  is the frame or exposure time.

Photoelectron noise is signal level dependent, i.e., the higher the photon flux, the larger the photoelectron noise. Photosurfaces may also exhibit a dark current due to thermionically generated electrons. For the S-20 or S-25 photosurface, this noise is generally negligible but may have to be considered in long exposure applications. The S-1 and S-10 photocathodes have a fairly large dark current and dark current noise must be included. The dark current noise due to a dark current,  $i_d$ , adds in quadrature in the  $SNR_D$  equation, i.e.,

$$SNR_{PC} = \left[ \frac{t_f \epsilon}{\alpha} \right]^{\frac{1}{2}} \frac{R_{SF}(N)}{\xi^2 \cdot N} \frac{2C_M i_{av}}{[e i_{av} + e i_d]^2} \quad (104)$$

Having noted the possibility of a dark current noise, we will elect to ignore it in the analysis that follows.

The above discussion applies equally well to active and passive sensors.

### 3.2.1 Objective Lens Parameters (Passive)

Passive television systems fall into two general categories - those which are primarily used in daylight and those which are primarily used at night. In the night case, high sensitivity is of considerable importance. As was shown in the previous section, the image  $SNR_{PC}$  is directly proportional to the lens diameter for a photoelectron noise limited camera. For a given field of view, therefore, the  $SNR_{PC}$  is directly proportional to the lens T-stop. In the current state of the art, viewing of nocturnal scenes requires objective lens T-stops of the order of 1 to 2. If system noise is a factor, then the  $SNR_{PC}$  is proportional to the T-stop raised to some power between 1 and 2. Thus, the further a



camera departs from a photoelectron noise-limited condition, the more important the T-stop becomes.

In daylight, the designer can use rather insensitive camera tubes such as the vidicon combined with relatively fast lenses (T/2 to T/4) or camera tubes of moderate to high sensitivity such as the silicon vidicon or EBSICON with rather slow lenses (T/4 to T/20). In the vidicon case, the system is system (preamp) noise limited and the  $SNR_{PC}$  is proportional to the T-stop squared. While the lens T-stop is not very important in bright sunlight conditions, it becomes very important under heavy overcast skies and at sunset. The more sensitive cameras such as the EBSICON are partly photoelectron and partly system noise limited for which the comments of the first paragraph apply.

In daylight operations, systems with long focal length lenses can be employed. Fields of view of the order of  $\frac{1}{2}^{\circ}$  to  $2^{\circ}$  are entirely feasible using lenses of focal length of about 10" to 50". The T-stops, using the more sensitive camera tubes can be quite large so that lens diameters need not be more than a few inches. Lens weights are not usually more than a few pounds except when optical zoom or other features are wanted. Even then, lens weights should be modest.

Very small fields of view are not feasible with current passive night sensors. With a 25 mm photocathode and a 250 mm focal length lens, the diagonal field of view will be about  $5.7^{\circ}$ . Lens weight for a T/1.5 lens will be typically 50 lbs. Halving the field of view to  $2.35^{\circ}$  while holding the T-stop constant will increase weight 8 fold to near 400 lbs.

To summarize, we note that lens T-stop is of considerable importance to passive systems where scene irradiance levels are low. In daylight,

camera systems using relatively insensitive camera tubes need fairly fast lenses and are restricted to moderately larger fields of view. Using the more sensitive camera tubes, T-stops can be increased and very small fields of view become possible. At night, the very small fields of view are not feasible due to the requirement of a low T-stop value.

### 3.2.2 Objective Lens Parameters (Active)

It is not now practical to construct range gated active TV systems for daylight use, because the amount of irradiator power available is insufficient to compete with the sunlit passive scene. However, the active optical imaging system makes possible small field of view systems at night without the need for immense objective lenses. This results from the fact that as the sensor field of view is reduced, the scene irradiator field of view also shrinks in direct proportion. To prove this result, we write the sensor photocurrent as

$$i = \frac{\pi S_T A_T \tau_o L_T}{4f^2} = \frac{\pi S_T A_T \tau_o D_o^2 L_T}{4F_L^2} \quad (105)$$

For small angles the solid angle field of view is

$$\Omega = \frac{\pi D_o^2}{4F_L^2} \quad , \quad (106)$$

so that

$$i = S_T A_T \tau_o \Omega L_T \quad , \quad (107)$$

and the scene irradiance due to the system source is

$$L_T = \frac{o\Phi_s \exp(-2\alpha_o P)}{\pi \Omega R^2} \quad , \quad (108)$$

and as a consequence,

$$i = \frac{S_T A_T \Omega_0 \Phi_s \exp(-2\alpha_0 R)}{\pi R^2} \quad (109)$$

That is, the sensor photocurrent is independent of the field of view for an active system whose field of view is matched to the irradiator field of view.

### 3.3 Image Tube Parameters, Image Motion Effects

The photosurface may be considered to be the sensor while that portion of the image tube following the photosurface is part of the signal processor. The primary function of the signal processor is to amplify and magnify the image prior to its viewing by an observer.

The simplest form of imaging tube is the image intensifier. In this device the photoelectron image generated by the input photosurface is accelerated to a phosphor which recreates a visible light image which may be directly viewed by an observer or coupled to other image tubes for the purpose of obtaining further image amplification and/or magnification. The phosphor usually provides a light gain, i.e., the output image will be brighter than that incident on the photosurface. The gain of a modified P-20 phosphor is typically 1,000 but since the photosurface quantum efficiency is generally about 5 to 10% (for white light), the overall gain is reduced to 50 - 100. Note also that the input image light level is less than the scene light level due to the light gathering efficiency of the lens. With a T/1.5 lens, the image irradiance is but 1/10 that of the reflected scene irradiance. Thus the overall gain of the image intensifier including the lens is but 5 - 10. Part of the gain results from the fact that a broad wavelength spectrum

of scene light is compressed spectrally to narrow band green by the phosphor. The eye is most sensitive to green and thus, even without a phosphor gain in terms of photons/electron, a gain of 2 - 4 is realized. Thus, the brightness gain of an intensifier (ignoring the losses in the objective lens) is typically 100 for a good intensifier with S-25/P-20 photocathode-phosphor combination. The gains above apply to an intensifier with unit magnification which implies a photosurface area equal to the phosphor area. If the areas are different, the net gain,  $G_I$ , is equal to

$$G_I = \frac{A_{pc}}{A_{ph}} G_B, \quad (110)$$

where  $A_{pc}$  is the photocathode area,  $A_{ph}$  is the phosphor area and  $G_B$  is the brightness gain for an intensifier of unit magnification. Observe however that the area gain is realized for the overall system only if the optic area is correspondingly increased as discussed in the previous section (for a given field of view).

Additional light amplification may be obtained by cascading one or more intensifiers to the first. To obtain appreciable gain (more than 1 - 4), the intensifiers must be coupled by means of fiber optic endplates rather than by an optical relay lens. With fiber optic coupling from P-20 phosphor to S-20 photocathode, a gain of 25 - 40 is typically obtained per intensifier. This is less than that obtained in the first stage viewed directly by the eye because the second stage intensifier photocathode is not as efficient as the retina in converting the green phosphor light. But note that the "green gain" is still obtained when the observer views the second stage phosphor.

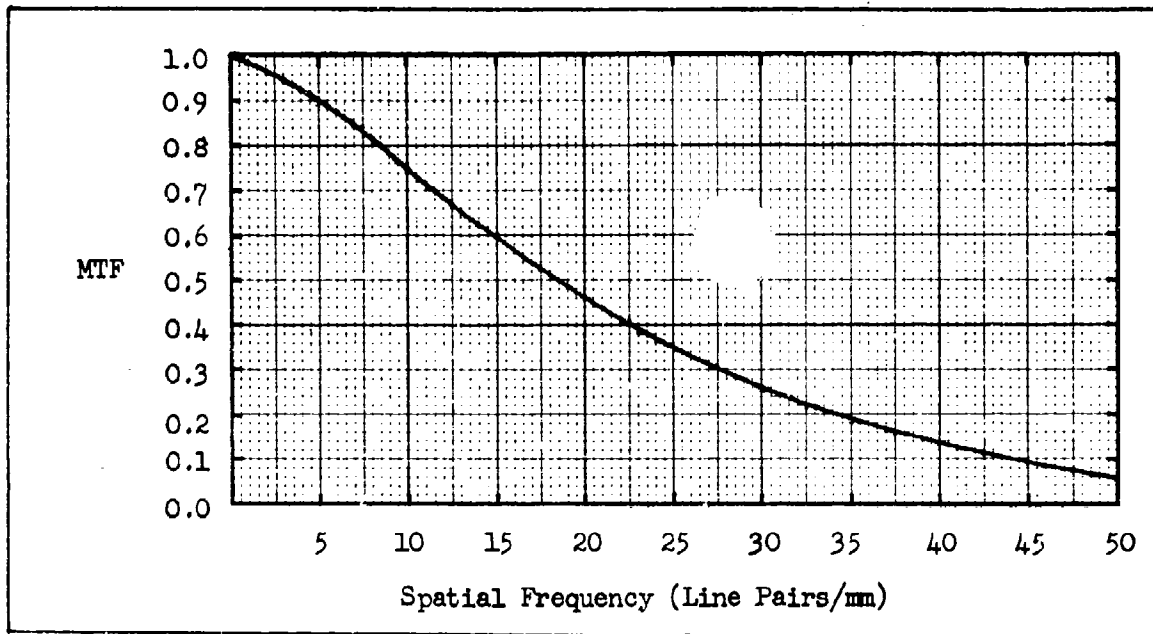


Fig. 31 Modulation Transfer Function for a Typical Image Intensifier.

The MTF of a typical intensifier is given in Fig. 31 for spatial frequencies in terms of line pairs/mm. With spatial frequency expressed in these terms, the MTF is relatively independent of photocathode or phosphor diameter except for photocathodes that are smaller than about 16 mm. Here it becomes necessary to take the MTF of the fiber optic faceplates into account. The principal MTF limiting factor in an intensifier with P-20 phosphor is the phosphor itself. With spatial frequency expressed in terms of lines/picture height, the MTF becomes phosphor diameter dependent as shown in Fig. 32.

In Fig. 33 we show an intensifier coupled to an EBSICON TV camera tube. This particular intensifier incorporates electronic viewfield zoom whereby the effective photosurface area can be varied from 80 to 40 mm. Since the intensifier MTF is limited by the phosphor, which is the same size

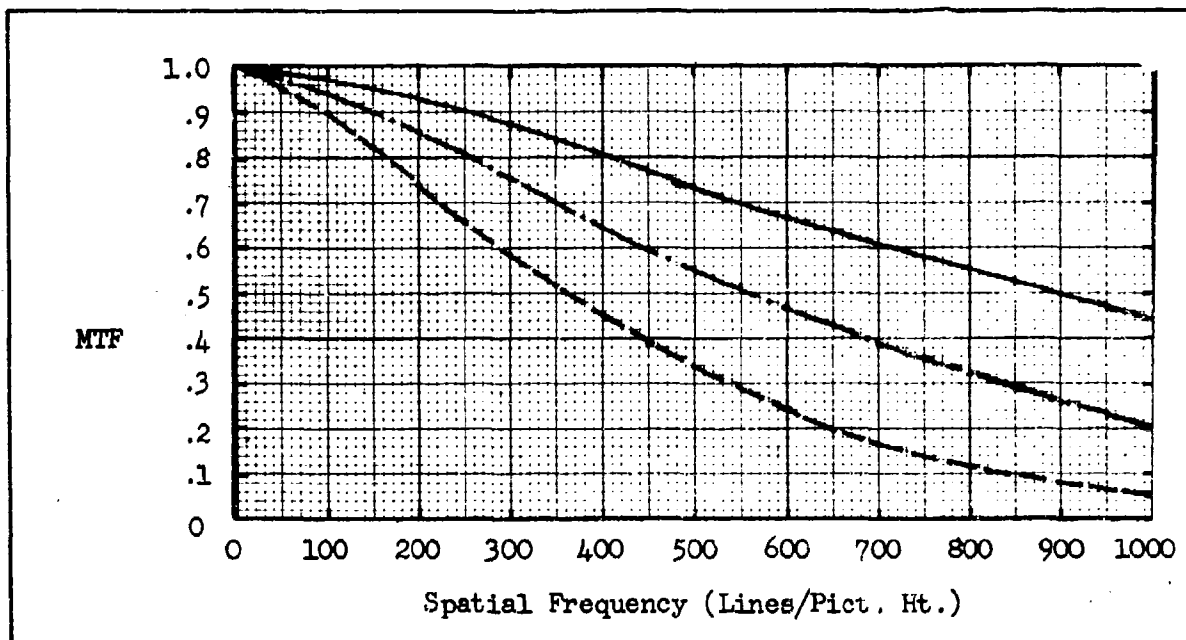


Fig. 32 Modulation Transfer Function for a Typical Image Intensifier with (—) 40, (— ·) 25 and (— —) 16 mm Phosphor Diameter.

for both the wide angle view (WAV) and narrow angle view (NAV), the effective scene resolution decreases in the WAV, i.e., scene resolution is exchanged for field of view. The lens T-stop is fully utilized in both the WAV and NAV but because of the larger effective photocathode area in the WAV, signal current in the WAV increases 4-fold. In general, electronic viewfield zoom is superior to optical zoom because of the difficulty in realizing a low T-stop in the WAV position in optical zoom lenses, i.e., sufficient to offset the photocathode area increase obtained in the electronic zoom case. If constant aperture could be realized with optical zoom, then electronic and optical zoom would be comparable. The intensifier phosphor has a finite time constant which results in some signal storage but generally this storage is

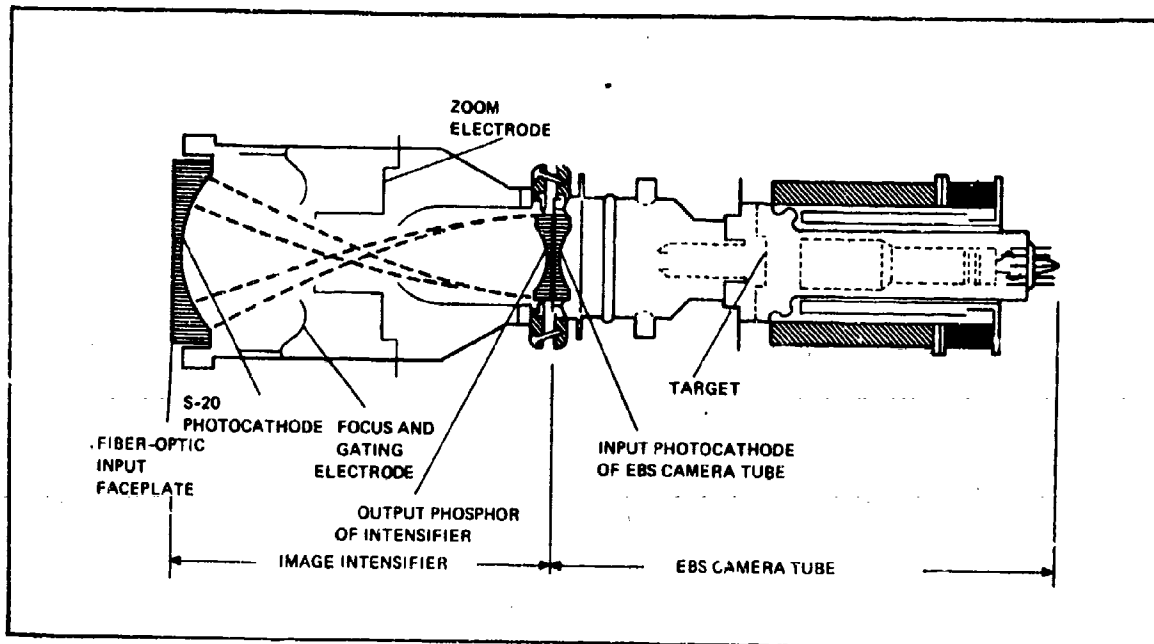


Fig. 33 Schematic of an Intensified-EBSICON Camera Tube.

negligible compared to that occurring in either the TV camera or the observer's eye.

The EBSICON TV pick-up tube may be used either with or without an image intensifier. In either case, a photon image is converted to a photoelectron image. The photoelectron image is then accelerated to the target. The target both amplifies the image and stores it for subsequent readout by the scanning electron beam. Target gain is proportional to the accelerating voltage between the photocathode and target and has a maximum value in the neighborhood of 2000 volts.

The MTF for EBSICON targets of diameter 16, 20 and 25 mm are shown in Fig. 34. The data here applies to targets as used in the newer EBSICONs manufactured by Westinghouse Electronic Tube Division. In general, the photocathodes of EBSICON tubes are either 16, 25, 32 or 40 mm in

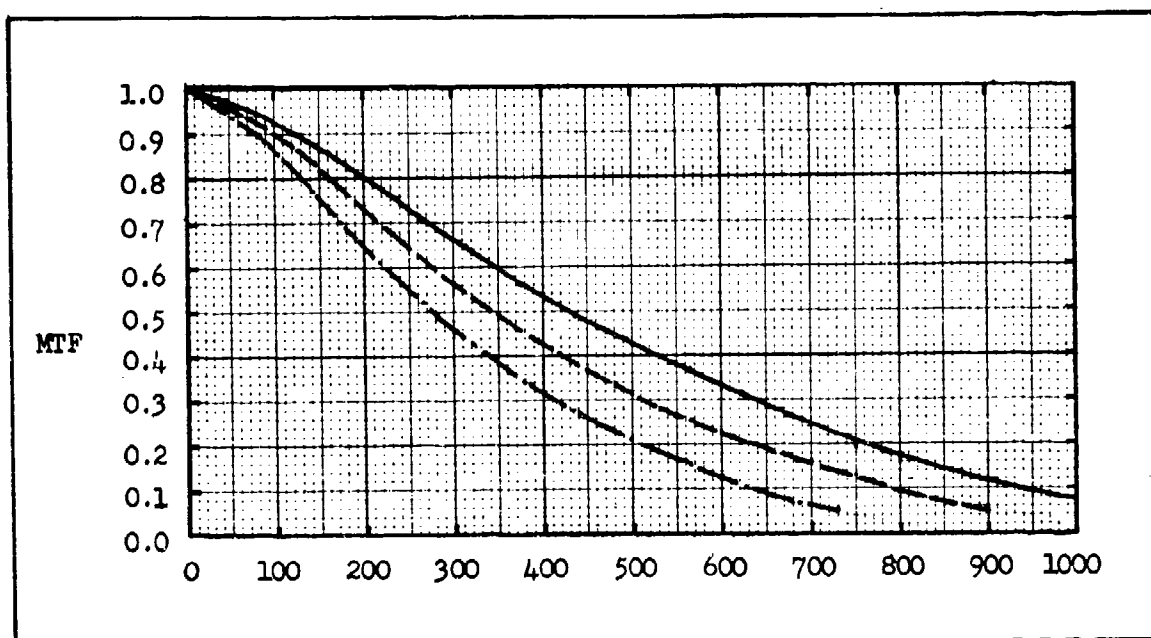


Fig. 34 Typical MTF's for EBSICON Camera Tubes with Targets of Diameter (—) 25 mm, (— —) 20 mm and (— · —) 16 mm. Targets are of the Deep Etch Variety.

diameter. The photocathode is generally larger than the target. Combinations such as 40/16, 25/16 and 16/16 are available. In this description the first two digits refer to the photocathode diameter in mm and the second two to the target diameter also in mm. When an EBSICON is to be mated to an intensifier, it is preferred to use a large diameter phosphor to keep MTF high. Thus, if the intensifier input photosurface is to be 25 mm, it is desirable to use a 25/25 mm (photosurface diameter/phosphor diameter) intensifier coupled to a 25/16 mm EBSICON rather than a 25/16 mm intensifier coupled to a 16/16 mm EBSICON. The benefit of the 25/25/16 mm I-EBSICON to MTF does however involve an increase in overall tube length. While the intensifier phosphor/EBSICON photosurface dimensions have an impact on MTF, the principal overall camera tube MTF is the EBSICON target. For high resolution, the EBSICON target should be as



large as possible. On the other hand, a large target will result in an increase in target lag.

It was noted that for a diffraction limited lens, that a field of view reduction through focal length increase while keeping lens diameter constant, does not result in an increase of scene resolution in the image plane. However, the image tube resolution, measured in lines per picture height in the image plane is independent of the field of view. Thus, the angular resolution in object space improves as lens focal length increases but not as much as it would if the lens resolution also improved. Stated differently, the increase in scene resolution is less than linear with respect to focal length increase.

Increasing the camera tube target diameter improves the camera tube MTF but increases lag. While lag can significantly affect imaging sensor performance, it is at least partially under the systems designers control. For example, the designer can use a smaller target, or decrease lens T-stop which minimizes lag through increase in signal current. Sometimes the target capacitance can be decreased without MTF loss (but at the expense of total signal storage capacity). However, the frame time of a camera tube is a fundamental time constant which cannot be escaped in normal operation.

The effect of a finite frame or exposure time on a number of different types of image motion was described in some detail in Ref. 3 but the results will be briefly reviewed herein and extended.

For linear image motion, the MTF is given by

$$R_o(N) = \frac{\sin(\pi N v_i t_f / 2Y)}{\pi N v_i t_f / 2Y} , \quad (111)$$

where  $N$  is the spatial frequency in lines/pict. ht.,  $v_i$  is the image velocity in mm/sec,  $t_f$  is the camera tube exposure time in seconds, and  $Y$  is the picture height in mm. To obtain the above result in terms of the angular motion, we note that

$$v_i = F_L \dot{\theta} \quad , \quad (112)$$

and also, that the total field of view,  $\phi$ , (for small angles) is

$$\phi = Y/F_L \quad , \quad (113)$$

so that Eq. (111) becomes

$$R_o(N) = \frac{\sin(\pi N \dot{\theta} t_f / 2\phi)}{\pi N \dot{\theta} t_f / 2\phi} \quad . \quad (114)$$

For the linear motion case, we noted in Ref. 3 that the motion MTF goes to zero when the image moves 2 lines (one cycle) in an exposure time.

For sinusoidal motion of peak-to-peak amplitude  $A$  mm in  $t_f$  seconds, the motion MTF is given by

$$R_o(N) = J_o\left(\frac{\pi AN}{2Y}\right) \quad , \quad (115)$$

where  $J_o$  is a Bessel function of zero order. In angular terms

$$R_o(N) = J_o\left(\frac{\pi \theta_A N}{2\phi}\right) \quad , \quad (116)$$

where  $\theta_A$  is the peak-to-peak angular motion per frame time. When the image moves about 1.53 lines in an exposure time,  $R_o(N) = 0$ .

For random motion of rms amplitude  $A$  per frame time,

$$R_o(N) = \exp - \frac{1}{2} \left[ \frac{\pi AN}{Y} \right]^2 \quad , \quad (117)$$

or alternatively,

$$R_o(N) = \exp - \frac{1}{2} \left[ \frac{\pi \theta_A N}{\phi} \right]^2 \quad (118)$$

For an image motion of about 0.89 lines per frame time,  $R_o(N) = 0.02$ .

The sightline motion MTF is a result of the integration time of the camera tube target. Because this integration takes place subsequent to the generation of photoelectron noise, the motion MTF filters the photoelectron noise. The filtering function is

$$\beta_M = \frac{1}{N} \int_0^N |R_o(N)|^2 dN \quad (119)$$

for periodic patterns. The objective lens, by contrast does not filter noise because its MTF precedes the point of noise insertion.

In Eq. (118), the random sightline motion MTF is given in terms of the spatial frequency  $N$  in lines/picture height in image space. To convert the image space resolution to object (scene) space we note that

$$N = 1.2 \phi k_\theta \quad (120)$$

where  $\phi$  is the field of view in the vertical and  $k_\theta$  is the angular frequency given in cycles/radian. Using this equation in Eq. (118), we have that

$$R_o(k_\theta) = - \frac{1}{2} [1.2 \pi \theta_A k_\theta]^2 \quad (121)$$

Thus, the sightline motion MTF, referenced to object space is independent of the field of view. Narrowing the field of view to gain

scene resolution, when the scene resolution is sightline motion limited is clearly fruitless.

We have seen the MTF's of both the diffraction limited lens and the sightline motion are independent of the field of view when the MTF is referenced to object space where it really counts. Only the sensor MTF referenced to object space improves. The net improvement in scene resolution with decrease in field of view will be substantially less than linear in most cases due to the combination of lens and sightline motion once the field of view has been decreased to the point where the lens and motion MTF's are significant.

### 3.3.1 Threshold Resolution of the TV Camera

The resolution of the TV camera is generally measured in the laboratory using a bar pattern projected directly on the faceplate of the camera tube. At a given light level, the spatial frequency of the bar pattern is increased until the observer can no longer discern the individual bars in the pattern. The highest spatial frequency that could be just barely discerned is designated the threshold spatial frequency or threshold resolution. The threshold spatial frequency is a function of the bar pattern irradiance level and the contrast of the pattern. While the threshold resolution vs irradiance level characteristic is directly measurable, it can also be calculated if the basic camera tube parameters are known as will be shown.

The first case to be considered will be the 25/20 mm EBSICON for which the MTF is plotted in Fig. 34. The target MTF also filters the noise. The filter factor  $\beta$  is calculated using Eq. (52) and the

square wave flux response is calculated and the values are given in Table 10. Next the  $SNR_D$  is calculated using the formula (see Eq. 55)

$$\frac{SNR_D}{C_M} = \left[ \frac{t\epsilon}{\alpha} \right]^{\frac{1}{2}} \frac{R_{SF}(N)}{N} \frac{2Gi_{av}}{[G^2 e i_{av}^2 B(N) + I_p^2 / 2\Delta f_V]^{\frac{1}{2}}}, \quad (122)$$

and the values,  $t = 0.1s$ ,  $\epsilon = 5$ ,  $\alpha = 4/3$ ,  $G = 2000$ ,  $e = 1.6 \times 10^{-19}$  Coul.,  $I_p = 5 \times 10^{-9}$  A, and  $\Delta f_V = 8.5 \times 10^6$  Hz. The results are plotted as  $SNR_D$  vs spatial frequency, in Fig. 35. Using a threshold value of 2.8 for  $C_M = 1$  and  $2.8/C_M$  for values of  $C_M = 0.316$ , 0.1 and 0.05, the threshold resolution is obtained as discussed in Section 2 and plotted in Fig. 36 as a function of input photocurrent. This result applies to a camera tube without lens. In laboratory practice, either the test pattern is placed directly against the fiber optic faceplate or, more commonly, projected onto the faceplate with a lens of very high resolution.

Next, we calculate the  $SNR_D$  for the same camera tube with an added intensifier. The MTF and MTF related parameters for this combination are given in Table 11. The Eq. (122) above and the same values for the constants are used for the calculation except that  $G$  is increased to 50,000 to reflect the added gain provided by the intensifier. The threshold resolution for the I-EBSICON is plotted in Fig. 37.

### 3.3.2 Effective Magnification of an Electro-Optical Sensor

When an observer employs a 7 power binocular the image of a scene object on the eye's retina is 7 times larger than it would be if the

SPATIAL FREQ TV <sub>L</sub> /P.H.	SQUARE WAVE AMPLITUDE RESPONSE	MODULATION TRANSFER FUNCTION	SQUARE WAVE FLUX RESPONSE	NOISE FILTER FACTOR (PERIODIC)
$N_{TV}$	$R_{SQ}(N)$	$R_o(N)$	$R_{SF}(N)$	$\beta(N)$
0	1.00	1.000	1.000	1.000
50	.98	.956	.898	.957
100	.96	.898	.792	.909
150	.92	.819	.701	.852
200	.85	.734	.616	.790
250	.77	.649	.538	.728
300	.70	.565	.462	.668
350	.63	.495	.401	.613
400	.55	.432	.350	.563
450	.47	.369	.299	.519
500	.40	.314	.255	.479
550	.34	.267	.216	.443
600	.29	.228	.185	.411
650	.25	.198	.160	.383
700	.21	.165	.134	.358
750	.17	.134	.109	.336
800	.12	.094	.076	.315
850	.09	.071	.058	.297
900	.06	.047	.038	.281
950	.03	.023	.019	.266
1000	.01	.008	.006	.253

Table 10 Amplitude and Flux Responses and Noise Filtering Factor vs Spatial Frequency for the 25/20 EBSICON.

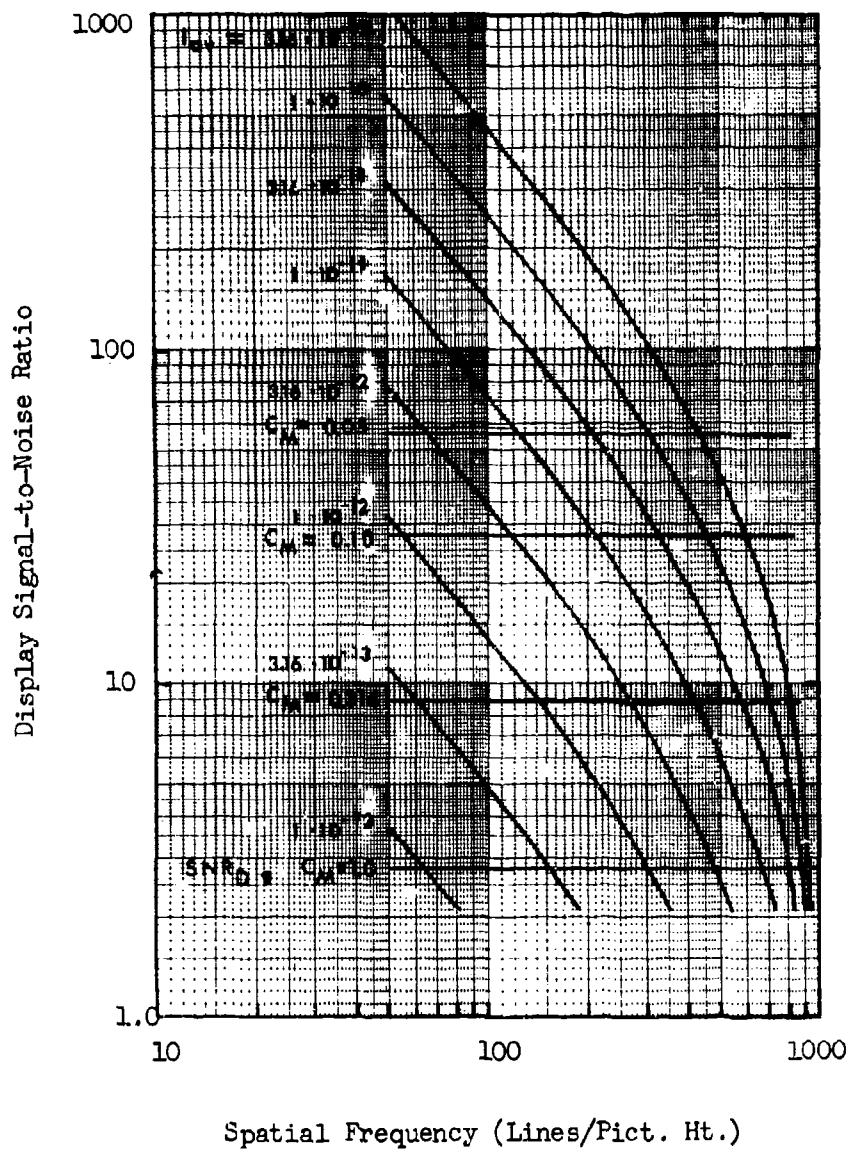


Fig. 35.  $SNR_D$  vs Spatial Frequency for the 25/20 mm EBSICON at Various Average Input Photocurrents. Lens MTF Assumed to be Unity. Horizontal Lines Represent Observer Thresholds for Various Image Modulation Contrasts.

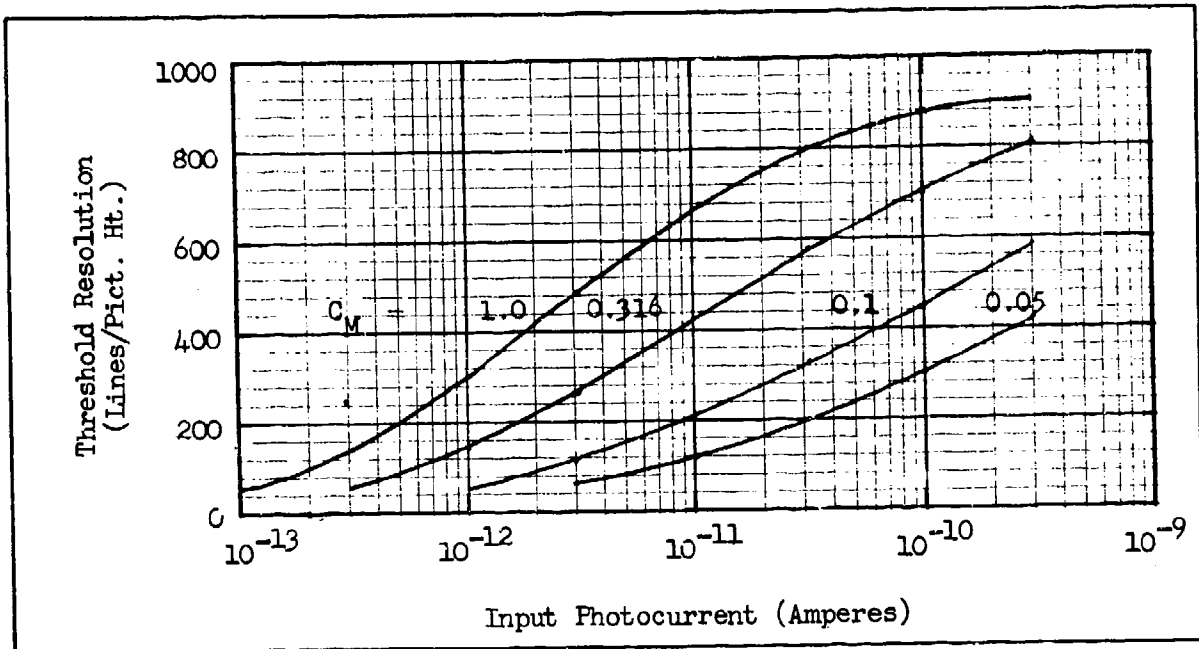


Fig. 36 Threshold Resolution vs Input Photocurrent for the EBSICON Camera Tube for Various Input Image Contrasts.

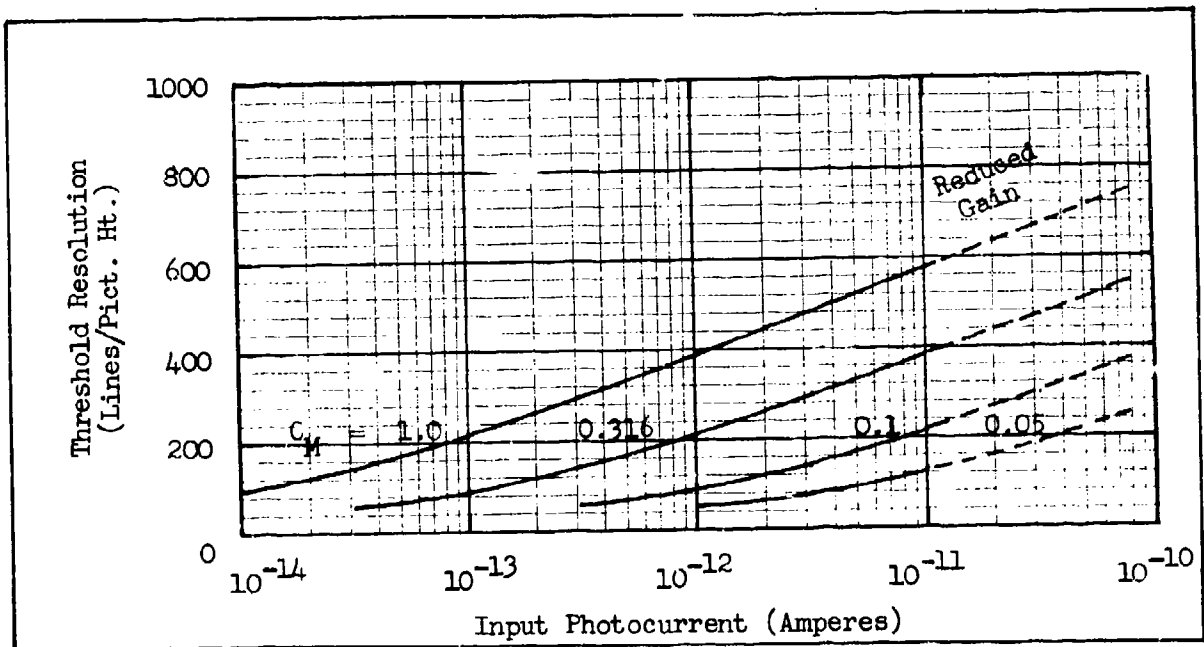


Fig. 37 Threshold Resolution vs Input Photocurrent for the  $D_{pc}/25/20$  I-EBSICON. The Above Result is Independent of the Input Photosurface Diameter,  $D_{pc}$ , to a Good Approximation.



I-EBS				I-EBS			
$N_{TV}$	MTF	$R_{SF}(N)$	$\beta(N)$	$N_{TV}$	MTF	$R_{SF}(N)$	$\beta(N)$
0	1.000	1.000	1.000	500	.173	.140	.371
50	.927	.844	.930	550	.135	.109	.339
100	.844	.729	.858	600	.106	.086	.312
150	.737	.619	.782	650	.084	.068	.288
200	.628	.519	.703	700	.064	.052	.269
250	.523	.428	.618	750	.047	.038	.251
300	.427	.347	.553	800	.030	.024	.235
350	.347	.281	.495	850	.021	.017	.221
400	.279	.226	.446	900	.012	.009	.209
450	.220	.178	.403				

Table 11 MTF and MTF Related Quantities for the 25/25/20 Intensified-EBSICON.

observer viewed the object directly. With a binocular, telescope or a microscope, magnification is a real and meaningful concept. Presumably, if the observer were equipped with a binocular of 7 x magnification, he could discern objects 1/7th as large as he could without the binocular. Because of the MTF of the binocular, the observer may not do quite that well but the binocular is a proven aid to visual acuity.

The concept of magnification is not so clear cut in the case of a television sensor even when the observer is close to the camera itself. One of the virtues of the TV system is that the display can be any size and the observer is free to adjust his viewing distance over a considerable range by simply leaning forward or backward. One possibility is to establish a standard viewing distance  $D_V$  to display height  $D_H$  ratio. For

fairly demanding applications a  $D_V/D_H$  ratio of 4 appears appropriate while for entertainment purposes 7 - 8 is more common (because of raster effects).

A more informative scheme might be to determine how much better (or worse) the observer can see with the sensor than without. In our current thinking, the preferred test pattern would be a bar pattern. One measure of sensor effectiveness might be the ratio of the angular extent of the bar which an observer can detect unaided to that which the observer can detect on the display. To obtain this ratio, we would need to know the observer's ability to detect bar patterns as a function of light level which data does not currently exist. This rating scheme may have some utility, but it has one principal shortcoming. At night, the observer's angular resolution becomes very poor and even a modest LLLTV would show a high figure of merit even though the practical utility of the sensor may in fact be quite low. Even so, it is conceptually useful.

As a more practical measure for this discussion, it is proposed to establish a standard sensor. The standard sensor for the television case would be one with a standard 525-line scan, bandlimited to give equal horizontal and vertical resolution and with field of view adjusted to give an absolute threshold resolution comparable to that of the unaided human eye under good scene illumination conditions. This leaves one important question, what is the threshold resolution of the unaided eye for bar patterns (under good lighting)? To estimate the threshold resolution, we note that according to the Rayleigh criterion, the eye should resolve two point images separated by  $1/10$  mm at 250 mm, and does. This corresponds to an angular separation of 0.4 mr. Bars, should be easier to resolve than points so that the eye's angular

resolution for high contrast patterns should be less than 0.4 mr.

Observers watching a 525-line (490-line active) display with pronounced raster line structure generally back up until the display height subtends somewhat less than  $8^\circ$ , at which point the line structure tends to disappear. When the display height subtends  $8^\circ$ , each of the 490 scan lines subtends about 0.285 mr. Also, a figure of 1' of arc is sometimes taken as the eyes acuity for scene detail which corresponds to 0.291 mr. Thus, we will assume that the limit of the eye's resolution is approximately 0.3 mr per line for repetitive bars of high contrast.

The absolute limiting resolution of a broadcast TV camera is usually taken to be about 343 lines per picture height. If the angular resolution per line corresponds to 0.3 mr, the total vertical field of view will be approximately  $6^\circ$ . That is, an observer viewing a broadcast camera's display when the camera's vertical field of view is  $6^\circ$ , should be able to do about as well as he would viewing the scene directly. A good closed circuit camera can of course have higher resolution than a typical bandpass-limited broadcast camera which would permit a wider field of view or a superior resolution of scene detail with the same field of view. The main effort here is to establish some sort of a reference level against which a system's effectiveness can be gauged. We do not imply that the reference level is absolute or even very precise.

Given a threshold resolution of N lines per picture height, the angular resolution  $\Delta\theta$  is given by

$$\Delta\theta = \frac{v}{N} \cdot F_L \quad , \quad (123)$$

where  $Y$  is the picture height and  $F_L$  is the lens focal length.

It should be observed that while the absolute resolution of a broadcast camera in the vertical is balanced with the resolution in the horizontal, i.e., the vertical and horizontal resolutions are approximately equal. This is not usually the case in closed circuit TV where the horizontal resolution quite often exceeds that in the vertical by a substantial amount. This disparity becomes smaller as the field of view is reduced and as sightline motion effects, if any, are reduced. For simplicity in the discussion that follows, we will assume that the vertical and horizontal resolutions are balanced and equal to the resolution measured or calculated in the horizontal. For wide fields of view, the above assumption will lead to an optimistic view of the camera resolution and for very narrow angles, a somewhat pessimistic view.

The effective magnification will be calculated as

$$m_e = \frac{3 \times 10^{-4}}{\Delta\theta_r} \quad (124)$$

where  $\Delta\theta_L$  is the resolution of the TV augmented observer. We shall calculate  $m_e$  for the I-EBS camera discussed in Section 3.3 for various fields of view.

Also, we shall assume that the lens is of constant aperture (4") and that the lens MTF varies with focal length as shown in Fig. 38. The image motion is taken to be random with rms sightline variations of 30 microradians. The MTF of the motion, calculated using Eq. (117) is plotted in Fig. 39 for the four fields of view being considered. The  $SNR_D$  are plotted in Fig. 40 for an average photocurrent of  $1 \times 10^{-11}$  Ampere. In Table 12, we give the threshold resolution both in lines

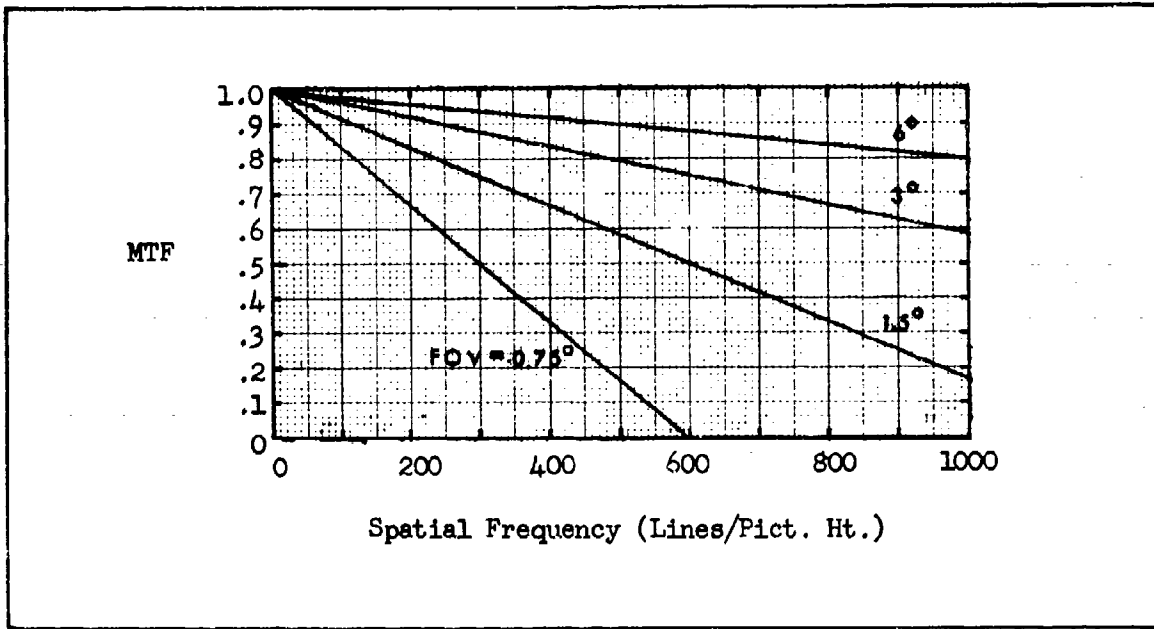


Fig. 38. MTF of Typical Lenses with Various Fields-of-View (in the Vertical).

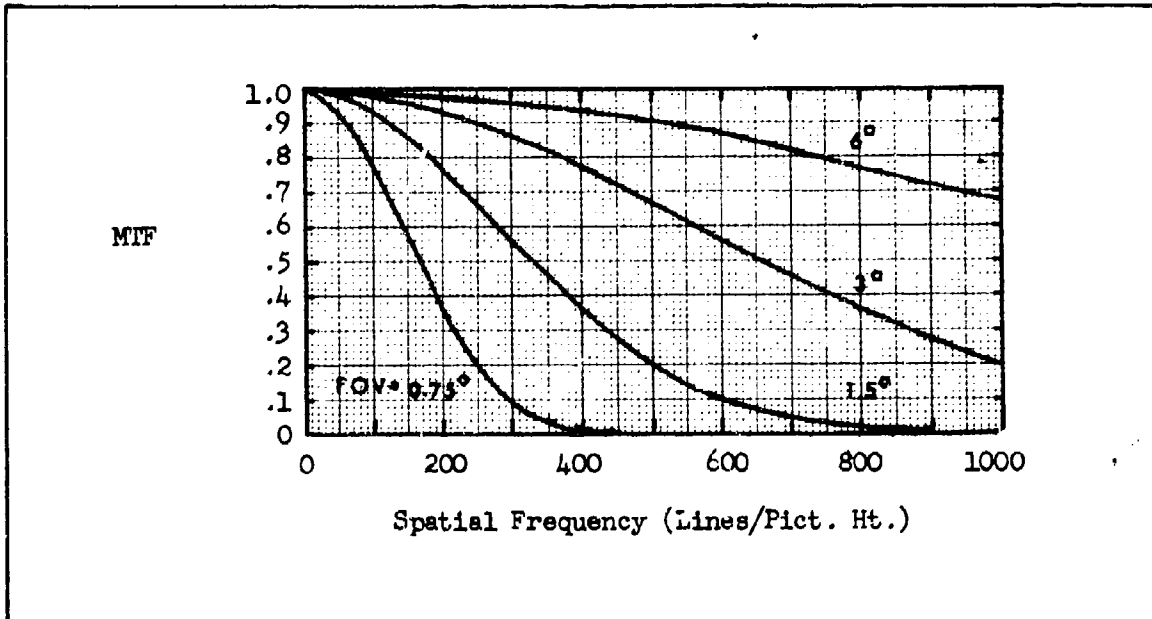


Fig. 39. MTF Due to Random Image Motion Expressed in Lines/Picture Height for Various Fields-of-View.

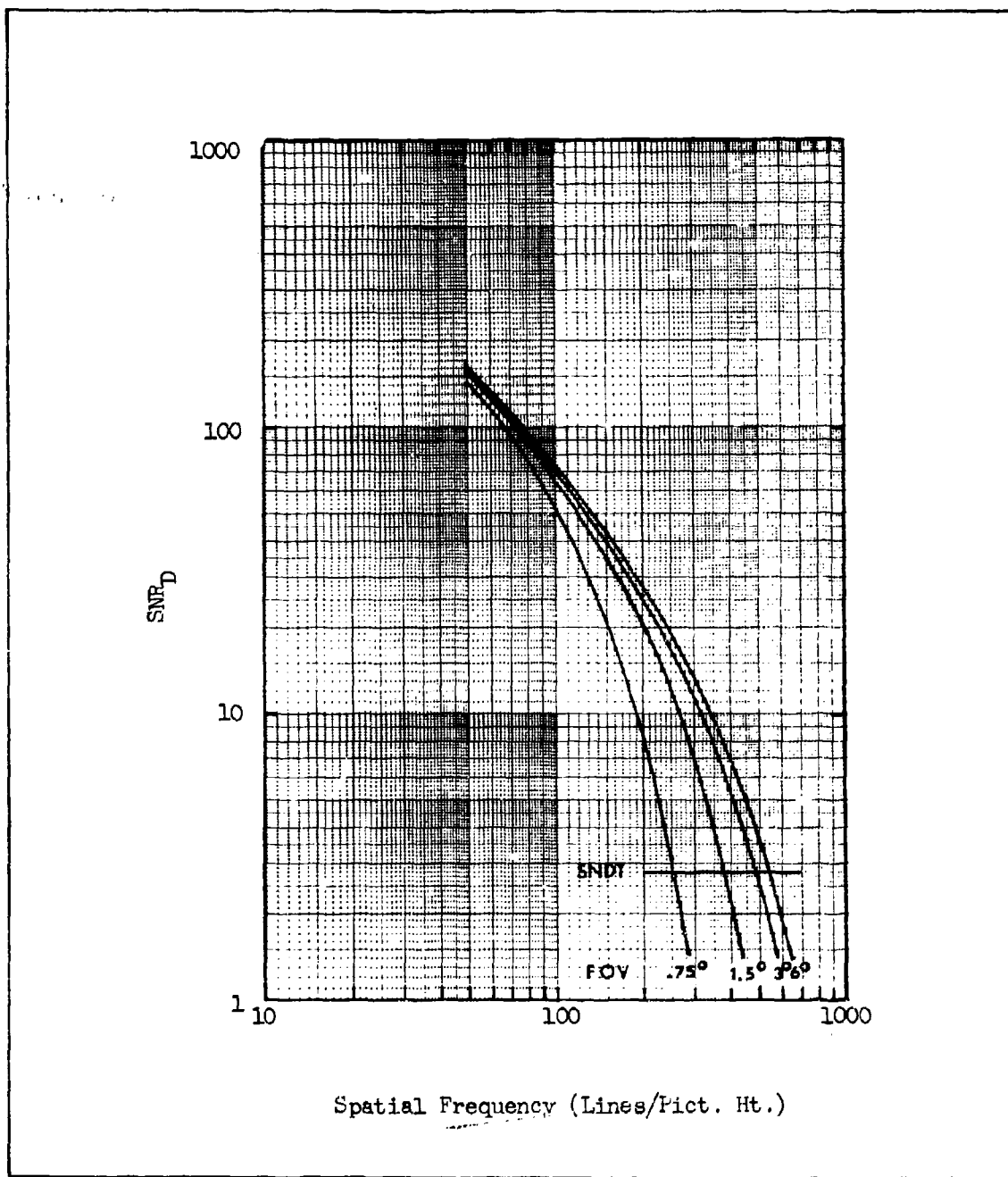


Fig. 40.  $SNR_D$  vs Spatial Frequency for the Assumed Camera with 4 Different Fields-of-View. Sightline Instability is 30 Micro-radians rms (random).

VERTICAL FIELD OF VIEW	THRESHOLD RESOLUTION ( $\frac{\text{Lines}}{\text{Pict. Ht.}}$ )	THRESHOLD RESOLUTION ( $\frac{\text{mr}}{\text{line}}$ )	EXPECTED MAGNI- FICATION INCREASE	ACTUAL* MAGNI- FICATION INCREASE	EFFECTIVE MAGNI- FICATION
6°	540	.194	1	1.00	1.55
3°	480	.109	2	1.80	2.75
1.5°	380	.069	4	2.81	4.34
0.75°	252	.052	8	3.73	5.76

\* Less than expected due to Lens and Motion MTF.

Table 12. Effect of Field of View Decrease and Sightline Motion on Effective Magnification.

per picture height and in mr/line. In decreasing the field of view 8 fold, the expected increase in threshold angular resolution is 8 fold. As can be seen, the actual increase is but 3.73:1 due to the lens and motion MTF. The effective magnification, based on Eq. (124) is also tabulated. Observe that with a 6° field of view, the effective magnification is 1.55 which is above that for our "standard TV camera." This is entirely possible: however, an 875-line scan or larger will be needed to realize an effective resolution of over 500 lines in the vertical. Even with a 1.5° field of view, a line number somewhat greater than the standard 525 can be profitably used.

### 3.4 Range Analysis

In section 3.3, the primary concern was with sensor parameters without regard for atmospheric or range to the scene. For passive systems, the primary effect of the atmosphere is to degrade image contrast while for active systems, the primary effect is to absorb system source power.

In performing range analysis, it has been customary to assume a particular scene object size. However, to make results more general, it is preferred to express results in terms of angular resolution (either  $\Delta\theta$  or  $k_\theta$ ) for then, the results apply to any scene object size.

It should not be inferred that range prediction is a highly refined science. The recognition of an object, for example, may vary radically depending on the type of object and the complexity of its background. In time, better guide lines will evolve based on further experimentation both in the laboratory and in the field. At this point in time, the systems designer must use judgement based on past experience. In the equivalent bar pattern approach, it was implied that if the system is capable of resolving a bar pattern of bar spacing equal to 8 lines per minimum target dimension and of bar length equal to the objects maximum dimension, then the object should be recognizable. This is felt to be generally true if the object is in a relatively uniform background. On the other hand, more resolution lines will probably be needed if the object is in a complex background. At other times, less resolution can be tolerated when the level of discrimination is lower or when other clues are available. For example, a task may be that of detecting a moving vehicle on the road. The object may be "recognized" as a



vehicle by virtue of its presence on a road and by virtue of its rapid motion. This level of "recognition" is lower than ordinarily implied, i.e., telling the difference between a jeep and a truck and the vehicle velocity may differentiate it from ox carts.

However, with good judgement, the ability of a system to resolve bar patterns in the field should be indicative of its ability to detect, recognize and identify many scene objects. In the next two sections, we will analyze the range performance of both active and passive TV sensors assuming the scene object is a bar pattern.

#### 3.4.1 Range Analysis (Active)

The photocurrent obtainable from an active scene is obtainable by combining Eqs. (105) and (108) to obtain

$$i_{av} = \frac{SA\tau_o \rho_{av} \Phi_s \exp(-2\alpha_o R)}{4f^2 \Omega R^2} \quad (125)$$

For a sample calculation, we will assume that  $S = 1.5 \times 10^{-2}$  A/W,  $A = 3 \times 10^{-4} \text{ m}^2$ ,  $T = f/\sqrt{\tau_o} = 4$ ,  $\Omega = 9 \cdot 137 \cdot 10^{-4} \text{ sr}$ ,  $\rho_{av} = 0.2$  and  $\Phi_s = 40 \text{ Watts}$ . Then,

$$i_{av} = 6.16 \times 10^{-4} \exp(-2\alpha_o R)/R^2, \quad (126)$$

for  $R$  in meters. This equation is plotted in Fig. 41 for sea level visibilities of 3, 5, and 10 n. mi. using the values of Table 8 for  $\alpha_o$ .

In general, the photocurrents expected are quite low. Thus, the camera tubes will be operated at high gain. In this case, the camera will be photoelectron limited and the  $SNR_D$  becomes

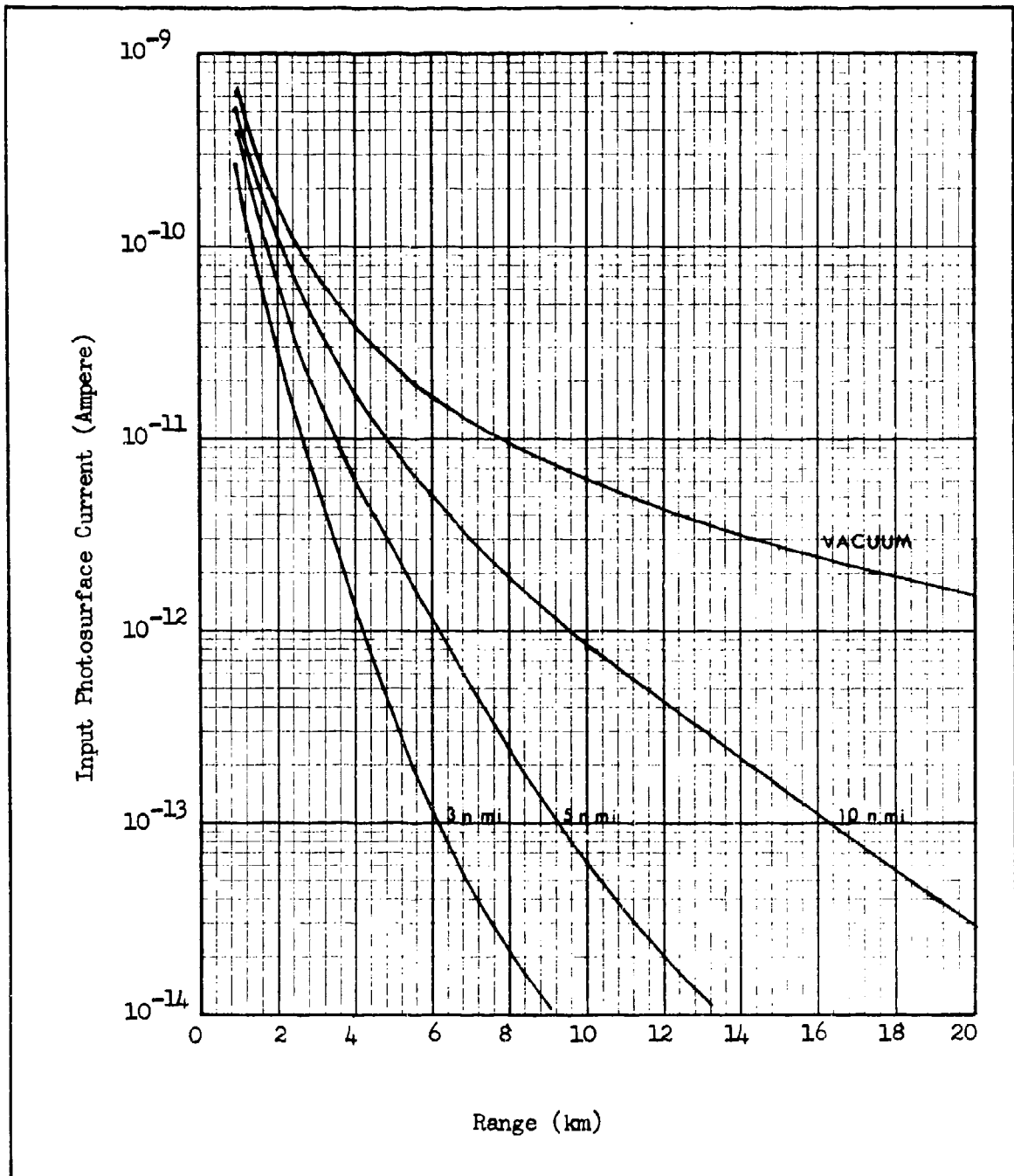


Fig. 41. Input Photocurrent vs Range for Various Sea Level Visibilities. System Source Power is 40 Watts, Lens T Stop is 4, Average Scene Reflectivity is 0.2, Field-of-View is  $1.5^\circ \times 2^\circ$  and Photoresponse is 15 mA/W.

$$\frac{\text{SNR}_D}{C_M} = \left[ \frac{t_s}{\alpha} \right]^{\frac{1}{2}} \frac{R_{SF}(N)}{\beta^{\frac{1}{2}}(N) \cdot N} \frac{2i_{av}^{\frac{1}{2}}}{e^{\frac{1}{2}}} \quad (127)$$

The photocurrent per Eq. (126) above is range dependent. For a specific case, say, a visibility of 10 n. mi. we can plot  $\text{SNR}_D$  equations for a number of ranges as shown in Fig. 42 using Fig. 41 to relate photocurrent and range. From the calculated values of  $\text{SNR}_D$  and the threshold  $\text{SNR}_{DT}$  (assumed equal to  $2.8/C_M$ ), we can obtain the threshold resolution in lines per picture height vs range as shown in Fig. 43. In making the  $\text{SNR}_D$  calculation we assumed the lens MTF of Fig. 38 ( $1.5^\circ$  field of view), the EBSICON MTF of Fig. 34, the intensifier MTF of Fig. 32 (25 mm phosphor diameter) and the sightline MTF of Fig. 39 (sightline motion of 30  $\mu$ r,  $1.5^\circ$  field of view). Using Eq. (123), we can convert the threshold resolution in lines per picture height to angular resolution in radians/line (actually plotted as microrad/line). The result is plotted vs range in Fig. 44. Alternatively, the threshold resolution can be plotted in terms of angular frequency,  $k_\theta$ , using Eqs. (90) and (123) as shown in Fig. 45.

As a first cut at recognition range, we suppose the task to be that of recognizing a jeep at 3 km. If we suppose the jeeps minimum dimension to be 2 meters, the angular resolution required is 83 microrad if we are to resolve 8 lines across the minimum dimension. As can be seen from Fig. 44, this implies that the jeep's modulation contrast must be above about 30%.

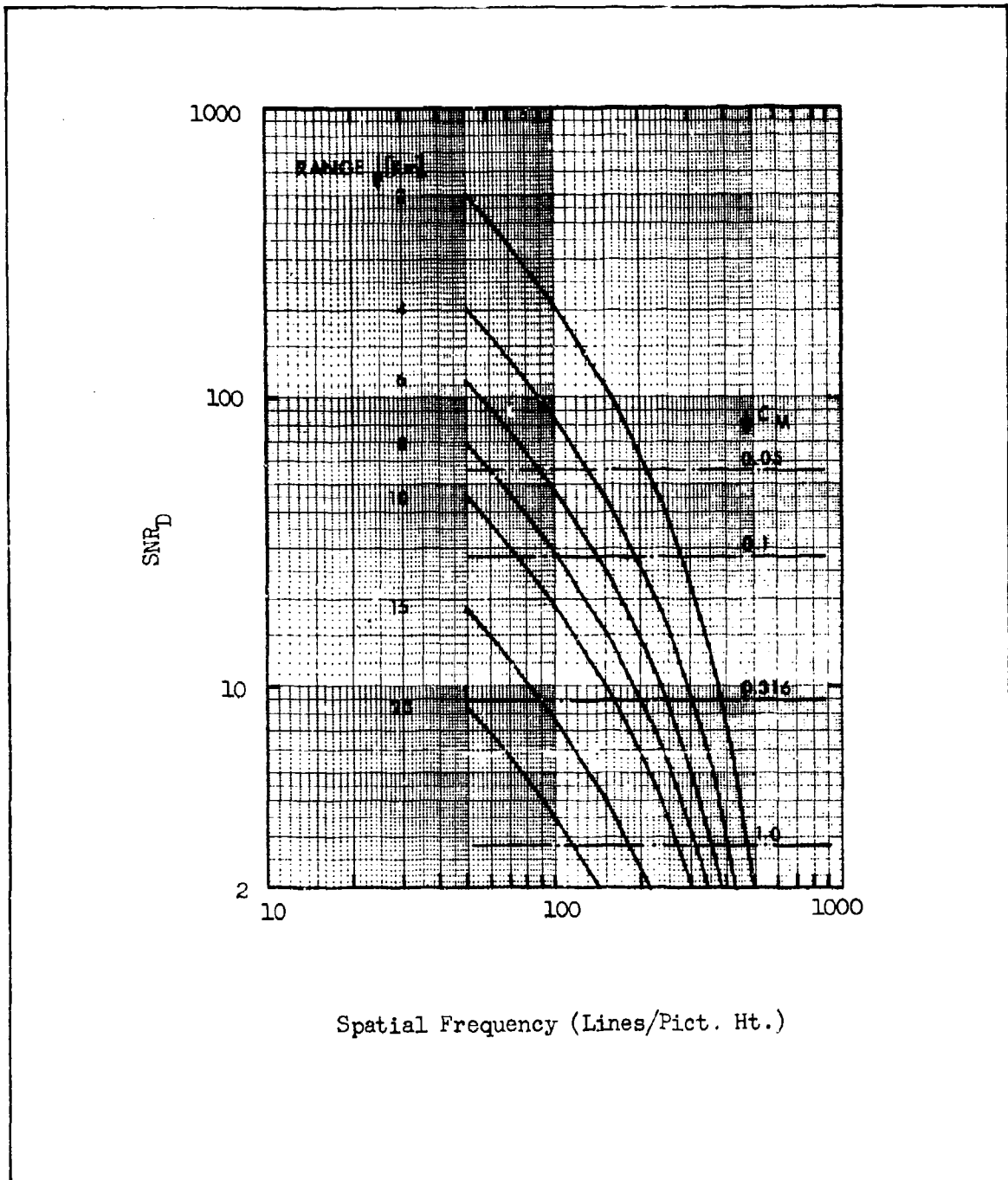


Fig. 42. SNR<sub>D</sub> vs Spatial Frequency as a Function of Range for the Assumed Active System.

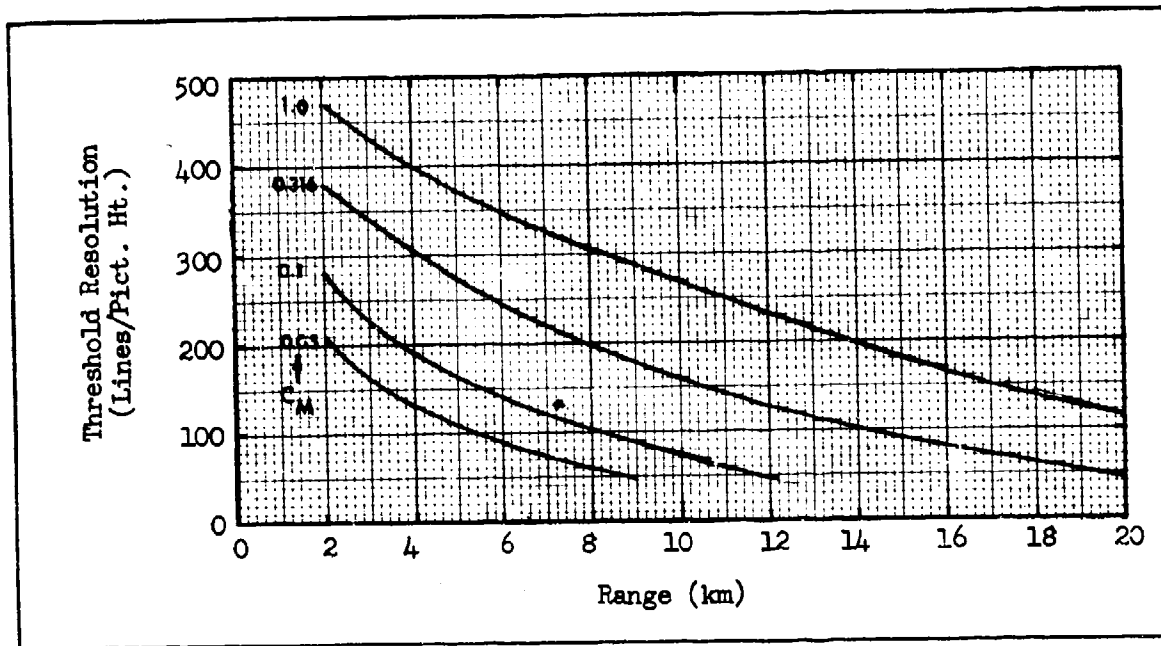


Fig. 43. Threshold Resolution vs Range for the Assumed Active System with Various Input Image Contrasts.

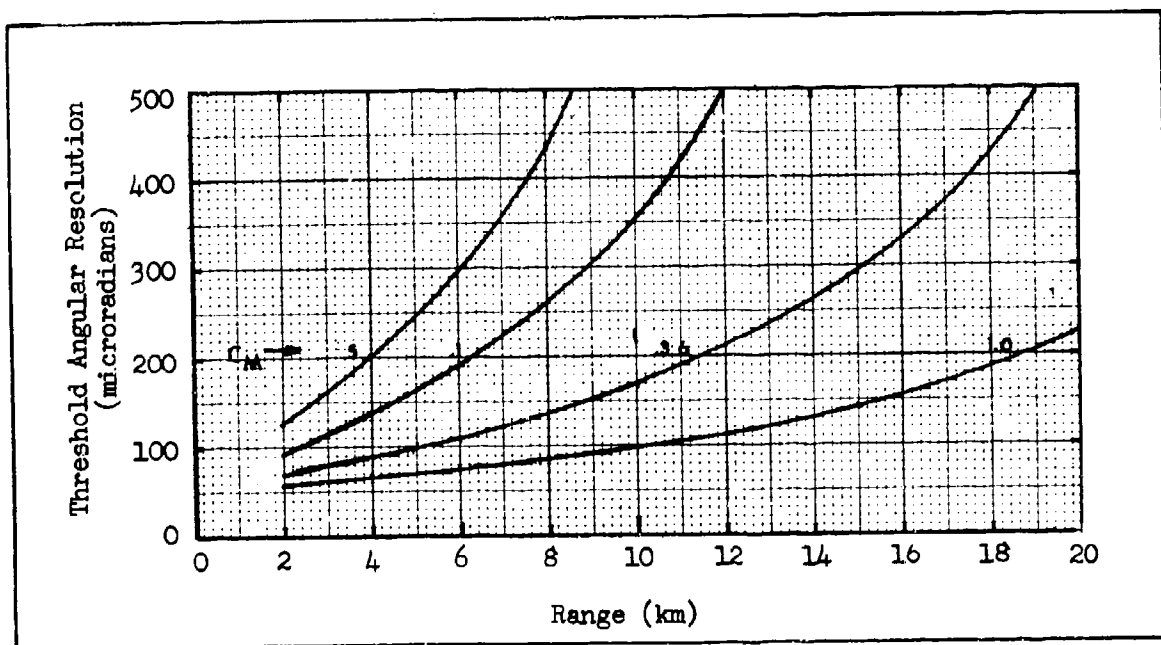


Fig. 44. Threshold Angular Resolution vs Range for the Assumed Active System with Various Input Image Contrasts.

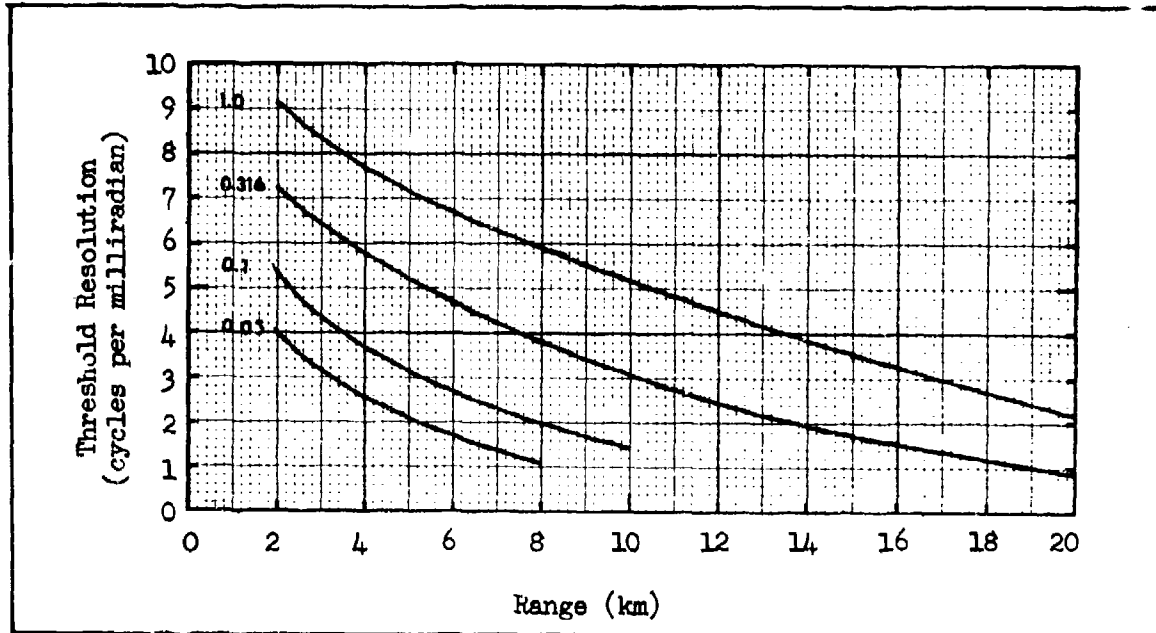


Fig. 45. Threshold Resolution vs Range for the Assumed Active System with Various Input Image Contrasts.

### 3.4.2 Range Analysis - Passive Case

The basic  $SNR_D$  Eq. (122), repeated below applies to both active and passive TV:

$$\frac{SNR_D}{C_M} = \left[ \frac{t_e}{\alpha} \right]^{\frac{1}{2}} \frac{R_{SF(N)}}{N} \frac{10i_{av}}{[G^2 e i_{av} \beta(N) + I_p^2 / 2\Delta f_V]^{\frac{1}{2}}} \quad (128)$$

Specifically, this equation applies to bar patterns. In the active case, we noted that the scene irradiance levels are very low except at very short ranges. Hence, the TV camera is operated at near maximum gain and the preamp noise is negligible. This is not true in the passive case where scene irradiance levels can vary by a factor of  $10^9$  or more in a 24-hour day.

For a diffuse scene, the photocurrent  $i_{av}$  can be written as

$$i_{av} = \frac{0.5\pi A \int_0^{\infty} S(\lambda) \tau_o(\lambda) [L_o(\lambda) + L_b(\lambda)] d\lambda}{4f^2}, \quad (129)$$

using the general formulation of Eq. (105) but noting the spectral dependence of the camera components and the scene object and background radiances,  $L_o(\lambda)$  and  $L_b(\lambda)$ , respectively. In the passive case, the image contrast is range dependent as noted in connection with Eq. (65) and Fig. 24. To acknowledge the range dependence of contrast we will set  $C_M$  in Eq. (128) equal to  $C_{MR}$ , the modulation contrast at range R which is

$$C_{MR} = C_{MO} \left[ 1 - \frac{S_K}{G_d} (1 - e^{-\alpha R}) \right]^{-1}, \quad (130)$$

and use  $C_{MR}$  as calculated using the above equation to adjust the  $SNR_D$  thresholds as will be shown.  $C_{MO}$  is the inherent contrast at range zero.

Operated at full gain, an I-EBSICON is photoelectron noise limited except at the very lowest light levels. As light level increases, a point will be reached where the tube saturates. Further increases in light must then be accompanied by a further decrease in gain. At the lowest gain achievable, the predominant noise will be that of the preamp. In Fig. 46, we plot the ratio of the total rms system noise to the photoelectron noise alone. At a gain of 50,000, the total system noise is seen to be almost entirely photoelectron while preamp noise completely dominates with a gain of 5. In the passive case, the full spectrum of sensor gain must be considered.

To illustrate the calculation of passive system performance using

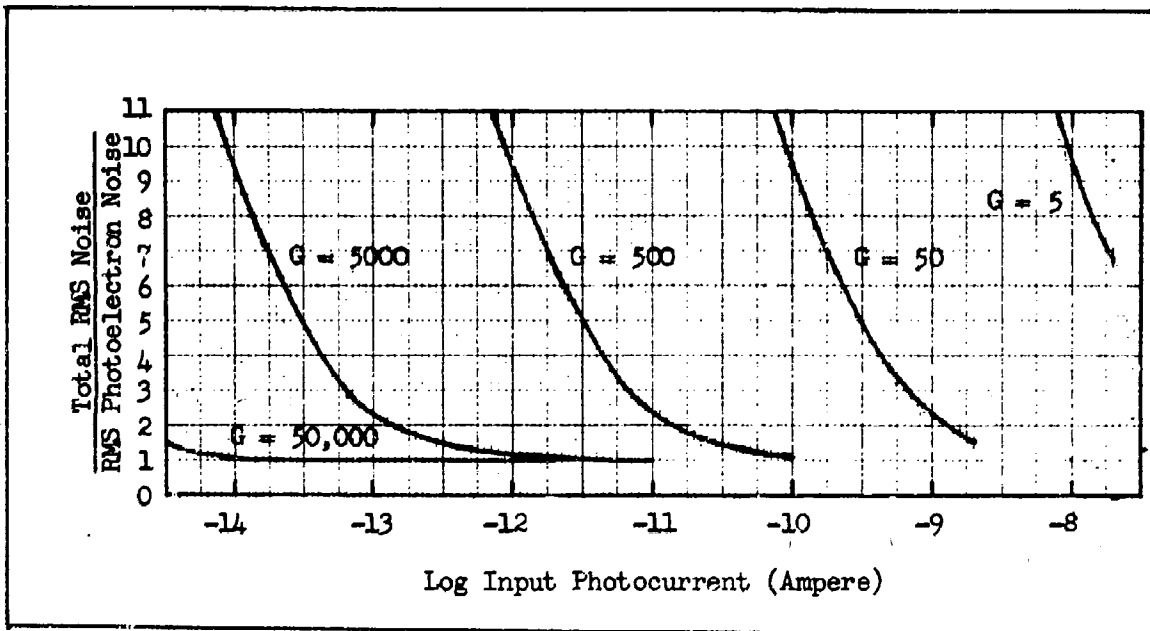


Fig. 46 Ratio of the Sum of Photoelectron and Preamp Noise to the Photoelectron Noise.

the 25/25/20 I-EBS previously considered in section 3.3.1 with a  $1.5^\circ$  vertical field of view of MTF and 30  $\mu$ r random sightline motion, the lens and motion MTFs are shown in Figs. 38 and 39. If the tube is operated at maximum gain, it will be photoelectron limited. The maximum average photocurrent obtainable is about  $5 \times 10^{-7}$  A. At max gain of  $5 \times 10^4$ , the maximum input photocurrent tolerable is  $5 \times 10^{-7} / 5 \times 10^4$  or  $1 \times 10^{-11}$  A. Suppose we are operating with maximum photocurrent and gain. Then the  $SNR_D$  is as plotted in Fig. 47.

Next, suppose we increase the input photocurrent (by increasing the input photosurface irradiance) by a factor of 100 which requires a 100-fold gain reduction. Preamp noise must now be considered. The  $SNR_D$  for this case is plotted in Fig. 48 for an input photocurrent of  $10^{-9}$  A, a gain of 500 and a preamp noise of  $5 \times 10^{-9}$  A in a



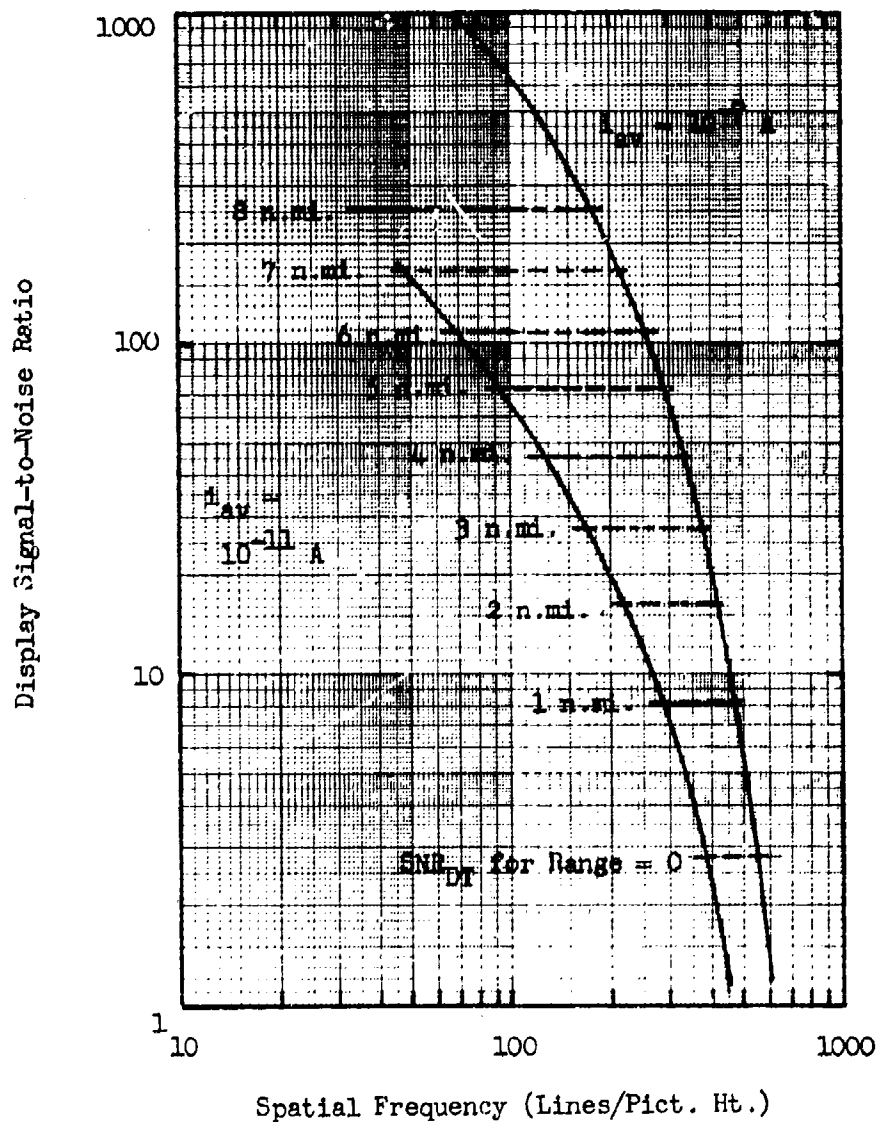


Fig. 47 Display Signal-To-Noise Ratio vs Range for the Assumed Passive System. SNR<sub>D</sub> Thresholds are for a 10 n.mi. Visibility of 10 n.mi. and a Sky to Ground Ratio of 4. Inherent Image Contrast is 100%.

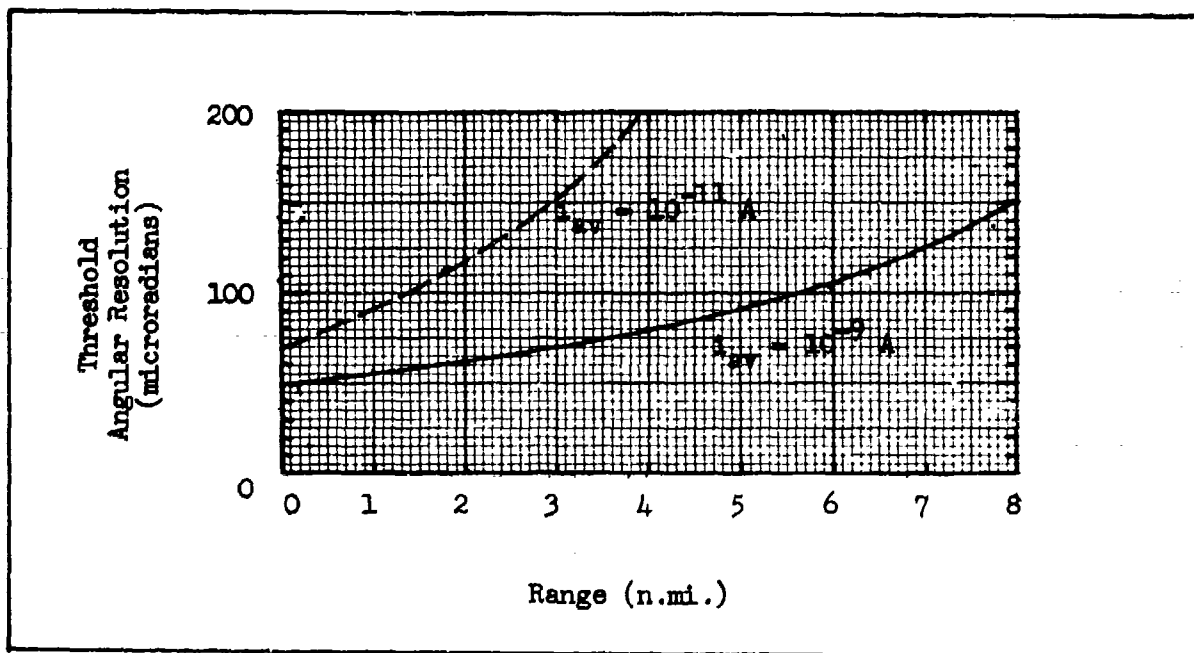


Fig. 48 Threshold Angular Resolution vs Range for the Assumed Passive System for Two Values of Average Input Photocurrent.

$5 \times 10^6$  Hz bandwidth. The  $SNR_{DT}$  for this case is also plotted in Fig. 47. To enter the range dependence of image contrast we adjust the threshold using the formula

$$SNR_{DT} \text{ at Range } R = \frac{SNR_{DT} \text{ at Range Zero}}{C \text{ at Range } R} \quad (131)$$

These  $SNR_{DT}$  are indicated in Fig. 47. From the intersections of the SNR and  $SNR_{DT}$  curves, we obtain the threshold resolutions. Next the resolution in lines per picture height is converted to angular resolution and plotted in Fig. 48. Note that without an atmosphere the angular resolution is a constant independent of range. The atmosphere causes the angular resolution to increase with range.

#### 4.0 Electro-Optical System Requirements and Specifications

A mission requirement can result from either a current or a projected need or by new technology which offers new mission possibilities. Assuming that the existence of a mission requirement can be established, an equipment specification will begin to take form based on technical exchange of information and preproposal activities. Finally, request for proposal will be generated. This RFQ will generally convey the mission requirements to the potential contractors and a number of performance objectives. In general, several proposals will be prepared by contractors. The contracting agency must then select the preferred approach. This selection process is difficult at best when a variety of approaches are taken but it is made more difficult than necessary by the lack of standards in nomenclature, in models for natural phenomena such as atmospheric transmission, or in methods of analysis or prediction of the overall system performance.

In the following, a performance specification outline is prepared with recommended nomenclature and methods of analysis. The objective is to obtain from a potential contractor, sufficient data and performance estimates to assure that the equipment will have a reasonable expectation of meeting the mission requirements and to serve as a basis for the comparison of competitive approaches on as common a basis as possible.

The approach to obtaining the data and performance predictions is to require:

- (1) detailed system component parameters and specifications,
- (2) prediction of the laboratory performance of the proposed system,
- (3) prediction of the field performance including scene parameters and other factors such as sightline motion, and
- (4) that the contractor provide his understanding of the mission requirements and show that equipment proposed by the contractor has a reasonable expectation of meeting the requirements.

The data required in the outline below emphasizes system parameters bearing on the capability to convey information to the user rather than physical details such as finish of parts, quality of construction, etc.

It is realized that methods of predicting system performance have not been fully developed and also, that judgment factors must enter into any system design. Alternative methods of analysis or interpretation may be provided in addition to the analysis as outlined below. To the extent possible, the preferred nomenclature of section 4.5 shall be employed.

In general, it is noted that the primary function of an imaging system is to enable an observer to resolve scene details with sufficient clarity to perform some desired function over an acceptably large fraction of the time that the equipment would be expected to have applicability. The fraction of the time when the equipment will not perform the desired function should mainly depend upon factors beyond the observer's control such as scene contrasts or atmospheric visibilities which are well below the expected average. The maximum level of scene resolution obtainable depends upon the designed-in system parameters and must perforce reflect a compromise between the user's desires and needs, the levels of

performance physically realizable and, the very real constraints of system size, weight, power and cost. The purpose of the data requested below is to establish the predicted level of proposed sensory system performance, to judge the adequacy of the design in view of the mission requirements and to compare the proposed design with other competitive approaches.

#### 4.1 Component Specifications

In order to estimate overall system performance, the parameters of the component parts must be known. The paragraphs below pertain to both active and passive sensors unless otherwise noted.

##### 4.1.1 System Component Blocks (Passive)

The basic components of a passive sensor are the window assembly, the line of sight stabilization and steering mechanisms, the objective lens assembly and the television sensor including the display and the observer.

##### 4.1.2 System Component Blocks (Active)

The active sensor includes all of the components for a passive sensor in addition to a system source (or scene irradiator) and the required range gating controls for the TV sensor.

##### 4.1.3 System Source (Active)

The system source consists of a source of radiant energy, a steerable line of sight mechanism, a lens assembly and a heat exchanger. For the source of radiant energy, specify

- (1) source type and dimensions of the radiant area.
- (2) beam uniformity.
- (3) source wavelength vs power output.

- (4) pulse rise time, duration and repetition rate.
- (5) type and basis for power output control.

For the steerable line of sight mechanism and lens assembly, specify

- (1) fields of view, line of sight steering coverage, line of sight stability.
- (2) separation of the source and TV sensor.
- (3) lens aperture, effective source power including any transmission losses through windows or filters.
- (4) aerodynamic drag of the window configuration if applicable.

For the heat exchanger, specify

- (1) heat load.
- (2) coolant type.
- (3) coolant capacity and consumption rate.

For the total system source, specify

- (1) overall component dimensions.
- (2) location of components.
- (3) size, weight and power requirements.

#### 4.1.4 Window Assembly

For the window assembly, specify

- (1) type of material and dimensions.
- (2) optical properties including the modulation transfer function as function of LOS angle if applicable.
- (3) aerodynamic drag if applicable.

#### 4.1.5 Stabilization and LOS Steering Mechanisms

For the stabilization and LOS steering mechanisms, specify

- (1) line of sight steering angle coverage, obscurations and objective

lens vignetting.

- (2) boresight and alignment accuracies.
- (3) degree of stabilization.
- (4) type of steering and stabilization control.
- (5) maximum slew rates.
- (6) image derotation method and accuracy, if applicable.
- (7) reflection and transmission losses in the optical path.
- (8) MTF of any optical components and MTF of any image motion due to the stabilizing components.
- (9) overall size, weight and power requirements.

#### 4.1.6 Objective Lens Assembly

For the objective lens assembly, specify

- (1) fields of view.
- (2) lens type.
- (3) lens focal lengths.
- (4) lens T/stop range obtainable including method of control using iris and neutral density filters.
- (5) transmission of spectral and polarizing filters.
- (6) depth of field, reticle and focus provisions.
- (7) degree of athermalization.
- (8) lens flare at max and min T/stop.
- (9) relative image plane irradiance.
- (10) lens MTF at center, half field and full field and for min and max T/stop in active mode and passive mode, if applicable.
- (11) overall size, weight and power requirements.

#### 4.1.7 Television Camera Assembly

The television camera typically consists of an image intensifier, a television camera tube, a preamplifier and a video signal processor. If an image intensifier is not used the input photosurface becomes that of the TV camera tube.

For the intensifier, specify

- (1) input photosurface spectral responsivity, effective areas, spectral responsivity and effective background irradiance.
- (2) input photosurface responsivity to a  $2854^{\circ}$  K source.
- (3) input photosurface uniformity.
- (4) phosphor type, effective diameters and persistence.
- (5) max gain and max net gain change obtainable due to intensifier phosphor/TV camera tube photosurface.
- (6) exposure gating range, if applicable.
- (7) exposure gating on-off ratio, if applicable.
- (8) scintillations.
- (9) intensifier MTF; center, half field and full field at max and min gain.
- (10) blemish specification.

For the television camera tube, specify the

- (1) items 1 through 3 of the intensifier specification if an intensifier is not used.
- (2) max gain and max net gain change obtainable from the gain-storage target.
- (3) effective gain-storage target diameter.
- (4) MTF of the combined TV camera tube's image section, gain storage target and scanning electron beam at the center, half field and full field.



- (5) linearity of the MTF and its functional dependence on input irradiance level, or temperature if any.
- (6) gain-storage target dark current and its temperature dependence.
- (7) maximum signal current storage capacity of the gain-storage target.
- (8) interelectrode capacitance of the output signal lead.
- (9) all sources of noise and their point of insertion within the camera tube including the functional relationship between noise sources, input photocurrent, gains and other tube operating parameters as applicable.
- (10) gain of any preamplifiers internal to the TV camera tube.
- (11) saturation characteristics and susceptibility of the gain-storage target to blooming and halting.
- (12) temperature dependence of TV camera lag characteristic.
- (13) blemish specification.

#### 4.1.8 Television Camera Assembly (Active)

In addition to the parameters specified in paragraph 4.1.7, for the range and exposure gating system, specify the

- (1) max and min range gate duration limits.
- (2) range gate voltage rise times from full on to full off.
- (3) method of range gate selection.

#### 4.1.9 Signal Processor

The signal processor consists of the preamplifier gain control circuitry aperture and gamma correction circuitry and the video amplifier. For the signal processor, specify

- (1) rms preamplifier noise referenced to its input.
- (2) frequency response and implementation of any aperture correcting networks.

- (3) video bandwidth.
- (4) method of automatic irradiance control signal generation and automatic irradiance control range.
- (5) automatic gain control characteristics.
- (6) gamma correction characteristics.

#### 4.1.10 Display

For the display, specify the

- (1) effective display dimensions.
- (2) display viewing distance.
- (3) display MTF, center, half field and full field including dependence on display luminance.
- (4) display luminance range.
- (5) aperture and gamma control characteristics.

#### 4.2 Predicted Laboratory Performance

While the true test of an equipment is its performance in the field, equipments are generally accepted on the basis of measurements made in the laboratory. Also some tests can only or can be best made in the laboratory. Consequently, the laboratory performance is of considerable interest. In the laboratory, the maximum performance of the system, which depends mainly on the designed-in system parameters as opposed to uncontrollable factors such as atmospherics, should be realized. Prior to equipment development, the expected maximum performance is calculated while in production, the performance is measured.

#### 4.2.1 Standardized Laboratory Test Patterns

The laboratory performance is predicted or measured using standardized test objects or patterns. The primary test pattern is the standard Air Force bar pattern consisting of 5 bars counting both the alternating bright and dark bars individually. The bars are of equal width and of length 5 times larger than the width. Three of the bars shall be dark and two white. The background surrounding the bars shall be of radiance equal to the radiance of the white bars. A number of bar patterns shall be employed of various spatial frequencies and contrasts with the spatial frequencies being appropriate to the system under test. The absolute test pattern irradiance levels shall be variable over an appropriate range.

If the proposed system is non-existent, the performance must be analytically predicted. The resolution predicted is expected to serve as a basis for the acceptance test of the actual system.

The test pattern modulation contrast is defined as

$$C_M = \frac{L_{\max} - L_{\min}}{L_{\max} + L_{\min}}, \quad (132)$$

where  $L_{\max}$  and  $L_{\min}$  are the highlight and low light irradiance levels respectively.

For system components, spatial resolution is specified in units of lines or half cycles per picture height. For example, if the effective input photosurface height is  $Y$  and the bar spacing is  $\Delta Y$ , the spatial frequency,  $N$ , will be

$$N = Y/\Delta y \text{ lines per picture height.} \quad (133)$$

By use of  $N$  as spatial frequency, which is dimensionless, component MTFs can be multiplied together (if the components are linear) to find the MTF of a group of components, or the overall system.

For the overall system, spatial frequency shall be specified in units of line pairs or cycles per milliradian referenced to object (or scene) space. If the spatial frequency of a pattern is given in terms of  $N$ , the spatial frequency  $k_\theta$  in line pairs per milliradian will be given by

$$k_\theta = \frac{N \cdot F_L}{2000 Y} \quad (134)$$

where  $F_L$  is the lens focal length. In addition, scene resolution may be reported in terms of a resolution angle  $\Delta\theta$ , where  $\Delta\theta$  is equal to

$$\Delta\theta = \frac{1}{2k_\theta} \quad (135)$$

The units of  $\Delta\theta$  are milliradians per line. If threshold values of  $\Delta\theta$  are reported, they shall be in addition to data given in terms of  $k_\theta$ .

#### 4.2.2 The Idealized Scene

The idealized scene shall consist of standard bar patterns as defined in 4.2.1. The scene is considered to be diffusely reflecting and normal to the line of sight. The range of scene irradiance levels to be expected shall be estimated for the passive case and calculated for the active case using the formula

$$E_S = \Phi_S / \Omega R^2 \quad (136)$$

where  $\Phi_S$  is the system source power,  $\Omega$  is the solid angle irradiated and  $R$  is the scene to camera range. The expected spectral scene

reflectivities,  $\rho_{\max}(\lambda)$  and  $\rho_{\min}(\lambda)$ , shall be and

Next the average photocurrent shall be calculated using the formula\*

$$i_{av} = \frac{A}{4T^2} \int_0^{\infty} \frac{[\rho_{\max}(\lambda) + \rho_{\min}(\lambda)]}{2} S(\lambda) \tau_f(\lambda) E_S(\lambda) d\lambda, \quad (137)$$

where A is the effective photosurface area, T is the lens T-stop,  $\rho_{\max}(\lambda)$  is the highlight reflectivity,  $\rho_{\min}$  is the lowlight reflectivity,  $S(\lambda)$  is the photosurfaces responsivity,  $\tau_f(\lambda)$  is the transmittance of any optical elements or filters other than the lens, and  $E_S$  is the scene irradiance level. Under laboratory conditions, atmospheric can be neglected. For passive sensors  $i_{av}$  will be independent of range while for active sensors  $i_{av}$  will be range dependent. In general, the use of photocurrent as a parameter is preferred when analyzing camera systems due to its spectral independence. Photocurrent can be readily converted to scene radiance knowing the scene and lens parameters.

#### 4.2.3 Overall System MTFs

For system SNR estimates, it is necessary that all of the MTFs which precede or follow points of noise insertion be separately indicated. However, the MTFs of any components which fall between two points of noise insertion can be lumped. From the MTF data, the following derived data shall be provided.

1.  $N_e$ , the overall system noise equivalent passband equal to

$$N_e = \int_0^{\infty} R_{oS}^2(N) dN, \quad (138)$$

where  $R_{oS}(N)$  is the overall system MTF.

---

\* if photoresponse is linear with irradiance level

2.  $R_{SF}(N)$ , the overall system square wave flux response equal to

$$R_{SF}(N) = \frac{8}{\pi^2} \sum_{k=1}^{\infty} \frac{R_o^2(kN)}{k^2} \quad \text{for } k \text{ odd.} \quad (139)$$

3.  $\beta(N)$ , the noise filtering function in the periodic direction equal to

$$\beta_c(N) = \frac{\int_0^N R_{of}^2(N) dN}{N}, \quad (140)$$

where  $R_{of}(N)$  is the MTF of those components following a point of noise insertion. One or more functions  $\beta(N)$  may be involved in a system depending on the noise sources.

4.  $\xi_s(N)$ , the noise increase factor along the bar lengths, equal to

$$\xi_s(N) = \left[ 1 + \left[ \frac{N}{N_{eC}} \right]^2 \right]^{\frac{1}{2}}, \quad (141)$$

where  $N_{eC}$  is the noise equivalent passband of the overall system. Ordinarily  $\xi_s(N)$  may be neglected.

5.  $\Gamma_C(N)$ , the noise filtering function along the bar lengths equal to

$$\Gamma_C(N) = \frac{\xi_{LT}(N)^{\frac{1}{2}}}{\left[ 1 + \left[ \frac{N}{N_{eB}} \right]^2 + 2 \left[ \frac{N}{N_{eC}} \right]^2 \right]^{\frac{1}{2}}}, \quad (142)$$

where  $N_{eB}$  refers to those noise equivalent passbands occurring before a point of noise insertion and  $N_{ef}$  represents those passbands following a point of noise insertion.

The linearity of the overall system shall be estimated or the functional dependence of the MTF on the system operating parameters shall be indicated.

In the above, it is assumed that the MTF characteristics are measured with patterns which are periodic in the direction of scan and aperiodic in the direction perpendicular to the scan. It is assumed that resolution in the scan and cross scan direction are balanced to be approximately equal. If not, the differences shall be noted. Also, raster interference effects expected shall be noted.

#### 4.2.4 Signal-to-Noise Ratio Obtainable

An analytical expression shall be provided for the display signal-to-noise ratio obtainable from the sensor when the input image is the standard laboratory test pattern of section 4.2.1. This expression shall include the lens MTF and the display MTF if applicable. All signal transfer factors and noise sources shall be included in the equation. The display signal-to-noise ratio shall be calculated for fixed values of photocurrent over the appropriate range of photocurrents and plotted as a function of spatial frequency in lines/picture height assuming a modulation contrast of unity.

For a typical TV camera of the type employing a photoemissive photosurface, a gain storage target and a preamp whose noise is essentially white in character, the following equation applies with good accuracy.

$$\frac{\text{SNR}_D}{C_M} = \left[ \frac{st}{\alpha} \right]^{\frac{1}{2}} \frac{R_{\text{SF}}(N)}{N \xi_y^{\frac{1}{2}}(N)} \frac{2Gi_{\text{av}}/e_v e_h}{\left[ \frac{eG^2 \beta_x(N) \Gamma_y(N) i_{\text{av}}}{(e_v e_h)^2} + \frac{I_p^2}{2\Delta f_V} \right]^{\frac{1}{2}}}, \quad (143)$$

where

$e$  = the length to width ratio of the bars in the test pattern  
(equal to 5 for the standard pattern).

$t$  = the temporal integration time of the observer's eye  
(assumed equal to 0.1 sec).

$\alpha$  = the effective focal plane width to height ratio.

$N$  = the bar pattern spatial frequency in lines per picture  
height.

$R_{\text{SF}}(N)$  = the overall system square wave flux response.

$\xi_y(N)$  = the noise increase function along the bar lengths.

$G$  = the combined gain of the intensifier, if used, and the  
gain-storage target.

$i_{\text{av}}$  = the average input image photocurrent due to the test  
pattern (Ampere).

$e_v e_h$  = the read-out electron beam scan efficiency.

$e$  = the charge of an electron (Coul).



$\beta_x(N)$  = the noise filtering function in the periodic direction  
of the bars.

$\Gamma_y(N)$  = the noise filtering function along the bar lengths.

$I_p$  = the rms preamp noise (Ampere).

$\Delta f_v$  = the video bandwidth (Hertz).

#### 4.2.5 Display Signal-to-Noise Ratio Required

In laboratory measurement, the observer is usually permitted to optimize the display viewing distance. For optimum viewing distance, the threshold value of  $SNR_D$  required by the observer is equal to 2.5 (assuming an eye integration time of 0.1 sec) for 50% probability of bar pattern detection. The observer's threshold  $SNR_D$  is independent of image contrast. However, to avoid the need for separate sets of display signal-to-noise ratio curves, it can be assumed that the observer's threshold is equal to  $2.5/C_M$  for values of  $C_M$  other than 1.0. The intersections of the threshold  $SNR_D$  curves with the  $SNR_D$  obtainable curves gives the threshold resolution which shall be determined and plotted for values of  $C_M =$   
and

#### 4.3 Predicted Field Performance

The maximum performance as predicted in section 4 will not in general be realized in a real environment due mainly to the atmosphere and sightline instability but the performance may also be degraded due to imaging geometries, scene radiance characteristics, extremes of temperature or other degradations commonly encountered in field use such as dirty windows, condensation, aging of components, etc. In any given mission,

certain degrading effects such as the atmosphere, will be beyond the control of the system designer and user. Certain effects, such as the selection of camera operating parameters, range gate selection, automatic irradiance level control, quality of stabilization, etc., are under partial control. To the extent possible, field performance degradations shall be estimated through calculations, simulations or through considerations based on previous experience. The extent to which partially controllable degrading effects are minimized through system design shall be indicated. For field performance calculations, the test pattern shall be considered to be a bar pattern similar to that used in the laboratory measurements and predictions.

#### 4.3.1 Effect of Sightline Vibration or Motion

For systems with small fields of view, sightline instability can become the dominant factor limiting system angular resolution. The instability may be due to aircraft perturbations, aerodynamic buffeting, structural resonances, gyro noise, stiction, etc. For the more common motions, i.e., linear, sinusoidal or random, motional MTFs can be derived. The contractor shall estimate the sightline instability, derive the motional MTF and include this MTF in the  $SNR_D$  analysis along with the other factors affecting field performance. Sightline instability causes MTF loss by its interaction with the storage or exposure time of the TV sensor. Because the motional MTF occurs after the generation of photoelectrons in tubes with photoemissive photocathodes and gain-storage targets, the motion MTF also has a noise filtering action (this is not true of vidicon type camera tubes).

Image motion may also cause sensor lag effects which have an MTF effect in addition to those involved in the interaction of motion with exposure time. To the extent possible, these effects shall be included in the analysis.

#### 4.3.2 Effect of Atmosphere (Passive)

The apparent contrast  $C_R$  of an object at range  $R$  is generally less than the inherent contrast  $C_0$  at zero range when a substantial amount of atmosphere intervenes between the sensor and the scene. For calculation purposes, the contrast degradation can be estimated from the relation

$$\frac{C_R}{C_0} = [1 - \frac{S_K}{G_D} (1 - e^{-\sigma R})]^{-1} , \quad (144)$$

where  $S_K/G_D$  is the sky-to-ground radiance ratio,  $\sigma$  is the atmospheric extinction coefficient and  $R$  is the optical slant range. For the purpose of calculation,  $S_K/G_D$  shall be assumed to be \_\_\_\_\_ and \_\_\_\_\_, and the atmospheric extinction coefficient shall be taken to be \_\_\_\_\_ and \_\_\_\_\_. Atmospheric MTF shall be taken into account if appropriate.

#### 4.3.3 Effects of Atmosphere (Active)

The effect of atmosphere at particular laser wavelengths such as  $0.855 \mu$  are not well known. Preliminary measurements indicate that the scene irradiance may fall off at a slower than exponential rate. However, for calculation purposes, it shall be assumed that the atmospheric transmittance  $\tau_A$  in the two-way path is exponential of the form

$$\tau_A = \exp(-2\alpha_0 R) . \quad (145)$$

The atmospheric extinction coefficients shall be taken to be \_\_\_\_\_ and \_\_\_\_\_, atmospheric MTF shall be taken into account if appropriate.

#### 4.3.4 Scene Irradiator - Sensor Gating Characteristics (Active)

The exposure duty cycle is defined as the ratio of the time the sensor is gated on to the total frame time. It, together with such spectral filters as may be used, will dictate the highest natural irradiance tolerable upon the scene before the passive scene image begins to mix with the active scene image. These effects shall be considered and their impact on system performance estimated for both general ambient scene irradiance levels and for bright light sources within the field of view.

The exposure gating ratio is the ratio of signal current with the sensor gated on continuously to that when it is gated off. The minimum exposure gating ratio shall be stipulated and the effect of incomplete gating on image contrast at the nearest point of intersection of the source and sensor fields of view shall be estimated.

The effect of uneven scene irradiance, such as may occur in low altitude flight and small sightline depression angles, shall be investigated and discussed. The methods proposed for scene irradiance and sensor sensitivity control shall be indicated including the sequence in which controls are activated, e.g., step 1, reduce intensifier and camera tube gain; step 2, reduce laser power; step 3, reduce iris opening, etc.

#### 4.3.5 Miscellaneous Environmental Considerations

In addition to sightline instability and atmospheric effects the effects of other environmental effects which bear on resolution shall be taken into account. Typical factors to be included are the effect of

temperature extremes, veiling glare, lens or dome defocus, sensor microphonics, increased dark current, window joints, split windows, increased observer thresholds, vignetting, etc.

#### 4.3.6 System Resolution (Passive)

Based on the new factors expected to be encountered in the field such as sightline instability, image contrast loss, atmospheric MTF, and the miscellaneous environmental conditions, new  $SNR_D$  calculations shall be made for various values of input photocurrent using a modulation contrast of unity. A technique of adjusting observer threshold  $SNR_D$  as a function of image contrast was discussed in section 4.2.5. This same technique can be used to plot observer thresholds as a function of range. The procedure is to assume a value of inherent image contrast, calculate the apparent image contrast at a given range and then adjust the threshold  $SNR_D$ . The intersection of the  $SNR_D$  obtainable curves with the threshold  $SNR_D$  curves gives the threshold resolution as a function of range for the particular value of inherent contrast chosen. For this calculation the inherent object contrast shall be \_\_\_\_\_ and \_\_\_\_\_. The threshold resolution shall be plotted as threshold angular frequency vs range for the specified contrasts. The predicted results will serve as a specification for flight measured bar pattern resolution.

#### 4.3.7 System Resolution (Active)

Based on the new factors expected to be encountered in the field such as sightline instability atmospheric scattering, atmospheric MTF and miscellaneous environmental factors, new  $SNR_D$  calculations shall be made for various values of input photocurrent. The values of photocurrent

shall be selected according to the expected value of input photocurrent at various regularly spaced range increments. To compute the expected value of input photocurrent vs range, the average value of scene reflectivity shall be taken to be \_\_\_\_\_ and \_\_\_\_\_, and the atmospheric extinction coefficient shall be as specified in section 4.3.4.

With a perfect range-gated system or with the near gate at the object to be detected, the apparent image contrast will be very nearly equal to the inherent image contrast. However, it is more likely that the scene object of interest will be in the center of the field-of-view. Also, some loss of contrast due to finite scene irradiator pulse duration may be expected. This loss of contrast shall be calculated and then used to adjust the range dependent  $SNR_D$  obtainable vs spatial frequency curves.

The intersection of the  $SNR_D$  obtainable curves with the threshold  $SNR_D$  curves gives the threshold resolution as a function of range. By adjustment of the threshold  $SNR_D$  as described in section 4.2.5 curves can be provided for various values of inherent object contrast. The values of contrast selected shall be \_\_\_\_\_, \_\_\_\_\_ and \_\_\_\_\_. The threshold resolution shall be plotted as threshold angular frequency vs range for the specified contrasts. The predicted results will serve as a specification for flight measured bar pattern resolution.

#### 4.4 Mission Requirements

The contractors understanding of the mission requirements shall be documented in this section starting with a general description of the mission including typical mission profiles, typical scenes, and tasks to be performed by the observer-user. From the general requirements,

the system requirements are to be generated in terms of the tasks to be performed. These specifics shall include but are not limited to

- (1) scene parameters such as target sizes, reflectivities, contrasts, geometries, etc.
- (2) typical and extremes of atmospherics expected in the world areas of greatest interest.
- (3) typical flight geometries, V/H ratios, time line analysis.
- (4) tasks to be performed, primary and secondary.
- (5) fields of view and line of sight steering coverage required to perform the desired primary and secondary tasks.
- (6) levels of scene-object discrimination required, e.g., detection, recognition, etc.

#### 4.4.1 Expectation of Meeting Mission Requirements

In the previous section, the test object is assumed to be a periodic bar pattern. There is some evidence that the detection of bar patterns correlates with the detection, recognition and identification of real scene objects. As a minimum, the bar pattern results serve as a basis of comparison.

It is incumbent upon the contractor to show that the system proposed have a reasonable chance of meeting the mission requirements. The criteria used in making the judgment that mission requirements are met are optional but must be clearly stated and supported through reference, documents or original investigation.

#### 4.4.2 Levels of Discrimination

The general mission requirements will dictate that certain levels of target discrimination be achieved. The contractor shall report his criteria for each level of discrimination in terms of the observer's requirements and in terms that can be related to the performance expected from the sensory system.

#### 4.4.3 Targets and Range Prediction

The contractor shall specify the primary targets of interest and predict the range at which these targets can be discerned at the desired level of discrimination. The contractor shall then show that the ranges predicted are sufficient to accomplish the mission.

#### 4.4.4 Mission Profile Recommendations

The contractor shall recommend flight profiles which optimize the probability of timely acquisition of targets.

#### 4.5 Nomenclature, Symbols and Units

The nomenclature and symbols shall be those used in these specifications and Table 13. The units are MKS and as specified in the International System (SI).



Table 13. International System (SI) for Fundamental Photometric and Radiometric Units

QUANTITY	SYMBOL <sup>(1)</sup>	DEFINING EQUATION <sup>(2)</sup>	UNITS	UNITS SYMBOL
Radiant Energy	Q	= $\int \phi dt$	{Joule lumen-sec (Talbot)	J
Luminous Energy				lm-s
Radiant Density	w	= $dQ/dV$	{Joule/cubic meter lumen-second/cubic meter	J/m <sup>3</sup>
Luminous Density				lm-s/m <sup>3</sup>
Radiant Flux	φ	= $dQ^*$	{Watt lumen	W
Luminous Flux				lm
Flux Density at a Surface				
Radiant Exitance <sup>(3)</sup>	M	= $d\phi/m^2$	{Watt/square meter lux (lumen/square meter)	W/m <sup>2</sup>
Luminous Exitance <sup>(3)</sup>				lx
Irradiance	E	= $d\phi/m^2$	{Watt/square meter lux (lumen/square meter)	W/m <sup>2</sup>
Illuminance				lx
Radiant Intensity	I	= $d\phi/d\omega$ (4)	{Watt/steradian candela (lumen/steradian)	W/sr
Luminous Intensity				cd
Radiance	L	= $d^2\phi/d\omega(d\alpha \cos \theta)$ (5)	{Watt/steradian - square meter nit (candela/square meter)	W/sr-m <sup>2</sup>
Luminance				nt
Dimensionless Ratios				
Emissivity	- ε	= $M/M_{\text{blackbody}}$		
Absorbance	- α	= $\phi_i/\phi_a$ (6)		
Reflectance	- ρ	= $\phi_r/\phi_i$ (6)		
Transmittance	- τ	= $\phi_t/\phi_i$ (6)		
Luminous Efficacy	- K	= $\phi_v/\phi_e$ (6)		
Luminous Efficiency	- v	= $k/k_{\text{maximum}}$ (7)		

(1) The symbols for radiometric and photometric quantities are the same. When it is necessary to differentiate between the two use subscript v for photometric and e for radiometric quantities; e.g.,  $Q_v, Q_e$ . Quantities may be restricted to narrow wavelength band by adding the word spectral and changing symbols with subscript λ; e.g.,  $\phi_\lambda$  for a spectral concentration, or a λ in parentheses; e.g.,  $K(\lambda)$  for a function of wavelength.

(2) Equations are given merely for identification.

(3) Emittance may be used for exitance but emittance is to be deprecated.

(4) ω is the solid angle through which flux from a point source is radiated.

(5) θ is angle between line of sight and normal to surface being considered.

(6) φ<sub>i</sub> is incident flux, φ<sub>a</sub> is absorbed flux, φ<sub>r</sub> is reflected flux, φ<sub>t</sub> is transmitted flux.

(7) K<sub>maximum</sub> is the maximum of the K<sub>(λ)</sub> function.

## 5.0 Dynamic Range

Suppose a specific image is projected onto the photosurface of an electro-optical sensor. As the image irradiance is reduced, a point will be reached where the image becomes undetectable due to a combination of photoelectron and system generated noises. On the other hand, if the image irradiance is increased, a point will be reached where some element of the sensory system, such as the camera tube's gain-storage target, the video amplifier, or the display, saturates. Further increases in image irradiance, beyond saturation will usually result in a distortion of the displayed images amplitude or shape. Two adjacent images may become discerned as one due either to image spread or to a loss of differential amplitude. Presumably, a lower and an upper limit to an image's irradiance which yields acceptable imagery could be specified and the difference between the limits could be designated the dynamic range of the sensor. If it were this simple, the dynamic range of a sensor would have been defined long ago.

Part of the problem stems from the fact that the discernability of an image at any irradiance level depends upon its dimensions. A large image can be discerned by an observer at a much lower photosurface irradiance level than can a small one. This problem can be alleviated if a standard image size can be agreed upon.

At low irradiance levels, the limit of a standard test image's discernability could be quite well defined. However, at high irradiance

levels, the limit will not be nearly so well defined due to differences in the saturation characteristics of various sensors. Sometimes, the saturation characteristic is abrupt, sometimes gradual and sometimes a sensor will move into a new mode of operation. In addition, the effects of saturation differ. In some cases, the displayed image area simply increases in proportion to the increase in image irradiance. The displayed image may be simply white or white surrounded by concentric black rings. In newer camera tubes, image growth is confined either by the target structure or by barriers. In a FLIR, the saturation may be seen primarily as streaking in the direction of scan.

For practical purposes, it may be desirable or even necessary to divide the "dynamic range" into two intervals. One interval would be that region over which the sensor's output current increases with increase in image irradiance and the second region over which the output current is substantially independent of input irradiance.

The "dynamic range" for a given sensor is usually a function of the operating point and thus, is variable. For example, the gain of camera tube image sections can be electronically controlled, input photosurface area can be electronically zoomed and displayed image brightness and contrast can be varied at will. Therefore, it will be necessary to include operating point as a parameter in describing dynamic range.

In the initial analysis, any dynamic range limitations due to the display or observer will be ignored. This is equivalent to assuming that the display and observer have an infinitely wide dynamic range.

The most common measure of dynamic range in the below saturation region of a sensor is the use of a grey scale. A test pattern is

constructed consisting of a series of adjacent rectangles whose brightnesses progressively increase (or decrease) from one end to the other in a staircase fashion. The dynamic range is specified in terms of the number of shades of grey that the observer can detect, i.e., he counts the number of steps he can perceive. The grey scale specification is not necessarily a bad one if it is properly defined and standardized. Its single most glaring fault is that the system requirements to discern a number of shades of grey are not known. Thus, it is almost impossible at this time to synthesize a system to meet a grey shade specification with assurance, beforehand, that the specification will be met. Furthermore, it may be more important in some applications to have more shades in the white (or the black) end of the scale even at the expense of the total number discernible.

Ordinarily, the grey scale test patterns are of low spatial frequency in order to avoid MTF effects. The effect of MTF is to decrease grey scale rendition at high spatial frequencies and as a consequence, two sensors with equal grey scale rendition as classically defined may be far different at high spatial frequencies. A possible solution is to include the MTF curve as part of the grey scale - dynamic range specification. Another is to make use of the threshold resolution vs irradiance level curves if some means of interpreting the results can be found.

On a more absolute basis, dynamic range may be defined on the basis of electrically measured, or possibly calculated, signal-to-noise ratios. This has appeal in that it avoids the use of an observer but it does not necessarily correlate directly with observed image quality. However,

since signal-to-noise ratio, as electrically measured is fundamental to the whole subject of dynamic range, we shall treat this subject first.

### 5.1 Signal Transfer Characteristic and Video Signal-to-Noise Ratio

For television camera systems, the signal transfer characteristic is defined as a plot of the current output of the tube as a function of the input photosurface irradiance (or illuminance). For our purposes, it is convenient to redefine the signal transfer characteristic as a plot of the output signal current  $I_H$  as a function of input photocurrent  $i_H$ . The subscript H is added to indicate that the peak-to-peak current swing is measured. Also, the signal transfer characteristic is always measured using a test image of large size so as to eliminate MTF as a factor. The current  $i_H$  is related to the photosurface irradiance through the formula

$$i_H = \int_0^{\infty} S_{\lambda} A E_{\lambda} d\lambda \quad , \quad (146)$$

where  $S_{\lambda}$  is the spectral responsivity,  $A$  is the total effective area and  $E_{\lambda}$  is the highlight spectral irradiance of the input photosurface.

A typical signal transfer characteristic is shown in Fig. 49 for an Intensified Electron-Bombarded-Silicon or I-EBSICON camera tube. A number of curves are shown for various values of camera tube gain. The overall I-EBSICON gain is the product of the intensifier phosphor/EBSICON photocathode gain,  $G_I$ , the EBSICON target gain,  $G_T$ , and the inverse of the scan efficiency  $e_v e_h$ . Quantitatively,

$$I_H = \frac{G_I G_T}{e_v e_h} i_H \quad . \quad (147)$$

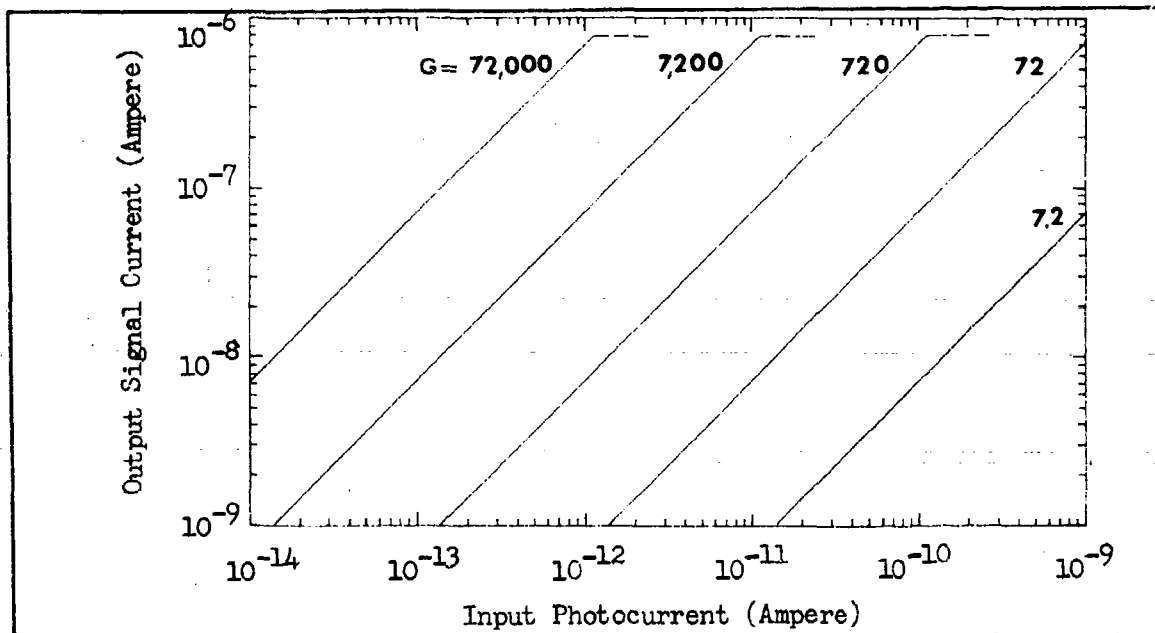


Fig. 49 Typical Output Signal Current vs Input Photocurrent for the Intensified-EBSICON Camera.

Typically,  $e_v e_h = 0.79$  and the maximum values of  $G_I$  and  $G_T$  are about 30 and 1890 respectively. Then  $I_H = 72,000 i_H$ . The product of  $G_I$  and  $G_T$  can be reduced to of the order of 4 - 10. The lower limits of the gains  $G_I$  and  $G_T$  are set by the onset of image defocus and rotation as the accelerating voltages are reduced below a certain point. The scan efficiency term results from the finite time required to retrace the electron scanning beam. Because of the loss of scanning time, the actual effective photosurface area must be scanned more rapidly. Since the same amount of charge on the target is read-out in less time, the output current increases. Thus, the inverse of scan efficiency may be thought of as a gain. Note, however, that as scan efficiency is reduced the system's video bandwidth must be increased.

The signal transfer curves of Fig. 49 are shown to change abruptly

at  $8 \times 10^{-7}$  Ampere. The "knee" in the curve is not really abrupt for the I-EBSICON but will be considered to be so for simplicity in the discussion and analysis. High contrast, low spatial frequency images can be discerned with very low output signal currents - perhaps as low as  $10^{-10}$  Ampere. Thus, for a given gain setting, the range of input photocurrents that can result in perceptable images is nearly  $10^4$ . Also, by gain change, this  $10^4$  range can be positioned over an additional range of  $10^4$ . However, it should not be inferred that a  $10^8$  range is obtainable in one scene. As the camera tube gain is reduced, the input photocurrent must increase to maintain image resolution.

In the preceding paragraph, it is inferred that the output current is maintained below the knee of the curve. A bright light in a low light level scene will usually drive the camera tube storage target to above saturation in a local area about the image of the light. In the older camera tubes, the image of the bright light grew in area in proportion to the intensity of the light. This extended image could have two effects. The first is to obscure images in the vicinity of the light and the second is to cause automatic light level circuitry, if used, to decrease camera gain and thus decrease sensitivity over the entire field of view. While the latter effect can be minimized by proper circuit design and operational procedures, it is nevertheless a serious problem. Fortunately, camera tubes with "anti-blooming" characteristics are now becoming available. While bright light problems still exist, they are much less troublesome.

It has been suggested, on occasion, that dynamic range, for operation

below the knee of the signal transfer characteristic be defined in terms of the video signal-to-noise ratio. The video signal-to-noise ratio is electrically measurable in principle although in practice, it is difficult to achieve high precision. On the other hand, for many camera tubes such as the I-EBSICON, the  $SNR_v$  can be calculated with greater confidence that it can be measured.

One problem with the video signal-to-noise ratio is its dependence on the video bandwidth. As is well known, the ability of an observer to perceive an image is relatively independent of video bandwidth except as it may affect the signal waveform (too narrow a bandwidth) or increase a system generated noise density. A typical system generated noise is the preamp noise. If the preamp noise is white, video bandwidth would have no effect on a displayed images discernability so long as the signal is not affected. However, many preamps have a noise spectrum which increases with frequency and thus a too wide video bandwidth increases the perceived noise. The main point is that the video signal-to-noise ratio measured is a function of video bandwidth and the video bandwidth may or may not affect the quality of the perceived image on the display. One possible remedy would be to specify a particular bandwidth but this condition would either handicap high resolution sensors if the bandwidth is too narrow or low resolution systems if the bandwidth is too wide. The best solution would appear to be to define a reference bandwidth,  $\Delta f_r$  equal numerically to

$$\Delta f_r = \frac{\alpha N_s N_v}{2t_f e_v e_h} \quad , \quad (148)$$



where  $\alpha$  is the horizontal-to-vertical picture aspect ratio,  $N_v$  is the number of active scan lines on the effective photocathode area (with the scanned direction presumed to be horizontal),  $t_f$  is the frame time and  $e_v e_h$  are the vertical and horizontal scan efficiencies respectively. The quantity  $N_H$  represents the horizontal resolution specified in units of lines per picture height.  $N_H$  can be limited artificially by limiting the bandwidth. In commercial TV broadcast, it may not be unreasonable to use a fixed bandwidth equal to or related to the bandwidth that can be transmitted. In closed circuit applications, the video bandwidth can be as large as desired but the maximum horizontal resolution will be limited by the camera parameters. These parameters include the camera tube MTF, the maximum signal storage capability and the sources of noise whether internal to the camera tube or in its associated circuitry. In general, a manufacturer will claim some maximum (or absolute limiting) value for  $N_H$ . In this case, the reference bandwidth should be consistent with the claimed maximum resolution.

In the case of the I-EBSICON, the principal noises are the photoelectron noise generated in the primary scene photon-to-photoelectron process and the preamplifier noise. The preamplifier noise is generally video bandwidth limited but the photoelectron noise is camera MTF limited. The principal MTF's are due to the intensifier phosphor and the EBSICON gain storage target. If the combined MTF of the intensifier phosphor and EBSICON target is  $R_{OT}$  in the horizontal, the noise equivalent bandwidth is

$$N_{eT} = \int_0^{\infty} |R_{OT}(N)|^2 dN \quad (149)$$

This bandwidth is substituted for  $N_H$  in Eq. (148). Typically,  $N_{eT}$  is of the order of 150 to 250 lines. If the noise in the vertical is uncorrelated line-to-line, the  $N_v$  in the equation would remain equal to the number of scanning lines. However, the noise in a TV camera shows line-to-line correlation and thus it would appear more reasonable to use  $N_{eT}$  as an estimate of the number of vertical lines in the equivalent noise bandwidth calculation. That is, for the photoelectron noise, the bandwidth  $\Delta f_p$  is

$$\Delta f_p = \frac{\alpha N_{eT}^2}{2t_f \cdot e_v \cdot e_h} \quad (150)$$

Suppose the rms preamp noise in the reference bandwidth  $\Delta f_r$  is  $I_p^2$ , then the peak-to-peak video signal to rms noise in the picture whites with a 100% contrast broad area image input is given approximately by

$$SNR_{Vo} = \frac{G_I G_T i_H / e_v e_h}{\left[ 2e \left( \frac{G_I G_T}{e_v e_h} \right)^2 i_H \Delta f_p + I_p^2 \right]^{1/2}} \quad (151)$$

where  $e$  is the charge of an electron usually the noise in the whites and in the blacks are averaged. With a 100% input image contrast, the noise in the picture blacks should be only the preamp noise while in the whites, it is the quadratic sum of preamp and photoelectron noise. Thus, the peak-to-peak signal-to-averaged rms noise ratio becomes

$$\overline{\text{SNR}}_{V_0} = \frac{2G_I G_T i_H / e_v e_h}{\left[ 2e \left( \frac{G_I G_T}{e_v e_h} \right)^2 i_H \Delta f_p + 2I_p^2 \right]^{1/2}} \quad (152)$$

In the above expression, we note that when  $G_I G_T$  is very high, that the photoelectron noise will dominate and

$$\overline{\text{SNR}}_{V_0} \approx \left[ \frac{2i_H}{e \Delta f_p} \right]^{1/2} \quad (153)$$

A high gain is not necessarily an advantage since the value of  $i_H$  is limited to a maximum value of

$$i_{H\text{max}} = \frac{I_{H\text{max}}}{(G_I G_T / e_v e_h)} \quad (154)$$

The larger the gain, the smaller the  $i_{H\text{max}}$  and the smaller will be the maximum obtainable  $\overline{\text{SNR}}_{V_0}$ .

To increase the maximum obtainable  $\overline{\text{SNR}}_{V_0}$ , it is necessary to reduce the gain.  $\overline{\text{SNR}}_{V_0}$ , of course, will not actually increase as gain is reduced unless  $i_H$  increases in proportion to the gain reduction. Recall that  $i_H$  is proportional to the input image's irradiance. Eventually, as gain is reduced and  $i_H$  is increased, the maximum  $\overline{\text{SNR}}_{V_0}$  will reach a limit given by

$$\overline{\text{SNR}}_{V_0} = \frac{2^{1/2} I_{H\text{max}}}{I_p} \quad (155)$$

These processes are illustrated in Fig. 50 where the  $\overline{\text{SNR}}_{V_0}$  is calculated for a number of values of gain as a function of highlight photo-

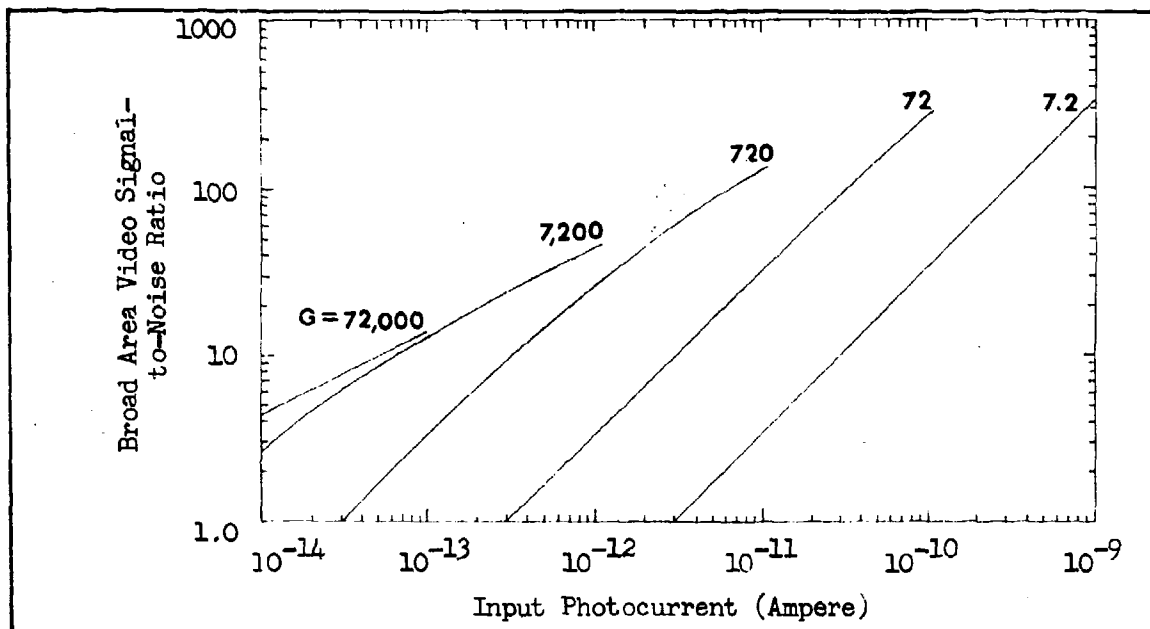


Fig. 50 Typical Broad Area Video Signal-to-Noise Ratio vs Input Photocurrent for the Intensified-EBSICON Camera.

current. For these calculations, it is assumed that  $N_{eT} = 160$ ,  $I_p^2 = 9 \times 10^{-18}$  Amperes<sup>2</sup>,  $\alpha = 4/3$ ,  $t_f = 1/30$  sec,  $e_v e_h = 0.79$  and  $[G_I G_T / e_v e_h]$  has a maximum value of 72,000 and for the successive curves, gain is decreased in decade steps. The maximum output signal current is assumed to be  $8 \times 10^{-7}$  Amperes.

As can be seen in Fig. 50, the maximum value of  $\overline{SNR}_{V_0}$  with a gain of 72,000 is about 14.5 with an input photocurrent of  $10^{-11}$  Ampere. By decreasing the gain to 7,200, the maximum value of  $\overline{SNR}_{V_0}$  increases to about 46. Below  $10^{-11}$  Ampere, the high gain is seen to give superior performance but does limit the dynamic  $\overline{SNR}_{V_0}$  range. With very large input photocurrents (high photocathode irradiance levels), the maximum  $\overline{SNR}_{V_0}$  obtainable increases to about 350:1.

We noted previously that the  $\overline{\text{SNR}}_{V_0}$  as defined above applies only to broad area input images. This is done purposely to eliminate the effect of sensor MTF's on output signal amplitude. As the input image dimensions are decreased, the amplitude of the video signal will eventually begin to decrease in turn. Generally, this will begin to happen when the image dimensions approach the size of the noise equivalent aperture  $\delta_{eT}$  given by

$$\delta_{eT} = \frac{1}{N_{eT}}, \quad (156)$$

where  $N_{eT}$  is defined by Eq. (149). This image is quite small -- of the order of 1/100 to 1/200 of the picture height as a rule. However, two sensors, with identical  $\overline{\text{SNR}}_{V_0}$  curves may differ appreciably with respect to their ability to detect small images. With small image inputs, the video signal-to-noise ratio obtainable from a high resolution camera can be many times larger than that obtainable from a low resolution camera. The high resolution camera must be interpreted as having a wider dynamic range. One possibility is to measure  $\overline{\text{SNR}}_V$  with a variety of test images of varying dimensions.

We note, however, that it is customary to measure the response of camera tubes using bar patterns of various spatial frequencies. The peak-to-peak amplitude of the video signal is measured as bar pattern spatial frequency is increased in discrete steps. The result, normalized to zero spatial frequency is known as the square wave amplitude response  $R_{SQ}(N)$  and has the typical numerical values shown in Table 10. This can be used to modify the broad area  $\text{SNR}_V$  as follows:

$$\overline{\text{SNR}}_V(N) = \frac{2R_{SQ}(N)G_I G_T i_H / e_v e_h}{\left[ 2e \left( \frac{G_I G_T}{e_v e_h} \right)^2 i_H \Delta f_p + 2I_p^2 \right]^{\frac{1}{2}}} \quad (157)$$

This could be offered as a three dimensional plot but ordinarily, the combination of the  $\overline{\text{SNR}}_{V_0}$  and the  $R_{SQ}(N)$  curves individually should be sufficient.

We note further that the video signal-to-noise ratio is a function of the test pattern contrast. We define modulation contrast as

$$C_M = \frac{i_H - i_L}{i_H + i_L} \quad (158)$$

where  $i_H$  and  $i_L$  are the highlight and low light input photocurrents respectively. With this definition, the video signal-to-noise ratio becomes

$$\overline{\text{SNR}}_V(N, C) = \frac{2C_M R_{SQ}(N)G_I G_T i_{av}}{\left[ 2e \left( \frac{G_I G_T}{e_v e_h} \right)^2 i_{av} \Delta f_p + I_p^2 \right]^{\frac{1}{2}}} \quad (159)$$

where  $i_{av} = (i_H + i_L)/2$ .

Aside from the difficulty in defining the noise bandwidths, the video signal-to-noise ratio has some attraction as a dynamic range specification. Presumably the video signal-to-noise ratio is measurable but a good measurement is not easy. The most common method of estimating noise is to use a line selector oscilloscope. This method is of highly questionable accuracy. The preferred method is to use an rms meter which has been designed so as to eliminate the video synchronizing

pulses or some of the newer computer based measuring methods.

The principal shortcoming of the video SNR method is that it does not include either the display or the observer as parts of the sensory process and thus does not relate directly to the overall sensory system dynamic range.

## 5.2 Shades of Grey

Many multipurpose television test patterns include a grey scale. The grey scales consist of a series of adjacent rectangles. Each rectangle varies in reflectivity from its neighbor in graded steps from one end to the other in staircase fashion. The background may be either black or white. The grey scale is widely used by broadcast engineers to set up their cameras. One use is to detect overshoot or ringing at the video amplifier. A second use is to insert black or white stretch. A third use is to test amplifier linearity. Black stretch, a higher amplification of images in the scene low lights, is used when the scene contains many shadow areas while white stretch, a higher amplification of images in the scene highlights is used when the scene is brightly lighted but of low contrast.

The number of shades of grey that can be discerned on the display of a TV camera is often used as a TV camera specification. This may not be totally inappropriate if the meaning of the specification is fully understood. In general, it is desired to discern a large number of shades of grey but under certain conditions, a large number of grey shade requirement can work at cross purposes to the overall system objectives. For example, it may be necessary to increase the capacitance of a camera tube's gain storage target to obtain the

necessary shades of grey but this will have an adverse effect on the camera tube's lag (response time) characteristic. Also, black stretch may be introduced to achieve the grey shade number which will look best in the laboratory while white stretch may be more appropriate for a specific air-to-ground reconnaissance application.

The grey shade measurement includes both the display and the observer in addition to the camera tube. Thus, it has the potential of being an overall measure of sensory system dynamic range. However, MTF effects probably play a rather minor role in the detection of grey shades and resolving capability should probably be part of a dynamic range specification.

In one common grey scale pattern, the incremental reflectance per step is a constant. The signal waveform is typically as shown in Fig. 51. The incremental signal current at any given step is equal to a constant  $k_I i_H$ . The photoelectron noise is a function of the average photocurrent. If the maximum photocurrent in the white portion of the display is  $i_H$ , the average photocurrent at the  $n$ th step is  $i_H(1 - nk_I/2)$ .

### 5.3 Psychophysical Experiments - Shades of Grey

Since the grey shade pattern is in common use as a system specification and has some potential as a dynamic range specification, it was considered worthwhile to obtain observer requirements with regard to grey shade detection. The hope is that if observer requirements are known, then systems could be synthesized to meet a grey shade specification or as a minimum, to determine the conditions under which a grey shade specification is unrealistic.



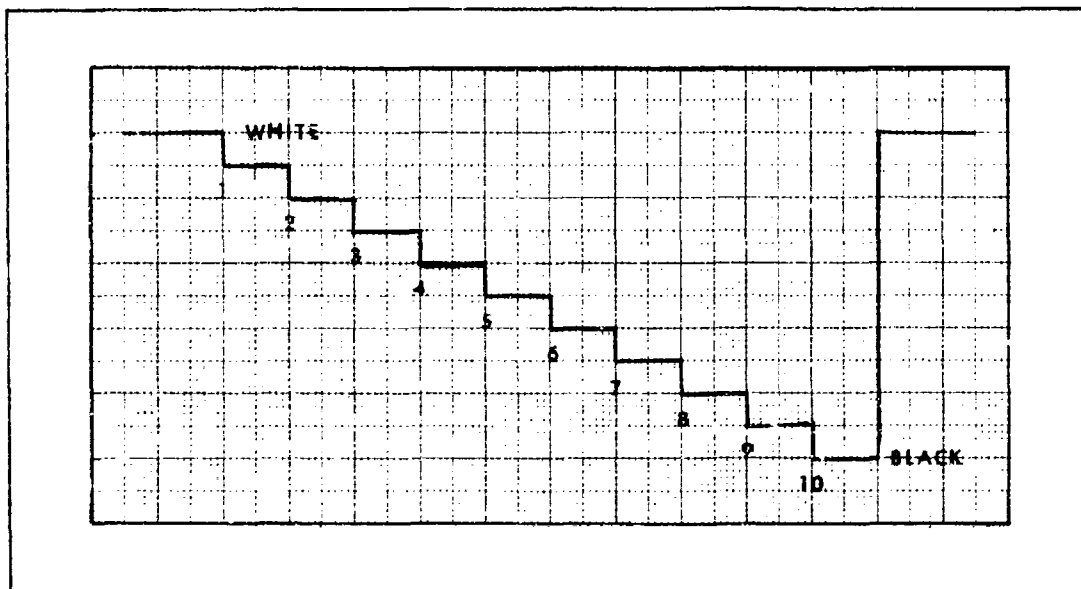


Fig. 51 Video Waveform for a Typical Linear Grey Scale.

The usual grey shade scale, shown as part of a resolution pattern, consists of a linear array of 9 rectangles. Each rectangle is  $1/18$  of a picture height high and  $1/16$  of a picture height wide. Measured in terms of scan lines, assuming 490 active lines per picture height, each rectangle is 28 lines high and 30.5 lines wide. Most commonly, the background of the grey scale is white so that each rectangle in the grey scale is surrounded by white on two sides and by a rectangle that is slightly brighter than the rectangle of interest on one side and by one which is slightly darker on the other side. In the rectangle detection studies discussed in section 2, the rectangles were surrounded by a uniform background on all four sides. Furthermore, at threshold, the background brightness is not far different from the brightness of the rectangle being detected. In detecting a grey scale, two rectangles,

differing in brightness by a small amount must be distinguished one from the other while surrounded on two sides by a background which is very much brighter than either of the two in question. Thus, we suspected and did find, that the detection of a grey scale rectangle differs from the problem of detecting an isolated rectangle on a uniform background.

In the isolated rectangle case, the incremental signal is defined as the difference between the rectangle and background brightness and the noise is proportional to the average of the rectangle and background brightness. Obviously, neither signal nor noise can be so precisely defined when the background brightness differs on the various sides of a given grey rectangle, i.e., the background would be the same on two sides of the grey scale and different on the other two sides for all but the two ends of the grey scale where three sides are the same. Thus, at the onset of the experimentation we are at a loss with respect to defining a clear cut hypothetical model for image signal-to-noise ratio to either verify or discredit.

In the first grey shade experiment an electronically generated 2-step staircase was generated with the waveform shown in Fig. 54. The length of the rectangle corresponded to 73 scan lines (relative to 490 active scan lines in the total picture height). The width of the rectangle in the vertical directions was varied from 2 to 32 scan lines. The system was operated at 30 frames/sec with 490 active scan lines in the vertical. The experimental setup is shown in Fig. 53. The observers were 28" distance from the 8" high monitor of 1 ft-Lambert brightness. Four observers participated in the experiment and a total

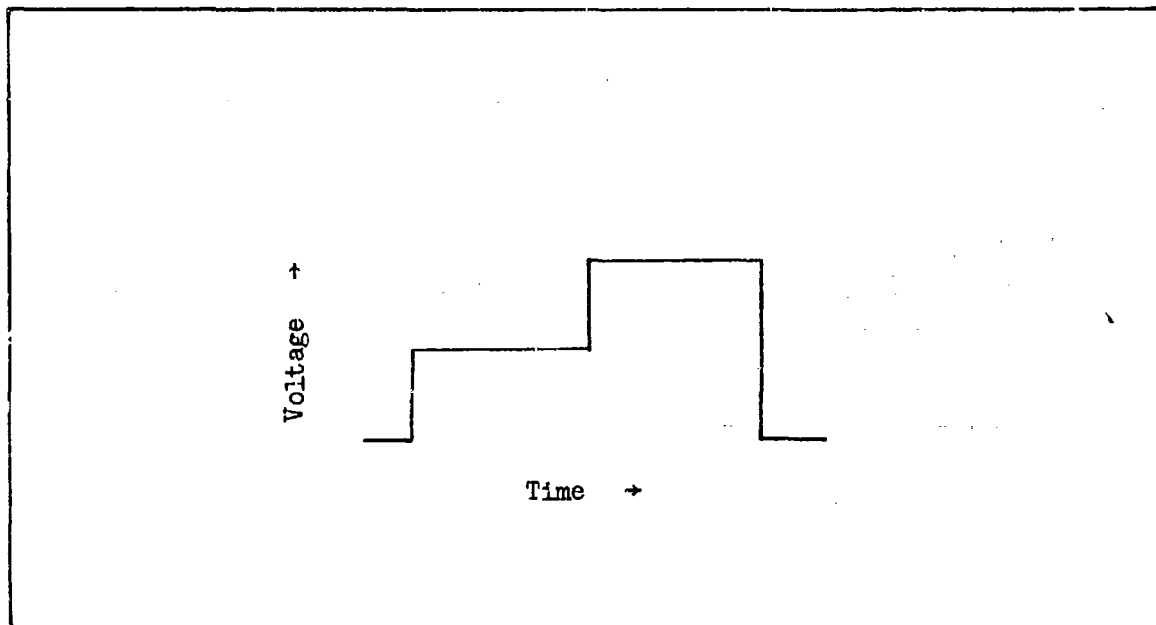


Fig. 52 Video Waveform Used for the Double Rectangle Experiments.

of 1643 data points were taken.

In the psychophysical experiment the observer was asked to determine whether or not he could discern a line between two shades of grey. The threshold value\* of video signal-to-noise ratio required to discern the line between the two rectangles is plotted in Fig. 53. The abscissa is a log scale and it is seen that the  $SNR_v$  required decreases at approximately the  $1/2$  power of the line length, i.e., the threshold signal to noise ratio is inversely proportional to the length of the line separating two grey shade rectangles. At line lengths greater than 8 scan lines, the threshold did not fall off as fast. This is undoubtedly due to the eye's inability to spatially integrate over the entire line

\* By threshold, we mean that average value where the line was discerned 50% of the time.

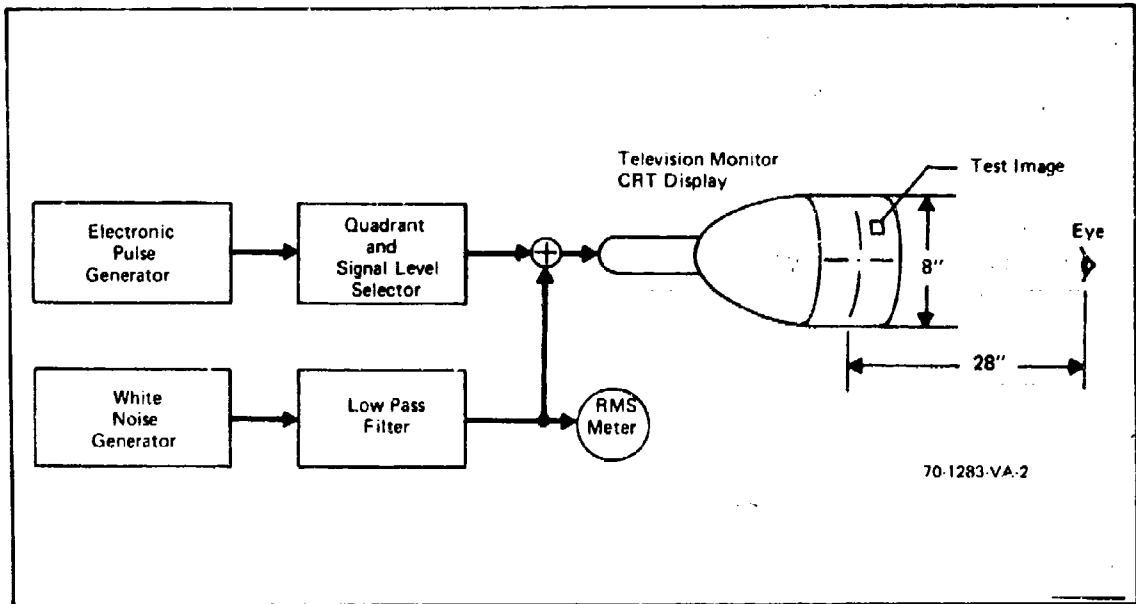


Fig. 53 The Display Signal-to-Noise Ratio Experiment.

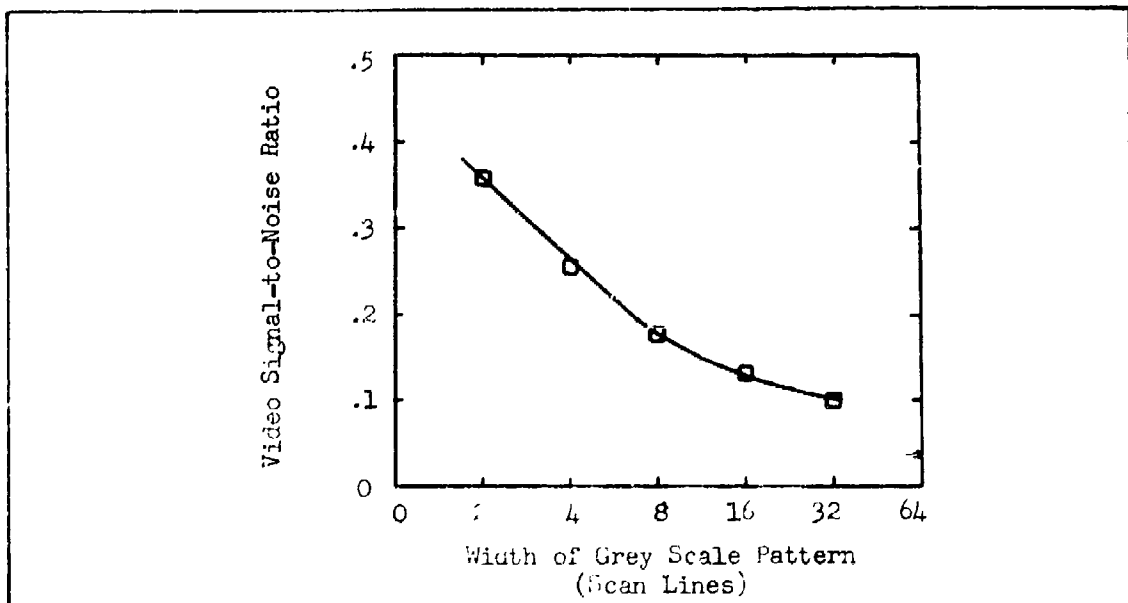


Fig. 54 Video Signal-to-Noise Ratio for Electronically Generated Shades of Grey as a Function of the Number of Scan Lines in a Bar Width.

length once the lines angular subtense increases beyond about  $\frac{1}{2}^\circ$  relative to the observer's eye.

Since the images in the above experiment were electronically generated with near perfect edges, MTF effects can be ignored. In this case, the image's display signal-to-noise ratio may be written as

$$\text{SNR}_D = [t\Delta f_V \left(\frac{a}{A}\right)]^{\frac{1}{2}} \text{SNR}_V, \quad (160)$$

where  $t$  is the observer's integration time,  $\Delta f_V$  is the video bandwidth,  $a/A$  is the ratio of image area to total picture area and  $\text{SNR}_V$  is the video signal-to-noise ratio. It is hypothesized that the eye does not integrate over the entire area of the grey shade rectangle when discerning the edge between two rectangles but rather, integrates over some distance to the left and right of the edge. We wish to estimate the distance over which the eye apparently integrates. For this purpose, let  $X_L$  be the length of the line dividing the two grey shades and let  $X_W$  be the effective integration distance expressed in units of scan lines. The relative area  $a/A$  is then

$$\frac{a}{A} = \frac{X_L X_W}{\alpha (490)^2}, \quad (161)$$

and Eq. (160) becomes

$$\text{SNR}_D = \left[ \frac{X_L X_W t \Delta f_V}{\alpha (490)^2} \right]^{\frac{1}{2}} \cdot \text{SNR}_V. \quad (162)$$

We know that the threshold value of  $\text{SNR}_D$  is equal to 2.8 for rectangles that are not of too large an extent in two directions simultaneously

(Ref. 2). If we solve the above equation for  $X_W$ , set  $SNR_D = 2.8$  and use the threshold value of 0.26 for  $SNR_V$  (for the 4-line high line width of Fig. 53), we can obtain a value for  $X_W$ . The value of  $X_W$  was found to be 7.7 scan lines. The presumption in the above analysis is that the detection of the line of demarcation between two grey shades is equivalent to the detection of a rectangle of height equal to the line length and of some width which, in the specific case tried was 7.7 scan lines. The angular subtense of the width determined, at the observer's eye, was 15.5 minutes of arc. In the previous large rectangle experiments of Ref. 2, an angular width of between 10 - 15' of arc was determined for the eye "integration distance." While the tasks are similar they are not exactly the same and we would not necessarily expect to get the exact same number. On the other hand, the results are probably within the experimental error.

In the second experiment, a 1.5-inch vidicon was used to generate the image of a 10-step grey scale. The camera was operated with an 875-line raster at 25 frames/sec. Relative to a conventional system with 490 scan lines, the height and width of each grey scale rectangle was 28 x 30 lines. The observer to display viewing distance to display height ratio was 3.5. The grey scale used is one that appears on a standard EIA test pattern as shown in Fig. 55.

The incremental reflectance per step was approximately constant. The white noise is added uniformly to all the steps and thus the video signal-to-noise ratio per step is a constant. Assuming the SNR to be constant, we would hypothesize that all of the steps should become simultaneously discernable when the SNR increases to above its threshold

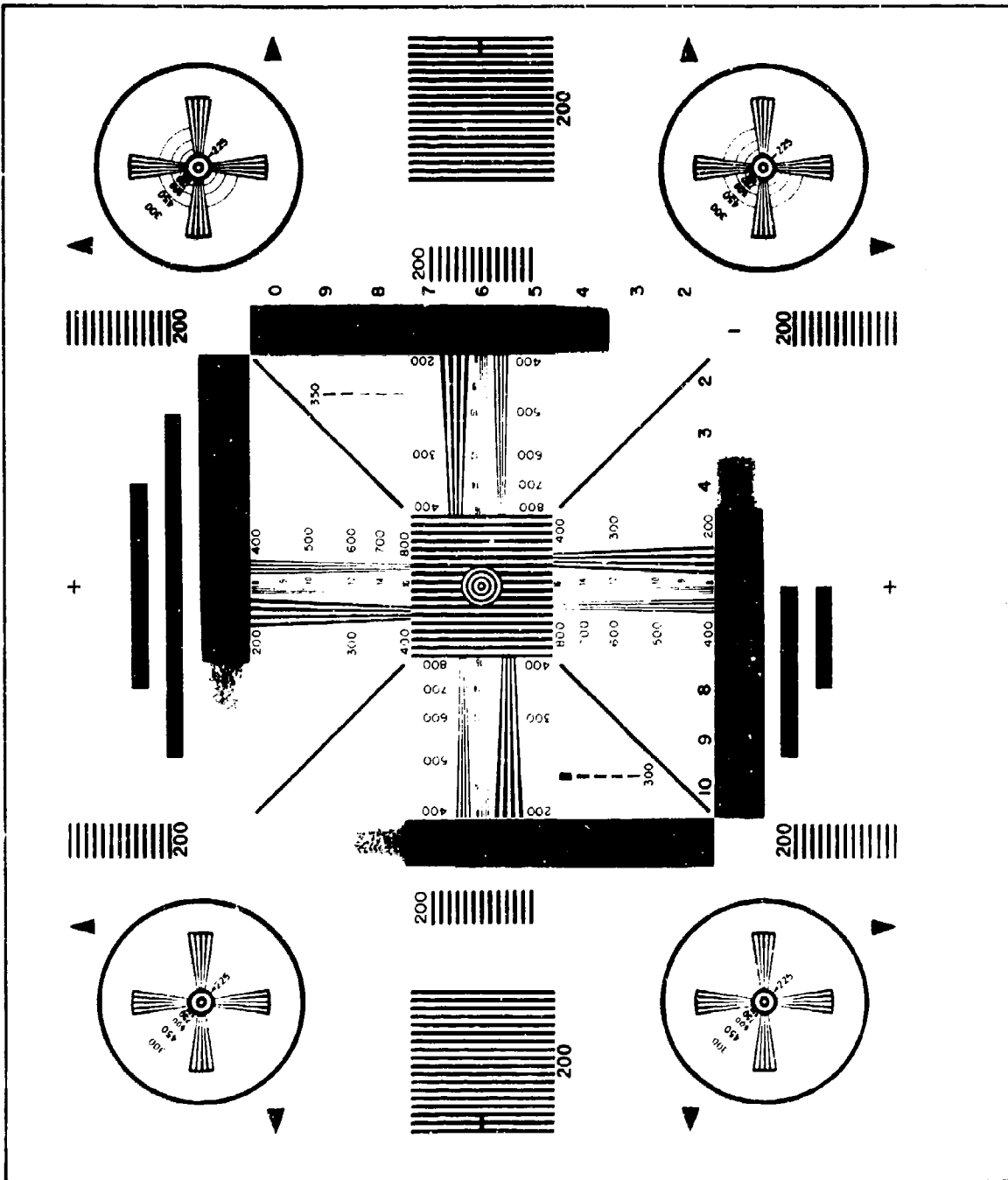


Fig. 55 Test Pattern Showing Grey Scale Pattern.

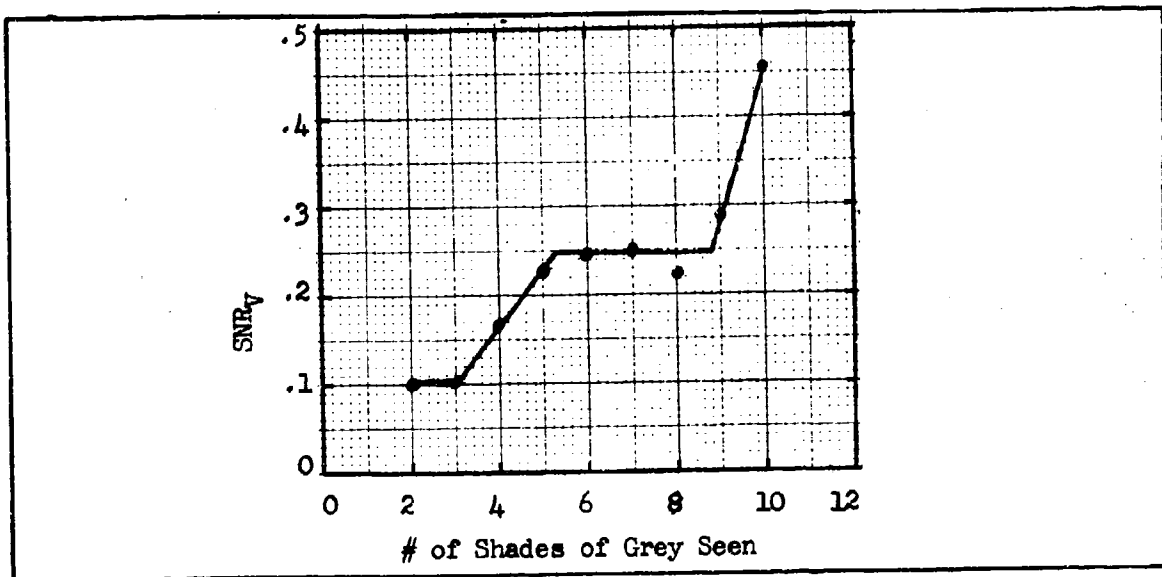


Fig. 56 Video Signal-to-Noise Ratio for EIA Grey Scale as a Function of Number of Shades of Grey

value. Based on the results obtained with the electronically generated grey steps, this should occur when the  $SNR_V$  is increased to its threshold value of 0.11 independent of the step number (see Fig. 54). From past experience, we know that this is not the case.

The threshold  $SNR_V$  values from the EIA grey scale experiment are plotted in Fig. 56 vs grey shade number. Number 1 corresponds to white and number 10 corresponds to black. The expected result is obtained for step number 2 and 3 but larger values of  $SNR_V$  are needed for the higher steps. Notice that the surround for step number 2 and 3 is similar to that for the electronically generated shade of grey and it is not surprising that the threshold value of  $SNR_V$  is the same for the two experiments due to the similarity of conditions. For the higher steps, the adjacent steps are dim and are surrounded on each side by the bright background



which undoubtedly adds perceived noise. This noise is not included in the calculation of the threshold  $SNR_V$  and therefore it is expected that a larger calculated  $SNR_V$  value is required for the darker steps. The problem in including this noise in the  $SNR_V$  calculation is in the modeling and a new model will be necessary to correctly account for this change of brightness conditions. Practically, the implications are that fewer shades of grey will be seen with the bright surround than would be seen if the surround were dark.

A third experiment was performed with a black background around the EIA grey scale. One observer was used and 260 data prints were taken. Two cases were considered, the first step (#2 on the chart) was 10 f-L with no noise and became 14 f-L when the noise was added. The second case had the last step (#10 on the chart) at 10 f-L without noise and 14 f-L with noise. The experimental results plotted as threshold  $SNR_V$  vs grey scale step number are shown in Fig. 57. The required value of  $SNR_V$  is nearly a constant for the two cases and the average threshold value is equal to 0.1, the previous value obtained for the ideal case of the electronic generated double rectangle.

Evidently when the signal-to-noise ratio for a grey step is determined completely by that ratio in the video channel then, for a constant noise the required threshold  $SNR_V$  value is a constant but if the monitor conditions are such that the signal-to-noise of the image changes such as is the case with a bright surround on the scale then different results will be obtained if this added monitor conditions are not taken into account in the model.

In summary, we see that the ability to detect a grey scale depends

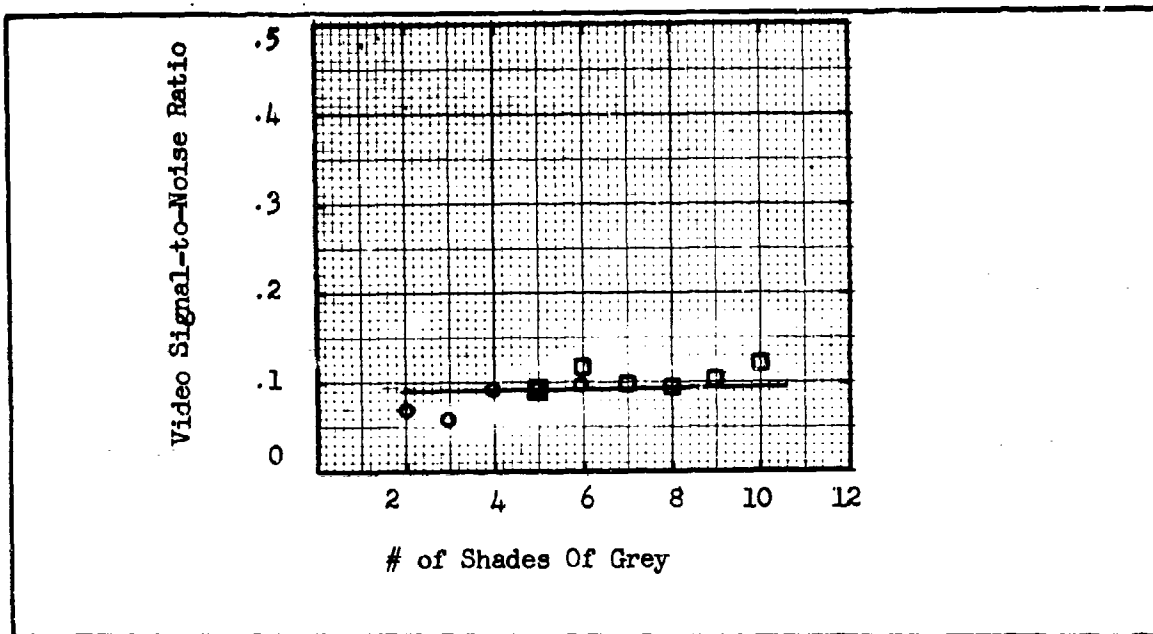


Fig. 57 Threshold  $SNR_V$  as a Function of # of Shades of Grey in EIA Grey Scale  $\circ$  10 FL in Step #2,  $\square$  10 FL in Step #10.

upon the brightness of the area surrounding the grey scale. In Ref. 2, a number of experiments were performed which indicated that a retinal fluctuation noise could be associated with the display brightness and that this noise component can decrease an observer's ability to discern an image. We feel that one of the most serious problems remaining in image sensor modeling is to include display brightness related retinal fluctuation noise. While retinal fluctuation noise is important in television imaging, it is even more important to the analysis of FLIR performance.

## 6.0 Effects of Image Motion

Except when an object moves relative to a stationary background, relative scene/sensor motion is degrading to image quality. These degrading effects can be divided into three distinct mechanisms; the effect of the motion on the observer directly, the interaction of image motion and camera exposure time, and sensor time constant effects. These various effects were previously considered in Ref. 2 and 3 in some detail and will be further considered herein. In general, the effects of image motion on the observer are considered to be nearly negligible for the image motion rates commonly encountered in television practice. The interaction of image motion and exposure time is considered to be quite serious as was discerned from the analytical treatment of Ref. 3. Also, sensor time constants can be limiting to system sensitivity and dynamic range.

In this section, motion experiments were performed to test the validity of certain of the image motion concepts and to gain further insight into the image motion problem. Specifically, psychophysical experiments were performed using moving bar patterns moving isolated bars and moving complex images (vehicles). The vidicon camera was used to generate the imagery. In these experiments, the light level was high enough so that sensor time constants are usually negligible and the primary effect of motion is due to exposure time.

For bar patterns, the current motion MTF model was used (motion effects only -- not lag), and it appears to be adequate for the particular

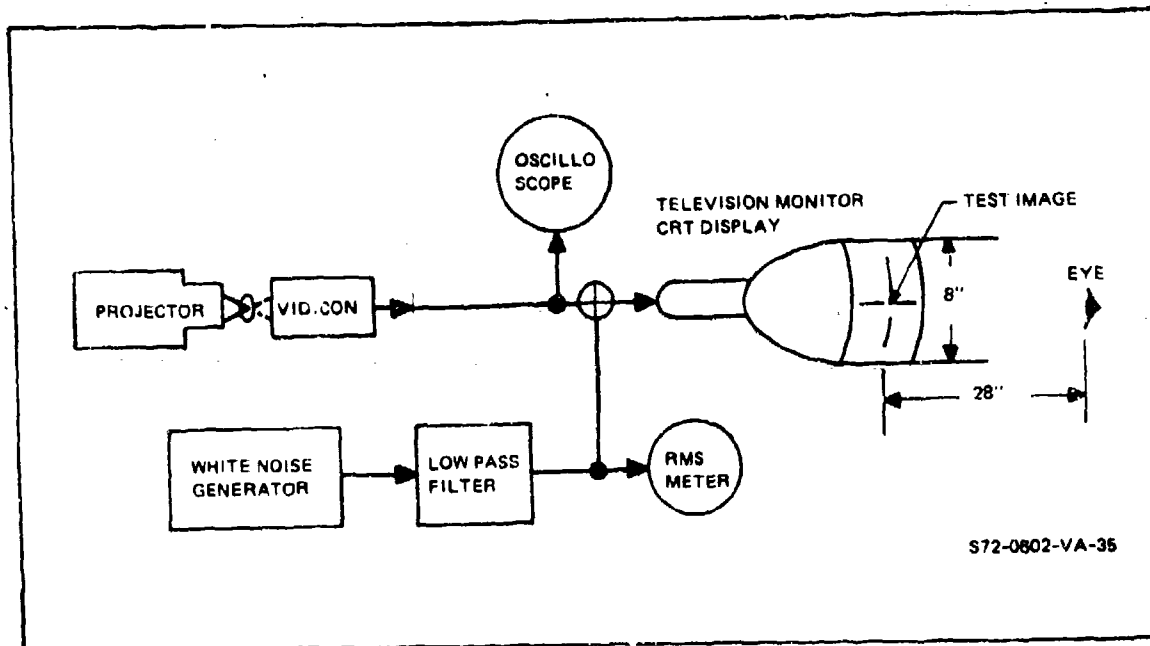


Fig. 58 Experimental Set-up for the Television Camera Generated Imagery.

cases considered. For the vehicular imagery, an aperiodic model was applied with apparent success but the results must be considered tentative.

#### 6.1 Psychophysical Experiments Involving Image Motion

The experimental set-up of Fig. 58 was used to perform the psychophysical experiments. The test images are projected on the faceplate of a high resolution 1-1/2" vidicon operated at highlight video signal-to-noise ratios of 50:1 or better. The camera and TV monitor were operated at 25 frames/second with 875 scanning lines (825 active). Band-limited white noise of Gaussian distribution was mixed with the camera generated signals. The noise was passed through a filter (noise equivalent bandwidth of 12.5 MHz) prior to mixing in the monitor. The monitor luminance was approximately 1 ft. Lambert unless otherwise specified. The displayed picture height was 8" and the observer-display distance was 28".

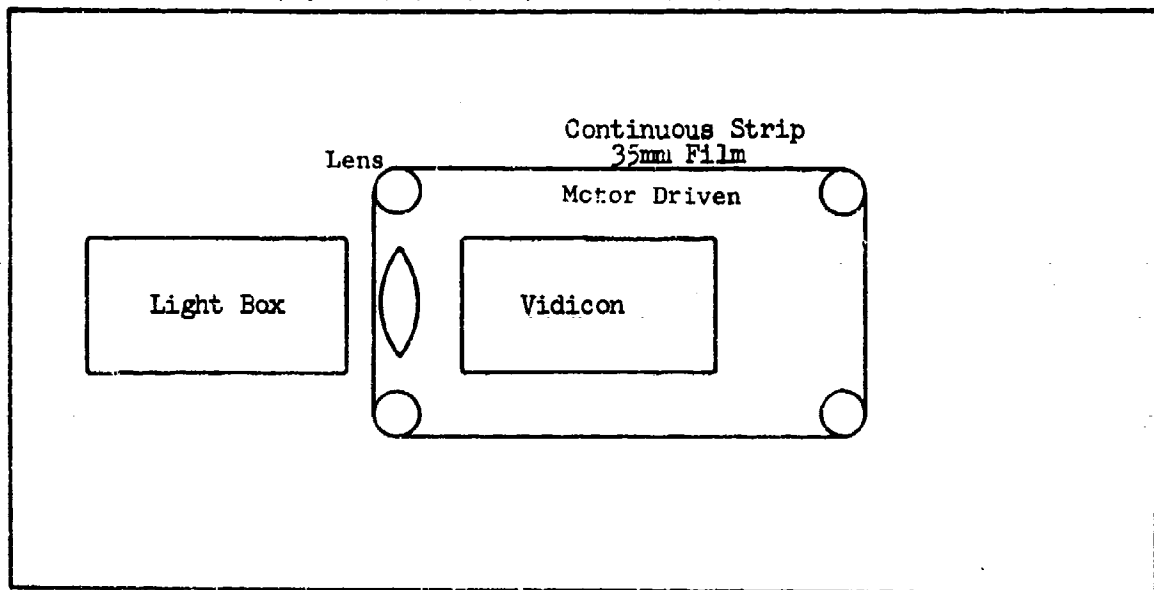


Fig. 59 Experimental Set Up for Motion Experiments .

The specific set-up for the motion experiments is shown in Fig. 59. A continuous strip of 35mm film was moved, at a constant speed, past the vidicon camera. Speed could be varied from less than 60 seconds per picture width to faster than 5 seconds per picture width. Motion could be either from left-to-right or right-to-left.

The transparencies which were used were made from high quality photographs of vehicles amid a uniform white background. The photographs were taken at a depression angle of  $45^{\circ}$  from the horizontal and perpendicular to the vehicle's longitudinal axis, i.e., the sides and tops of the vehicles were imaged as is shown in Fig. 60. The vehicles included a tank, a van truck, a half track with top-mounted radar antenna and a tracked bulldozer with derrick. The areas of the various vehicles were approximately  $.17 \text{ in}^2$

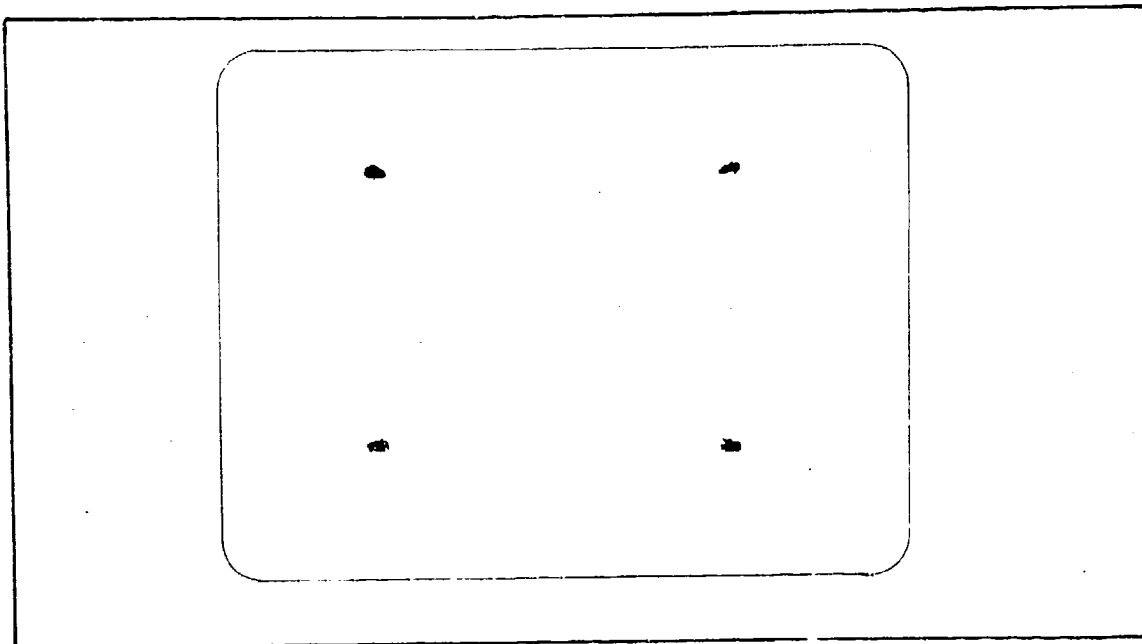


Fig. 60 Photographs of Models Used for Recognition Experiments - Upper Left, Tank; Upper Right, Van Truck; Lower Left, Half Track with Antenna; and Lower Right, Derrick Half Track.

on the 8" x 10.7" display and subtended angles of about  $1^\circ$  by  $2^\circ$  at the observer's eye. The vehicle types and video SNR were randomly varied; and the probabilities of recognition, corrected for change, were determined. The  $SNR_D$ 's for the various images were calculated on the basis of the area of a bar whose length and width are equal to the length of the vehicle's image and the width of the vehicle's image divided by 8 for recognition and divided by 2 for detection. This is in accord with the equivalent bar pattern concept discussed in Ref. 2. We note, however, one difference between the calculations for the bar pattern and the vehicular image's  $SNR_D$ . In the case of the vehicular image, the signal amplitude was measured from the background signal level which was approximately constant, to the peak object signal level. For the "equivalent bar patterns," the signal levels were measured in terms of the mean signal excursion within the bar pattern area in the periodic

direction. Had the peak-to-peak excursions about the average signal within the vehicle area been used (when the object is imaged against a uniform background), the thresholds  $SNR_D$  would have been somewhat lower.

These difficulties result from the necessity of defining an image area and a signal excursion in order to calculate an  $SNR_D$  threshold. In this connection, we observe that the criterion for bar pattern recognition is that the observer must be able to discern a modulation within the bar pattern whereas for vehicle image recognition, the vehicle's outline must be discerned. This outline may have periodic features but is more likely to be aperiodic. With vehicle imagery reported here, a film speed of 5 seconds per picture width was used and the motion, as seen on the monitor, went from right to left. For the vehicle detection experiment, an image of a tank was used and it was randomly positioned in either the upper one third, middle one third or bottom one third of the monitor. One observer participated in the experiment and a total of 180 data points were taken. For the vehicle recognition experiment, four vehicle images were used, a tank, a van truck, a truck with a radar antenna on top and a mobile derrick with a bulldozer blade as shown in Fig. 60. The order of the images on the film was randomly chosen as was the signal-to-noise ratio of the image. One observer participated in the experiment and a total of 200 data prints were taken.

For the calculation of display signal-to-noise ratio, the following formula was used

$$SNR_D = \left[ \frac{2t\Delta fa}{\xi_{x_{LT}} \xi_{y_{LT}} K_d A} \right]^{\frac{1}{2}} SNR_V, \quad (163)$$

where

$$\xi_{x_{LT}} \xi_{y_{LT}} = \left[ 1 + \left( \frac{\delta_L}{x_o} \right)^2 + \left( \frac{\delta_T}{x_o} \right)^2 + \left( \frac{\delta_M}{x_o} \right)^2 \right]^{\frac{1}{2}} \left[ 1 + \left( \frac{\delta_L}{y_o} \right)^2 + \left( \frac{\delta_T}{y_o} \right)^2 \right]^{\frac{1}{2}}, \quad (164)$$

$$\text{SNR}_V = 0.08$$

$$\delta_L = 1.07 \times 10^{-3}$$

$$\delta_T = 3.64 \times 10^{-3}$$

$$\delta_M = 1.067 \times 10^{-2}$$

$$a/A = 0.002$$

$$x_0 = 2.155 \times 10^{-2}$$

$$y_0 = 6.31 \times 10^{-2}$$

Table 14 Values Used for Tactical Image Detection Calculations.

and where  $t = 0.1$  sec,  $\Delta f = 12.04 \times 10^6$  Hz and  $\text{SNR}_V$  is the peak-to-peak video signal to noise ratio with image motion. The value of  $a/A$  that was used was the area of the image,  $a$ , on the photo-surface divided by the active area of the photosurface,  $A$ , assuming a perfect lens with no MTF's effects. The factor of  $K_D$  in the equation comes from the assumption that we are to calculate  $\text{SNR}_D$  of an equivalent bar pattern basis, that is, for recognition, the bars are each  $a/8$  in area where as for detection the bars are each  $a/2$ .

In Table 14, the value of  $a/A$ , the unattenuated  $\text{SNR}_V$  value and various  $\delta$  values are listed which apply for the detection experiment.

The definitions of the various  $\delta$ 's are:

$$\delta_L = \frac{1}{N_{eL}} = \frac{1}{\int |R_{oL}|^2 dN} \quad (165)$$



$$\delta_T = \frac{1}{N_{eT}} = \frac{1}{\int |R_{OT}|^2 dN} \quad , \quad (166)$$

$$\delta_M = \frac{1}{N_{eM}} = \frac{1}{\int |R_{OM}|^2 dN} \quad , \quad (167)$$

where  $R_{OL}$  is the MTF of the lens,  $R_{OT}$  the MTF of the tube and  $R_{OM}$  the motion MTF. For simple linear motion,  $\delta_M = 4t_f/3t_s$  where  $t_f$  is the frame time (1/25 sec for the vidicon experiments) and  $t_s$  is the image speed, sec/P.W., (5 sec/P.W., here).

In Figs. 61 and 62, photographs of the tank, as seen on the monitor (without noise) statically and in motion at a speed of 5 sec/P.W. are shown. In Figs. 63 and 64, a trace through the tank for static and dynamic conditions are shown. The edges of the waveform are rounded off and the peak value is somewhat reduced by the motion. In the calculation of  $SNR_D$ , the peak value of the signal was used.

Using the values of the parameters in Table 14 and Eqs. 163 and 164, we have that the threshold value (50% value) of  $SNR_D$  for detection of the tank is 3.7.

For vehicle recognition, a new value of  $x_0$  is required, one that is 1/4 of that in Table 14. Using this value, the experimentally determined  $SNR_V$  values (averaged for the four images) and the other values from Table 14, we have that for tactical image recognition, the threshold value of  $SNR_D$  is 3.2 which is the same value as reported for  $SNR_D$  for static recognition of the tactical images.

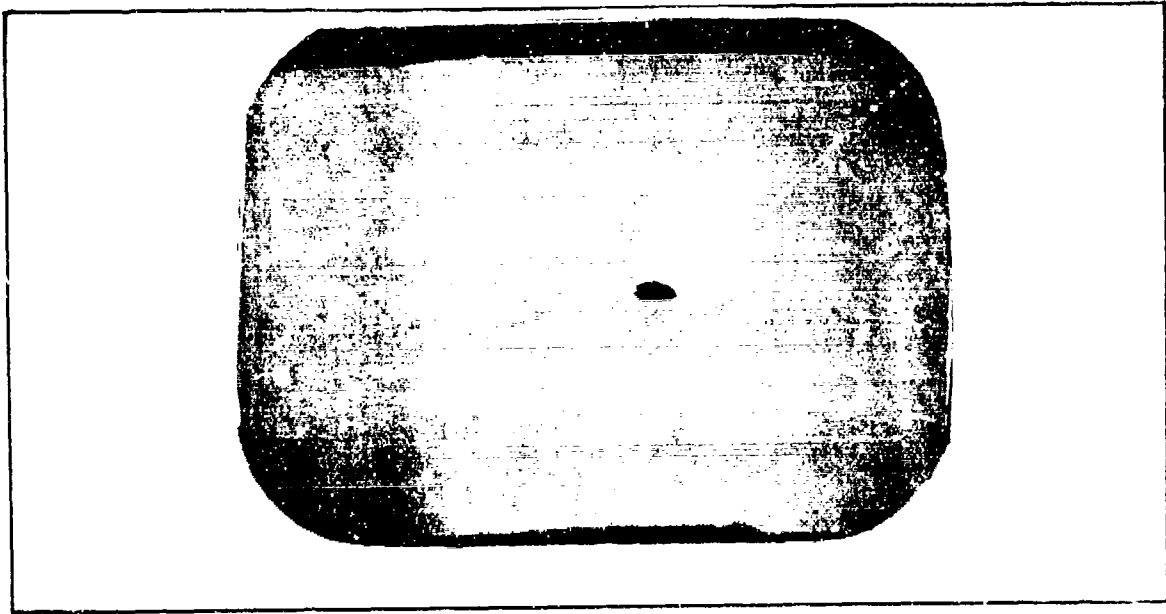


Fig. 61 Static Tank-Detection Experiment.

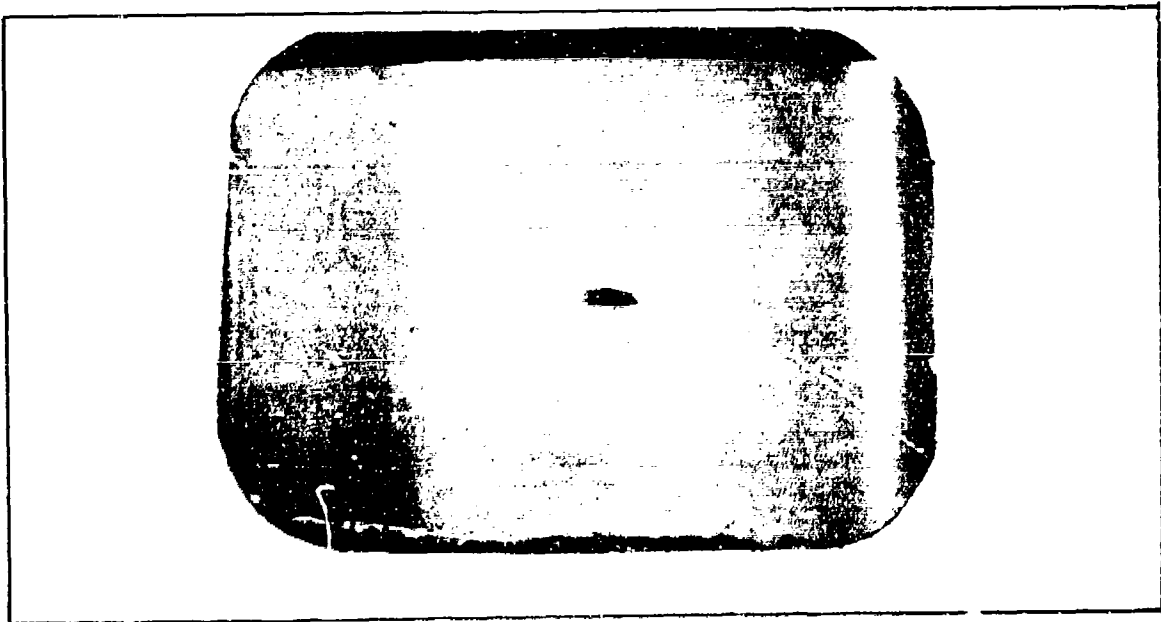


Fig. 62 Tank in Motion-5 Sec/P.W. Detection Experiment.

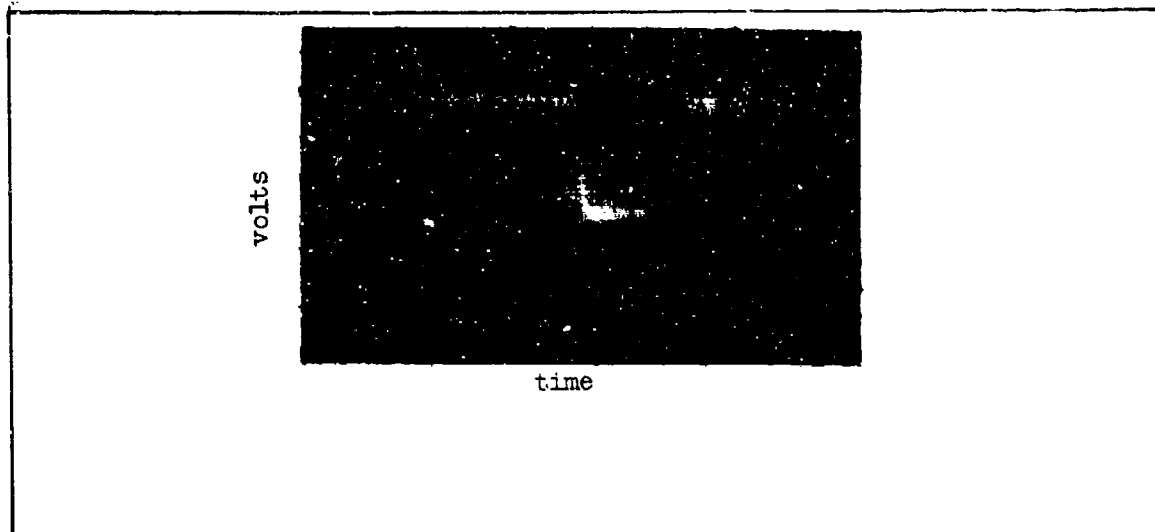


Fig. 63 Static Tank - A Trace Waveform.

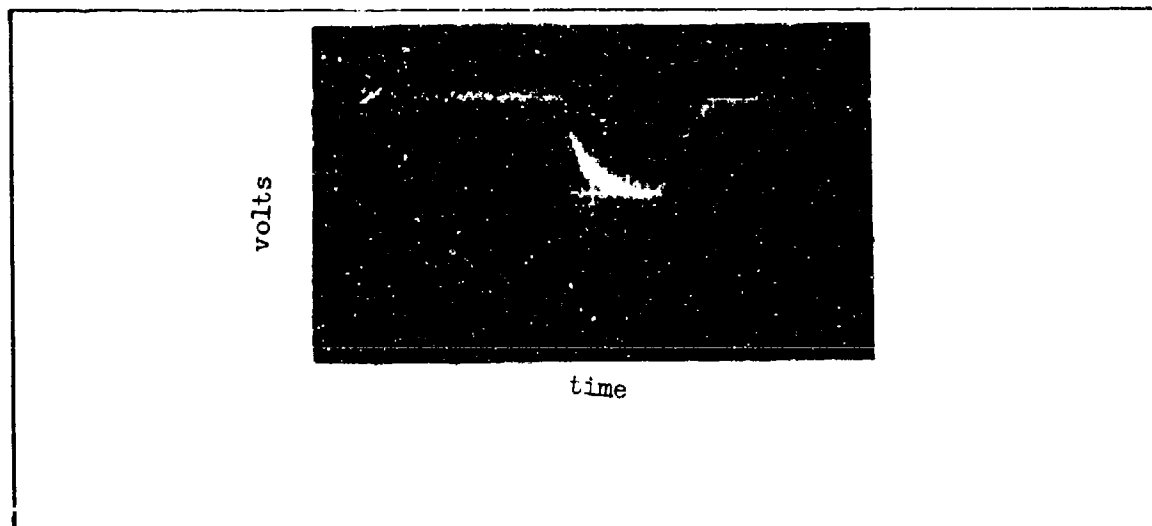


Fig. 64 Tank Moving 5 sec/P.W. - A Trace Waveform.

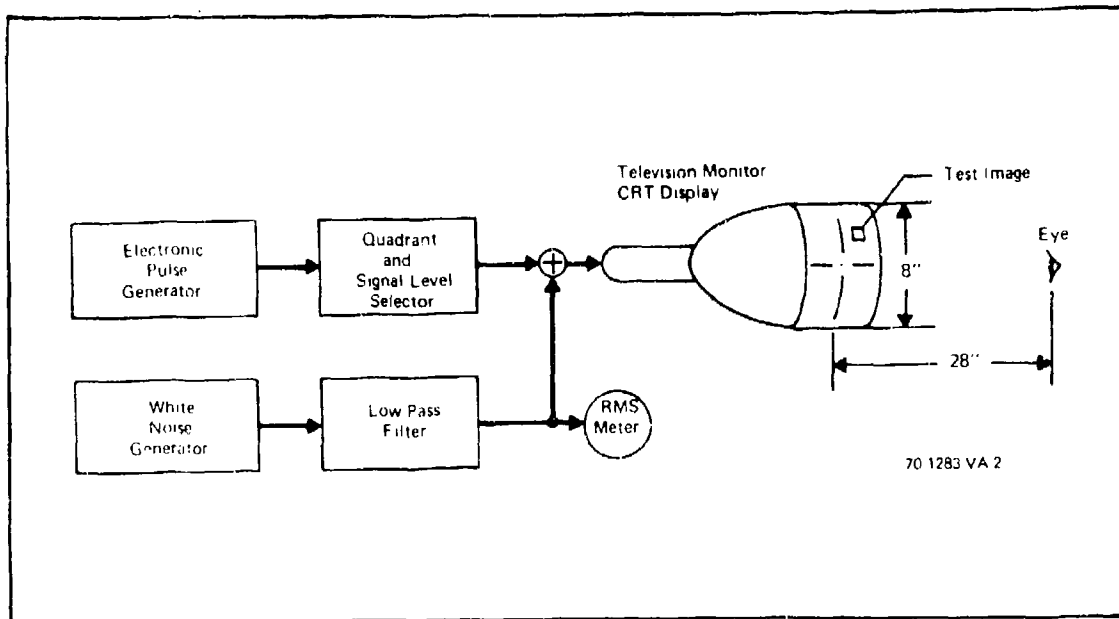


Fig. 65 The Display Signal-to-Noise Ratio Experiment.

It is of interest to compare these values with those required for the detection of electronically generated squares. The experimental setup is shown in Fig. 65. With electronic generation, the lag and exposure time effects normally associated with camera tube imagery are absent. The system operated at 30 frames/sec with 490 scan lines/picture height. The display itself has some lag but this lag is negligible for the image sizes and pattern speeds used. The test squares could appear in either the top, middle or lower third of the displayed picture and the motion was from left-to-right at speeds of 20 and 5 seconds per picture width (only 93% of the actual picture width was used). Monitor brightness was 1 fL and the observer-to-display distance was 28". The effects of these speeds on the threshold signal-to-noise ratio is shown in Fig. 66 for various image sizes. It is seen

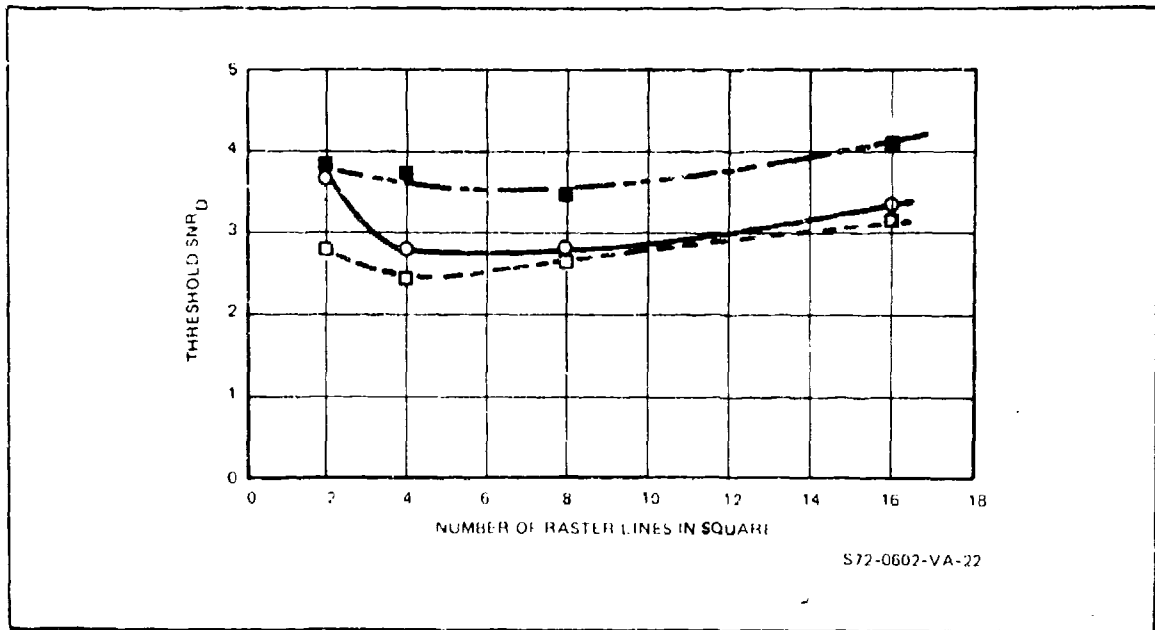


Fig. 66 Threshold  $SNR_D$  vs Number of Raster Lines in Square for ○ Stationary Patterns □ 20 Seconds/Picture Width Motion and ■ 5 Seconds/Picture Width Motion.

that at 20 sec./picture width, motion has almost no effect on the required SNR except for the smallest object which increased in detectability since the  $SNR_D$  required was 24% lower than for the static case. With a rate of 5 sec/picture width, the threshold  $SNR_D$  is the same as for the static case for the smallest square but is 26% higher for the larger squares.

For tactical image detection, the width of one bar of the equivalent bar patterns is about 10 scan lines/picture height. From Fig. 66, a threshold  $SNR_D$  value, for the detection of an ideal square this size, is 3.6. Thus the value for tactical image detection and ideal square detection is very similar which suggests that the equations which were used to calculate  $SNR_D$  for the tactical image are at least approximately true.

For tactical image recognition, the equivalent bar width is about 2 raster lines wide (relative to 490 active raster lines per picture height)

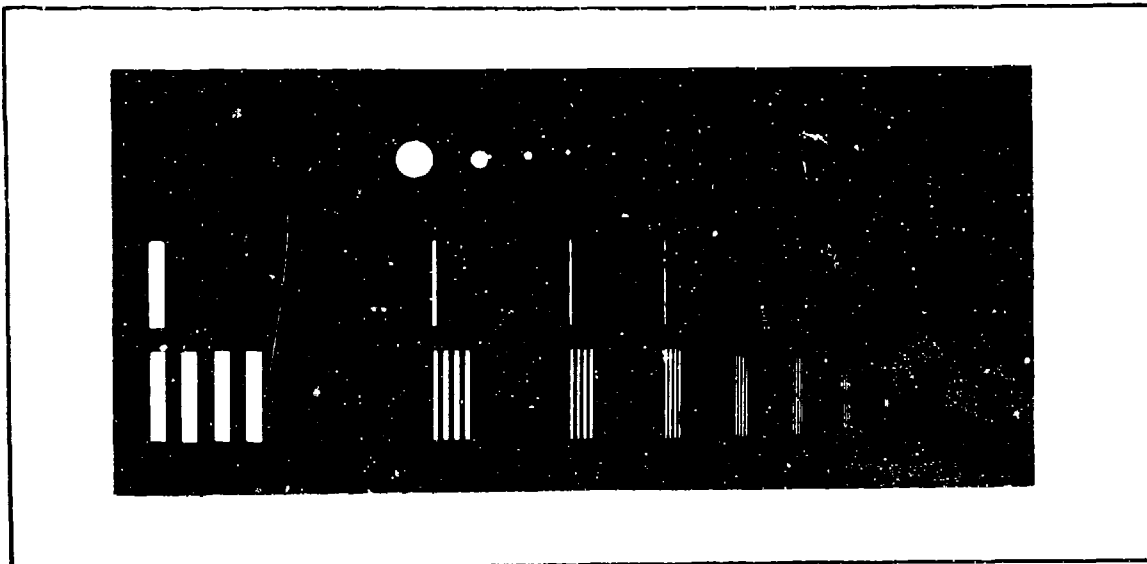


Fig. 67 Bar Patterns of Variable Aspect, Isolated Bars and Isolated Circles Used for Experiments.

and from Fig. 66,  $SNR_D = 3.8$ . This value is 42% higher than that determined for the recognition of tactical images.

Motion experiments were also performed with periodic bar patterns using the motion, vidicon setup. A photograph of the bar pattern which was used is shown in Fig. 67.

For bar patterns,  $SNR_{DI}$  is calculated on the basis of the total area of a single bar. Specifically, the equation

$$SNR_D = \left[ \frac{2tn_v \Delta f_v}{\alpha} \right]^{\frac{1}{2}} \frac{R_{SF}(N)}{N \xi_y^{\frac{1}{2}}} \left( \frac{\Delta i}{I_n} \right), \quad (168)$$

is used. In the above,  $\Delta i$  is the peak-to-peak signal current for a broad area pattern (unity modulation transfer function) and  $I_n$  is the rms noise that is added to the camera generated image. Real cameras, of course, have a response that is a function of frequency and the value of  $\Delta i$  in

the video channel for square wave inputs becomes  $\Delta i_{p-p}$ , the peak-to-peak value of the video signal when the frequency effects are included. That is,

$$\Delta i_{p-p} = \Delta i R_{SQ}(N) , \quad (169)$$

and

$$SNR_D = \left[ \frac{2tn_v \Delta f_v}{\alpha} \right]^{\frac{1}{2}} \left( \frac{1}{N} \right) \frac{R_{SF}(N)}{R_{SQ}(N) \xi_y^{\frac{1}{2}}} \frac{\Delta i_{p-p}}{I_N} , \quad (169)$$

where  $R_{SF}(N)$  is the value of the flux factor at  $N$ ,  $R_{SQ}(N)$  is the value of the square wave response at  $N$  and  $\Delta i_{p-p}$  the value of the peak-to-peak signal corresponding to  $N$  as measured in the output of the video channel.

Alternately, one could measure  $\Delta i$  for a broad area pattern and use Eq. (168).

In any event,  $\xi_y$  is given by

$$\xi_y = \left[ 1 + \left( \frac{N}{n_v N_{eL}} \right)^2 + \left( \frac{N}{n_v N_{eT}} \right)^2 \right]^{\frac{1}{2}} , \quad (170)$$

where  $N_{eL}$  and  $N_{eT}$  are given by Eqs. (165) and (166). For calculation purposes,  $t$ , the integration time of the eye is taken to be 0.1 sec and  $\alpha$ , the picture aspect ratio is 4/3. At low spatial frequencies the displayed images approach a squarewave while at high spatial frequencies, above about 300 lines/picture height, the displayed images were nearly pure sine waves.

Experiments were performed with the periodic patterns at 5 and 10 sec/P.W. speeds. The psychophysically determined  $SNR_D$  values are similar for the two pattern speeds and are very similar to the values which were obtained statically. For the calculation of  $SNR_D$  the measured dynamic characteristics of the sensor were used.

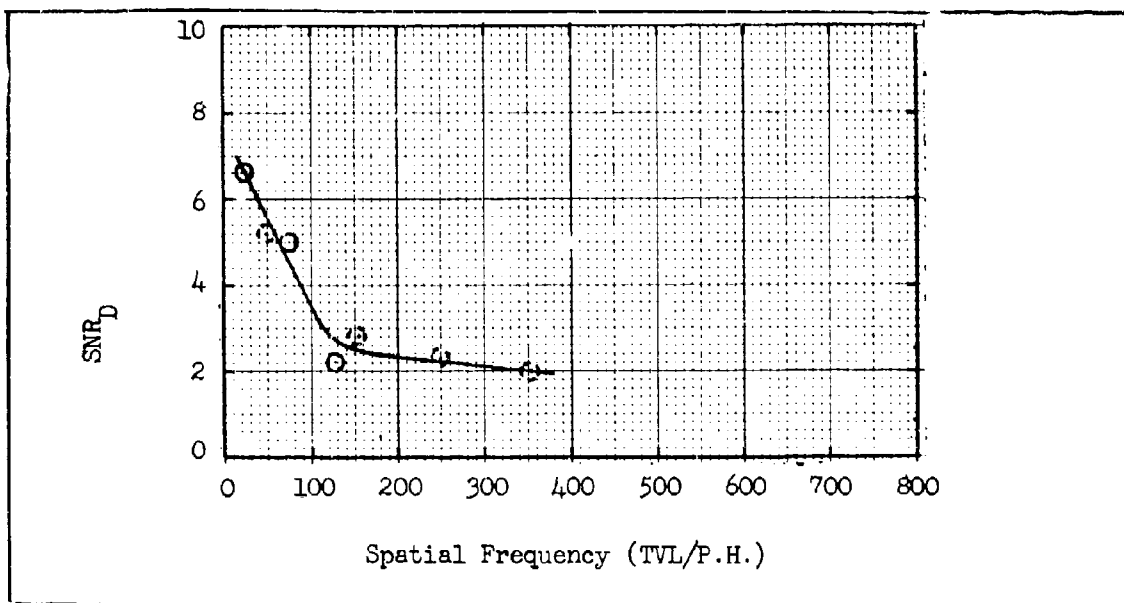


Fig. 68 Threshold SNR<sub>D</sub> vs Spatial Frequency for Pattern Speeds of (○) 10 Sec/P.W. and (○) 5 Sec/P.W.

In Fig. 68, the threshold SNR<sub>D</sub> values are plotted as a function of spatial frequency for the two speeds. As can be seen, the results are very similar and agree well within the experimental accuracy. In Figs. 69 and 70, the predicted and measured squarewave responses (dynamic) are shown. More signal is lost than is accounted for by the theoretical curve and this loss is most likely due to the lag of the camera. The amount that is lost is greater at the higher pattern speed.

Finally an experiment was performed with the isolated bars shown in Fig. 67 with one observer. A total of 250 data points were taken. Monitor-observer conditions were the same as the rest of the vidicon experiments reported in this section. For the calculation of SNR<sub>D</sub>, Eqs. 163 and 164 were used. Pattern speed was 10 sec/P.W. and the results of the experiment are shown in Fig. 71 by the squares. Comparing these values with the



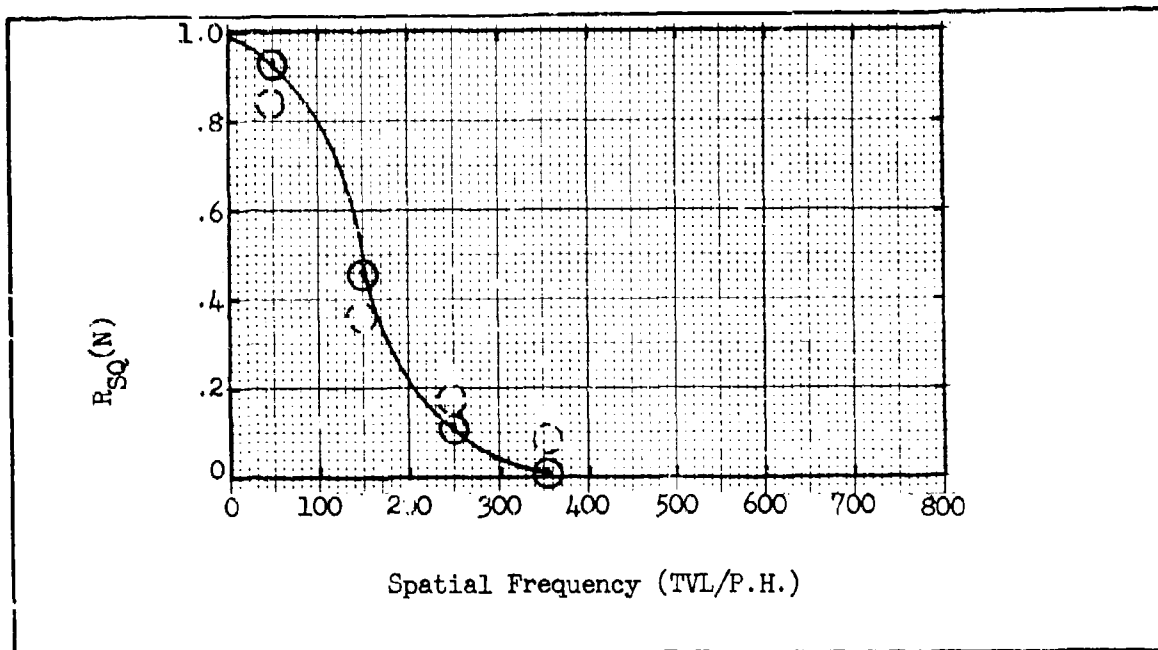


Fig. 69 Dynamic Square Wave Response - Theory  $\circ$  Measured  $\circ$  for 10 Sec/P.W. Linear Pattern Speed.

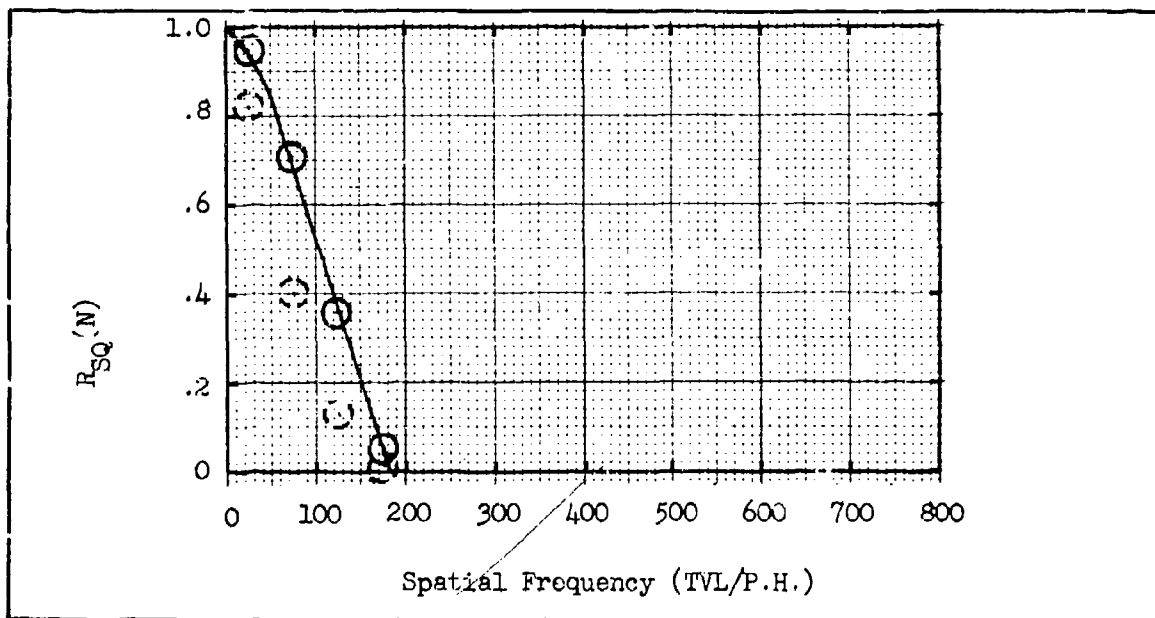


Fig. 70 Dynamic Square Wave Response - Theory  $\circ$  Measured  $\circ$  for 5 Sec/P.W. Linear Pattern Speed.

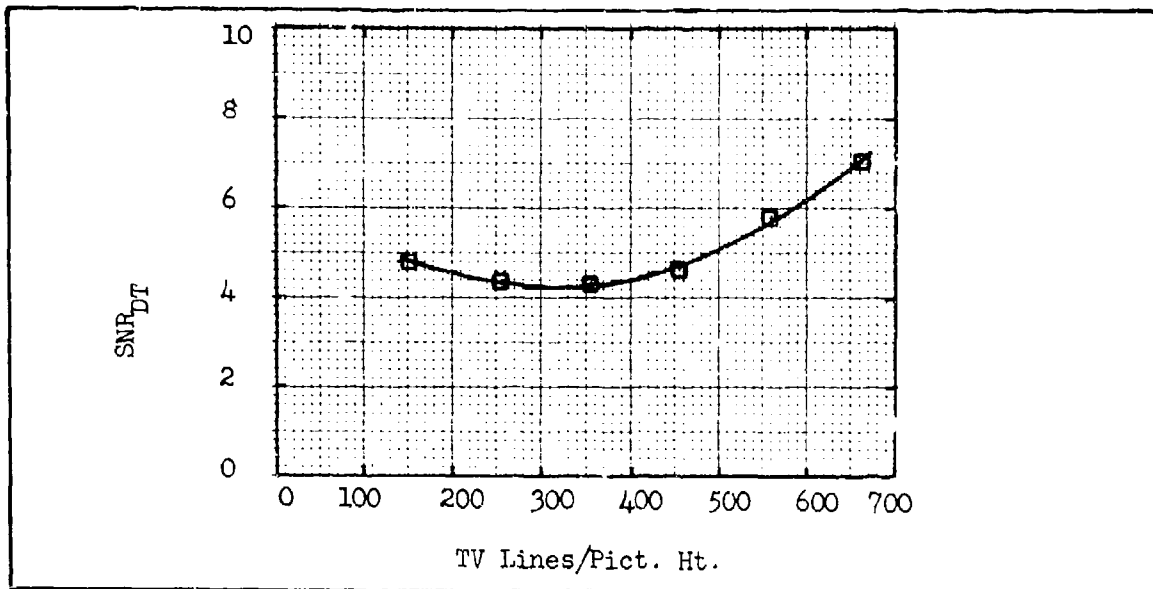


Fig. 71 Threshold  $SNR_D$  vs Line Number for Aperiodic Bars Moving at a Speed of 10 Seconds per Picture Width.

corresponding ones for ideal squares in motion of Fig. 66 shows that the present values are high by about 30%.

In conclusion it was seen that motion effects are reasonably accounted for by using the motion MTF and calculating  $SNR_D$  using the standard models for either periodic or aperiodic images. The biggest discrepancy occurs for periodic images at the highest pattern speeds where lag effects apparently cause added losses in the available signals over and above those predicted by pure motion effects above.

## 7.0 Computer Programs For System Resolution Prediction

It is quite common to judge electro-optical system performance in terms of the overall systems ability, including the observer, to resolve simple geometric patterns which are easy to make and to quantitatively describe. The most common test pattern used, by far is the square wave bar pattern consisting of alternating black and white stripes. A number of patterns are employed, each of a different spatial frequency. The higher the spatial frequency that can be resolved, the better the system is presumed to be. Bar patterns are used both in the laboratory and in the field. In the 698DF Performance Synthesis Program (Ref's 1-3) efforts have been made to correlate the ability to resolve bar patterns with the ability to detect, recognize and identify real scene objects. It would be presumptuous to claim that a one-to-one correlation was observed but a degree of correlation does definitely exist.

In any event, real imagery is almost impossible to describe quantitatively and is generally unsuitable for use in an analytical model and thus the bar pattern has been adopted by most workers as the standard of performance. In general, the ability of an electro-optical sensor augmented observer to resolve a bar pattern on the sensor's display can be analytically predicted, knowing the sensor's parameters. The prediction is ordinarily quite precise, subject mainly to the statistical variation from observe-to-observer.

In the following, we will provide computer programs for the purpose of predicting a systems' ability to resolve bar patterns. In general, the procedure is to calculate the bar pattern signal-to-noise ratio as it appears on the display and then compare that to the signal-to-noise ratio required by the observer. While we have suggested methods of correlating the discernability of bar patterns with real images, these methods must be considered preliminary and subject to further improvement and revision in the future. Thus, while the prediction of bar pattern resolution should be quite accurate, the estimation of the range at which real objects are recognized must be considered to be an approximation.

In the following various computer programs are developed which are suitable for both component tradeoff and overall system analysis. Before discussing the main programs, smaller speciality programs will be discussed which generate the system functions and constants needed as inputs to the main programs.

#### 7.1 Calculation of $N_e$

The format which will be followed in the following will be to first give the algebraic expression that is being calculated, then the program and a description of symbols, and finally an example. The first program calculates  $N_e$  where  $N_e$  is given by

$$N_e = \int_0^{\infty} R_o(N)^2 dN \quad (171)$$

```

10 REM***PROGRAM CALCULATES NE***
20 N=16
30 DIM R(20)
50 FOR J=1 TO N
60 READ R(J)
70 DATA .887, .774, .630, .485, .350, .250, .166, .10
80 DATA .061, .036, .019, .010, .004, .002, .001, .0
90 NEXT J
95 N1=50
97 S1=0
100 FOR J=1 TO N
110 S=(R(J)^2)
120 S1=S1+S
130 NEXT J
140 PRINT "NE="N1*(S1+.5)
150 END

```

Table 15 Program for Calculation of  $N_e$ .

For evaluation of the integral, a linear fit between data points is used. The program is shown above. In the program,  $N$  is the number of data points, 16 in this case. Equal increments in  $\Delta N$  are assumed and  $N_1$  is  $\Delta N = 50$  here.  $N_e = NE$  in the program and  $R(J)$  is the sine wave response of interest (e.g., of the tube,  $N_{et}$ ; of the lens,  $N_{el}$ ; or of motion,  $N_{em}$ ) at each value of  $N$ , e.g., 50, 100, 150, etc. For the data given,  $N_e = 137$ .

```

10 REM***PROGRAM CALCULATES XI AND GAMMA***
20 E=5
30 N1=137
40 N2=300
50 N3=350
60 PRINT "N=", "XI=", "GAMMA="
70 FOR N=50 TO 700 STEP 50
80 S1=SQR(1+(N/(E*N1))^2+(N/(E*N2))^2+(N/(E*N3))^2)
90 S2=S1/SQR(1+(N/(E*N1))^2+2*(N/(E*N2))^2+2*(N/(E*N3))^2)
100 PRINT N, S1, S2
110 NEXT N
120 END

```

Table 16 Program for Calculation of  $x_1$  and Gamma.

## 7.2 Calculation of $\xi$ and $\Gamma$

The next program calculates  $\xi$  and  $\Gamma$ . The equation for  $\xi$  and  $\Gamma$  are:

$$\xi_{yLT} = \left[ 1 + \left( \frac{N}{\epsilon N_{el}} \right)^2 + \left( \frac{N}{\epsilon N_{et}} \right)^2 + \left( \frac{N}{\epsilon N_{em}} \right)^2 \right]^{1/2} \quad (172)$$

$$\Gamma_{yLT} = \frac{\xi_{yLT}}{\left[ 1 + \left( \frac{N}{\epsilon N_{el}} \right)^2 + 2 \left( \frac{N}{\epsilon N_{et}} \right)^2 + 2 \left( \frac{N}{\epsilon N_{em}} \right)^2 \right]^{1/2}} \quad (173)$$

where  $\epsilon$  is the bar length/width ratio,  $N_{el}$ ,  $N_{et}$  and  $N_{em}$  the  $N_e$  for the lens, tube and motion, respectively.

The program for calculating  $\xi$ , called  $S_1$  and  $\Gamma$ , called  $S_2$  is above. In the program, E is  $\epsilon$ ,  $N_1$  is  $N_{et}$ ,  $N_2$  is  $N_{el}$  and  $N_3$  is  $N_{em}$ .

Below is listed the result of the sample calculation for  $\xi$  and  $\Gamma$ .

N=	KI=	GAMMA=
50	1.00352	.999045
100	1.01441	.996273
150	1.03213	.991958
200	1.05645	.985484
250	1.08692	.976921
300	1.12303	.966577
350	1.16427	.953834
400	1.21101	.938087
450	1.26363	.919838
500	1.31300	.899432
550	1.37036	.877143
600	1.42996	.853342
650	1.49203	.828399
700	1.55629	.802092

Table 17  $x_i$  and Gamma Calculated with Program.

### 7.3 Calculation of $R_{SF}(N)$

The next program calculates the flux factor  $R_{SF}(N)$ , called F in the program. The flux factor is given by

$$R_{SF}(N) = \frac{8}{\pi^2} \sum \frac{|R_o(kN)|}{k^2}, \quad (174)$$

where  $R_o$  is the overall sine wave response of the system.  $k$  is the harmonic, 1, 3, 5, etc. of  $N$ .

As in the calculation of  $N_e$ ,  $R(J)$  is the sine wave response of the whole system, at each increment and  $N$  the number of data points.

```

00 REM***PROGRAM CALCULATES FLUX FACTOR***
20 N=16
30 DIM R(200)
50 FOR J=1 TO N
60 READ R(J)
70 DATA .887, .774, .630, .485, .350, .250, .166, .103
80 DATA .061, .036, .019, .010, .004, .002, .001, .0
90 NEXT J
92 FOR J=N+1 TO 11*N
94 R(J)=0
96 NEXT J
98 PRINT "N=", "FLUX FACTOR="
100 FOR K=1 TO N
110 J=K
160 A=R(K)+R(3*K)/9+R(5*K)/25+R(7*K)/49+R(9*K)/81+R(11*K)/121
170 F=A*8/(3.14156^2)
200 PRINT K*50, F
250 NEXT K

```

Table 18 Program for Calculation of Flux Factor.

PROGRAM	FLUX FACTOR
N=	FLUX FACTOR =
50	.799553
100	.56111
150	.315196
200	.181556
250	.102795
300	.062507
350	.038557
400	1.34904E-2
450	4.24432E-2
500	1.91211E-2
550	1.54911E-2
600	5.13535E-3
650	3.24835E-3
700	1.52117E-3
750	3.10535E-4
800	0

Table 19 Flux Factor as Calculated with Program.



```

10 REM***PROGRAM CALCULATES BETA FACTOR***
20 N=16
30 DIM R(20)
40 DIM B(20)
50 FOR J=1 TO N
60 READ R(J)
70 DATA .887, .774, .630, .485, .350, .250, .166, .103
80 DATA .061, .036, .019, .010, .004, .002, .001, .0
90 NEXT J
95 N1=50
100 PRINT "N=", "B="
110 B(1)=(1+(R(1))^2)/2
115 PRINT N1, B(1)
120 FOR J=2 TO N
140 B(J)=((J-1)*B(J-1)+((R(J-1))^2)/2+((R(J))^2)/2)/J
150 PRINT N1*J, B(J)
160 NEXT J
170 END

```

Table 20 Program for Calculation of Beta Factor.

#### 7.4 Calculation of $\beta(N)$

The beta factor,  $\beta(N)$ , is calculated in the next program and  $\beta(N)$  is given by

$$\beta(N) = \frac{1}{N} \int_0^N \frac{|R_{ot}(N)|^2}{N} dN, \quad (175)$$

where  $R_{ot}$  is the sine wave response of the tube (with motion). For the program, a linear fit is used between data points in the calculation and a total 16 data points are used.  $\Delta N = 50 = N_1$  in the program and  $\beta(N)$  is called B(J).

PROGRAM	BETAFAC
N=	B=
50	.393384
100	.793153
150	.694755
200	.500039
250	.515344
300	.445237
350	.333167
400	.341979
450	.304777
500	.27455
550	.249567
600	.22333
650	.211279
700	.195135
750	.183109
800	.171665

Table 21 Beta Factor as Calculated with Program.

### 7.5 Calculation of $R_{om}(N)$

The next program calculates the value of  $R_{om}(N)$ , the sine wave response due to random motion.  $R_{om}(N)$  is given by

$$R_{om}(N) = \exp\left(-\frac{1}{2} \frac{(\pi F_L \Delta\theta N)^2}{Y}\right), \quad (176)$$

where  $F_L$  is the lens focal length,  $\Delta\theta$  the RMS value of stability (in rad.),  $N$  TV lines/picture height and  $Y$  the active height of the picture on the photocathode. For the program  $F_L = F$ ,  $\Delta\theta = 0$  (this is the letter O)  $Y$  is  $Y$ .

$R_{om}(N)$  is given by R.

```

10 REM***PROGRAM CALCULATES R0 DUE TO RANDOM MOTION***
20 F=26
30 O=30E-6
40 Y=(.707*25/25.4)
50 P=3.14159
55 PRINT"N=", "R0="
60 FOR N=50 TO 700 STEP 50
70 R=EXP(-.5*(P*F*O*N/Y)^2)
80 PRINT N,R
90 NEXT N
100 END

```

Tabl 22 Program for Calculating  $R_{om}$  Due to Random Motion.

N	R0=
50	.984310
100	.920891
150	.860780
200	.799353
250	.678742
300	.572342
350	.467888
400	.370821
450	.284021
500	.212237
550	.153260
600	.107305
650	7.23326E-2
700	4.70255E-3

Table 23  $R_{om}$  as Calculated with Program.

## 7.6 Calculation for Passive Day Operation

For the analysis or design of passive television systems, whether at the component level or the system level the starting point is the same, the  $SNR_D$  equation. The value of  $SNR_D$  is given by

$$SNR_D = \left[ \frac{t\epsilon}{\alpha} \right]^{\frac{1}{2}} \frac{1}{\xi_{yLT}^{\frac{1}{2}}} \frac{R_{SF}(N)}{N} \frac{2C_M G_{i_{av}}}{[G^2 \epsilon \Gamma_{yLT} \beta_{yt} i_{av} + I_p^2 / 2\Delta F_V]^{\frac{1}{2}}}, \quad (177)$$

where  $t$  is the eye integration time, usually taken to be 0.1 sec, the bar length-to-width ratio,  $\epsilon$  the  $\xi$  factor given by Eq. (172) which accounts for the increase in size of the bar in the  $y$  direction due to the MTF's.

$R_{SF}(N)$  is the flux factor,  $C_M$  the modulation contrast of the pattern,  $C(0)$  is the intrinsic contrast of the pattern for a lab test,  $C_M$  is given by

$$C_M = C(0) \left[ 1 - \left( \frac{S_K}{G_D} \right) (1 - e^{\alpha R}) \right]^{-1}, \quad (178)$$

for viewing of the pattern through an atmosphere. In the above  $S_K/G_D$  is the sky-to-ground ratio which is taken to be 3 in the example which follows. The atmosphere attenuation coefficient is given by  $\alpha$  and the slant range from the sensor to the object  $R$ . Resolution in radians is given by  $\Delta\theta$  (radians) where

$$\Delta\theta = \frac{Y}{NF_L}, \quad (179)$$

or  $K_\theta$  (cycles/mradian) where

$$K_\theta = \frac{NF_L}{2000Y}, \quad (180)$$

and  $N$  is TV lines/pict. ht.,  $Y$  the height of the photocathode and  $F_L$  the lens focal length. The average photocurrent is given by

$$i_{av} = i_{av \text{ max}}/G \quad , \quad (181)$$

where  $i_{av \text{ max}}$  is the maximum average current out of the tube and  $G$  is the minimum gain. For the analysis  $SNR_D$  is calculated as a function of  $N$ ,  $\Delta\theta$  or  $K_\theta$ .

The program which calculates  $SNR_D$  vs  $N$  as a function of  $R$  and atmosphere attenuation coefficient  $\alpha$  is the following.

The program is listed in Tables 24 and 25. Table 26 identifies the relationships between algebraic and alphanumeric symbols. Tables 27 and 28 list a sample calculation and the results of the calculation are plotted in Fig. 72. For the calculation a threshold  $SNR_D$  of 6.0 was used for recognition of the object in a cluttered environment. Also plotted in Fig. 72 is the required resolution to recognize the target where the required resolution,  $\Delta\theta_R$ , is given by

$$\Delta\theta_R = \frac{X_t}{kR} \quad , \quad (182)$$

where  $X_t$  is the minimum object dimension,  $k = 2$  for detection, 8 for recognition and 13 for identification and  $R$  is the slant range from the sensor to the object. The intersection of the two curves, the resolution required to recognize the system and the resolution available from the system yields the range for the threshold operation of the system. For the present case  $R = 24,000$  ft.

```

100 REM*****THIS PROGRAM CALCULATES SNRD VS N AND R FOR PASSIVE DAY**
120 PRINT"PASSIVE DAY"
130 N=12
135 M=3
140 DIM A(20)
150 DIM P(20)
160 DIM G(20)
170 DIM R(20)
180 DIM B(20)
185 REM ***PUT ATMOSPHERE ATTENUATION COEFFICIENTS HERE***
190 FOR L=1 TO M
200 READ A(L)
210 DATA3.3E-5,7.58E-5,1.37E-4
220 NEXT L
250 FOR J=1 TO N
260 READ P(J),G(J)
270 DATA1.00,1.00,1.01,1.00,1.03,.99
280 DATA1.06,.99,1.09,.98,1.12,.97
290 DATA1.16,.97,1.21,.96,1.25,.95
300 DATA1.31,.95,1.37,.94,1.40,.93
310 NEXT J
350 FOR J=1 TO N
360 READ R(J),B(J)
370 DATA.791,.893,.651,.793,.516,.695
380 DATA.394,.600,.284,.516,.203,.445
390 DATA.135,.388,.083,.342,.049,.305
400 DATA.029,.275,.015,.250,.008,.229
410 NEXT J
500 REM*****PROGRAM CONSTANTS FOLLOW*****
510 T=.1
515 E=1.6E-19
520 A=1
525 D2=50
530 I1=.6E-6
540 G=10
550 I2=3E-9
560 D1=1E7
580 D=25

```

Table 24. Program for Passive Day.

```

600 F1=10
605 F=26
610 C0=.3
615 X1=10
620 Y1=30
630 K3=3
650 REM****N1=13 IDENTIFICATION,8 RECOGNITION,2 DETECTION***
660 N1=8
661 IF N1=2 THEN 669
662 IF N1=8 THEN 667
663 PRINT"IDENTIFICATION"
665 GO TO 670
667 PRINT"RECOGNITION"
668 GO TO 670
669 PRINT"DETECTION"
670 E1=N1*Y1/X1
680 REM***MAIN CALCULATION STARTS HERE****
700 FOR L=1 TO M
710 PRINT"ATTENUATION COEFICIENT*A(L)"
720 FOR R=6000 TO 30000 STEP 6000
722 C=C0/(1-K3*(1-EXP(A(L)*R)))
723 PRINT"R="R,"C(R)="C
725 PRINT"N=", "SNRD=", "DELTA THETA=", "K THETA="
727 FOR J=1 TO N
730 I=I1/G
750 S=SQR(T*E1/(A*P(J)))*R(J)/(J*D2)
760 S=S*2*C*G*I
762 LET D9=(G^2)*E*G(J)*B(J)*I
764 LET D8=(I2^2)/(2*D1)
766 LET S=S/SQR(D9+D8)
780 D3=((D/25.4)/SQR(A^2+1))/(J*D2*F)
800 PRINT J*D2, S, D3, 1/(2000*D3)
825 IF S<3 THEN 860
850 NEXT J
860 PRINT
890 NEXT R
895 PRINT
900 NEXT L
925 PRINT
930 PRINT
950 END

```

Table 25 Continuation of Passive Day Program.

<u>Name</u>	<u>Algebraic Symbol</u>	<u>Computer Program Equivalent</u>
Atmospheric Attenuation Coefficient	$\alpha$	A(L)
Psi	$\xi(N)$	P(J)
Gamma	$\Gamma(N)$	G(J)
Flux Factor	$R_{SF}(N)$	R(J)
Beta Factor	$\beta(N)$	B(N)
Eye Integration Factor	t	t
Display Aspect Ratio	$\alpha$	A
Delta N	$\Delta N$	D <sub>2</sub>
$i_{av \text{ max}}$	$i_{av \text{ max}}$	I <sub>1</sub>
Minimum Gain	G	G
$I_{pa \text{ rms}}$	$I_{pa}$	I <sub>2</sub>
Bandwidth (Hz)	$\Delta f$	D <sub>1</sub>
Photocathode Diameter	$D_{pc}$	D
Focal Number	F#	F <sub>1</sub>
Focal Length (in)	$F_1$	F
Intrinsic Contrast	C(O)	CO
Target Minimum Height	$X_t$	X <sub>1</sub>
Target Length	$Y_t$	Y <sub>1</sub>
Sky-to-Ground Ratio	$S_K/G_D$	K <sub>3</sub>

Table 26 Correspondence Between Symbols.



PASSIVE DAY  
 IDENTIFICATION

AFTERMATH COEFFICIENT = 000033

N = 3000

C(D) = .131052

N#	S.I.D.=	DELTA THETA=	K THETA=
50	4887.83	5.35352E-4	.933947
100	1951.15	2.57531E-4	1.35739
150	1032.85	1.73454E-4	2.30174
200	637.843	1.33341E-4	3.73579
250	373.577	1.07072E-4	4.66973
300	251.474	8.22271E-5	5.30353
350	133.532	7.54304E-5	6.53753
400	72.5865	6.69203E-5	7.47157
450	37.8349	5.74347E-5	8.40552
500	25.2755	5.25352E-5	9.33947
550	15.54193	4.35593E-5	10.2734
600	8.55914	4.45135E-5	11.2074

N = 1,000

C(D) = .12267

N#	S.I.D.=	DELTA THETA=	K THETA=
50	3139.91	5.35352E-4	.933947
100	1326.65	2.57531E-4	1.35739
150	729.912	1.73454E-4	2.30174
200	429.39	1.33341E-4	3.73579
250	255.299	1.07072E-4	4.66973
300	155.855	8.22271E-5	5.30353
350	95.1277	7.54304E-5	6.53753
400	55.987	6.69203E-5	7.47157
450	35.7077	5.74347E-5	8.40552
500	15.737	5.25352E-5	9.33947
550	8.43393	4.35593E-5	10.2734
600	5.10772	4.45135E-5	11.2074

Table 27 Passive Day Calculations.

**COPY AVAILABLE TO DDC DOES NOT  
 PERMIT FULLY LEGIBLE PRODUCTION**

C(1) = 3.73704E-3		C(1) = 3.73704E-3	
0	217.730	5.35352E-4	9.33947
100	208.771	2.57531E-4	1.75719
150	201.227	1.74864E-4	3.40104
200	197.09	1.33341E-4	3.73579
250	182.723	1.07072E-4	4.66973
300	111.703	8.92271E-5	5.60363
350	64.5797	7.64594E-5	6.53753
400	32.0100	5.92232E-5	7.47157
450	14.7024	5.24347E-5	8.40552
500	9.45111	5.35352E-5	9.33947
550	4.83412	4.36593E-5	10.2734
600	2.17301	4.46130E-5	11.2074
C(1) = 4.13400E-3		C(1) = 4.13400E-3	
0	180.734	5.35352E-4	9.33947
100	797.374	2.57531E-4	1.75719
150	347.977	1.74864E-4	3.40104
200	237.011	1.33341E-4	3.73579
250	130.750	1.07072E-4	4.66973
300	71.5777	8.92271E-5	5.60363
350	47.0611	7.64594E-5	6.53753
400	26.0127	5.92232E-5	7.47157
450	13.7179	5.24347E-5	8.40552
500	7.59197	5.35352E-5	9.33947
550	3.41950	4.36593E-5	10.2734
600	1.55100	4.46130E-5	11.2074
C(1) = 4.73133E-3		C(1) = 4.73133E-3	
0	1270.51	5.35352E-4	9.33947
100	140.945	2.57531E-4	1.75719
150	195.340	1.74864E-4	3.40104
200	173.247	1.33341E-4	3.73579
250	103.002	1.07072E-4	4.66973
300	33.1491	8.92271E-5	5.60363
350	35.0633	7.64594E-5	6.53753
400	19.1014	5.92232E-5	7.47157
450	14.4345	5.24347E-5	8.40552
500	5.5034	5.35352E-5	9.33947
550	2.50397	4.36593E-5	10.2734

Table 28 More Passive Day Calculations.

COPY AVAILABLE TO DDC DOES NOT  
 PERMIT FULLY LEGIBLE PRODUCTION

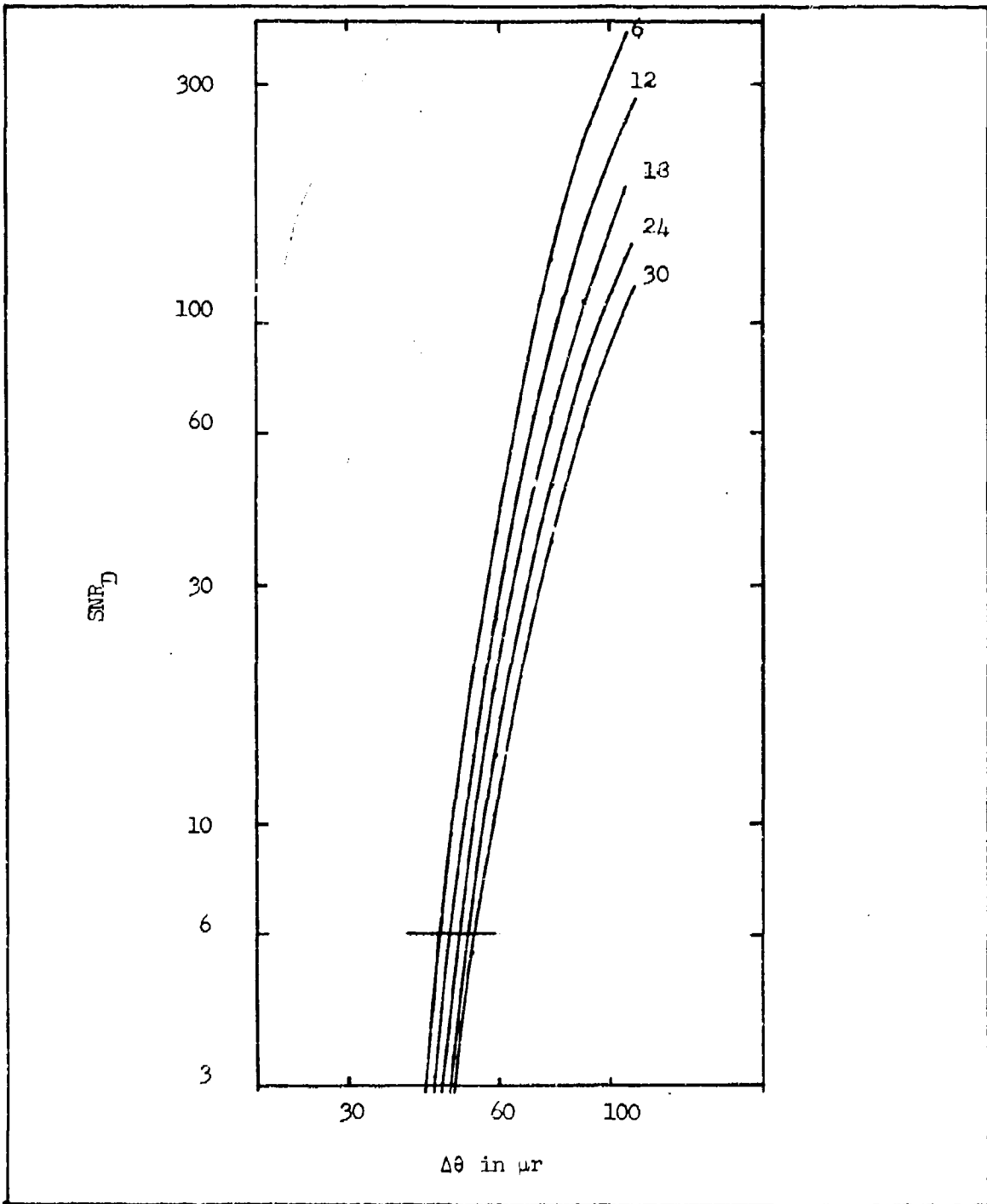


Fig. 72 SNR<sub>D</sub> vs Δθ for 6, 12, 18, 24 and 30 K ft.

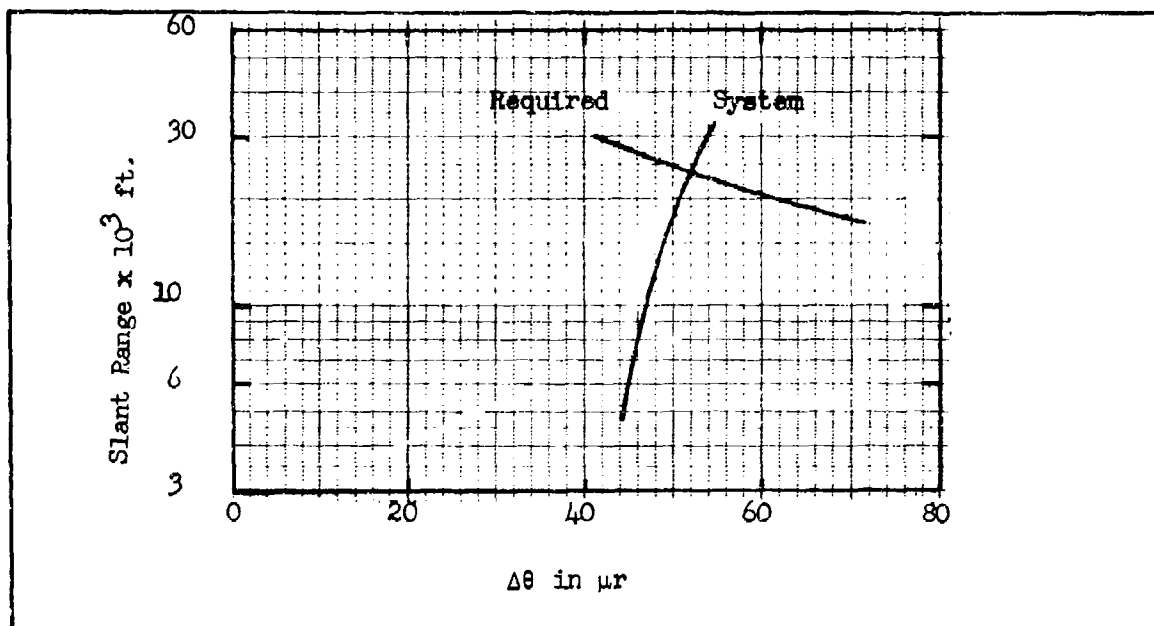


Fig. 73 Required vs Available Resolution,  $\Delta\theta$  vs Slant Range.

#### 7.7 Calculation for Passive Night

The basic calculations for the passive system at night are similar to the passive system during the day but now the signal current depends on the ambient light level as

$$i_{av} = \frac{\rho_{av} S A E_S}{4T^2}, \quad (183)$$

where  $\rho_{av}$  is the average reflectivity of the object,  $SAE_S$  must be given in consistent units for a specified source such as a 2870° K tungsten light, e.g., S in amps/watt, A in m squared and  $E_S$  scene light level in watts/m squared. T is the lens T number. The program steps  $\alpha$  the attenuation coefficient, ambient light level and range. The program is shown below. For simplicity, light levels of  $E_S$  below  $1 \text{ W/m}^2$  were not run in order to

```

100 REM***PROGRAM CALCULATES SNRD VS N AND R FOR NIGHT PASSIVE*
120 PRINT"PASSIVE TWILIGHT/NIGHT"
130 N=:2
135 M=3
140 DIM A(20)
150 DIM P(20)
160 DIM G(20)
170 DIM R(20)
180 DIM B(20)
185 REM ***PUT ATMOSPHERE ATTENUATION COEFFICIENTS HERE***
190 FOR L=1 TO M
200 READ A(L)
210 DATA3.3E-5,7.58E-5,1.37E-4
220 NEXT L
250 FOR J=1 TO N
260 READ P(J),G(J)
270 DATA1.00,1.00,1.01,1.00,1.03,.99
280 DATA1.06,.99,1.09,.98,1.12,.97
290 DATA1.16,.97,1.21,.96,1.26,.95
300 DATA1.31,.95,1.37,.94,1.43,.93
310 NEXT J
350 FOR J=1 TO N
360 READ R(J),B(J)
370 DATA.791,.893,.651,.793,.516,.695
380 DATA.394,.600,.284,.516,.203,.445
390 DATA.135,.388,.083,.342,.049,.305
400 DATA.029,.275,.015,.250,.008,.229
410 NEXT J
500 REM*****PROGRAM CONSTANTS FOLLOW*****
510 T=.1
515 E=1.6E-19
520 A=1
525 D2=50
530 G1=10
532 I1=.6E-6
535 G2=30000
540 S1=20E-3
542 D=25
545 A1=((D*1E-3)^2)*(A/((A^2)+1))
548 P=.3
550 I2=3E-9
560 D1=1E7
590 T0=10
600 F1=10
605 F=26
610 C0=.3
615 X1=10

```

Table 29 Program for Passive Night.

```

620 Y1=30
630 K3=3
650 REM***N1=13 IDENTIFICATION,8 RECOGNITION,2 DETECTION***
660 N1=8
661 IF N1=2 THEN 669
662 IF N1=8 THEN 667
663 PRINT"IDENTIFICATION"
665 GO TO 670
667 PRINT"RECOGNITION"
668 GO TO 670
669 PRINT"DETECTION"
670 E1=N1*Y1/X1
680 REM***MAIN CALCULATION STARTS HERE*****
700 FOR L=1 TO M
710 PRINT"ATTENUATION COEFICIENT"(A(L))
712 FOR Q=3 TO -5 STEP -1
715 PRINT"ES="10^Q
720 FOR R=6000 TO 30000 STEP 6000
722 C=C0/(1-K3*(1-EXP(A(L)*R)))
723 PRINT"R="R,"C(R)="C
725 PRINT"N=", "SNRD=", "DELTA THETA=", "K THETA="
727 FOR J=1 TO N
729 E2=10^Q
730 I=P*S1*A1*E2/(4*(T0^2))
732 IF I*G2<I1 THEN 750
736 G=I1/(P*S1*A1*E2/(4*(T0^2)))
738 IF G>G1 THEN 751
740 PRINT"E IS TO LARGE FOR MIN G1, REDUCE E"
741 PRINT
742 GO TO 894
750 G=G2
751 S=SQR(T*E1/(A*P(J)))*R(J)/(J*D2)
752 S=S*2*C*G*I
754 D9=(G^2)*E*G(J)*B(J)*I
756 D8=(I2^2)/(2*D1)
758 S=S/SQR(D9+D8)
760 D3={(D/25.4)/SQR(A^2+1)}/(J*D2*F)
800 PRINT J*D2, S, D3, 1/(2000*D3)
825 IF S<3 THEN 860
850 NEXT J
860 PRINT
890 NEXT R
893 PRINT
894 NEXT Q
895 PRINT
900 NEXT L
925 PRINT
930 PRINT
950 END

```

Table 30 Continuation of Program for Passive Night.

PASSIVE NIGHTTIME  
RECOGNITION

ATTENUATION COEFFICIENT .000033

ES= 1000

R= 0000

C(R)= .181062

N=

SNRD=

DELTA THETA=

K THETA=

E IS TOO LARGE FOR MIN G1, REDUCE E

ES= 100

R= 0000

C(R)= .181062

N=

SNRD=

DELTA THETA=

K THETA=

E IS TOO LARGE FOR MIN G1, REDUCE E

ES= 10

R= 0000

C(R)= .181062

N=

SNRD=

DELTA THETA=

K THETA=

50

1255.17

5.35838E-4

.933947

100

1115.9

2.67531E-4

1.30739

150

1002.8

1.73484E-4

2.30174

200

891.932

1.13741E-4

3.73579

250

803.341

1.07073E-4

4.20973

300

717.359

7.72971E-5

5.56355

350

643.195

7.04894E-5

6.56763

400

58.7312

5.39203E-5

7.47157

450

55.3682

5.94247E-5

8.40552

500

49.4255

5.35302E-5

9.33947

550

4.12793

4.66073E-5

10.2734

600

4.58275

4.45135E-5

11.2074

ES= 10000

N=

C(R)= .18207

SNRD=

DELTA THETA=

K THETA=

50

1255.11

5.35358E-4

.933947

100

1115.57

2.67531E-4

1.30739

150

1002.8

1.73484E-4

2.30174

200

891.747

1.13741E-4

3.73579

250

803.355

1.07073E-4

4.20973

300

717.34

7.72971E-5

5.56355

350

643.6791

7.04894E-5

6.56763

400

49.3577

5.39203E-5

7.47157

450

45.3195

5.94247E-5

8.40552

500

43.1955

5.35302E-5

9.33947

550

4.12191

4.66073E-5

10.2734

600

4.59929

4.45135E-5

11.2074

Table 31. Calculations for Passive Night.

COPY AVAILABLE TO DDC DOES NOT  
PERMIT FULLY LEGIBLE PRODUCTION

N=	C(R)=	DELTA TILTA=	K TILTA=
50	2055.7	3.35308E-4	.933947
100	341.355	2.57631E-4	1.50739
150	433.7	1.73454E-4	2.30134
200	236.115	1.33341E-4	3.73579
300	170.744	1.07072E-4	4.66973
350	164.335	8.2271E-5	5.30363
380	60.3946	7.84304E-5	6.53753
400	33.1553	6.69293E-5	7.47157
450	17.5497	5.94347E-5	8.40552
500	9.37357	5.35352E-5	9.33947
550	4.48317	4.85693E-5	10.2734
600	2.14671	4.45135E-5	11.2074

N=	C(R)=	DELTA TILTA=	K TILTA=
50	1034.13	3.55352E-4	.933947
100	554.721	2.57631E-4	1.50739
150	301.253	1.73454E-4	2.30134
200	212.431	1.33341E-4	3.73579
300	136.365	1.07072E-4	4.66973
350	77.3944	8.2271E-5	5.30363
380	43.2443	7.84304E-5	6.53753
400	24.6511	6.69293E-5	7.47157
450	13.6536	5.94347E-5	8.40552
500	6.7513	5.35352E-5	9.33947
550	3.77005	4.85693E-5	10.2734
600	1.97403	4.45135E-5	11.2074

N=	C(R)=	DELTA TILTA=	K TILTA=
50	1157.31	3.55352E-4	.933947
100	554.371	2.57631E-4	1.50739
150	301.451	1.73454E-4	2.30134
200	151.75	1.33341E-4	3.73579
300	78.25	1.07072E-4	4.66973
350	23.3547	8.2271E-5	5.30363
380	12.7556	7.84304E-5	6.53753
400	11.7137	6.69293E-5	7.47157
450	6.25461	5.94347E-5	8.40552
500	3.55933	5.35352E-5	9.33947
550	2.43925	4.85693E-5	10.2734

Table 32 More Calculations for Passive Night.

COPY AVAILABLE TO DDC DOES NOT PERMIT FULLY LEGIBLE PRODUCTION



$\Delta t = 1$	$\Delta t = 0.001$	$\Delta t = 0.002$	$\Delta t = 0.004$	$\Delta t = 0.008$
50	1075.84	533.327	266.664	133.332
100	537.92	266.664	133.332	66.666
150	358.613	177.776	88.888	44.444
200	269.059	133.332	66.666	33.333
250	215.247	107.546	53.773	26.909
300	177.776	88.888	44.444	22.222
350	148.148	74.074	37.037	18.519
400	123.094	62.371	31.186	15.593
450	101.511	52.756	26.378	13.189
500	82.839	44.637	22.319	11.159
550	66.666	37.778	18.889	9.444
600	52.778	32.037	15.819	7.909
650	40.741	27.186	13.593	6.797
700	30.909	23.094	11.547	5.773
750	22.909	19.519	9.759	4.879
800	16.222	16.222	8.111	4.074
850	10.741	13.186	6.797	3.398
900	6.797	10.741	5.773	2.889
950	3.773	8.111	4.879	2.444
1000	2.000	6.000	4.000	2.000

$\Delta t = 1.000$	$\Delta t = 0.001$	$\Delta t = 0.002$	$\Delta t = 0.004$	$\Delta t = 0.008$
50	1000.00	500.000	250.000	125.000
100	500.000	250.000	125.000	62.500
150	333.333	166.667	83.333	41.667
200	250.000	125.000	62.500	31.250
250	200.000	100.000	50.000	25.000
300	166.667	83.333	41.667	20.833
350	142.857	71.429	35.714	17.857
400	125.000	62.500	31.250	15.625
450	111.111	55.556	27.778	13.889
500	100.000	50.000	25.000	12.500
550	90.909	45.455	22.727	11.364
600	83.333	41.667	20.833	10.417
650	76.923	38.462	19.231	9.615
700	71.429	35.714	18.182	8.929
750	66.667	33.333	17.222	8.333
800	62.500	31.250	16.316	7.813
850	59.091	29.545	15.476	7.368
900	56.250	28.125	14.706	6.979
950	53.846	26.923	14.000	6.630
1000	50.000	25.000	13.333	6.333

$\Delta t = 1.000$	$\Delta t = 0.001$	$\Delta t = 0.002$	$\Delta t = 0.004$	$\Delta t = 0.008$
50	1000.00	500.000	250.000	125.000
100	500.000	250.000	125.000	62.500
150	333.333	166.667	83.333	41.667
200	250.000	125.000	62.500	31.250
250	200.000	100.000	50.000	25.000
300	166.667	83.333	41.667	20.833
350	142.857	71.429	35.714	17.857
400	125.000	62.500	31.250	15.625
450	111.111	55.556	27.778	13.889
500	100.000	50.000	25.000	12.500
550	90.909	45.455	22.727	11.364
600	83.333	41.667	20.833	10.417
650	76.923	38.462	19.231	9.615
700	71.429	35.714	18.182	8.929
750	66.667	33.333	17.222	8.333
800	62.500	31.250	16.316	7.813
850	59.091	29.545	15.476	7.368
900	56.250	28.125	14.706	6.979
950	53.846	26.923	14.000	6.630
1000	50.000	25.000	13.333	6.333

Table 33 More Passive Night Calculations.

COPY AVAILABLE TO DDC DOES NOT PERMIT FULLY LEGIBLE PRODUCTION

N = 24000	C(O) = .054437		
N =	S(I) =	DELTA TILTA =	K TILTA =
57	584.521	5.35362E-4	.933947
100	244.723	2.87531E-4	1.38779
150	137.917	1.72454E-4	2.39134
200	82.915	1.33341E-4	3.73579
250	55.1451	1.07072E-4	4.86973
300	39.153	7.92271E-5	5.80567
350	28.1753	7.54304E-5	6.53753
400	19.7153	6.39203E-5	7.47157
450	9.4314	5.24247E-5	7.40552
500	3.19881	5.35362E-5	9.33947
550	1.35347	4.18893E-5	10.2734
N = 30000	C(O) = 4.93933E-2		
N =	S(I) =	DELTA TILTA =	K TILTA =
57	429.881	5.35362E-4	.933947
100	136.202	2.87531E-4	1.38779
150	101.3	1.72454E-4	2.39134
200	53.1155	1.33341E-4	3.73579
250	34.7043	1.07072E-4	4.86973
300	24.4755	7.92271E-5	5.80357
350	14.5777	7.54304E-5	6.53753
400	8.17352	6.39203E-5	7.47157
450	4.14791	5.24247E-5	7.40552
500	2.43215	5.35362E-5	9.33947

Table 34 More Passive Night Calculations.

limit the amount of printout but, of course, in practice, light levels all the way down to starlight are of interest.

#### 7.8 Calculation for Active System

For the active system,  $i_{av}$  is given by

$$i_{av} = \frac{\rho_{av} SAP \exp(-2\alpha R)}{4T^2 R^2 \Omega}, \quad (184)$$

where P is the transmitted power,  $\Omega$  the solid angle into which the power is transmitted. Term S has units of amps/watt, T is the lens T number and photocathode area A has the same units as  $R^2$ , usually ft. squared.

The program for the active system follows. In the program, it is assumed that  $C(R) = C(0)$  which is approximately true for moderate to good

```

100 REM***PROGRAM CALCULATES SNRD VS N AND R FOR ACTIVE NIGHT*
120 PRINT"ACTIVE NIGHT"
130 N=12
135 M=3
140 DIM A(20)
150 DIM P(20)
160 DIM G(20)
170 DIM R(20)
180 DIM B(20)
185 REM ***PUT ATMOSPHERE ATTENUATION COEFFICIENTS HERE***
190 FOR L=1 TO M
200 READ A(L)
210 DATA3.3E-5,7.58E-5,1.37E-4
220 NEXT L
250 FOR J=1 TO N
260 READ P(J),G(J)
270 DATA1.00,1.00,1.01,1.00,1.03,.99
280 DATA1.06,.99,1.09,.98,1.12,.97
290 DATA1.16,.97,1.21,.96,1.26,.95
300 DATA1.31,.95,1.37,.94,1.43,.93
310 NEXT J
350 FOR J=1 TO N
360 READ R(J),B(J)
370 DATA.791,.893,.651,.793,.516,.695
380 DATA.394,.600,.284,.516,.203,.445
390 DATA.135,.388,.083,.342,.049,.305
400 DATA.029,.275,.015,.250,.008,.229
410 NEXT J
500 REM*****PROGRAM CONSTANTS FOLLOW*****
510 T=.1
515 E=1.6E-19
517 P3=30
518 S1=20E-3
520 A=1
525 D2=50
532 I1=.6E-6
540 G=30000
542 D=25
545 A1=(((D/25.4)2)/144)*(A/((A2)+1))
548 P=.3
550 I2=3E-9
560 D1=1E7
590 T0=10

```

Table 35 Program for Active System.

```

605 F=26
608 O1=1.5*1.5
609 O1=O1*(3.14156/180)^2
610 C0=.3
612 C=C0
615 X1=10
620 Y1=30
650 REM*****N1=13 IDENTIFICATION,8 RECOGNITION,2 DETECTION***
660 N1=8
661 IF N1=2 THEN 669
662 IF N1=8 THEN 667
663 PRINT"IDENTIFICATION"
665 GO TO 670
667 PRINT"RECOGNITION"
668 GO TO 670
669 PRINT"DETECTION"
670 E1=N1*Y1/X1
680 REM***MAIN CALCULATION STARTS HERE*****
700 FOR L=1 TO M
710 PRINT"ATTENUATION COEFICIENT"A(L)
720 FOR R=6000 TO 30000 STEP 6000
722 I=P*S1*A1*P3*EXP(-2*A(L)*R)/(4*(T0^2)*(R^2)*O1)
723 PRINT"R="R,"I="I
725 PRINT"N=", "SNRD=", "DELTA THETA=", "K THETA="
727 FOR J=1 TO N
751 S=SQR(T*E1/(A*P(J)))*R(J)/(J*D2)
752 S=S*2*C*G*I
754 D9=(G^2)*E*G(J)*B(J)*I
756 D8=(I2^2)/(2*D1)
758 S=S/SQR(D9+D8)
760 D3=((D/25.4)/SQR(A^2+1))/(J*D2*F)
800 PRINT J*D2,S,D3,1/(2000*D3)
825 IF S<3 THEN 860
850 NEXT J
860 PRINT
890 NEXT R
893 PRINT
894 GO TO 895
895 PRINT
900 NEXT L
925 PRINT
930 PRINT
950 END

```

Table 36 Rest of Program for Active System.

ACTIVE NIGHT

ACQUISITION

INTERPOLATION COEFFICIENT .000033

N = 8000

I = 4.12473E-11

N	SIN $\theta$	DELTA THETA	K THETA
50	34.735	3.35332E-4	4.33747
100	16.731	1.67331E-4	1.67331
150	11.0117	1.73334E-4	2.73334
200	8.6541	1.65412E-4	3.65412
250	6.8433	1.67332E-4	4.67332
300	5.5331	1.53337E-4	5.53337
350	4.71533	1.47153E-4	6.47153
400	4.01510	1.40151E-4	7.40151
450	3.42851	1.34285E-4	8.34285

N = 12000

I = 3.94673E-11

N	SIN $\theta$	DELTA THETA	K THETA
50	19.070	3.80332E-4	4.80332
100	9.53377	1.95331E-4	1.95331
150	6.3173	1.73334E-4	2.73334
200	4.5	1.33341E-4	3.73379
250	3.33743	1.67332E-4	4.67332
300	2.98746	1.63337E-4	5.63337
350	2.67333	1.64334E-4	6.64334
400	2.31433	1.53333E-4	7.53333

N = 14000

I = 2.97737E-11

N	SIN $\theta$	DELTA THETA	K THETA
50	13.03	3.23332E-4	4.23332
100	6.3433	1.67331E-4	1.67331
150	4.3727	1.73334E-4	2.73334
200	3.33371	1.33341E-4	3.73379
250	2.11736	1.67332E-4	4.67332
300	1.63333	1.63337E-4	5.63337
350	1.23133	1.64334E-4	6.64334

N = 24000

I = 7.33310E-13

N	SIN $\theta$	DELTA THETA	K THETA
50	34.0333	3.33332E-4	4.33332
100	14.9343	1.67331E-4	1.67331
150	9.39732	1.73334E-4	2.73334
200	6.3973	1.33341E-4	3.73379
250	4.14133	1.67332E-4	4.67332
300	3.33333	1.63337E-4	5.63337

N = 30000

I = 3.23313E-13

N	SIN $\theta$	DELTA THETA	K THETA
50	23.3333	3.33332E-4	4.33332
100	11.7334	1.67331E-4	1.67331
150	7.63333	1.73334E-4	2.73334
200	5.33333	1.33341E-4	3.73379
250	3.63333	1.67332E-4	4.67332

Table 37 Calculations for Active TV.

COPY AVAILABLE TO DDC DOES NOT PERMIT FULLY LEGIBLE PRODUCTION

viewing and with a reasonable separation between the transmitter and the receiver. If a more exact calculation is required, the techniques discussed in AFAL-TR-72-229 should be used and  $G(R)$  calculated at each range value.

A sample calculation is shown after the program.

#### REFERENCES

1. Rosell, F. A., and Willson, R. H., Performance Synthesis (Electro-Optical Sensors) AFAL-TP-71-137, Air Force Avionics Laboratory, WPAFB, Ohio, May 1971.
2. Rosell, F. A., and Willson, R. H., Performance Synthesis (Electro-Optical Sensors) AFAL-TR-72-279, Air Force Avionics Laboratory, WPAFB, Ohio, August 1972, AD-905-291L.
3. Rosell, F. A., and Willson, R. H., Performance Synthesis of Electro-Optical Sensors, AFAL-TR-73-260, Air Force Avionics Laboratory, WPAFB, Ohio, August 1973.
4. Biberman, L. M., "Perception of Displayed Information," Plenum Press, New York, May 1973.
5. Biberman and Nudelman, "Photoelectronic Imaging Devices," Vol. I, Plenum Press, New York, 1971.
6. Middleton, WEK, "Vision Through the Atmosphere," University of Toronto Press, 1952.
7. "Electro-Optics Handbook," RCA Defense Electronics Products, Burlington, Mass., 1968.
8. McClatchey, et.al., "Optical Properties of the Atmosphere," AFCRL-71-0279, Air Force Cambridge Research Laboratories, 10 May 1971.
9. Steingold, H., and Strauch, R., Applied Optics, Jan. 1969.

UNCLASSIFIED

Security Classification

DOCUMENT CONTROL DATA - R&D		
<i>(Security classification of title, body of abstract and indexing annotation must be entered when the overall report is classified)</i>		
1 ORIGINATING ACTIVITY (Corporate author) Westinghouse Defense and Space Center Aerospace Division, Baltimore, Maryland	2a REPORT SECURITY CLASSIFICATION Unclassified	
	2b GROUP None	
3 REPORT TITLE  PERFORMANCE SYNTHESIS OF ELECTRO-OPTICAL SENSORS		
4 DESCRIPTIVE NOTES (Type of report and inclusive dates) Final Report April 1973 - April 1974		
5 AUTHOR(S) (Last name, first name, initial) Rosell Frederick A. William, Robert H.		
6 REPORT DATE April 1974	7a TOTAL NO OF PAGES 221	7b NO OF REFS 9
8a CONTRACT OR GRANT NO F33615-73-Q-4132	9a ORIGINATOR'S REPORT NUMBER(S)	
b PROJECT NO		
c 698DF	9b OTHER REPORT NO(S) (Any other numbers that may be assigned this report) AFAL-TR-74-104	
d		
10 AVAILABILITY/LIMITATION NOTES Distribution limited to United States government agencies only; test and evaluation; 30 April 1974. Other requests for this document must be referred to Air Force Avionics Laboratory (NVA-698DF), Wright-Patterson Air Force Base, Ohio 45433.		
11 SUPPLEMENTARY NOTES	12 SPONSORING MILITARY ACTIVITY Air Force Avionics Laboratories Wright-Patterson AFB, Ohio 45433	
13 ABSTRACT This effort is a continuation of the Performance Synthesis Study (Electro-Optical Sensors) reported in Technical Report AFAL-TR-73-260, dated August 1973 analytical sensor models are updated and refined. Procedures for performing systems trade-off analysis are discussed, general requirements and specifications for typical electro-optical imaging sensors are derived and reported. Psychophysical testing was performed in order to determine grey scale detection and other dynamic range requirements and to further improve the understanding of image motion effects. Finally computer programs for system resolution prediction are developed.		

DD FORM 1473  
1 JAN 64

UNCLASSIFIED

Security Classification



UNCLASSIFIED

Security Classification

KEY WORDS	LINK A		LINK B		LINK C	
	ROLE	WT	ROLE	WT	ROLE	WT
Synthesis						
698DF						
Low-Light-Level Television						
Model						
Range						
Electro-Optics						
Sensors						
Video						
Perception						
Vision						
Signal-to-Noise Ratio Display						
Motion						
Apertures						

UNCLASSIFIED

Security Classification